Technische Universität München

Physik Department

MPQ

An Ultracold Gas of Electrically Trapped Formaldehyde

Alexander Volker Prehn

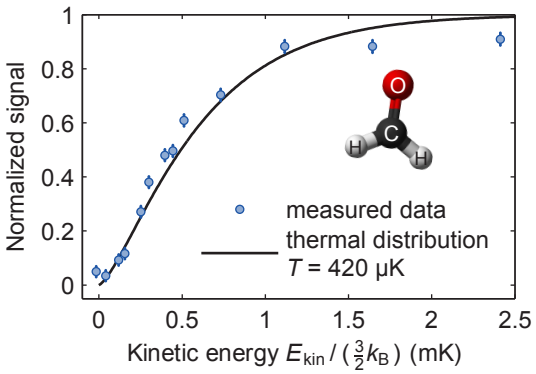

Dissertation

Physik-Department, Technische Universität München
and Max-Planck-Institut für Quantenoptik, Garching

May 2018

Cover illustration: The figure shows the main experimental result of this thesis, the measured integral of the kinetic energy distribution of the electrically trapped, ultracold ($T < 1\,\mathrm{mK}$) gas of formaldehyde molecules. The solid curve represents the expected distribution for a thermal ensemble at a temperature of 420 µK in a perfect box potential and serves as a comparison. As an inset, the chemical formula and structure of the formaldehyde molecule is sketched.

Technische Universität München

Max-Planck-Institut für Quantenoptik

An Ultracold Gas of Electrically Trapped Formaldehyde

Alexander Volker Prehn

Vollständiger Abdruck der von der Fakultät für Physik der Technischen Universität München zur Erlangung des akademischen Grades eines

Doktors der Naturwissenschaften (Dr. rer. nat.)

genehmigten Dissertation.

Vorsitzender :		Prof. Dr. Wilhelm Zwerger
Prüfer der Dissertation :	1.	Hon.-Prof. Dr. Gerhard Rempe
	2.	Prof. Dr. Reinhard Kienberger

Die Dissertation wurde am 18.05.2018 bei der Technischen Universität München eingereicht und durch die Fakultät für Physik am 18.09.2018 angenommen.

Abstract

Fascinating applications of ultracold ($T < 1\,\mathrm{mK}$) polar molecules ranging from controlled chemistry to the investigation of dipolar quantum gases or precision tests of fundamental physical theories exploit the rich internal level structure and the electric dipole moment of the molecules. Realizing such applications demands a high level of control over both external and internal degrees of freedom of the molecules. Moreover, many of the envisioned experiments rely on structurally and chemically diverse species, motivating the development of various 'direct' cooling and control techniques which are applicable to preexisting molecules. To date, the long-standing goal of direct cooling to the submillikelvin temperature regime has been demonstrated with two methods, with one of the two first experimental realizations being the main focus of this thesis: Using optoelectrical Sisyphus cooling, an ensemble of 3×10^5 formaldehyde (H_2CO) molecules was generated at a temperature of about $400\,\mu\mathrm{K}$, with the molecules populating a single rotational state with more than 80 % purity and staying electrically trapped for tens of seconds.

Optoelectrical Sisyphus cooling proceeds in an electrostatic trap which produces box-like potentials for low-field-seeking molecular states. Kinetic energy is removed by allowing molecules to repeatedly move up the electric-field gradient of the trapping potential in a rotational state with strong Stark interaction, and back down in a state with weaker Stark interaction. Dissipation is provided by a vibrational spontaneous decay. The approach makes use of generic properties of polar polyatomic molecules and should thus be widely applicable. With formaldehyde, we demonstrate a reduction in temperature by three orders of magnitude and an increase in phase-space density by a factor of about 10^4, only limited by technical imperfections. In the thesis, the structural requirements of the molecule species and the experimental implementation of the scheme are detailed. In particular, the consequences of the asymmetric-rotor structure of formaldehyde for experiments and technical improvements of the electric trap, resulting in a better homogeneity of the box-like trapping fields, are illuminated. Moreover, the produced molecule sample is characterized thoroughly.

A major motivation for cold and ultracold molecule research is the interest in spectroscopy with ever-increasing precision. The low temperature of our cooled molecules and the box-like trapping potential with its tunable offset field offer ideal conditions for high-resolution spectroscopy on trapped molecules. Thus, the second focus of this thesis is on the demonstration of a novel method to observe narrow spectral lines with trapped polar molecules. Specifically, we combine techniques well-known from optical atomic clocks, i.e. the choice of a 'clock' transition with vanishing first-order differential Stark shift and measurement at a 'magic' electric field with minimal residual Stark broadening, with the preparation methods developed in the first part of the thesis to perform precise microwave spectroscopy. As a result, Doppler-limited line widths down to 3.8 kHz are measured, the narrowest spectral features observed with electrically trapped molecules so far, yielding a relative uncertainty of 10^{-8}.

Contents

1 Introduction

The study of molecules plays a central role in physics. On the one hand, at present smaller molecules consisting of only a few atoms make up the most complex physical systems which scientists can anticipate to model and understand in full detail, from first principles based on quantum mechanics. Therefore, experiments on quantum-controlled molecules of increasing complexity are ideal tools to test and develop our ever-improving fundamental theoretical understanding as well as precise predictions and calculations. On the other hand, molecules play important roles in more complex structures and phenomena, including not only chemistry or condensed matter but also star formation and life. A better understanding of molecules and their interaction with each other hence can give valuable insight into much more intricate processes and help solve fundamental open questions in science and technology.

Molecules are investigated with diverse methods in a number of fields of physics. For example, femtosecond physics [Kra09] aims at resolving fast processes, within molecules or during molecular interactions, with ultrashort laser pulses. Laser pulses also permit the manipulation of internal molecular states with coherent control techniques [Sha12b]. Full control of the internal and external degrees of freedom of a molecule, and hence of its individual molecular quantum states, however, requires cooling to very low temperatures. It is the availability and further development of cooling techniques for molecules which allowed the observation of subtle physical effects related to molecules and established the research field of cold and ultracold molecules [Car09, Kre09]. This discipline, which this thesis contributes to, is introduced in the following with a focus on neutral polar molecules.

Typically, two temperature ranges are distinguished in the field, the cold (1 mK to $\sim$ K) and the ultracold ($<$ 1 mK) regime [Bel09, Car09, Lem13]. In the cold regime, the thermal energy is comparable to an interaction energy caused by strong external electric or magnetic fields available in the laboratory. This allows trapping of molecular samples and isolation from the environment with such external fields. Further cooling can lead to the ultracold temperature regime. In atomic physics, this regime is reached when (non-dipolar) scattering processes can be entirely modeled with a single partial wave which is the case at submillikelvin temperatures, motivating the above definition. For molecules, however, a rigorous definition based on scattering properties is more involved and depends on the species, the existence of an electric dipole moment, and in the case of a non-zero dipole moment on the applied electric field [Boh09].

Investigations of ultracold matter started with the demonstration of laser cooling and trapping of alkali atoms [Chu98, Coh98, Phi98] and, among other spectacular achievements, led to the creation of Bose-Einstein condensates in 1995 [Cor02, Ket02], boosting this line of research. More recently, quantum-controlled, ultracold atomic systems are routinely used for applications like quantum simulation of condensed matter systems [Gro17], quantum information processing and the investigation of light-matter interaction [Rei15], or precision measurements with interferometric techniques [Cro09].

Despite the unsurpassed quantum-control achieved over alkali, alkaline earth or similar atoms, attaining likewise control over other, more complicated forms of matter is desirable. Molecules offer a wide range of internal degrees of freedom, including electronic, vibrational, rotational, and hyperfine states, which can be used for manipulation. Additionally, polar molecules can carry a strong permanent electric dipole moment which lets them react to external electric fields and provides a long-ranged, anisotropic, state-dependent, and thus tunable interaction between individual molecules. Moreover, due to the more complex structure, external degrees of freedom like orientation and alignment also influence interactions of molecules with each other and their environment and can be exploited for the purpose of control.

These properties render cold and ultracold polar molecules ideal systems for a number of research directions. Unsurprisingly, molecular systems are the natural choice for the investigation of chemistry at low temperatures where tunneling effects and resonances can dominate collisions or chemical reactions (see below). Less obviously, certain molecules are very sensitive probes of fundamental physics [Wal16, DeM17]. For instance, precision spectroscopy is used to investigate the shape of the electron [Hud11, Bar14a, Bar17] or the chirality of matter [Dau99, Die15, Tok17]. Advancing control over molecular quantum states also enables applications in quantum physics, where in particular the strong dipole-dipole interaction can be harnessed to investigate interacting many-body systems [Yan13], to perform quantum simulations [Wal13, Wal15], or to process quantum information. A few of these applications of ultracold polar molecules are discussed in more detail in the following section.

The diverse structure of molecules, appealing to various research interests, however, also makes it challenging to cool and control them. Consequently, there is no general approach to producing ultracold molecules yet. The existing strategies include 'indirect' methods for the assembly of ultracold molecules from laser-cooled ultracold alkali atoms, accessing the lowest temperatures but being restricted to diatomic molecules with laser-coolable constituent atoms. Wider applicable are 'direct' techniques for cooling of preexisting molecules. Both approaches are summarized in Sec. 1.2. In fact, at the time this thesis work began, direct cooling to the ultracold temperature regime had not yet been reported. One such demonstration is the main topic of this thesis: optoelectrical Sisyphus cooling allowed the creation of an electrically trapped, rotational-state-controlled gas of formaldehyde (H_2CO) molecules at submillikelvin temperatures. To date, this is still the largest ensemble of molecules ever produced in a laboratory in this temperature regime. In the meantime, other groups used 'direct' laser cooling, only applicable to special molecules, to generate diatomic radicals at similar temperatures. These recent and complementary results are outlined in Sec. 1.3.

Cooling and trapping of the molecules, a prerequisite of many applications, is not the only challenge which has to be addressed towards improved control over molecules. For example, the strong interaction of polar molecules with external electric fields which we exploit for both cooling and trapping often causes a broadening of spectral lines if cold molecules are spectroscopically investigated inside an electric trap. Nevertheless, very narrow spectral features can be observed if the motion of the molecules and the trapping environment are controlled well, as shown in the last part of this thesis. By combining the unique design of our electric trap [Eng11] with a clever choice of experimental parameters we demonstrate a method to obtain narrow spectral lines with cooled and electrically trapped molecules—a first application of optoelectrical Sisyphus cooling.

Formaldehyde, the molecule used for all experiments in this thesis work, is a prototypical polar polyatomic molecule. It is sufficiently simple to allow for a deep theoretical understanding [Hud06c]. Yet, it is a generic representative of asymmetric rotor molecules and features electronic, vibrational, rotational and hyperfine states with transition frequencies encompassing the ultraviolet-, infrared-, microwave- and radio frequency domains. Next to being a model system for molecular spectroscopy [Eli12], formaldehyde is extensively studied in various other fields of physics because it is, for example, an important interstellar [Brü03] and atmospheric [Per09] molecule. Previous investigations of formaldehyde in the context of cold molecules are specifically mentioned in the following introductory sections.

1.1 Applications of ultracold polar molecules

Ultracold molecules carrying a permanent electric dipole moment are of interest in many fields of physics and physical chemistry. A few intriguing applications are discussed in the following paragraphs. For a more comprehensive overview of the field, the reader is directed to recent reviews or special issue collections of articles [Car09, Kre09, Dul11, Jin12, Lem13, Doy16]. Besides the following topics, recent results and future prospects of using molecules for tests of fundamental physical theories by performing precise spectroscopy are outlined in the introduction to Ch. 5 which covers the results on precision spectroscopy of electrically trapped formaldehyde obtained during this thesis. Not discussed at all are the fascinating perspectives of quantum-many-body physics and quantum simulations with polar molecules (see e.g. the review [Mos16] and references therein).

Ultracold collisions and chemistry. Investigations of ultracold molecular collisions and chemical reactions are ultimately driven by the desire to completely probe and, as an extension, control the scattering properties and reaction paths of molecules on the quantum level [Bel09, Bal16, Boh17]. At low temperatures where the de-Broglie wavelength of a molecule exceeds its size or even the separation of molecules, quantum effects play an important role in these processes. In this regime, resonances in the interaction energy are predicted for collisions and, more specifically, chemical reactions. For example, high reaction rates and resonances at ultralow temperature were calculated for several reactions [Wec05b, Wec05a, Qué08], despite usually very high classical reaction barriers of up to a few hundred Kelvin, as first shown for the reaction $\mathrm{F} + \mathrm{H_2} \rightarrow \mathrm{H} + \mathrm{HF}$ by Balakrishnan and Dalgarno [Bal01]. Moreover, a dependence on external fields can give a handle for control over collisions [Kre05] and chemical reactions [Tsc15], allowing the adjustment of reaction rates or reaction resonances. This is particularly interesting for polar molecules with their long-ranged and electric-field-dependent dipole-dipole interaction.

Towards control of chemical reactions at low temperatures, a process involving formaldehyde, $\mathrm{H_2CO} + \mathrm{OH} \rightarrow \mathrm{HCO} + \mathrm{H_2O}$, was theoretically investigated in detail by Hudson *et al.*, suggesting that the collision and reaction cross sections can be modified by orders of magnitude by changing either the molecular state, or the external electric field [Hud06c]. This reaction is of interest in atmospheric chemistry, for instance. Both reactants can be cooled to low temperatures and even electrically trapped, allowing

controlled experiments. While Hudson *et al.* were able to produce cold molecular beams of both species via Stark deceleration (see Sec. 1.2), the predicted reaction rates at low temperature were not large enough for observation in their experiment. They recommended trapping of at least one species and secondary cooling of the reactants, increasing the sample density, to make measurements feasible [Hud06c].

Collisions and chemistry at ultracold temperatures have been extensively studied in the context of molecule formation with 'indirect' methods (see Sec. 1.2). However, chemistry in the ultracold regime with a polar molecule as a reactant has only been observed with the alkali dimer KRb in the group of Ye. Their results are summarized in a very recent review [Boh17] and include observation of a dependence of the reaction rate on the number of populated initial internal states by Ospelkaus *et al.* [Osp10] and on the applied electric field by Ni *et al.* [Ni10]. Further, exploiting the anisotropic dipole-dipole interaction, preparation in a single molecular quantum state, and Fermi statistics, de Miranda *et al.* [Mir11] could suppress the reaction rate by two orders of magnitude by confining the molecules in a two-dimensional trap and the motional ground state. However, due to the reliance on molecule production with 'indirect' methods, the developed techniques are restricted to few chemical species.

For the use with more diverse molecule species, the lowest collision temperatures down to 10 mK and the finest energy resolution are currently achieved with the very promising merged beam approach: two atomic or molecular beams with reactants are joined by bending one of them with a magnetic [Hen12] or electric [Ber14] guide into the other. This allowed the observation of resonances in the Penning ionization reaction of metastable He with H_2 by Henson *et al.* [Hen12]. By controlling the rotational state of H_2, Klein *et al.* showed that a subkelvin reaction resonance appears only if the molecule is rotationally excited which in this case probes the anisotropy of the collision [Kle16]. Jankunas *et al.* investigated electron-transfer reactions with more complex molecules, namely ammonia [Jan14a, Jan15] and CH_3F [Jan14b]. This technique is in principle applicable to all molecules with a magnetic or electric dipole moment, with the drawback of short interaction times due to the relatively large forward velocity of the beams.

Longer interaction times, allowing the study of weak or slow processes, can be obtained with trapped molecules. In this direction, Wu *et al.* observed dipolar collisions in slow and dense beams of CH_3F and ND_3 molecules confined in an electric guide [Wu17]. Further, the effect of electric fields on atom-molecule collisions potentially useful for sympathetic cooling was investigated by Parazzoli *et al.* by overlapping electrically trapped ND_3 with Rb in a magneto-optical trap [Par11]. A dependence of collisional loss on an external electric field was also observed for magnetically trapped OH [Stu13]. Recently, Akerman *et al.* demonstrated cotrapping of O_2 with Li in a magnetic trap, however, to date without results on collisions [Ake17]. 'Direct' cooling of diverse species to ultracold temperatures would expand the research possibilities in this field.

Physics and chemistry in space and the earth's atmosphere. Small molecules are present not only in the atmosphere of our planet [Rot13] but also in interstellar space. Radio telescopes and infrared spectrometers allow the observation of distant molecules and determination of their abundance which gives insight into the formation of more complex molecules and stars [Ber07]. In interstellar space, H_2 is the most abundant molecule accounting for 99.99 % of all molecules, followed by, e.g., CO, H_2O, OH, CO_2 and H_2CO [Agú13]. In fact, formaldehyde, H_2CO, was the first polyatomic organic

molecule to be detected in the interstellar medium by microwave spectroscopy [Sny69][1] and, formed from CO and various hydrogen compounds, it plays an important role during star formation in so-called cold dark interstellar clouds. In these clouds, molecules with mean densities from 10^2 to $10^6\,\mathrm{cm}^{-3}$ collide and react at temperatures around 10 K [Ber07]. Thus, laboratory investigations of chemical reactions in this [Smi11] or a lower [Kra16] temperature regime are of great interest.

Precise spectroscopic studies under controlled laboratory conditions are also useful for comparison with astronomy data. Then, spectroscopic data from space reveals the temperature, the density, the kinetic temperature and other important characteristics of these clouds [Ber07]. Moreover, accurately calculated potential energy surfaces of the molecules are needed to model collisions and chemical reactions [Boh17]. Verification of these calculations requires precise knowledge of the molecular structure. Consequently, while the processes in interstellar clouds happen at temperatures of $\sim 10\,\mathrm{K}$ or more, investigating the structure of the molecules and collisions between them at significantly lower temperatures could be useful to gain more insight into astrophysical chemistry.

Quantum information processing. A large variety of physical systems are already utilized and considered for quantum information processing [Nie10], a field with huge scientific and technological interest and progress. Ultracold polar molecules combine a few attributes which make them particularly interesting. On the one hand, long-lived rotational or hyperfine states allow for information storage with potentially long coherence times and information access with microwave radiation. On the other hand, the long range dipole-dipole interaction facilitates entanglement generation and gate operations encompassing qubits in distinct molecules. These specific features are exploited in a number of concrete proposals relying entirely on polar molecules [DeM02, Yel06, Kuz08] or making use of the coupling of molecular rotational states to superconducting microwave stripline resonators in hybrid systems [And06, Rab06, Rab07]. All approaches require trapped ultracold molecules and control over all quantum states. Towards this, an important experimental achievement was the observation of a coherence time on the order of one second between hyperfine levels of ultracold $^{23}\mathrm{Na}^{40}\mathrm{K}$ molecules by Park *et al.* [Par17].

More complex molecules can have additional benefits for quantum computing. Wei and coworkers pointed out the upside of polar symmetric top molecules, similar to those used in this thesis, as qubits: “These offer advantages resulting from a first-order Stark effect, which renders the effective dipole moments nearly independent of the field strength. That permits use of much lower external field strengths for addressing sites” [Wei11]. As a second example, the many internal degrees of freedom can be used to build an entire quantum computer from a single molecule, as proposed by Tesch and de Vivie-Riedle [Tes02]. In contrast to having one qubit per particle, as in the case of atoms or diatomic molecules, the various vibrational modes of one polyatomic molecule serve as qubits. As a first experimental step in that direction, Hosaka *et al.* implemented a Fourier transform in iodine molecules based on population transfer via shaped femtosecond laser pulses [Hos10]. The authors pointed out that for future scalability of the approach, cooling, trapping and addressing of individual molecules will be necessary.

[1] Various isotopologues of formaldehyde were detected in different environments in space, see, e.g., the introduction of Ref. [Mül17].

1.2 Approaches to generating ultracold polar molecules

Molecular structure and the envisioned applications of ultracold polar molecules are diverse. So are the methods to produce ultracold polar molecules. As it was pointed out before, 'indirect' techniques associating molecules from laser-cooled ultracold atoms and 'direct' cooling of preexisting molecules are distinguished and briefly outlined. While 'indirect' approaches presently give access to the lowest temperatures, various applications of ultracold molecules profit from chemically and structurally diverse species. Therefore, a growing number of research groups pushes the development of 'direct' cooling technology. In the following, the focus is on a summary of the state of the art, not on a detailed explanation of the techniques which can be found in the cited references.

Indirect methods. Formation of ground-state molecules from ultracold atoms is always a two-step process. First, weakly bound, highly excited molecules are created during atomic collisions via Feshbach association or photoassociation [Ni09]. Second, the molecules are transferred to their ground state via a coherent state transfer [Ni08] or internal state cooling by optical pumping [Vit08, Man12], carrying away the binding energy of ground-state molecules of a few thousand Kelvin with photons in both cases. The aim is to map the temperature of the ultracold atoms to the newly created molecules and avoid heating in the formation process.

The coldest temperatures, the highest densities, and the best control over the internal state of the molecules is achieved with experiments pursuing Feshbach association because this is a fully coherent and therefore reversible process which can in principle be controlled extremely well [Ni09, Mos15]. Two near-quantum-degenerate atomic gases are overlapped and the magnetic field is scanned adiabatically over a Fano-Feshbach scattering resonance such that the two free atom states are converted to a highly vibrationally excited bound molecular state via the avoided crossing of the resonance. The adiabatic transfer to the ground state is achieved with a coherent two-photon STIRAP process [Ber98]. This approach requires a high initial phase-space density and was first demonstrated with non-polar Cs_2 [Dan08] and Rb_2 [Lan08] and polar KRb. Notably, in the latter case Ni *et al.* produced about 30000 ground-state KRb molecules at a temperature of 350 nK and a density of $10^{12}\,\mathrm{cm}^{-3}$, resulting in a near-quantum-degenerate gas of polar molecules with a phase space density of 0.02 [Ni08, Ni09]. More recently, ultracold ground-state molecules were produced with a few more species using the same techniques, namely bosonic RbCs [Mol14, Tak14] and NaRb [Guo16] as well as fermionic NaK [Par15, See18]. All these experiments produced 10^3 to 10^4 molecules at temperatures of a few hundred nanokelvin and densities around $10^{11}\,\mathrm{cm}^{-3}$. Despite these successful demonstrations, a major drawback of the method is its limited applicability. It can only produce polar diatomic molecules consisting of certain laser-coolable alkali or similar atoms. Moreover, the experiments are very complex and demanding which can also be seen from the fact that it took many years to apply the techniques demonstrated in 2008 for KRb to other polar species, regardless of substantial effort by a number of research groups.

In the second indirect approach, photoassociation [Ulm12], two laser-cooled atoms sufficiently close to each other are transferred to an electronically excited, bound molecular state via laser excitation. A subsequent photon emission, stimulated or sponta-

neous, transfers the molecule to the molecular electronic ground state, usually a vibrationally excited state, from which a transfer to the absolute ground state is possible. A number of polar alkali dimers have been produced in the vibrational and electronic ground state, e.g., RbCs [Sag05] and LiCs [Dei08]. However, the temperatures of $\sim 100\,\mu\mathrm{K}$ achieved with this technique are higher and the densities of $\sim 10^4\,\mathrm{cm}^{-3}$ and phase-space densities of $\sim 10^{-14}$ are orders of magnitude lower than what was demonstrated with Feshbach association [Ni09]. The reasons are a finite transition probability from the free atom states into the bound molecular excited state and spontaneous decay from the excited state to many molecular electronic ground states, limiting the efficiency of molecule production [Ulm12]. Therefore, it seems that Feshbach association is being established as the technique of choice to produce trapped ultracold gases of alkali dimers, despite the high complexity of the scheme discussed above.

Direct production of cold and slow molecular beams. Direct cooling to the ultracold regime, potentially applicable to a huge variety of molecule species, essentially always starts with the production of a cold molecular beam and subsequent trapping of the molecules. We give an overview of the three most common techniques to produce cold beams, each of them used by various research groups at present and applicable fairly generally. Two of the methods produce internally cold molecular beams with a large forward velocity. In these cases further deceleration is necessary to allow for trapping, as discussed in the following.

One approach to produce a beam of slow and thus motionally cold polar molecules is velocity filtering, as first demonstrated by Rangwala *et al.* with H_2CO and ND_3 [Ran03]. It is based on separating the slowest fraction of molecules which are present in any thermal ensemble from the fast molecules by selectively trapping low-velocity molecules in two dimensions in an electrostatic quadrupole guide, or any other electric or magnetic guide, and directing them away from the faster ones. It can produce an intense beam of slow, trappable molecules ($T < 1\,\mathrm{K}$) in low-field-seeking rotational states [Rie05, Eng11]. In this thesis, velocity filtering is used as a very simple and robust source of formaldehyde molecules to load our electrostatic trap [Eng11]. The drawback is that the distribution of internal states reflects the much higher temperature of the effusive nozzle used to load the quadrupole guide[2].

Cooling of internal and external degrees of freedom to a temperature of a few Kelvin is achieved via a pulsed supersonic expansion of a high pressure gas into vacuum. Adiabatic cooling and collisions in the nozzle convert the thermal energy of the gas to forward velocity of the beam resulting in a beam of molecules which are cold in the co-moving frame of reference and travel with a longitudinal velocity of many hundred meters per second in the laboratory frame. Deceleration of the beam with conservative forces then delivers cold, trappable molecules [Bet00].

The very dense and short pulses of molecules produced in a supersonic expansion can be decelerated effectively by using time-varying and inhomogeneous electric fields in a Stark decelerator for polar molecules or magnetic fields in a Zeeman decelerator for paramagnetic molecules, as summarized in Refs. [Hog11, Mee12]. In this approach, the electromagnetic fields are tailored such that the traveling molecular beam always sees

[2]See thesis of M. Motsch [Mot09b] for details on operation and characterization of velocity filtering. The thesis also includes further experiments on guided beams of cold formaldehyde [Mot07].

a potential hill allowing deceleration to a selectable longitudinal velocity or almost to rest. It was first demonstrated by Bethlem *et al.* with CO molecules employing a Stark decelerator [Bet99] and resulted in production of the first ensemble of trapped molecules where ND_3 was held in a quadrupole electric trap [Bet00]. Hudson *et al.* produced a cold beam of formaldehyde with a similar Stark decelerator [Hud06c]. In a more advanced design, so called moving-trap or traveling-wave decelerators confine the packet of molecules in three dimensions during the slow-down process, reducing losses due to transverse motion of the molecules and allowing trapping in the decelerator [Qui13] or an efficient transfer to an adjacent trap [Liu17, Ake17]. In particular, the group of Bethlem used their moving-trap Stark decelerator to trap 2×10^4 CH_3F molecules at a temperature of 40 mK [Men15], to prepare a small number of ammonia molecules at submillikelvin temperatures via adiabatic cooling [Qui14], and to construct a molecular fountain [Che16]. Note that deceleration can also be accomplished with chip-based Stark decelerators [Mee09], microwave [Mer12], or intense optical fields [Ful04]. The described variations of a supersonic expansion followed by deceleration of the beam are widely applicable. The pulsed operation, however, makes it difficult to obtain both large numbers of slow molecules and high densities. Moreover, production of a large number of ultracold molecules requires application of a dissipative cooling scheme to the trapped molecules.

A third option to produce an internally cold molecular beam is via collisions with a cryogenic buffer gas of Helium or Neon, first demonstrated for CaH molecules in the group of Doyle [Wei98] and reviewed comprehensively by Hutzler *et al.* [Hut12]. Cryogenic buffer-gas cooling is the most general technique as it does not set any requirements on the structure of the cooled molecules. Recently, it allowed cooling molecules as complex as CH_3ReO_3 [Tok17] or CF_3CCH [Wu17]. While the first experiments were performed inside the cryogenic buffer-gas cell, it is now most common to create an aperture in the cell and work with the resulting molecular beam, allowing separation of the cooled molecules from the buffer gas [Hut12]. Combining a buffer gas cell with an electric quadrupole guide, van Buuren *et al.* created an internally cold beam of formaldehyde molecules [Buu09].

Depending on the operating conditions of the cell (and the mass of the molecule species), cold beams of buffer-gas-cooled molecules have a mean forward velocity of about 50 m/s to 200 m/s. Even for comparatively low buffer-gas densities, leading to smaller forward velocities, very slow, trappable molecules are absent in the beam due to inevitable collisions in the vicinity of the nozzle, accelerating the slow molecules [Mot09a]. Hence, for subsequent trapping of a substantial fraction of the beam the molecules have to be further decelerated to below ~ 20 m/s, a typical capture velocity of a molecule trap [Tru17b].

A beam of buffer-gas-cooled molecules can be pulsed, but with larger pulse durations and relative velocity spreads than after supersonic expansion, or continuous. Therefore, conventional Stark and Zeeman decelerators cannot be applied efficiently[3]. Continuous deceleration of electrically guided polar molecules was demonstrated by exploiting conservative centrifugal forces on a rotating disc [Che14]. The combination of a cryogenic buffer-gas cell with this centrifuge decelerator recently lead to the construction of a very bright source of slow molecules in our group, delivering record-large fluxes of 10^{10}

[3]The use of a traveling wave decelerator was proposed though [Fab14].

CH_3F, ND_3, or CF_3CCH molecules per second at velocities $< 20\,\mathrm{m/s}$ and densities $\sim 10^9\,\mathrm{cm}^{-3}$ [Wu17]. This approach is widely applicable to polar molecules and ideal for loading a trap. An alternative for molecules amenable to laser cooling (see below) is the use of Doppler slowing [Met99]. With this technique, buffer-gas cooled molecules have been successfully slowed to below the capture velocity of a trap [Bar12, Yeo15]. As Doppler cooling is a dissipative process allowing compression of the phase space, it can also compress the velocity distribution while slowing the molecules, as recently proven by Truppe *et al.* [Tru17b]. However, laser slowing to date delivers substantially smaller samples of molecules and is less general than other techniques.

Direct cooling to the ultracold regime. In order to bring molecules deep into the submillikelvin temperature regime, trapping and application of a dissipative cooling process allowing an increase of the phase-space density is mandatory. In particular, this also requires some means to remove entropy. In this paragraph, we outline the existing strategies, while the experimental demonstrations of cooling to submillikelvin temperatures are summarized in the next section.

A general method of dissipating energy and entropy is via collisions between particles. Evaporative cooling, i.e. removal of hot particles and rethermalization to lower temperatures of the remaining ones, or sympathetic cooling with colder particles of a different (atomic or molecular) species requires dense samples of trapped molecules. Despite the generality of this approach only very few results in this direction have been reported. Evaporative cooling of OH molecules in a quadrupole trap was investigated by Stuhl *et al.* [Stu13]. Regardless of possible first indications of evaporative cooling [Stu13], the ultracold temperature regime has not been reached yet and control over collisions and molecule losses turned out to be surprisingly difficult [Ree17]. Towards sympathetic cooling of molecules with ultracold atoms many theoretical calculations have been performed, see, for example, Refs. [Lar06, Tok11, Lut14]. A preparatory experimental achievement was already mentioned before: Akerman *et al.* trapped 10^9 oxygen molecules and 10^5 lithium atoms in the same trap, a prerequisite for future investigations of inter-species collisions [Ake17].

Another approach is to use a large number of spontaneously emitted photons for dissipation in laser cooling and magneto-optical trapping (MOT), the standard methods to produce ultracold atoms [Met99]. However, as significant cooling requires ten thousands of photons to be resonantly scattered from the molecule, Doppler cooling and similar techniques can only be applied to a special class of molecules which feature fast-decaying electronic transitions with highly diagonal Franck-Condon factors. Only then the molecules decay to a small number of vibrational states after spontaneous emission of a photon, allowing Doppler cooling with a manageable number of repumping lasers. These conditions are fulfilled for a number of diatomic radicals [Di 04] and selected polyatomic radicals [Isa16, Koz16, Koz17b].

Experimentally, transverse laser cooling of a molecular beam of SrF was demonstrated by Shuman *et al.* [Shu10] and a MOT of the same species by Barry *et al.* [Bar14b]. These first results later led to the production of diatomic radicals at submillikelvin temperatures, as discussed in Sec. 1.3. Laser cooling using an electronic cycling transition was recently also demonstrated for the polyatomic molecule SrOH by cooling the transverse motion of a molecular beam [Koz17a]. Nonetheless, for the large majority of molecule species other cooling mechanism have to be found, notably as many of

the more complex and chemically stable molecules including formaldehyde predissociate with high probability and are hence destroyed upon electronic excitation with an ultraviolet laser [Moo83].

The aforementioned difficulties arising from exciting molecules electronically motivated the development of alternative cooling methods using spontaneously emitted photons more efficiently. These dissipative cooling techniques rely on using inhomogeneous, internal-state-dependent potential landscapes created with electric or magnetic fields for energy extraction and a single or only a small number of spontaneous photon emissions to remove entropy and ensure the irreversibility of the process. One such method, single photon cooling, was proposed by Narevicius *et al.* [Nar09]: Molecules in their initial state move in a strongly varying potential and are optically excited at the classical turning point where they maximize the potential energy and minimize the kinetic energy. A single spontaneous decay to a final state exhibiting a shallow potential thereby takes out a large fraction of the molecular kinetic energy. Such an optical pumping process could also be used to transfer molecules from one to another trapping environment [Sha12a]. Although it did not involve cooling, part of these ideas were realized by accumulating NH molecules in a magnetic trap via optical pumping from an untrapped state to a trapped state [Mee01, Rie11]. Combining state-dependent electric potentials with optical pumping via a vibrational excitation allows construction of a closed, repeatable, Sisyphus-type cooling scheme for polyatomic molecules. Here, only a few tens of spontaneous decays are needed to reduce the kinetic energy of the molecules by orders of magnitude. The method was developed by Zeppenfeld *et al.* in our group [Zep09] and implemented in a proof-of-principle experiment reducing the temperature of CH_3F molecules by a factor of 13 to 29 mK shortly before this thesis work began [Zep12, Zep13, Eng13, Pre12]. The aim of this thesis was pushing forward the technique and accessing the ultracold temperature regime with polyatomic molecules.

1.3 Directly cooled polar molecules at submillikelvin temperatures

Direct cooling with a dissipative method to the ultracold temperature regime was only realized very recently, with one of the two first demonstrations being the main focus of this thesis [Pre16]: 3×10^5 electrically trapped formaldehyde (H_2CO) molecules at a temperature of about 400 µK were produced. In this section, complementary results obtained with three-dimensional laser cooling of diatomic radicals [Di 04] are summarized. Other techniques, including the remaining ones mentioned in Sec. 1.2, have not yet been successful in producing directly cooled ultracold molecules.

The first diatomic radical cooled to below 1 mK was SrF. Norrgard *et al.* built a magneto-optical trap (MOT) confining 2000 SrF molecules at a temperature of 400 µK and with a lifetime in the trap of 0.5 s. Their results [Nor16] were published back-to-back with the main results of this thesis work and slightly improved later [Ste16], reaching a temperature of 250 µK with 10^4 molecules. More recently, two groups independently realized a MOT of CaF. Truppe and Williams *et al.* trapped about 2×10^4 CaF molecules in their MOT at temperatures down to 730 µK [Tru17a, Wil17]. Anderegg *et al.* obtain larger ensembles of $(1.0 \pm 0.3) \times 10^5$ CaF molecules at a temperature

of $(340 \pm 20)\,\mu K$ with their setup [And17]. Consequently, the latter group reaches the largest particle density of $(7 \pm 3) \times 10^6\,cm^{-3}$ in a MOT. All of these experiments start with a molecular beam produced with cryogenic-buffer-gas cooling and laser slowing (see above paragraph on production of cold beams) to produce molecules with velocities smaller than the capture velocity of a MOT. To be more specific, Truppe and Williams *et al.* report a capture velocity of their MOT of 11 m/s [Wil17]. The achievable particle numbers are thereby limited mainly by difficulties in efficiently slowing the molecular beam, while the temperature of the ensembles comes close to the theoretical temperature limit of a MOT, the Doppler temperature [Met99], in all three experiments.

Going one step further, Truppe and Williams *et al.* used a three-dimensional optical molasses [Met99] to cool their ensemble of CaF to 50 µK, to below the Doppler limit, reaching a number density of $(0.8 \pm 0.1) \times 10^5\,cm^{-3}$ and a phase-space density of $(2.4 \pm 0.6) \times 10^{-12}$ [Tru17a]. The group also transferred the molecules to a magnetic trap [Wil18], a step towards investigation of molecule collisions at ultracold temperatures. However, these impressive results of cooling to submillikelvin temperatures obtained with direct laser cooling have been restricted to two metal fluoride molecule species up to now, SrF and CaF.

1.4 Outline of this thesis

This thesis presents experiments proving direct cooling of polyatomic polar molecules to the ultracold temperature regime and showing high-precision spectroscopy of electrically trapped molecules. Using the method of optoelectrical Sisyphus cooling, a record-large ensemble of electrically trapped formaldehyde, H_2CO, was prepared at submillikelvin temperatures and in a single rotational state. The molecules were then used to implement a method for precision spectroscopy in our box-like electric trap.

The general idea of optoelectrical Sisyphus cooling, the relevant aspects of the internal structure of formaldehyde, and the choice of internal states for the implementation of cooling are detailed in **Chapter 2**. In this theoretical discussion, the consequences of the asymmetric rotor structure of formaldehyde and its properties in the electric field are emphasized. Despite the complexity of the molecule, the resulting level scheme for cooling is simple and clearly structured.

To achieve the long-standing goal of direct cooling to the ultracold regime, the experimental apparatus and methods were improved substantially, based on conclusions drawn from previous thesis work with optoelectrical Sisyphus cooling and rotational-state control of CH_3F molecules [Zep13, Eng13, Glö16]. **Chapter 3** introduces the electric trap and the surrounding apparatus as well as important improvements implemented in the course of this thesis. In particular, the homogeneity of the box-like trapping fields could be enhanced, a significant step not only for cooling but also for the spectroscopy work. Additionally, experimental techniques on rotational-state detection and rotational-state preparation which have been refined and adapted to formaldehyde are presented in the same chapter along with new measurements of molecular parameters and characteristics of our system.

The experimental results on optoelectrical Sisyphus cooling of formaldehyde are elucidated in great detail in **Chapter 4**. This part includes a thorough explanation of

the method to measure the kinetic energy of the trapped molecules, details of the experimental sequence, and a characterization of the molecule ensemble obtained after cooling. The main outcomes of the experiments covered in this chapter were previously published in an article [Pre16].

As a first application of the preparation techniques, and as a demonstration of the high level of control achieved, high-precision spectroscopy of trapped formaldehyde molecules is investigated in **Chapter 5**. Stark broadening has been eliminated and Doppler-limited spectroscopic lines have been observed by probing a rotational transition with vanishing first-order differential Stark shift in a 'magic' electric field. The proof-of-principle experiments performed with this method result in measured line widths of a few kHz for rotational transitions in formaldehyde, the narrowest spectral features observed with electrically trapped molecules so far, with prospects to attain much higher precision in the future. The text concludes with an outlook to future experiments in **Chapter 6**.

2 Theory essentials: optoelectrical Sisyphus cooling and the formaldehyde molecule

In this chapter it will be shown that optoelectrical Sisyphus cooling which was proposed [Zep09] for and first demonstrated [Zep12, Zep13, Eng13, Pre12] with symmetric top molecules is applicable to formaldehyde, a small asymmetric rotor molecule. It turns out that the resulting level scheme for cooling of the external motion, which makes use of the rotational and vibrational degrees of freedom of the molecule, is fairly simple and can be implemented with decent experimental complexity. On the one hand, the slightly asymmetric rotor structure of formaldehyde makes the choice of internal states for cooling a little more intricate. On the other hand, the diverse structure offers extreme flexibility for future applications in quantum optics because state manifolds with different properties and widely varying transition frequencies are available, as will be illustrated throughout the chapter. For example, this could allow to couple cooled formaldehyde molecules with other physical systems in a wide frequency range.

Besides the vibrational and rotational level structure of formaldehyde, its properties in a static electric field are most important for optoelectrical Sisyphus cooling. Some of the theoretical calculations for formaldehyde leading to the presented cooling scheme were worked out by Martin Ibrügger in his diploma thesis [Ibr13]. In this chapter we demonstrate that the main characteristics for our experiments can be understood with a simple analytical model.

Accordingly, the chapter describes the theoretical concepts this thesis work is based on and is structured as follows: Section 2.1 explains the general idea and requirements of optoelectrical Sisyphus cooling and motivates the choice of the molecule species. Formaldehyde and the relevant aspects of its molecular structure are introduced in Sec. 2.2. Section 2.3 describes the interaction of the molecule with a static electric field. With these foundations at hand, the internal states for Sisyphus cooling are chosen in Sec. 2.4 and the detailed level scheme is developed in Sec. 2.5.

2.1 Optoelectrical Sisyphus cooling

In general, any mechanism that cools the external degrees of freedom of a particle has to fulfill the following requirements. There has to be a means to extract kinetic energy from the particle and a dissipative process to remove entropy. If the scheme does not dissipate the entire kinetic energy in a single step, the cooling process should also be repeatable to allow cooling by a large factor. Additionally, trapping of the particle or the ensemble of particles is desirable to maintain control over it during the experiment.

Figure 2.1 sketches how these requirements are implemented in optoelectrical Sisyphus cooling, a cooling method designed for polar molecules with a strong electric-field

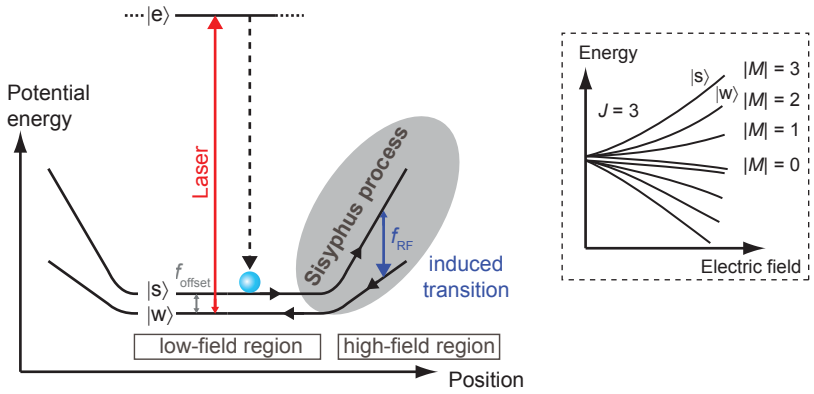

Figure 2.1: Working principle of optoelectrical Sisyphus cooling shown in an energy-level and state-transition diagram. A molecule initially residing in a strongly trapped low-field-seeking state $|s\rangle$ looses kinetic energy by performing an induced transition (f_{RF}) to the more weakly trapped state $|w\rangle$ in the high-field region of the trap. Coupling $|w\rangle$ and a vibrational excited state $|e\rangle$ with an infrared laser in the low-field region of the trap closes the cooling cycle because the molecule is pumped back to its initial state $|s\rangle$. Due to the irreversible spontaneous emission in the last step the process only works in the direction which leads to cooling. The frequency f_{offset} is defined in the text. The inset shows a sketch of the Stark-shifted set of M sublevels of the rotational state $J = 3$ of a molecule, including one possible choice of the states $|s\rangle$ and $|w\rangle$.

interaction. A suitable electrostatic trap featuring low electric fields in the central part and strong trapping fields at the edges of the confining volume produces a box-like potential for low-field-seeking rotational states as shown. Kinetic energy is extracted by allowing molecules to repeatedly move up the electric-field gradient of the trapping potential in a state with strong Stark interaction, $|s\rangle$, and back down in a state with weaker Stark interaction, $|w\rangle$. This is achieved by constructing a unidirectional cycling process as follows. The two states are coupled with radio frequency (RF) radiation which resonantly induces transitions in the high-field region of the trap. Moreover, only the state $|w\rangle$ is coupled with an excited vibrational state $|e\rangle$ in the low-field region, allowing for spontaneous decays from $|e\rangle$ to (both of) the ground states. In combination, this constitutes a repeatable cooling cycle. Such a scheme, which exploits state-dependent potential energy curves along with optical pumping, is commonly called a Sisyphus cooling process [Pri83, Zep09].

For a practical implementation of the scheme, one can think of many different choices for the internal molecular states represented by $|s\rangle$, $|w\rangle$, and $|e\rangle$ if a few conditions are fulfilled. First, as we use electrostatic trapping fields all of the states have to be low-field seeking to keep the molecules trapped during cooling. Second, the electric-field interaction of state $|s\rangle$ has to be stronger than the one of state $|w\rangle$. Third, sufficiently strong transition dipole moments should exist between the pairs of states $|s\rangle$ and $|w\rangle$ as well as $|w\rangle$ and $|e\rangle$. Fourth, a spontaneous decay channel from state $|e\rangle$ to state $|s\rangle$ is required and other decays from state $|e\rangle$ should predominantly lead to trapped low-field-seeking states incorporated in the cooling scheme to minimize losses while allowing many repetitions of the Sisyphus cycle. Finally, the states have to be chosen such that unwanted transitions to states outside the cooling scheme induced by the

applied radiation fields or other processes such as black-body radiation are minimized.

As we will see throughout this chapter, a particularly simple scheme, sufficiently closed to allow many repetitions, can be constructed by using the rotational and vibrational degrees of freedom of a molecule: The states $|s\rangle$ and $|w\rangle$ are identified with successive trapped M sublevels of one rotational state J, split apart by the Stark effect (see inset of Fig. 2.1). Here J is the total angular momentum of rotation and M its projection on the external quantization axis [Tow75], as reviewed in the next section. The state $|e\rangle$ is a vibrational excited state with the same rotational quantum number J. In fact, this choice of states, used in the current and previous experimental implementations [Zep12, Zep13], differs from the initially proposed assignment [Zep09].

With the building blocks of optoelectrical Sisyphus cooling being established now, the following paragraphs are devoted to a more detailed explanation of a few important aspects of the cooling method and the choice of the molecule species for experiments. While the discussion is fairly general and does not require knowledge of the particular quantum states chosen for the implementation, it implies the choice of successive M sublevels as states $|s\rangle$ and $|w\rangle$.

Amount of extracted energy. A key benefit of this cooling method is the ability to choose and adjust the amount of kinetic energy which is extracted in one cycle of the process. Using a simple picture, this amount is given by the radio frequency f_{RF} which couples the two ground states $|s\rangle$ and $|w\rangle$ minus the offset splitting f_{offset} of the same two states in the low-field region of the trap (cf. Fig. 2.1). Consequently, the portion of energy which is dissipated can be chosen very high for uncooled molecules initially ($f_{\mathrm{RF}} - f_{\mathrm{offset}} \sim h \cdot 5\,\mathrm{GHz} \sim k_B \cdot 0.24\,\mathrm{K}$ in a realistic experimental sequence, see Sec. 4.2.1) to extract as much energy as possible. As cooling advances, f_{RF} has to be lowered such that molecules which now possess less kinetic energy still reach the point in the potential where the RF is resonant and cooling can continue. We choose stepwise adjustments of f_{RF}.

Selecting Stark-split M sublevels for the implementation, particles can in principle be cooled by a factor of ~ 2 per cycle, if the cooling RF is matched tightly to the molecular temperature and an appropriate set of internal states is chosen [Pri83]. In practice, however, it is beneficial to adjust f_{RF} such that molecules with a range of different kinetic energies are able to undergo a transition from $|s\rangle$ to $|w\rangle$ at the expense of slightly lower energy reduction per cycle. Considering this and the actual level scheme used in experiments (Sec. 2.5) an energy reduction by a factor of $\sim \sqrt{2}$ per Sisyphus cycle is realistic (Sec. 4.2.2 and [Zep12]). Even with the reduced cooling factor, only about 20 cycles are needed to decrease the molecules' kinetic energy by a factor of 1000.

Optical pumping via a vibrational transition. Optical pumping to the strongly trapped state $|s\rangle$ is a crucial part of the cooling cycle. Because of the efficient energy extraction discussed previously, a vibrational excitation can be used for this purpose. Although spontaneous decay rates of vibrational modes for most molecule species are slow, $\lesssim 100\,\mathrm{Hz}$, limiting the speed of cooling, this choice offers several advantages.

First, from electronically excited states non-radiative decays dominate over purely radiative transitions for many molecule species, and especially polyatomic molecules suffer from rapid predissociation upon electronic excitation [Her66]. Second, electronically excited molecules would decay to a large number of final vibrational states because

there are very few selection rules for the vibrational degree of freedom for electronic transitions. This precludes construction of a closed cycling scheme via an electronic transition, except for special molecules with highly-diagonal Franck-Condon factors, which are (mostly diatomic) radicals [Di 04, Isa16, Koz16]. In contrast, molecules with a single quantum of excitation in a single vibrational mode will predominantly decay back to the ground state with strict selection rules for the rotational quantum numbers, except in cases of strong resonances with other vibrational modes [Zep09]. Consequently, construction of a closed cycling scheme based on vibrational excitation is possible. Finally, vibrational transition wavelengths lie in the mid-infrared which is more easily accessible with present-day laser technology than the (deep) ultraviolet radiation required to excite electrons in many chemically stable molecules.

Fundamental limit of cooling. Fundamentally, the lowest temperatures reachable by optoelectrical Sisyphus cooling are limited to a few times the recoil temperature of the photons used for optical pumping [Pri83, Zep12]. The recoil temperature [Met99] associated with the fundamental excitation of the v_1 C-H stretch vibrational mode of formaldehyde is 25 nK and is similar for other molecule species suitable for optoelectrical cooling. The factor "a few times" stems from the fact that a molecule will typically scatter more than one photon during optical pumping from state $|w\rangle$ to the state $|s\rangle$ because the excited state $|e\rangle$ usually decays to both of the ground states. However, in our large-volume, box-like trap most likely the cooling process will turn out to be inefficient at considerably larger temperatures in the low µK-regime due to slow diffusion of molecules to the trap boundaries or due to other limitations of the trapping geometry[1]. Further, rather technical limitations of the present experiments will be discussed after the experimental results in Sec. 4.4.

Suitable molecule species. In principle, optoelectrical Sisyphus cooling can be applied to all polar molecules with a strong Stark interaction and pure rovibrational states. The former, a large Stark shift, is needed for electric trapping (see also Sec. 3.1). The latter requirement is twofold: First, low-field-seeking excited vibrational states should decay to low-field-seeking ground states to keep the molecules trapped during the cooling sequence. This is naturally the case for symmetric-top molecules [Tow75]. For asymmetric rotors this condition is fulfilled, if the molecule possesses near-degenerate inversion-doublet rotational states which are coupled strongly already by the moderate electric field in the central low-field region of the trap. Then, a linear Stark shift and appropriate selection rules are found. Such states exist for the slightly asymmetric molecule formaldehyde as will be shown throughout the chapter. Presumably, such states can also be found for many more molecule species. Second, the molecule should possess a suitable vibrational transition which is sufficiently isolated (in energy space) from other vibrational modes such that Fermi resonances which lead to losses from the closed cycling scheme do not occur or are sufficiently suppressed.

Additionally, the decay rate of the vibrational mode should be large enough to achieve substantial cooling in a time shorter than the lifetime of molecules in the electric trap (which will be finite in any real experiment). Many symmetric-top molecules with

[1] General requirements for the trapping geometry for optoelectrical Sisyphus cooling are discussed in Barbara Englert's thesis [Eng13]. Optoelectrical Sisyphus cooling to temperatures close to the recoil temperature might be possible in a harmonic trap.

permanent electric dipole moments $\gtrsim 1$ Debye and a vibrational decay rate of 10–100 Hz fulfill these requirements and were identified in the original proposal [Zep09].

The present experimental setup, in particular the molecule source, puts another constraint on the choice of the molecule species. Our effusive nozzle which is cooled with liquid nitrogen produces thermal ensembles in a temperature range of 110–300 K [Mie10]. On the one hand, the rotational constants of the species determine the number of states populated after the limited precooling, which can range from dozens of states to many thousand or more. The smaller the rotational constants are, the more states are populated in this temperature range. On the other hand, Sisyphus cooling acts only on a small set of states. Consequently, the choice of a molecule with rather small mass and therefore large rotational constants greatly enhances the population in the set of rotational states used for the experiments. Apart from the more fundamental requirements discussed earlier this was an important reason for the choice of fluoromethane (CH_3F) for the first demonstration of optoelectrical Sisyphus cooling [Zep12, Eng13].

Note that the possibility of applying our method to diatomic polar molecules with highly diagonal Franck-Condon factors and with optical pumping via an electronic transition is currently being investigated in our group by Manuel Koller. First results indicate that for this class of molecules Doppler cooling is often the preferable technique.

Formaldehyde as an ideal test molecule. Formaldehyde (H_2CO)[2], the molecule species chosen for the experiments in this thesis, has several properties making it an ideal candidate to substantially advance optoelectrical Sisyphus cooling compared to the experiments with fluoromethane, without the need to construct a more complex experimental apparatus. The key points are summarized in the following list.

- Although being an asymmetric rotor, formaldehyde features sets of rotational states in which inversion doublets are coupled already at moderate electric field strengths in the trap, resulting in a strong linear Stark shift and allowing creation of closed cycling schemes of trapped low-field-seeking states (Secs. 2.3 – 2.5).

- A large vibronic-ground-state electric dipole moment of 2.33 Debye [Fab77], 25% larger than the one of CH_3F, ensures strong electric trapping of molecular states with a linear Stark shift (see Sec. 3.1).

- The v_1 C-H stretch vibrational mode suitable for optoelectrical Sisyphus cooling decays with a rate of ~ 60 Hz [Rot13], 4 times faster than the v_1 mode of CH_3F used before [Zep12]. This allows much faster cooling and in particular results in a larger fraction of hot molecules being cooled initially during trap loading and therefore kept in the trap (see Sec. 4.2.1).

- The large rotational constants of formaldehyde ($A = 282$ GHz, $B = 38.8$ GHz, $C = 34.0$ GHz [Brü03]) lead to a sufficiently narrow thermal rotational state distribution already at ~ 150 K permitting the use of a simple and robust effusive nozzle with liquid nitrogen precooling as a molecule source (Secs. 2.4 and 3.2).

[2]The systematic IUPAC name for formaldehyde is methanal and following the newest standards the chemical formula is written CH_2O. In this thesis, the name and the symbol most common in the literature of molecular physics are used, formaldehyde and H_2CO.

2.2 The slightly asymmetric rotor formaldehyde

In this section, the formaldehyde molecule (H_2CO) is introduced and the structural properties playing a role for the development of the cooling scheme are summarized. As it was shown in the introduction, formaldehyde is extensively studied in physics. The spectrum of formaldehyde and its structure has been investigated from early analyses of infrared (IR) [Nie34, Her45] and ultraviolet (UV) [Die34] absorption spectra and the advent of microwave spectroscopy [Bra49, Law51] to the present [Mül17] in different spectral ranges corresponding to different internal degrees of freedom: pure rotational spectra (and hyperfine structure) in the radio frequency, microwave, and recently Terahertz domain [Cha73, Fab77, Cor80, Brü03, Mül17], vibrational transitions in the IR [Pin78, Bro78, Bro79, Rot13], as well as electronic excitations in the UV spectral range [Mou75, Clo83, Zep07, Mot08].

The theory of molecular structure is explained in great detail in textbooks [Her45, Tow75, Kro75, Bun12]. In earlier theses from our group several aspects of the theory relevant to our experiments with cold molecules were already presented. Christian Sommer described the molecular Hamiltonian with emphasis on rotation and electric-field interaction [Som11]. The rotational energy structure in an electric field was calculated specifically for optoelectrical Sisyphus cooling of formaldehyde by Martin Ibrügger [Ibr13]. Erich Dobler summarized how selection rules for electric dipole transitions in formaldehyde involving all degrees of freedom can be derived from symmetry considerations of the molecule structure [Dob16].

Here, the emphasis is on the identification of suitable internal states for optoelectrical Sisyphus cooling of formaldehyde and previous knowledge of the basic structure of molecules is assumed. Understanding the choice of internal states for cooling of this slightly asymmetric rotor molecule, should allow readers to assess whether other similar or even more asymmetric molecules of interest could be cooled with our method.

The general molecule structure and the relevant internal degrees of freedom, vibration, rotation, and effects of the nuclear spins are discussed briefly. In particular, the rotational level structure is investigated with respect to finding the desired inversion-doublet rotational states (defined below) which are coupled strongly already at moderate electric field strengths. Further, the hyperfine interaction due to the spins of the hydrogen nuclei strongly influences the thermal population of rotational states and hence the choice of states for experiments. Moreover, the experiments on precision spectroscopy presented in Ch. 5 have almost reached an accuracy which is comparable to the magnitude of the hyperfine interaction.

Molecule structure. Formaldehyde is a four-atom prolate asymmetric top molecule. Its structure along with its inertial axes (a, b, c) and the molecule-fixed coordinate system (x, y, z) in I^r representation [Kro75] is shown in Fig. 2.2. Here, the assignment of the axes (a, b, c) is given by the rotational constants $A > B > C$ [Kro75]. In the electronic and vibrational ground state formaldehyde is a planar molecule [Clo83] with a permanent electric dipole moment along the symmetry axis. Electronically excited states do not play a role in this work.

Vibrational modes. As the investigated cooling method makes use of vibrational spontaneous decays, a vibrational mode has to be picked for experiments. H_2CO has six

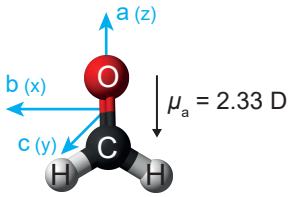

Figure 2.2: Structure of formaldehyde (H_2CO). A molecule-fixed right-handed coordinate system (x, y, z) is assigned to the principal axes (a, b, c) of the molecule using the I^r representation suitable for prolate asymmetric tops [Kro75]. The planar molecule lies in the xz plane. The magnitude of the electric dipole moment [Fab77], with the arrow pointing from negative to positive charge, is given in Debye (D) for the vibronic (vibrational and electronic) ground state. Formaldehyde has a mass of $m_{H_2CO} = 30.03\,\mathrm{u}$.

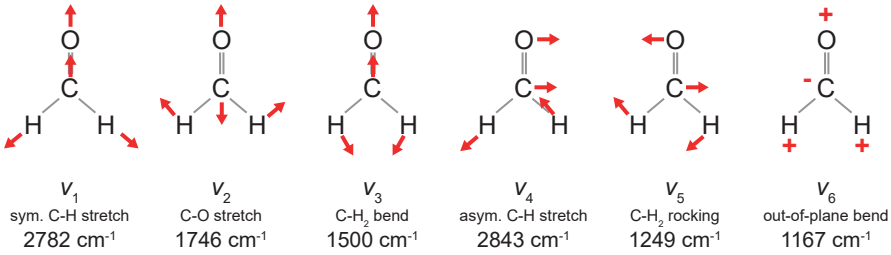

Figure 2.3: Vibrational modes of formaldehyde. Arrows indicate the motion of nuclei in the molecular plane, + and − show motion perpendicular to this plane. The numbering of modes ν_4 to ν_6 is not consistent in the literature. Here, the nomenclature follows Refs. [Her45, Rot13]. The transition energy of the fundamental excitation is given in wavenumbers [Rot13]. In this thesis only the totally symmetric ν_1 mode plays a role. Its fundamental excitation decays with a rate of $\sim 60\,\mathrm{Hz}$ [Rot13].

normal vibrational modes, all of them non-degenerate [Her45]. They are summarized in Fig. 2.3. Five modes live in the molecular plane, one of them, here labeled ν_6, leads to oscillations perpendicular to the plane.

Three considerations play a role in our experiments. First, the type of mode, i.e. the symmetry of the vibration, determines the selection rules for transitions between rotational states in the vibrational ground and excited state (see below). Thus, the totally symmetric or *parallel* vibrational modes, ν_1, ν_2, and ν_3, where the nuclei move symmetric to the axis of the electric dipole moment, and the three remaining *perpendicular* modes are distinguished and lead to distinct selection rules for the rotational quantum numbers. In particular, *perpendicular* vibrations cause a transition electric dipole moment along the axes b or c of the molecule. Second, for efficient cooling, a large spontaneous decay rate is desired. Third, the energy of the mode determines the laser frequency required to excite the vibration.

Considering all three points, in this work only the totally symmetric ν_1 C-H stretch mode is used for the purpose of optical pumping within optoelectrical Sisyphus cooling and rotational-state preparation. To this end, Q-branch transitions[3] to the first vibrational excited state $\nu_1 = 1$ are driven with an IR laser around a wavelength of

[3]The total angular momentum of rotation J is not changed, $\Delta J = 0$.

3.6 µm from different rotational ground states. With this choice, the transition electric dipole moment is always parallel to the a axis in the presented experiments, leading to relatively strict selection rules for the rotational quantum numbers. Thus, in our case, the angular momentum selection rules for rovibrational transitions are equal to those for purely rotational transitions.

Comparing the transition energy of the vibrational modes with the source temperature $T = 150\,\mathrm{K}$ in our apparatus, one finds that formaldehyde almost exclusively populates the vibrational ground state under the conditions of our experiments. More specifically, the ratio of the vibrational transition energy hf_{vib} and the thermal energy $k_B \cdot 150\,\mathrm{K}$ ranges from 11 to 27 for the vibrational modes of formaldehyde.

Rotational level structure and selection rules. Optoelectrical Sisyphus cooling takes place in an electrostatic trap and requires internal states with a strong electric-field interaction (Sec. 2.1) to achieve large trap depths and allow for the construction of closed cycling schemes of trapped, low-field-seeking states. Sizable Stark shifts varying linearly with the applied field are observed whenever two opposite-parity states with small separation Δ are coupled strongly by an external electric field [Tow75]. The electric-field interaction is investigated in the following Sec. 2.3. Here, we identify which rotational states of an asymmetric rotor are coupled by the electric field and investigate the separation of these doublets for formaldehyde.

In a symmetric-top molecule, the rotational state $|J, K, M\rangle$ is characterized by the quantum numbers J, the total angular momentum of rotation, K, the projection of J onto the molecular symmetry axis, and, in the case of an external field, M, the projection of J onto the external quantization axis [Tow75]. Without external field and neglecting hyperfine structure, the two states $|J, \pm|K|, M\rangle$ with $|K| > 0$ are degenerate. However, these states are not parity eigenstates, i.e. not eigenstates of the parity operator or the inversion of all space-fixed coordinates, because inversion leaves the pseudovector $\boldsymbol{J}$ unchanged but flips the axis of the molecule and thus the sign of K [Kro75]. As the molecular Hamiltonian is invariant under inversion, the molecules have to obey parity conservation in free space and one would expect the existence of energy eigenstates which are also parity eigenstates.

In fact, the states

$$\left|J, |K|^{\pm}\right\rangle = \frac{1}{\sqrt{2}} \left(|J, +|K|\rangle \pm |J, -|K|\rangle\right) \tag{2.1}$$

are parity eigenstates with parity $\pm$ [Kro75] and are formally the correct eigenstates if no external field is applied. The pair of states $\left|J, |K|^{\pm}\right\rangle$ is called an inversion doublet. Since the dipole moment of symmetric-top molecules is by definition parallel to the symmetry axis of the molecule, the inversion-doublet states are coupled by electric-dipole matrix elements governed by the symmetric-top selection rules for purely rotational transitions (or rovibrational transitions involving a parallel vibrational mode) [Tow75]

$$\Delta J = 0, \pm 1;\ \Delta K = 0;\ \Delta M = 0, \pm 1;\ (K = 0 :\ \Delta J = \pm 1). \tag{2.2}$$

Due to the degeneracy of the inversion doublets, the pair of states is strongly coupled already in tiny external electric fields, leading to large, linear Stark shifts even in the limit of zero field. In the field, inversion symmetry is broken and the degenerate

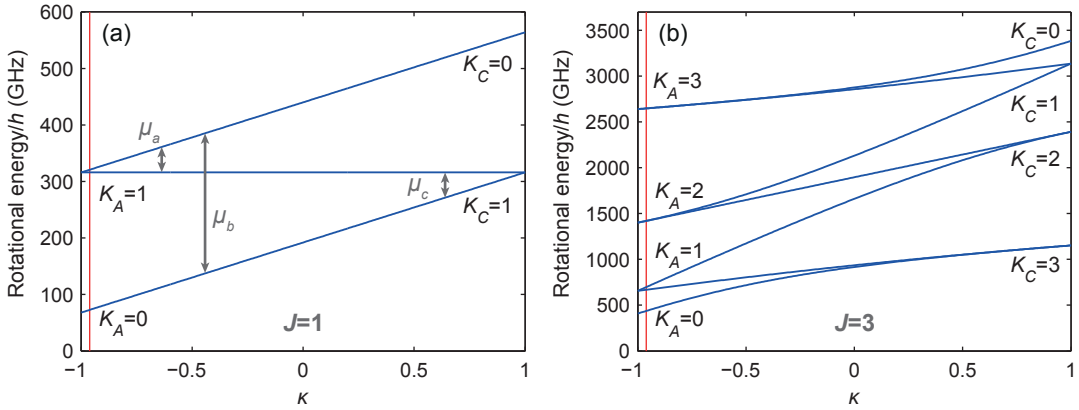

Figure 2.4: Rotational energy levels of asymmetric rotors. The levels are plotted for $J = 1$ **(a)** and $J = 3$ **(b)** as a function of asymmetry parameter κ. Formaldehyde has $\kappa = -0.961$ (red line). The calculation was performed with the rotational constants $A = 282\,\mathrm{GHz}$ and $C = 34.0\,\mathrm{GHz}$ of formaldehyde [Brü03], with varying B, $C \leq B \leq A$. The arrows in part (a) indicate which states are coupled by an external field if dipole moments along the corresponding principal axes are present in the molecule.

symmetric-top rotational states $|J, \pm|K|, M\rangle$, superpositions of the $\left|J, |K|^{\pm}\right\rangle$, are the correct eigenstates. Therefore, often the wave functions $|J, K, M\rangle$ are used to describe the molecule even if an external electric field is not explicitly applied.

For asymmetric rotors the situation is fundamentally different because a symmetry axis of molecular rotation, with respect to which the $|J, K, M\rangle$ were defined before, is no longer clearly defined. However, the $|J, K, M\rangle$ can still serve as a useful set of basis functions to describe an asymmetric-top rotational state, but are now defined with respect to one of the two 'special' axes a or c with which the largest or smallest rotational constant A or C is associated. Most relevant for our experiments is the following consequence of the asymmetric structure: the rotational Hamiltonian (in the basis of symmetric-top wave functions) couples states with $\Delta K = 0, \pm 2$ [Kro75], resulting in a splitting Δ between the inversion-doublet states $\left|J, |K|^{\pm}\right\rangle$.

One parameter determining the magnitude of the inversion splitting Δ is the degree of asymmetry, i.e. the deviation of the rotational level structure from the limiting symmetric-top cases. It is quantified by Ray's asymmetry parameter [Tow75]

$$\kappa = \frac{2B - A - C}{A - C} \tag{2.3}$$

which is a function of the rotational constants A, B, and C and is equal to -1 or $+1$ in the case of a prolate or oblate symmetric top with symmetry axis a or c, respectively. The rotational energy shows a universal behavior with respect to κ, as depicted in the so-called correlation diagrams of Fig. 2.4. With varying κ the rotational energy of a particular state smoothly changes between the two limiting cases. Hence, an asymmetric-top rotational state $|J, K_A, K_C, M\rangle$ is labeled by K_A and K_C, the K quantum numbers of the limiting symmetric top cases[4]. The $|J, K_A, K_C, M\rangle$ are parity eigenstates. In the limits of near-prolate or near-oblate slightly asymmetric tops, the two rotational states $|J, K_A, K_C\rangle$ with equal K_A or equal K_C are close-by in energy (cf.

[4] $0 \leq K_A, K_C \leq J$ and the sum $(K_A + K_C)$ is either J or $J + 1$.

Fig. 2.4) and are predominantly given by the symmetric-top inversion-doublet states $\left|J,|K|^{\pm}\right\rangle$ with $|K| = K_A$ or K_C, respectively.

Whether two asymmetric-rotor states with a small energy separation are actually coupled by an external electric field, depends on the specific direction of the molecular dipole moment with respect to the principal axes of the molecule (given by the principal moments of inertia). The following electric-dipole selection rules for K_A and K_C apply, if a dipole moment along the principal axes exists [Kro75]:

$$\begin{aligned} \mu_a \neq 0: &\ \Delta K_A = 0, \pm 2, ... \quad \Delta K_C = \pm 1, \pm 3, ... \\ \mu_b \neq 0: &\ \Delta K_A = \pm 1, \pm 3, ... \quad \Delta K_C = \pm 1, \pm 3, ... \\ \mu_c \neq 0: &\ \Delta K_A = \pm 1, \pm 3, ... \quad \Delta K_C = 0, \pm 2, ... \end{aligned} \tag{2.4}$$

States coupled by dipole moments along different axes are also marked with arrows in Fig. 2.4(a). Consequently, states are close-by in energy *and* can be coupled strongly by an external field if the asymmetry is moderate and reasonable dipole moments exist along the axes a or c for prolate or oblate asymmetric molecules, respectively. In case the dipole moment is only along the b axis, the coupled states are always separated by a large amount of energy. Then, linear Stark shifts cannot be observed, even with large laboratory electric fields, as shown in the thesis of Michael Motsch for the H_2O molecule which is of this type [Mot09b].

Focusing on the correlation diagram for $J = 3$ in Fig. 2.4(b) and prolate molecules (the left side of the plot), it is already obvious that the splitting of states with equal $K_A > 0$, the inversion doublets, also depends on the value of K_A relative to J. For fixed J and larger K_A the splitting becomes smaller. Moreover, the increase of the splitting with larger asymmetry is also slower. The situation is reversed for oblate rotors.

Since formaldehyde is a slightly asymmetric prolate top molecule with its dipole moment along the a axis, the states with equal $K_A > 0$ constitute the inversion doublets which can potentially be strongly coupled by an external electric field and exhibit linear Stark shifts. The inversion splitting Δ of these doublets and the effects of the slight asymmetry of formaldehyde will be investigated in more detail now.

The general form of the wave function of a prolate asymmetric top is [Tow75]

$$|J, K_A, K_C, M\rangle = \sum_{K=K_A \pm 2n} a_{JK}^{K_A K_C} |J, K, M\rangle \tag{2.5}$$

with expansion coefficients $a_{JK}^{K_A K_C}$ and the symmetric-top wave functions $|J, K, M\rangle$. Here, for symmetry reasons only states $|J, K, M\rangle$ with even or odd K appear in the sum. The above sum is also the reason for the presence of higher-order $\Delta K_A = \pm 2, \pm 4, ...$ and $\Delta K_C = \pm 3, \pm 5, ...$ electric-dipole transitions in the first row of Eq. (2.4). As formaldehyde is only slightly asymmetric, the above expansion is dominated by the two symmetric-top wave functions $|J, \pm|K|, M\rangle$ with $|K| = K_A$ which form the parity eigenstates $\left|J,|K|^{\pm}\right\rangle$ in Eq. (2.1). For the same reason, the higher-order transitions in Eq. (2.4) are greatly suppressed in our case, by at least a factor of 10^2 [Cor80, Rot13]. Thus, for many practical purposes the selection rules for electric-dipole transitions in formaldehyde reduce to the ones for symmetric-top molecules ($\Delta J = 0, \pm 1$, $\Delta K_A = 0$, and $\Delta M = 0, \pm 1$). We will come back to this during the discussion of loss channels from the cooling scheme.

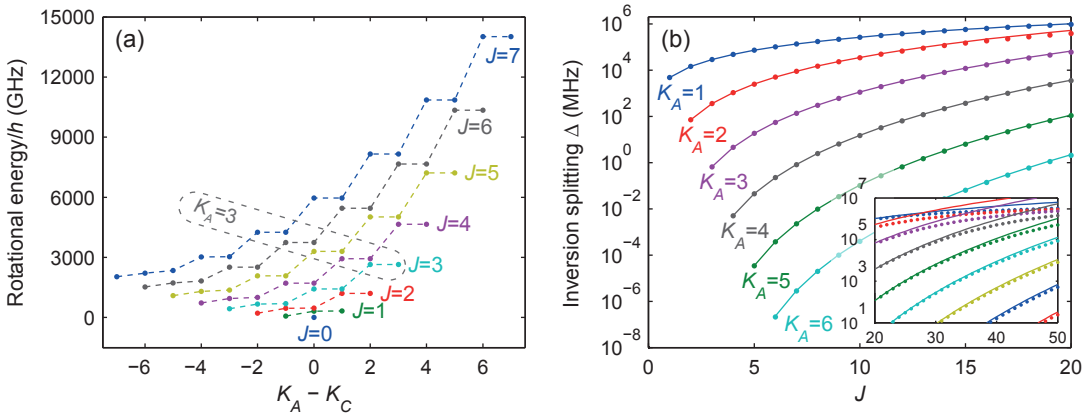

Figure 2.5: Rotational states of formaldehyde. (a) Energy levels of formaldehyde for the lowest J. For J fixed the energetic order of the states is given by $K_A - K_C$. The rotational constants are $A = 282\,\mathrm{GHz}$, $B = 38.8\,\mathrm{GHz}$, and $C = 34.0\,\mathrm{GHz}$ [Brü03]. **(b)** Inversion splitting Δ of the states with equal $K_A > 0$. The dots represent the splittings calculated with the full set of rotational and centrifugal distortion constants of Ref. [Brü03]. The lines are calculated with Eq. (2.6). The inset shows that the approximate formula of Eq. (2.6) is only valid for smaller J.

As a further consequence of the slight asymmetry, the inversion splitting $\Delta(J, K_A)$ can be approximated by an equation given by Wang [Wan29, Tow75]

$$\Delta(J, K_A) = \left(A - \frac{B+C}{2}\right) \frac{|b_p|^{K_A}\,(J+K_A)!}{8^{K_A-1}\,(J-K_A)!\,[(K_A-1)!]^2} \tag{2.6}$$

in terms of another asymmetry parameter for slightly asymmetric prolate molecules

$$b_p = \frac{C-B}{2A-B-C} = \frac{\kappa+1}{\kappa-3} \tag{2.7}$$

which varies from $-1/3$ to zero and is equal to -0.0098 for formaldehyde. Equation (2.6) enables quick calculations of the order of magnitude of the inversion splitting and reveals its scaling. Evidently, $\Delta(J, K_A)$ scales with the asymmetry b_p to the power of K_A. As $|b_p| \ll 1$ the splitting decreases for larger K_A. At the same time $\Delta(J, K_A)$ increases with larger J, for $K_A = 1$ proportional to $b_p \cdot J(J+1)$.

Figure 2.5 shows the rotational energy of formaldehyde for the lowest values of J and the inversion splitting $\Delta(J, K_A)$ for the states with equal $K_A > 0$ where the discussed effects are also observable. We note again that the smallest splittings Δ are observed for inversion doublets with $K_A = J$, as already seen in the previous Fig. 2.4(b). $\Delta(J, K_A{=}J)$ decreases by about two orders of magnitude per increment of $K_A = J$. The inset of Fig. 2.5(b) shows when the approximation of Eq. (2.6) breaks down due to centrifugal distortion of the rotational energy levels.

Even for the only slightly asymmetric molecule formaldehyde and already for small K_A the inversion splittings vary by orders of magnitude depending on the choice of states. This allows engineering the response of formaldehyde to an electric field which not only changes the energy levels due to the Stark shift but also modifies the selection rules for electric dipole transitions as will be discussed in the next section. Moreover, the flexibility to choose a suitable inversion splitting basically at will could be useful in

the future: it potentially allows to couple formaldehyde molecules resonantly to other physical systems in a wide frequency range (see also outlook, Ch. 6).

For optoelectrical Sisyphus cooling we desire states with a small inversion splitting such that linear Stark shifts occur already at small electric fields which speaks in favor of states with large $K_A = J$. However, the thermal population of the states in the source has to be considered as well (Sec. 2.4). From the foregoing discussion one can already see that suitable states for optoelectrical Sisyphus cooling can most probably be found for molecules with considerably larger asymmetry, too. Moreover, the inversion splitting is also relevant for the experiments on precision spectroscopy presented in Ch. 5: Since the splitting has a large effect on the response of the rotational states to an external field, as discussed in the next section, it strongly influences the 'magic' electric field in which Stark broadening is minimized for a transition with vanishing first-order differential Stark shift.

Hyperfine interaction and statistical weights. All isotopologues of formaldehyde exhibit hyperfine structure. If hyperfine structure is not resolved, the number of hyperfine states which is different for distinct rotational states, has to be considered as a statistical weight, e.g., if thermal rotational-state distributions are calculated. As it was pointed out before, this influences the choice of internal states for the implementation of Sisyphus cooling. In this paragraph, the statistical weights and the order of magnitude of hyperfine interaction are discussed.

In the naturally most abundant isotopologue[5], $H_2^{12}C^{16}O$, which is the one used in our experiments, the hyperfine interaction is only due to the spins of the two protons and therefore very weak. Two effects contribute to hyperfine structure, the magnetic spin-spin interaction of the two proton spins and the magnetic spin-rotation interaction of the total spin of the two protons I with the small magnetic field induced by the molecular rotation ($\boldsymbol{I} \cdot \boldsymbol{J}$-coupling) [Tow75].

The two spin-$\frac{1}{2}$ protons can couple to a spin-singlet state, $I = 0$, or to a spin-triplet state, $I = 1$. These nuclear spin states combine with rotational states of different symmetries because the complete molecular wave function has to be antisymmetric under permutation of the two identical protons (fermions) due to the generalized Pauli exclusion principle [Kro75]. In our case of a totally symmetric vibronic wave function, rotational states with a symmetric wave function (K_A even) combine with the antisymmetric nuclear spin singlet state, and states with K_A odd combine with the spin triplet state. These and the remaining allowed combinations of vibronic, rotational and nuclear spin wave functions along with the statistical weights are listed in Table 2.1. For experiments which rely on a thermal source as ours, it is therefore preferable to work with rotational states with odd K_A due to the higher statistical weight $S = 3$ and hence threefold thermal population. Note that these symmetry considerations also determine that only states $|J, K, M\rangle$ with even or odd K contribute in the expansion of prolate asymmetric-top states $|J, K_A, K_C, M\rangle$ with even or odd K_A in terms of symmetric-top states $|J, K, M\rangle$ in Eq. (2.5).

The experiments on precision spectroscopy presented in Ch. 5 reach line widths down to a couple of kHz. Thus, we briefly touch on the order of magnitude of hyperfine interaction in formaldehyde. In the absence of external electromagnetic fields, the angular

[5]The natural abundance of $H_2^{12}C^{16}O$ is 99% [Rot13].

K_A	$\chi(\psi_r)$	$\chi(\psi_{ev})$	$\chi(\psi_{ns})$	$\chi(\Psi)$	Statistical weight
even	$+1$	$+1$	-1	-1	1
odd	-1	$+1$	$+1$	-1	3
even	$+1$	-1	$+1$	-1	3
odd	-1	-1	-1	-1	1

Table 2.1: Statistical weights of rotational states of formaldehyde due to hyperfine structure. The character χ of the total wave function Ψ has to be antisymmetric (-1) under proton exchange due to the Pauli exclusion principle. The character of the rotational wave function $\chi(\psi_r)$ is determined by whether K_A is even or odd. The vibronic ground state and the $v_1 = 1$ vibrational excited state are totally symmetric $\chi(\psi_{ev}) = +1$. This fixes the character of the nuclear spin wave function $\chi(\psi_{ns})$ and determines whether the proton spins are coupled to the singlet (-1) or triplet $(+1)$ state with the respective statistical weights. Table adapted from Ref. [Kro75].

momentum of rotation $\boldsymbol{J}$ and the total spin of the protons $\boldsymbol{I}$ couple to the well-defined total angular momentum $\boldsymbol{F} = \boldsymbol{J} + \boldsymbol{I}$ [Tha64]. This results in hyperfine splittings of states with odd K_A from a few kHz to a few tens of kHz [Fab77]. When a moderately strong electric field is applied which results in Stark shifts much larger than the hyperfine splittings, F is not a good quantum number any more and the projections of $\boldsymbol{J}$ and $\boldsymbol{I}$ onto the external quantization axis, M_J and M_I, have to be considered separately. This strong-field limit is valid in our electric trap. Then, the hyperfine splitting is even smaller, $\lesssim 1\,\mathrm{kHz}$, for the rotational states used in our experiments [Fab77]. Consequently, even with the highest-precision measurements we have performed so far in the trap, hyperfine structure could not be resolved and will therefore not be examined in more detail. Notably, other isotopologues containing Deuterium or with nuclear spin in the carbon or oxygen atoms, like for example $H_2^{13}C^{16}O$, have larger hyperfine interactions [Tha64, Tuc71, Cha73, Fab77, Mül17].

2.3 Formaldehyde in a static electric field

Optoelectrical Sisyphus cooling and electric trapping rely on the Stark effect which is caused by the interaction of the rotating molecular dipole, described by the rotational quantum states, with an external electric field. In this section, it is shown that the relevant consequences of the electric field for our experiments can be understood with a simple model considering only single pairs of inversion-doublet states strongly coupled by the electric field. Besides causing a Stark shift of the energy levels, the strong mixing of the inversion doublets modifies transition probabilities for electric-dipole transitions such that a closed level scheme of low-field-seeking and thus trapped states for optoelectrical Sisyphus cooling can be constructed (Sec. 2.5). Additionally, unwanted but weakly allowed RF transitions from low-field-seeking to high-field-seeking states will play a role when strong RF radiation is applied to the molecules, as needed to measure their kinetic energy with RF knife-edge filters (Sec. 4.1).

2.3.1 The Stark interaction

Assuming a static electric field $\boldsymbol{\mathcal{E}} = \mathcal{E}_Z$ applied in Z-direction in the space-fixed coordinate system $F = (X, Y, Z)$, the combined Hamiltonian of rotation and electric-field interaction has the form [Tow75]

$$H = H_{\mathrm{rot}} + H_{\mathrm{s}} = H_{\mathrm{rot}} + \mathcal{E}_Z \sum_{g=x,y,z} \mu_g \lambda_Z^g = H_{\mathrm{rot}} + \mathcal{E}_Z \mu_z \lambda_Z^z \tag{2.8}$$

with the direction cosine matrix λ_F^g transforming the molecule-fixed coordinate system $g = (x, y, z)$ into the space-fixed system F. As formaldehyde has its dipole moment along the $z = a$ axis and the vibronic ground state is totally symmetric, only the z-component of the interaction Hamiltonian yields a non-zero contribution for symmetry reasons [Tow75] and $H_{\mathrm{s}} = \mathcal{E}_Z \mu_z \lambda_Z^z$, as shown in the last part of Eq. (2.8).

To obtain precise Stark shifts for the full range of electric fields used in the experiment, the total Hamiltonian $H(\mathcal{E}_Z)$ can be diagonalized numerically. The Stark shift ν_s of a state $|J, K_A, K_C, M\rangle$ is then given by the difference of the newly calculated energies and those in the field-free case. The eigenstates and energies of formaldehyde in an electric field are commonly calculated in the symmetric-top basis using the direction cosine matrix elements summarized in Table 2.2. Since only the factors λ_Z^z are non-zero in our case, states are coupled by the static field $\mathcal{E}_Z$ with the selection rules[6]

$$\Delta J = 0, \pm 1; \ \Delta M = 0. \tag{2.9}$$

Consequently, H_{s} is diagonal in M, but couples states with different J, leaving M as the only good quantum number in an external electric field. In the field, the M sublevels are split by the Stark effect and only states with $M \neq 0$ remain energetically degenerate in $\pm M$. The relevant factors of the direction cosine matrix element $\langle J, K_A, K_C, M | \lambda_Z^z | J', K_A', K_C', M \rangle$ are

$$\langle J | \lambda_Z^z | J' \rangle \langle J, M | \lambda_Z^z | J', M \rangle \sum_{K=K_A \pm 2n} a_{JK}^{K_A K_C} a_{J'K}^{K_A' K_C'} \langle J, K | \lambda_Z^z | J', K \rangle. \tag{2.10}$$

Electric-field-dependent energies of the lowest rotational states obtained by numerical diagonalization of the full Hamiltonian are shown in Fig. 2.6. As expected from the asymetric rotor structure, many states have only quadratic Stark shifts. We will see in the following that the properties of the states we are interested in can be understood with a simpler, analytical model. However, the selection rules and the factors of the direction cosine matrix elements summarized here will still be needed.

2.3.2 Two-level approximation for inversion-doublet states

When two states coupled by the electric field are energetically much closer to each other than to any other state, as it is the case for most sets of inversion doublets (Sec. 2.2), the energy shift due to the electric field is comparably large, can be linear, and is predominantly caused by the close-lying state [Tow75]. Then, the Stark shift and modified transition rates can be calculated approximately with excellent precision by

[6] The asymmetric rotor Hamiltonian H_{rot} couples states with ΔK_A even and ΔK_C odd (Sec. 2.2).

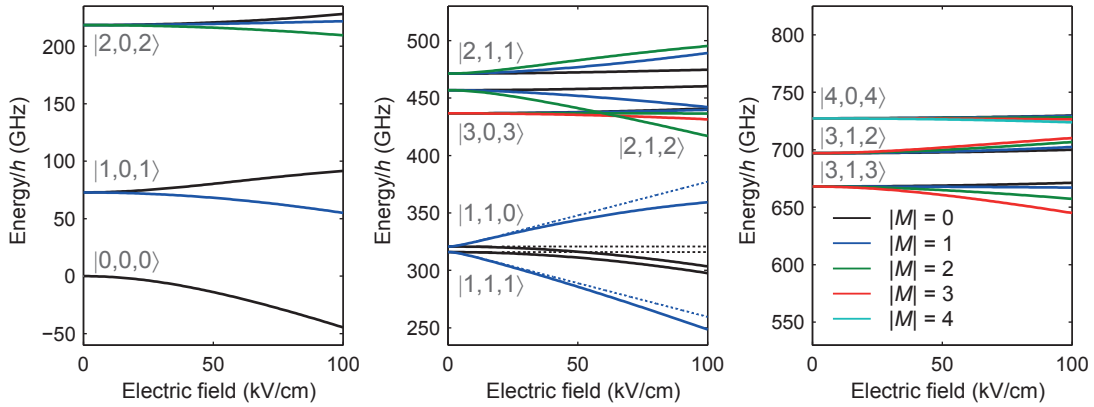

Figure 2.6: Stark-shifted lowest rotational energy levels of formaldehyde. The energy levels were calculated by numerical diagonalization of the full asymmetric rotor Hamiltonian with electric field interaction using the free software package PGOPHER [Wes17] and the molecular constants of Ref. [Brü03]. Rotational states $J \leq 20$ are included in the calculation. States are labeled with $|J, K_A, K_C\rangle$. Note that states with $M \neq 0$ are doubly degenerate in $\pm M$. The dotted lines in the central panel will be discussed later in the text. Stark energies for all rotational states $J \leq 20$ up to an energy of about 8 THz are plotted in Ref. [Ibr13].

	$J' = J + 1$	$J' = J$	$J' = J - 1$
$\langle J \vert \lambda_F^g \vert J' \rangle$	$\frac{1}{4(J+1)\sqrt{(2J+1)(2J+3)}}$	$\frac{1}{4J(J+1)}$	$\frac{1}{4J\sqrt{4J^2-1}}$
$\langle J, K \vert \lambda_F^z \vert J', K \rangle$	$2\sqrt{(J+K+1)\,(J-K+1)}$	$2K$	$-2\sqrt{J^2-K^2}$
$\langle J, K \vert \lambda_F^y \vert J', K\pm1 \rangle$ $= \mp i \langle J, K \vert \lambda_F^x \vert J', K\pm1 \rangle$	$\mp\sqrt{(J\pm K+1)\,(J\pm K+2)}$	$\sqrt{(J\mp K)\,(J\pm K+1)}$	$\mp\sqrt{(J\mp K)\,(J\mp K-1)}$
$\langle J, M \vert \lambda_Z^g \vert J', M \rangle$	$2\sqrt{(J+M+1)\,(J-M+1)}$	$2M$	$-2\sqrt{J^2-M^2}$
$\langle J, M \vert \lambda_Y^g \vert J', M\pm1 \rangle$ $= \mp i \langle J, M \vert \lambda_X^g \vert J', M\pm1 \rangle$	$\mp\sqrt{(J\pm M+1)\,(J\pm M+2)}$	$\sqrt{(J\mp M)\,(J\pm M+1)}$	$\mp\sqrt{(J\mp M)\,(J\mp M-1)}$

Table 2.2: Direction cosine matrix elements in the symmetric-top basis. The matrix elements $\langle J, K, M \vert \lambda_F^g \vert J', K', M' \rangle$ for the transformation from the molecule-fixed coordinate system $g = (x, y, z)$ into the space-fixed system $F = (X, Y, Z)$ can be separated into three factors [Cro44].

considering pairs of coupled inversion-doublet states and finding an analytical solution for the two-level system coupled by the electric field $\mathcal{E}$.

We consider the two states of an inversion doublet $|+\rangle = |J, K_A, K_C{=}J{-}K_A, M\rangle$ and $|-\rangle = |J, K_A, K_C{=}J{-}K_A{+}1, M\rangle$ of a prolate asymmetric rotor with energy $E_\pm$ ($H_\mathrm{rot}|\pm\rangle = E_\pm|\pm\rangle$), separation $\Delta = (E_+ - E_-)/h$, and opposite parity. After application of the field $\mathcal{E}$ the two states are coupled to a low-field-seeking state $|l\rangle$ and a high-field-seeking state $|h\rangle$

$$\begin{aligned} |l\rangle = &\quad a_{JK_A|M|}(\mathcal{E})\,|+\rangle + b_{JK_A|M|}(\mathcal{E})\,|-\rangle \\ |h\rangle = &-b_{JK_A|M|}(\mathcal{E})\,|+\rangle + a_{JK_A|M|}(\mathcal{E})\,|-\rangle \end{aligned} \tag{2.11}$$

where the Hamiltonian in the basis ($|+\rangle$, $|-\rangle$) is given by the matrix[7] [Tow75]

$$H_\mathrm{rot} + H_\mathrm{s} = \begin{pmatrix} E_+ & -\mu\mathcal{E}\lambda_Z^z \\ -\mu\mathcal{E}\lambda_Z^z & E_- \end{pmatrix}. \tag{2.12}$$

By diagonalizing the Hamiltonian, the energy of the coupled states

$$W_{l/h} = \frac{E_+ + E_-}{2} \pm h\sqrt{\left(\frac{\Delta}{2}\right)^2 + \frac{\mu^2\mathcal{E}^2}{h^2}\left|\langle+|\,\lambda_Z^z\,|-\rangle\right|^2} \tag{2.13}$$

and the coefficients a, b are obtained:

$$(a,b)_{JK_A|M|}(\mathcal{E}) = \sqrt{\frac{s \pm \Delta}{2s}} \text{ with } s = \sqrt{\Delta^2 + \frac{4\mu^2\mathcal{E}^2}{h^2}\left|\langle+|\,\lambda_Z^z\,|-\rangle\right|^2}. \tag{2.14}$$

Here, the direction cosine matrix element $\langle+|\,\lambda_Z^z\,|-\rangle$ is given by Eq. (2.10) with $J' = J$ and hence simplifies to (cf. Table 2.2)

$$\langle+|\,\lambda_Z^z\,|-\rangle_{JK_A|M|} = \frac{2M}{4J(J+1)} \sum_{K=K_A\pm 2n} 2K a_{JK}^{K_A K_C} a_{JK}^{K_A K_C'} \approx \frac{K_A M}{J(J+1)} \tag{2.15}$$

with $K_C' = K_C + 1$ as defined above.

The final approximately-equal sign in the preceding equation only holds for slightly asymmetric rotors: As already explained in Sec. 2.2, in the sum over K the absolute values of all but two expansion coefficients $a_{JK}^{K_A K_C}$ are very small and the asymmetric rotor state $|J, K_A, K_C\rangle$ in Eq. (2.5) is predominantly given by the two symmetric-top wave functions $|J, \pm|K|\rangle$ with $|K| = K_A$ forming the symmetric-top inversion doublets. Hence, the matrix element $\langle+|\,\lambda_Z^z\,|-\rangle_{JK_A|M|}$ for the slightly asymmetric rotor can be approximated by the corresponding symmetric-top matrix element $\langle J, K, M|\,\lambda_Z^z\,|J, K, M\rangle$ with $K = K_A$ for the purpose of this model[8]. However, this does not necessarily mean

[7] The indices of the dipole moment μ and the electric field $\mathcal{E}$ are omitted for simplicity.

[8] Approximating the sum over K in Eq. (2.15) with a single value, for the states with $J = K_A = 3$ of formaldehyde, induces an error on the 10^{-4} level for Stark energies and transition probabilities for strong $\Delta K_A = 0$, $\Delta K_C = 1$ transitions. This is much smaller than the deviation of, e.g., the energy levels obtained by the two-level model from the ones given by the diagonalization of the full Hamiltonian with electric-field interaction. The error is small because the asymmetry of formaldehyde is small and states with small inversion splitting are chosen for experiments. The small error induced by the approximation also indicates the strong suppression of $\Delta K_A \neq 0$ transitions (Secs. 2.2 and 2.5). If high accuracy is needed or higher-order $\Delta K_A, K_C$ transitions are investigated, the calculations of this and the next subsection can be performed in the $|J, K\rangle$ basis of symmetric-top states, including all states coupled by the asymmetric-rotor Hamiltonian. The stated error was estimated in this way.

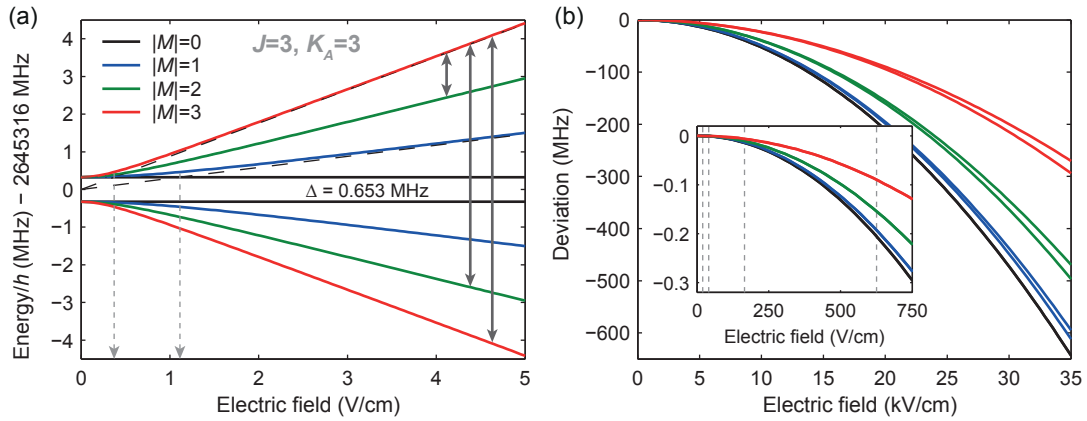

Figure 2.7: Inversion-doublet rotational levels in a static electric field. **(a)** Stark shift of the rotational levels $J = K_A = 3$ vs. electric field, calculated with the two-level Hamiltonian. The upper lines correspond to the low-field-seeking states $|l\rangle$. The dashed lines show the linear approximation obtained with Eq. (2.16). The electric field $\mathcal{E}$ where $h\Delta = \mu\mathcal{E}|\langle +|\,\lambda_Z^z\,|-\rangle|_{JK_A|M|}$ is marked with dashed arrows for $|M| = 1, 3$. The solid arrows denote the RF transitions investigated in Sec. 2.3.3. **(b)** Deviation of the Stark shift obtained with the two-level Hamiltonian from the exact computation for states shown in (a) and the complete range of electric fields relevant in experiments. The dashed lines in the inset denote the offset electric fields commonly applied during experiments in the central region of our trap, the fields for which transition frequencies are most often calculated (see also Sec. 3.1).

that the properties of the states $|l\rangle$ and $|h\rangle$ are equal to those of symmetric-top states because the model described here takes into account the non-zero inversion splitting Δ which can vary by orders of magnitude for formaldehyde as already established in Fig. 2.5(b).

Figure 2.7(a) shows the Stark shifts calculated with the two-level Hamiltonian for the inversion doublet characterized by $J = 3$ and $K_A = 3$, the states around which the cooling scheme will be developed later. The two-level Hamiltonian was solved for each $|M| > 0$ separately as a static electric field does not couple levels with distinct $|M|$. This model does not give a Stark shift for $M = 0$ states since the matrix element $\langle +|\,\lambda_Z^z\,|-\rangle$ vanishes in this case (Table 2.2). For the states $|M| > 0$ the transition from quadratic to linear Stark shift is evident. The electric field strength at which this happens is directly proportional to Δ and $1/|M|$. In the limit of vanishing field, $\mathcal{E} \to 0$, $|l\rangle = |+\rangle$ and $|h\rangle = |-\rangle$. Hence, the states are the parity eigenstates in this limit. In contrast, in the limits of $\Delta \to 0$ and $\mathcal{E} \to \infty$ the coefficients $(a, b)_{JK_A|M|} \to 1/\sqrt{2}$ and the states $|l\rangle$ and $|h\rangle$ are fifty-fifty mixtures of the states $|+\rangle$ and $|-\rangle$, i.e. approximately given by the $|J, \pm|K|\rangle$ symmetric-top states. Then, linear Stark shifts

$$\nu_s^{(1)} = -\frac{\mu\mathcal{E}}{h}\frac{K_A M}{J(J+1)} \tag{2.16}$$

are observed, as usually obtained for symmetric-top molecules by first-order quantum mechanical perturbation theory for states with $|K_A| > 0$. For $|M| = 1, 3$ the linear approximation is shown as a dashed line in Fig. 2.7(a). Thus, the inversion doublet investigated here is coupled strongly already at small electric fields.

The two-level approximation gives precise Stark shifts for electric fields sufficiently small such that interactions with other states $J' \neq J$ can be neglected. For very high electric fields this does not hold any longer, as shown in the central panel of Fig. 2.6 for the inversion doublet $J = 1$, $K_A = 1$: for large electric fields the Stark shift again depends quadratically on the applied field and the two-level approximation (dashed lines) deviates noticeably from the numerical diagonalization of the complete Hamiltonian because states $J' \neq J$ contribute significantly. However, for the states and electric fields used in experiments this is usually not an issue (see also the following Sec. 2.4). To give an idea of the order of magnitude, the deviation of the two-level calculation from the exact numerical solution is shown in Fig. 2.7(b) for the states investigated in part (a) and the range of electric fields used in experiments. Transitions between rotational states are usually driven in electric fields $\mathcal{E} \lesssim 1\,\mathrm{kV/cm}$, where inversion doublets are coupled strongly but interactions with states $J' \neq J$ can be neglected. Hence, frequencies for Stark shifted transitions are mostly calculated using the simple formula for linear Stark shifts, Eq. (2.16). Considering a Stark broadening in the electric trap of usually many MHz, the error caused by this procedure is completely negligible for most transitions driven in experiments, with one exception being the special transition with vanishing first-order differential Stark shift used for precise spectroscopy in Ch. 5.

2.3.3 Modified transition probabilities

An external electric field not only causes an energy shift but also modifies relative transition probabilities between individual M sublevels of an inversion doublet. This is investigated in the final part of this section using the coupled states $|l; J, K_A, |M|\rangle$ and $|h; J, K_A, |M|\rangle$ obtained before with the two-level Hamiltonian with applied electric field. More specifically, electric-field-dependent relative transition probabilities within the inversion doublet characterized by $J = K_A = 3$ and composed of the states $|l; 3, 3, |M|\rangle$ as well as $|h; 3, 3, |M|\rangle$ are calculated for the three RF transitions

$$|l; 3, 3, 3\rangle \rightarrow |l; 3, 3, 2\rangle\,,\ |l; 3, 3, 3\rangle \rightarrow |h; 3, 3, 2\rangle\,,\ \text{and}\ |l; 3, 3, 3\rangle \rightarrow |h; 3, 3, 3\rangle\,. \tag{2.17}$$

Here, the common initial state $|l; 3, 3, 3\rangle$ is low-field-seeking but two of the final states are high-field-seeking. The three transitions, which are marked with solid arrows in Fig. 2.7(a), constitute all allowed electric dipole transitions within the inversion doublet and from the chosen initial state because it holds $\Delta M = 0, \pm 1$.

Experimentally, the situation is relevant for the construction of the cooling scheme: optoelectrical Sisyphus cooling as described in Sec. 2.1 relies on induced RF transitions like $|l; 3, 3, 3\rangle \rightarrow |l; 3, 3, 2\rangle$, from strongly trapped states with large $|M|$ to more weakly trapped states with smaller $|M|$. At the same time, transitions to untrapped, high-field-seeking states, like the remaining two, cause losses and have to be avoided. From the following discussion, one can directly conclude which conditions have to be fulfilled for construction of a closed level scheme of trapped, low-field-seeking internal states for cooling. Moreover, the resulting quantitative predictions will later be used during the optimization of our method to measure the molecules' kinetic energy via RF knife-edge filters (Sec. 4.1). In the optimization process, unwanted transitions to high-field-seeking states were observed and had to be taken care of.

The transition rate r for a specific electric-dipole transition $|1\rangle \rightarrow |2\rangle$ is proportional to the matrix element squared of the two states with the electric dipole oper-

ator [Tow75]: $r \propto |\langle 2|\, \boldsymbol{\mu} \cdot \boldsymbol{E}_{\mathrm{RF}}\, |1\rangle|^2$ with the dipole moment vector $\boldsymbol{\mu}$ and the electric field of the RF $\boldsymbol{E}_{\mathrm{RF}}$. As $\boldsymbol{\mu} = \mu_z = \mu$ in formaldehyde this is essentially reduced to a direction cosine matrix element squared, $r \propto \mu^2 E_{\mathrm{RF}}^2 |\langle 2|\, \lambda_F^z\, |1\rangle|^2$. We are only interested in relative transition probabilities and will therefore solely evaluate the last factor $|\langle 2|\, \lambda_F^z\, |1\rangle|^2$ for the three chosen RF transitions. In contrast to our previous evaluation of direction cosine matrix elements, for RF transitions the matrix elements in all three space-fixed directions $F = (X, Y, Z)$ have to be considered in the calculation. For example,

$$\left| \langle h; 3, 3, 2|\, \frac{1}{\sqrt{2}} \left(\lambda_X^z - i\lambda_Y^z\right) |l; 3, 3, 3\rangle \right|^2 \tag{2.18}$$

has to be evaluated for the $\Delta M = -1$ transition $|l; 3, 3, 3\rangle \rightarrow |h; 3, 3, 2\rangle$.

The matrix elements are calculated using the expansion of the states $|l, h\rangle$ in terms of $|\pm\rangle$, as noted down in Eq. (2.11). Here, matrix elements $\langle \pm|\, \lambda_F^z\, |\pm\rangle$ vanish because they connect states with equal parity [also seen from the selection rule for ΔK_C in Eq. (2.4)]. Moreover, following Eq. (2.15), matrix elements of type $\langle \pm|\, \lambda_F^z\, |\mp\rangle$ are approximated with the respective ones for symmetric tops since formaldehyde is only slightly asymmetric and we consider "strong" $\Delta K_A = 0$, $\Delta K_C = 1$ transitions. Then, we find:

$$\begin{aligned}
|l; 3, 3, 3\rangle \rightarrow |l; 3, 3, 2\rangle: &\qquad r(\mathcal{E}) \propto \frac{3}{16} |a_2 b_3 + b_2 a_3|^2, \\
|l; 3, 3, 3\rangle \rightarrow |h; 3, 3, 2\rangle: &\qquad r(\mathcal{E}) \propto \frac{3}{16} |a_2 a_3 - b_2 b_3|^2, \\
|l; 3, 3, 3\rangle \rightarrow |h; 3, 3, 3\rangle: &\qquad r(\mathcal{E}) \propto \frac{9}{16} \left|a_3^2 - b_3^2\right|^2.
\end{aligned} \tag{2.19}$$

The relative transition rates r depend on the static electric field $\mathcal{E}$ applied to couple inversion doublets via the coefficients a and b [Eq. (2.14)]. The index of a coefficient represents the corresponding M sublevel the two-level Hamiltonian was solved for, e.g., $a_2 = a_{332}(\mathcal{E})$. The prefactors, the squared Clebsch-Gordan coefficients, 3/16 and 9/16 stem from the different $|\langle +|\, \lambda_F^z\, |-\rangle|^2$ which were approximated with $2|\langle 3, 3, 2|\, \lambda_Y^z\, |3, 3, 3\rangle|^2$ or $|\langle 3, 3, 3|\, \lambda_Z^z\, |3, 3, 3\rangle|^2$ in the symmetric-top basis $|J, K, M\rangle$.

The dependence of the transition probabilities on the applied electric field is shown in Fig. 2.8(a). Without or with very weak electric field the transitions $|l\rangle \rightarrow |h\rangle$ are strong as can be expected from parity considerations and the selection rule $\Delta K_C = 1$ for asymmetric rotors. In this case, RF or IR transitions with $\Delta J = 0$ from low-field-seeking to low-field-seeking states, $|l\rangle \rightarrow |l\rangle$, as needed for cooling cannot be driven effectively in asymmetric rotors. The two $\Delta M = -1$ transitions to $|l\rangle$ and $|h\rangle$ are equally probable for the static electric field $\mathcal{E} = h\Delta/(2\mu|\langle 3, 3, 2|\, \lambda_Y^z\, |3, 3, 3\rangle|)$. In electric fields much larger than that, the inversion doublets are strongly coupled and transitions $|l\rangle \rightarrow |l\rangle$ dominate as desired for cooling in the electrostatic trap.

Sisyphus cooling is performed with offset electric fields of 625 V/cm to 40 V/cm. Hence, unwanted transitions from low-field-seeking to high-field-seeking states inducing losses from the trap are suppressed at least four orders of magnitude compared to the desired transitions for this set of states and there is no indication that such transitions occur during cooling. However, very strong RF radiation was applied as a knife-edge filter to measure the energy distribution of the cooled molecules. During the optimization of these filters at offset electric fields of about 40 V/cm, $|l\rangle \rightarrow |h\rangle$ transitions had to be taken into account, despite their strong suppression (see Sec. 4.1). As

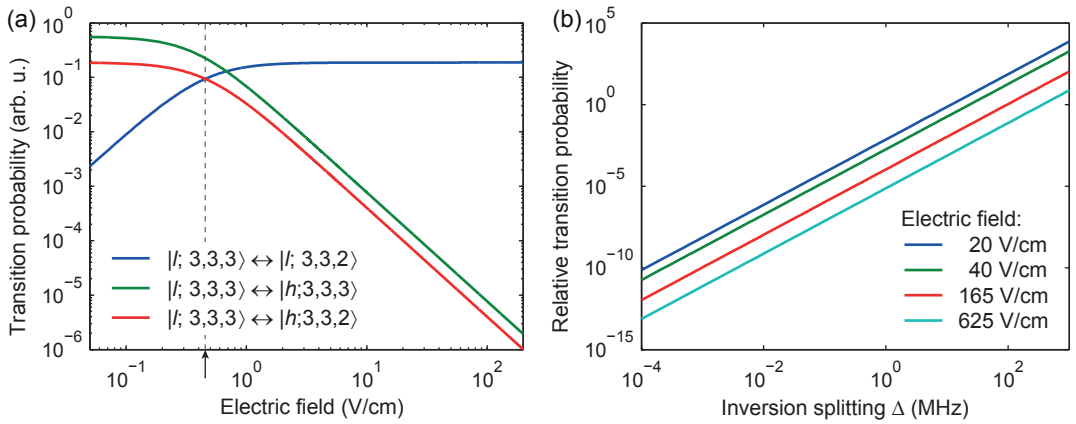

Figure 2.8: RF transition probabilities within inversion-doublet states in a static electric field. (a) Dependence of the relative transition probabilities on electric field for the three transitions discussed in the text (see legend). Transitions $|l\rangle \rightarrow |h\rangle$ dominate if the inversion doublet is only weakly perturbed by the external field. $|l\rangle \rightarrow |l\rangle$ and $|l\rangle \rightarrow |h\rangle$ are equally probable for electric fields satisfying $h\Delta/2 = \mu\mathcal{E}|\langle +|\,\lambda_F^z\,|-\rangle|$. For the $\Delta M = -1$ case this field is marked by the dashed line and the black arrow. For experiments, the inversion doublets should be strongly coupled such that transitions $|l\rangle \rightarrow |l\rangle$ dominate. **(b)** Ratio of transition probabilities of $|l\rangle \rightarrow |l\rangle$ over $|l\rangle \rightarrow |h\rangle$ transitions vs. inversion splitting Δ for the four most commonly applied offset electric fields in the trap. The calculation was performed for the transitions named in panel (a).

the unwanted transitions $|l\rangle \rightarrow |h\rangle$ reverse the sign of the interaction with the external field, i.e. flip the effective dipole moment, and couple states which have distinct K quantum numbers in the high-field case, we denote them as *K-flip transitions*.

So far, the discussion ignored transition frequencies. Assuming linear Stark shifts and a homogeneous electric field, the frequency of the $\Delta M = -1$ ($\Delta M = 0$) K-flip transition from the initial state $|l; 3, 3, 3\rangle$ is five (six) times larger than the frequency of the $|l\rangle \rightarrow |l\rangle$ transition. Thus, unwanted transitions induced by radiation sources would not be an issue if the electric field strength could be controlled precisely. Nonetheless, the strong coupling of the inversion doublet states by a static electric field is crucial for our experiments for two reasons. First, in any real electrostatic trap a distribution of electric-field strengths has to be present, simply to confine the molecules. Consequently, for a given applied frequency, molecules can accidentally come into resonance with the unwanted K-flip transition somewhere in the trap where the electric field is five (six) times smaller. As the RF for cooling f_{RF} is applied in the high-field region of the trap and is deliberately chosen much larger than the splitting of M-sublevels f_{offset} in the low-field region to extract a large amount of energy (Sec. 2.1), molecules indeed probe electric fields satisfying the unwanted resonance condition. Second, optoelectrical Sisyphus cooling relies on vibrational spontaneous decays which are governed by the same selection rules and relative transition probabilities. Both effects would cause molecule losses due to K-flips to untrapped, high-field-seeking states if the inversion doublets were not coupled strongly by an electric field. Thus, for the construction of the cooling scheme, the use of inversion doublets with small inversion splitting Δ is beneficial, as also illustrated by Fig. 2.8(b).

2.4 Internal states for Sisyphus cooling

With the principles of optoelectrical Sisyphus cooling and the key properties of formaldehyde having been established, suitable internal states for the implementation of the cooling scheme are now selected and their properties briefly discussed. After that, the nomenclature of internal molecular states used in the rest of the thesis is defined and precise frequencies for all used transitions are summarized.

2.4.1 The choice of rotational states

Building on the results of the previous sections, the following criteria can be established for the selection of a set of inversion-doublet rotational states for optoelectrical Sisyphus cooling. First, the picked inversion doublet should be coupled strongly already with small electric fields, much smaller than the offset electric field present in the trap (see Sec. 3.1), ensuring strong suppression of K-flip transitions and large, linear Stark shifts. This calls for inversion doublets with a small splitting (Sec. 2.3) and, thus, for states with large $J = K_A$ (Sec. 2.2). Second, the selected states should have large Stark shifts such that the trap depth for molecules in the (low-field-seeking) states is large. This condition, too, is fulfilled best by states with large $J = K_A$, since the Stark shift in linear approximation, given by Eq. (2.16), approaches $\mu\mathcal{E}/h$ for $J = K_A = M \to \infty$. Third, as a thermal source provides the initial molecule sample and Sisyphus cooling, as implemented here, acts only on a small set of states, the thermal population of the chosen states should be high to cool as many molecules as possible[9]. Due to the threefold statistical weight of rotational states with odd K_A (Sec. 2.2), an inversion doublet with $J = K_A$ odd is preferred, of which the one with $J = K_A = 3$ which was already investigated in Sec. 2.3 shows the highest population for our source parameters.

Thermal rotational-state distribution. Our source consists of a precooled nozzle and an electrostatic quadrupole guide for velocity filtering (see Sec. 3.2) delivering molecules in low-field-seeking states to our trap. The thermal population of low-field-seeking states in the guide is given by a Boltzmann distribution for the temperature of the nozzle, $T = 150\,\mathrm{K}$, weighted with the Stark shift squared at the confining electric field strength $\mathcal{E} = 30\,\mathrm{kV/cm}$ of the guide [Mot09b]. The calculated[10] rotational-state distribution is displayed in Fig. 2.9. The state manifold $K_A = 3$ is the most abundant one and fulfills the remaining criteria defined above as well. Therefore, it is used for experiments. Note that for the densities present in the quadrupole guide and in the trap, thermalization is slow. Consequently, the state distribution in the trap is initially equal to the distribution in the guide. The comparably narrow rotational-state distribution at $T = 150\,\mathrm{K}$ was an important reason for the choice of the molecule species, as already explained in Sec. 2.1.

[9] Rotational-state cooling, as demonstrated before in our group [Glö15a, Glö16], can increase the number of initially populated states addressed by Sisyphus cooling. However, for now, these techniques are limited to a state manifold with a single K_A quantum number.

[10] Rotational states $J \leq 30$ are included in the calculation. The Stark shifts at $\mathcal{E} = 30\,\mathrm{kV/cm}$ were obtained with two approaches to limit the computational effort. For most states, in particular the ones with high J, the two-level approximation of Sec. 2.3.2 was used. For states with smaller J, for which quadratic Stark shifts at high electric fields cause a significant deviation from the two-level model, the Stark shift was computed with the diagonalization of the full Hamiltonian with $J \leq 15$.

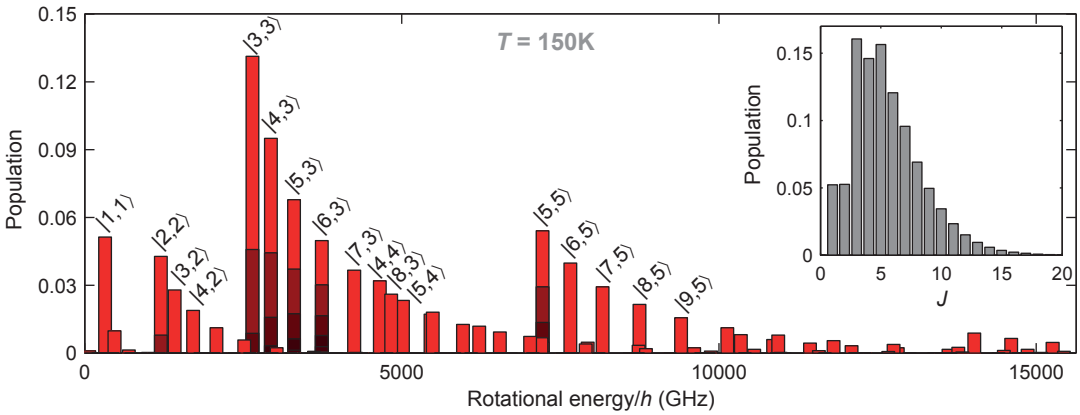

Figure 2.9: Thermal rotational-state distribution of formaldehyde in our molecule source. The population of rotational states is plotted vs. the rotational energy in zero electric field. The distribution is given by a Boltzmann distribution for the nozzle temperature $T = 150\,\mathrm{K}$ weighted with the Stark shift squared for the maximum electric field in the quadrupole guide of $30\,\mathrm{kV/cm}$ (see text). The occupation of states with large positive Stark shifts is enhanced strongly, states with negative Stark shift (high-field seekers) do not contribute because they are not trapped. Additionally, the threefold statistical weight of states with odd K_A is evident. States with higher population are labeled with $|J, K_A\rangle$. For a few bars the occupation of M sublevels is resolved: from top to bottom the segments of the bars represent sublevels with descending $|M|$. The inset shows the distribution vs. J.

Sisyphus cooling is implemented in the states $|J, K_A, K_C\rangle = |3, 3, \{0, 1\}\rangle$, with the second set $|4, 3, \{1, 2\}\rangle$ needed to close the cycling scheme. Further, the states $|5, 3, \{2, 3\}\rangle$ play a role in rotational-state preparation and detection. The thermal population of the low-field-seeking states of these sets is 13 %, 10 %, and 7 %, respectively, with the majority of molecules being in the highest M sublevels (Fig. 2.9). Molecules entering the trap in a state which is part of the first two sets have a chance to get cooled. Hence, almost a quarter of all molecules are addressed by optoelectrical Sisyphus cooling. For optical pumping to strongly trapped states, an essential part of the cooling scheme, the totally symmetric v_1 C-H stretch vibrational mode of formaldehyde is excited (Sec. 2.2). All involved states are summarized in Fig. 2.10.

Stark shifts. The calculated Stark shifts for the three experimentally relevant sets of rotational states are shown in Fig. 2.11. As expected, the Stark shift is linear[11] for larger electric fields (plots on the left). In a given set of rotational states as defined above, the state with the smaller value of K_C becomes the low-field-seeking state, whereas the one with larger K_C turns into the high-field seeking state (curves on the right). In the same plots, the transition from quadratic to linear Stark shift is seen and the inversion splitting Δ is specified. The inversion doublets are strongly coupled for electric fields greater than about $1\,\mathrm{V/cm}$, $10\,\mathrm{V/cm}$, and $40\,\mathrm{V/cm}$. As these conditions are fulfilled

[11] Careful inspection of the left panels of Fig. 2.11 reveals that the energy levels bend down slightly for the highest electric fields shown due to the onset of quadratic Stark shifts at large fields. Experimentally, the tiny deviation [cf. Fig. 2.7(b)] from the linear approximation of Eq. (2.16) is not relevant.

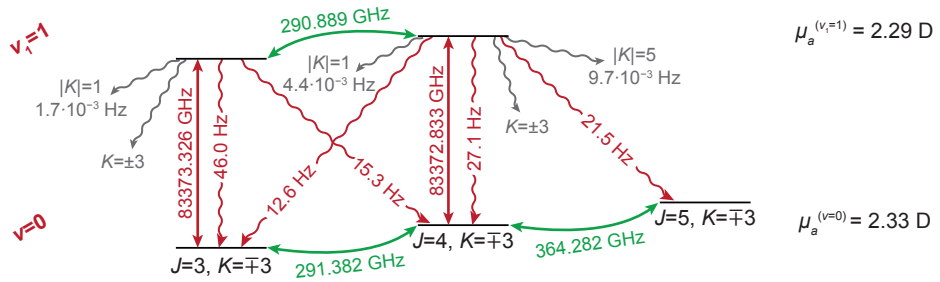

Figure 2.10: Level scheme showing all states and transitions of formaldehyde addressed in this thesis work (without M substructure). The states $|0;3,3,M\rangle$ and $|0;4,3,M\rangle$ are used for Sisyphus cooling, the manifold $|0;5,3,M\rangle$ plays a role for rotational-state preparation and detection (see Sec. 3.3) and the experiments on precision spectroscopy presented in Ch. 5. Long wavy arrows indicate the dominant spontaneous decay channels, whereas the short, gray wavy arrows indicate strongly suppressed loss channels (see Sec. 2.5). The rates [Rot13] for the dominant decay channels (red) hold if the inversion doublets are strongly coupled by the electric field. Rates for K-flip transitions (gray arrows to $K \pm 3$) strongly depend on the applied field and are therefore not specified. Rates for higher-order ΔK spontaneous decays to states with $|K| \neq 3$ due to the slightly asymmetric rotor structure of formaldehyde are found in the literature [Rot13].

almost always in experiments, unwanted K-flip transitions (Sec. 2.3.3) are strongly suppressed and formaldehyde in the chosen rotational states behaves very similarly to a symmetric-top molecule. Thus, the use of symmetric-top rotational quantum numbers J, $K = K_A$, and M is appropriate.

The precise calculation of Stark shifts from the full Hamiltonian was only performed for the vibrational ground state. In the excited state $v_1 = 1$, the dipole moment is slightly smaller. This leads to slightly smaller splittings of M sublevels without changing the general properties of the chosen rotational states in the vibrational excited state. These smaller splitting were measured via Stark spectroscopy allowing deduction of the dipole moment in the excited state (see Sec. 3.3.2) and subsequently the calculation of Stark shifts with Eq. (2.16).

2.4.2 Internal-state nomenclature

Experiments are performed on molecules in low-field-seeking states because only those are trapped in the electrostatic trap. To label internal states and distinguish low- and high-field seekers the following convention is used for the remainder of this thesis. With the vibrational quantum number v and symmetric-top rotational quantum numbers J, K, and M the doubly degenerate Stark shifted molecular states, strongly coupled by a static electric field, are identified with $|v;J,\mp K,\pm M\rangle$ where $\mp K \equiv |K| = K_A$ is chosen positive and M remains a signed integer. Then, the sign of M specifies the character of the state: $+M$ is a low-field-seeking energy level, whereas $-M$ is a high-field-seeking state. Consequently, the label, e.g., $|0;3,3,M{>}0\rangle$ refers to the trapped, low-field-seeking states characterized by the quantum numbers $J = 3$ and $K_A = 3$.

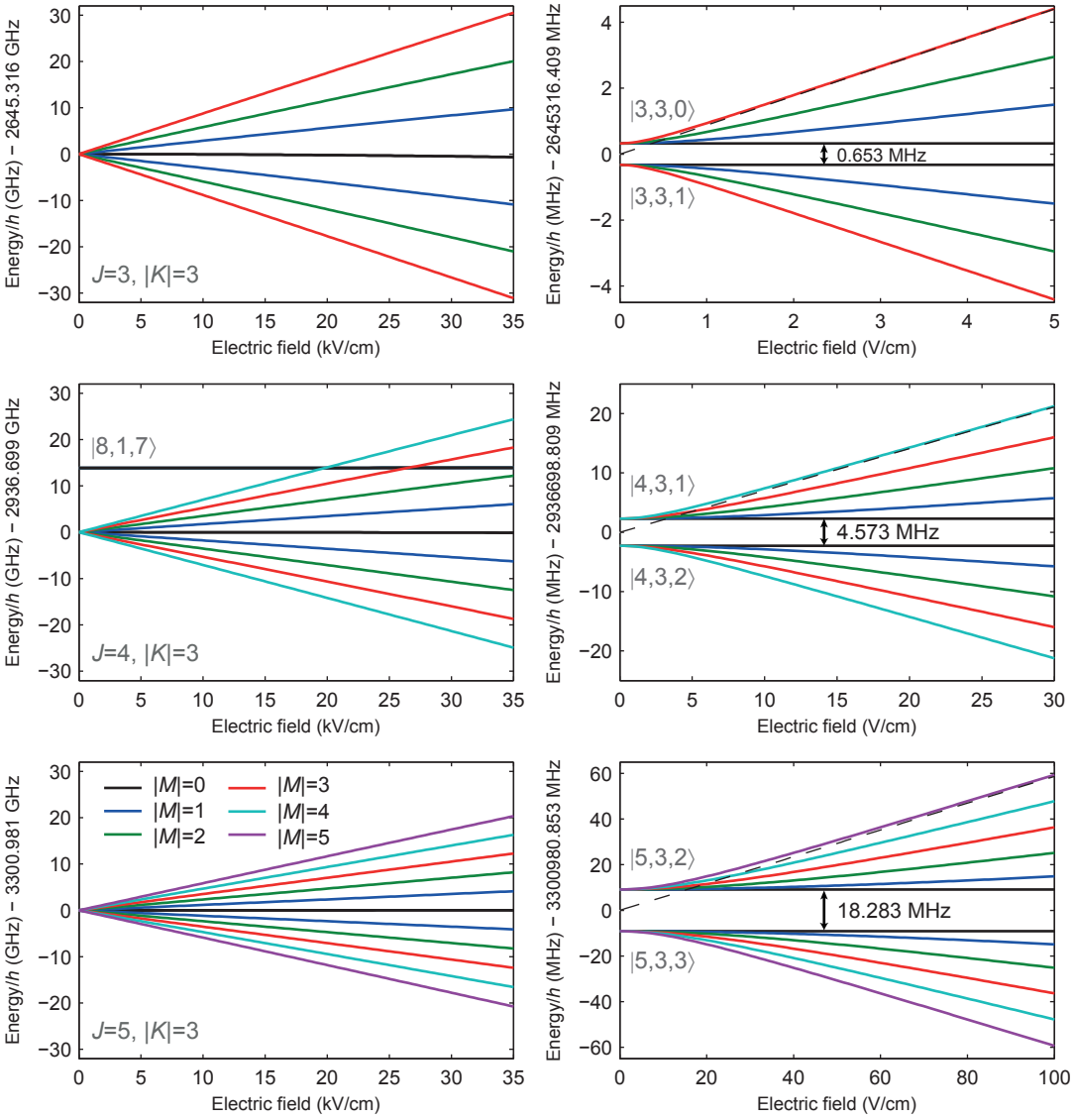

Figure 2.11: Stark shifts of the rotational states of formaldehyde which are addressed in experiments. The curves were calculated with the free software package PGOPHER [Wes17] using the molecular constants of Ref. [Brü03]. Rotational states $J \leq 20$ are included in the calculation. Plots in each row show the same set of states. On the left, the linear scaling for large electric fields up to 35 kV/cm is observed. The zoom-in on the right (with different scales for each row) displays the transition from quadratic to linear Stark shifts for small electric fields. The vertical axes are centered between the two states which are coupled strongly by the external field. The dashed line shows the Stark shift in linear approximation [Eq. (2.16)] for the highest M sublevel. States are labeled with symmetric-top quantum numbers on the left, and in asymmetric-rotor notation $|J, K_A, K_C\rangle$ on the right. The splitting of the inversion doublets without electric field is specified. State $|8, 1, 7\rangle$ is energetically close to $|4, 3, 1\rangle$ and $|4, 3, 2\rangle$ but is not coupled to these states and therefore does not cause problems.

Transition	Frequency (MHz)	Accuracy (MHz)	Reference
$\|0;3,3,0\rangle \leftrightarrow \|0;4,3,1\rangle$	291384.360	0.10	[Brü03, Wes17]
$\|0;3,3,1\rangle \leftrightarrow \|0;4,3,2\rangle$	291380.440		
$\|0;4,3,1\rangle \leftrightarrow \|0;5,3,2\rangle$	364288.899	0.03	
$\|0;4,3,2\rangle \leftrightarrow \|0;5,3,3\rangle$	364275.188		
$\|0;3,3,0\rangle \leftrightarrow \|1;3,3,1\rangle$	83 373 325.55	0.02	[Ibr13]
$\|0;3,3,1\rangle \leftrightarrow \|1;3,3,0\rangle$	83 373 326.79		
$\|0;4,3,1\rangle \leftrightarrow \|1;4,3,2\rangle$	83 372 828.58		
$\|0;4,3,2\rangle \leftrightarrow \|1;4,3,1\rangle$	83 272 838.23		

Table 2.3: Precise frequencies for relevant transitions of formaldehyde in the absence of external electric fields. States are labeled with $|v_1;J,K_A,K_C\rangle$. Purely rotational transition frequencies were calculated with PGOPHER [Wes17] using the molecular constants of Ref. [Brü03]. The listed vibrational transitions were measured precisely in our group by Martin Ibrügger with saturation spectroscopy using a multi-pass Herriot cell [Ibr13]. Data on the full infrared spectrum is available in the HITRAN database [Rot13]. In the relevant 3.6 µm range the HITRAN data is accurate to about 10-60 MHz [Per06, Per09].

2.4.3 Transition frequencies

Precise frequencies for transitions between distinct inversion doublets are calculated in the following way. Transition frequencies in the absence of external fields are listed in Table 2.3. Since experiments are performed in the regime of linear Stark shifts and Eq. (2.16) shall be used to calculate Stark-shifted transition frequencies, we first calculate a hypothetical center frequency coupling two inversion doublets. It is given by the mean of the frequencies of the two transitions allowed without electric field (those listed in the table). The resulting center frequencies are included in Fig. 2.10. The Stark shift in linear approximation is added to the center frequency using the electric dipole moments for the vibrational ground state ($v = 0$), 2.33 Debye [Fab77], and the vibrational excited state ($v_1 = 1$), 2.29 Debye (measurement in Sec. 3.3.2). If available, measured values for the offset electric field in the trap (Sec. 3.1.3) are used for the calculation of Stark-shifted transition frequencies.

2.5 A closed level scheme for cooling

Finally, the complete level scheme for optoelectrical Sisyphus cooling of formaldehyde is now introduced (Fig. 2.12) and potential loss channels are discussed. The two main ingredients of cooling (Sec. 2.1), namely optical pumping to strongly trapped states in low electric fields and induced transitions to more weakly trapped states in high electric fields, are implemented as follows.

For optical pumping a $\Delta M = +1$ infrared (IR) transition from states $|0;3,3,M{<}3\rangle$ is driven. From the excited state $|1;3,3,M\rangle$ molecules decay to two ground state manifolds due to the selection rule $\Delta J = 0, \pm 1$. Therefore, the states $|0;3,3,M{>}0\rangle$ and $|0;4,3,M{+}1\rangle$ are coupled with microwave (MW) radiation. This results in optical pumping to and accumulation of molecules in the strongly trapped highest M sublevels

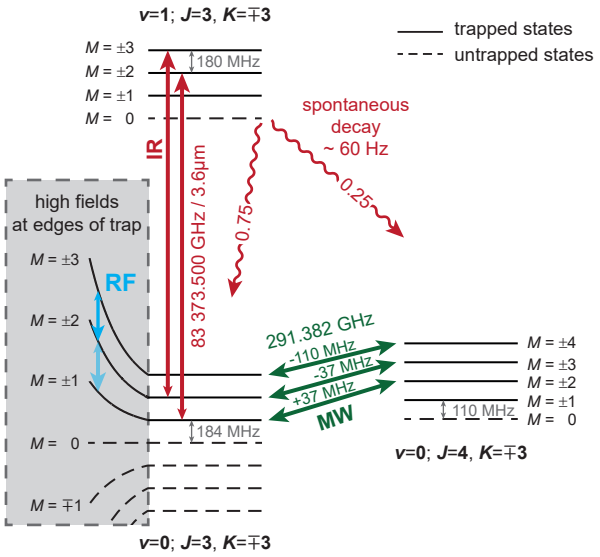

Figure 2.12: Detailed scheme for optoelectrical Sisyphus cooling of formaldehyde as explained in the main text. Radiation (solid arrows) couples rovibrational states, wavy arrows indicate spontaneous decay channels and their branching ratio (without resolving the M substates). The Stark splitting of neighboring M sublevels and transition frequencies [Cor80, Brü03, Rot13] are given for the homogeneous-field region of the trap ($V_{\mathrm{trap}} = \pm 1500\,\mathrm{V}$ as used for most experiments, see Sec. 3.1.1).

based on the selection rule $\Delta M = 0, \pm 1$. Note that the laser frequency is chosen such that the transition $|0;3,3,2\rangle \leftrightarrow |1;3,3,3\rangle$ is resonant in the offset electric field. Nevertheless, also the second marked IR transition is driven with that laser frequency at a slightly reduced rate as the Stark shifts in the ground and excited states are very similar for equal rotational quantum numbers (see also Sec. 3.3). In contrast, distinct MW frequencies are applied to drive several transitions with $\Delta J = \pm 1$.

Coupling neighboring M sublevels with RF radiation in the strong-field edge region of the trap closes the cooling cycle: transitions to more weakly trapped states remove kinetic energy. Consequently, the strongly trapped, $|s\rangle$, and more weakly trapped states, $|w\rangle$, used to introduce the cooling scheme in Sec. 2.1 are identified with successive M sublevels of the rotational-state manifolds $|0;\{3,4\},3,M\rangle$. Of course, the RF acts on all trapped molecules, although the potential energy curves and transitions in the high-field region of the trap are only sketched for one set of states in the figure. To minimize losses to untrapped states $M \leq 0$, the RF transitions have to be driven at a slow rate compared to the optical pumping rate to strongly trapped states since the M sublevels are equidistant [Zep12]. The spontaneous decay rate of $\sim 60\,\mathrm{Hz}$ limits the optical pumping and hence the speed of cooling. Despite this restriction, the choice to remove kinetic energy via RF transitions between successive M sublevels is appealing because the resulting level scheme is particularly simple.

An alternative would be to identify states with distinct J quantum number with the states $|s\rangle$ and $|w\rangle$, e.g. the states $|0;3,3,3\rangle$ and $|0;4,3,2\rangle$, and extract kinetic energy by driving a MW transition between those states in high electric field [Zep09, Eng13]. In theory, this could speed up cooling because the Stark-shifted transitions $|0;3,3,M\rangle \leftrightarrow |0;4,3,M\rangle$ differ in frequency and the chosen transition could be driven

selectively without causing losses to untrapped states if the electric fields are engineered carefully. In practice, however, driving the transition $|0;3,3,3\rangle \leftrightarrow |0;4,3,2\rangle$ selectively has proven difficult since it requires large MW power due to the large differential Stark shift and a small transition-dipole moment (cf. Sec. 3.3.1).

The presented scheme is sufficiently closed to allow many repetitions of the cooling cycle. However, minor loss channels exist and are discussed now. Foremost, the most weakly trapped state $|0;4,3,1\rangle$ is not repumped and therefore constitutes a loss channel. However, decays to this state happen rarely for two reasons. The squared Clebsch-Gordan coefficient for the decay from $|1;3,3,2\rangle$ to $|0;4,3,1\rangle$ is only 1/48. Furthermore, after initial accumulation of molecules in the strongly trapped states, the molecules predominantly cycle within the two highest M levels of the two sets of states because the rate of optical pumping to strongly trapped states is a lot larger than the coupling to lower M levels by the RF. In consequence, the excited state $|1;3,3,2\rangle$, which possesses the unwanted decay channel, is less populated because the state $|0;3,3,1\rangle$ is less populated. Combining the two reasons with the fact that only about 20 complete Sisyphus cycles are needed to cool the molecules by a factor of thousand (Sec. 2.1) it can be concluded that losses via the state $|0;4,3,1\rangle$ are not significant (see also Ref. [Zep12]).

Even weaker loss channels exist through K-flip transitions, either induced by the RF or via a vibrational spontaneous decay, as discussed in Sec. 2.3. These K-flip transitions to high-field-seeking and thus untrapped states with $K_A = 3$ are strongly suppressed because all inversion doublets used in experiments are strongly coupled by the electric field. For example, considering a spontaneous decay from the excited state $|1;3,3,3\rangle$ in the low-field region of the trap (offset electric field $\mathcal{E}_{\text{offset}} = 625\,\text{V/cm}$, as used in the beginning of the cooling sequence), decays to the untrapped states $|0;3,3,-M\rangle$ are suppressed by a factor of 4×10^{-7} compared to those to the trapped states $|0;3,3,M\rangle$. For the lowest offset field used for cooling, $\mathcal{E}_{\text{offset}} = 40\,\text{V/cm}$, the suppression still is 10^{-4}. These values were calculated with the model described in Sec. 2.3.3.

Finally, the asymmetric rotor Hamiltonian allows higher-order ΔK transitions with $\Delta K_A = \pm 2, \pm 4, ...$ and $\Delta K_C = \pm 1, \pm 3, ...$ (Sec. 2.2). Consequently, spontaneous decays to states with $J = 2, 3, 4$ and K_A odd can happen, but are strongly suppressed as well. For instance, the strongest of these weakly allowed decays, decays from our excited state to the inversion doublets characterized by $J = 3$, $K_A = 1$ and $J = 2$, $K_A = 1$ occur with rates of about $7 \times 10^{-4}\,\text{Hz}$ and $9 \times 10^{-4}\,\text{Hz}$ according to the HITRAN database [Rot13]. Such loss rates can be safely neglected for Sisyphus cooling. Nevertheless, these strongly suppressed decay channels are included in Fig. 2.10.

2.6 Summary

In conclusion, a scheme for optoelectrical Sisyphus cooling of formaldehyde was presented. Despite the asymmetric rotor structure of the molecule, rotational states with a strong electric-field interaction suitable for Sisyphus cooling, namely inversion doublets with a small splitting, can be identified. Towards this end, the splitting of inversion-doublet rotational states was investigated. The inversion splittings varying by orders of magnitude depending on the rotational state could potentially be useful for future experiments because this allows to couple formaldehyde to other physical systems in

a large range of frequencies. The inversion splitting is also relevant for the method developed for precision spectroscopy in the final part of the thesis as it is one factor determining the magnitude of the 'magic' field required to eliminate Stark broadening on the chosen transition.

Moreover, it was shown that the experimentally significant properties of the rotational states in a static electric field can be understood with a simple analytical model considering pairs of inversion-doublet states. It allows to quickly calculate Stark shifts and strengths of electric-dipole transitions in the electric field. The rotational states chosen for experiments have inversion splittings on the order of MHz, leading to strong coupling of the inversion-doublet states at small electric fields of a few V/cm and effective suppression of unwanted transitions to untrapped high-field-seeking states by a few orders of magnitude.

The complete level scheme for cooling incorporates only a small number of states and transitions and is sufficiently closed to allow many repetitions of the cooling cycle without loosing many molecules. Despite the many degrees of freedom formaldehyde possesses as an asymmetric polyatomic molecule, the experimenter can work with a simple and clearly structured level scheme. Moreover, only three radiation sources are needed to implement motional cooling, a single IR laser, a single microwave source, and a single RF generator. Thus, the experiment can be performed with a fairly uncomplicated setup, built around an electrostatic trap and the aforementioned radiation sources.

The cooling scheme makes use of quite general properties of polar molecules. Hence, it should be applicable to various other molecule species, for example the symmetric-top molecules suggested in the original proposal [Zep09]. In addition, however, this chapter showed that suitable states for cooling should also be identifiable in molecules with a larger rotational asymmetry than formaldehyde as long as the molecule has a sizable component of the dipole moment along the axis which would be the symmetry axis of the corresponding symmetric-top limiting case, a prerequisite for a strong coupling of inversion-doublet rotational states by a static electric field.

3 The electric trap and experimental foundations

The key device required for the implementation of optoelectrical Sisyphus cooling is a suitable electrostatic trap which confines molecules in low-field-seeking rotational states in clean potential landscapes. Therefore, in this chapter the electric trap and the surrounding apparatus are introduced. A general challenge for most experiments with cold and ultracold polyatomic molecules is the very limited performance of established detection methods. This has been and still is one of the big challenges we face with our experiments: A really robust, efficient, and accurate detection scheme which suits our experimental needs has not yet been developed (see outlook, Ch. 6). Nevertheless, by refining the experimental setup and transferring internal-state control techniques which were developed earlier during experiments with fluoromethane to formaldehyde, both data acquisition and diagnostics in the experiment could be improved substantially. For example, it is now possible to measure the population of all different M sublevels of a specific rotational state $|0; J, K, M\rangle$, whereas it was restricted to selected M sublevels before. As these developments were very helpful for cooling of formaldehyde to submillikelvin temperatures, a section on internal-state control and its applications is included in this chapter. The following description gives references to earlier publications and emphasizes how the setup was changed and how previously developed techniques were improved and adapted to formaldehyde.

The experimental foundations of this thesis are described in the following order. Section 3.1 introduces the electric trap, changes made to it during this thesis work, and its key properties which are verified with measurements on formaldehyde molecules. The experimental apparatus and its evolution are described in Sec. 3.2. Adaption of internal-state control techniques to formaldehyde and their use for diagnostic measurements are presented in Sec. 3.3. Two examples for the latter, which also yield molecular parameters, are discussed: an experiment determining the IR driving rate and verifying the spontaneous vibrational decay rate as well as the spectroscopic measurement of the dipole moment in the excited vibrational state.

3.1 The box-like electrostatic trap

The electric trap and the majority of the surrounding experimental setup where constructed before this thesis work began and are described in several articles and theses. The trap was designed by Martin Zeppenfeld [Zep13]. First trapping of molecules was achieved in 2011 with 1/e trap decay times of about 10 s [Eng11]. The characterization of the first version of the trap is described in Ref. [Eng13]. Successful operation of the trap led to the initial demonstration of optoelectrical Sisyphus cooling [Zep12] and internal state control [Glö15a] of fluoromethane.

Knowledge gained with previous experiments suggested that cooling to submillikelvin

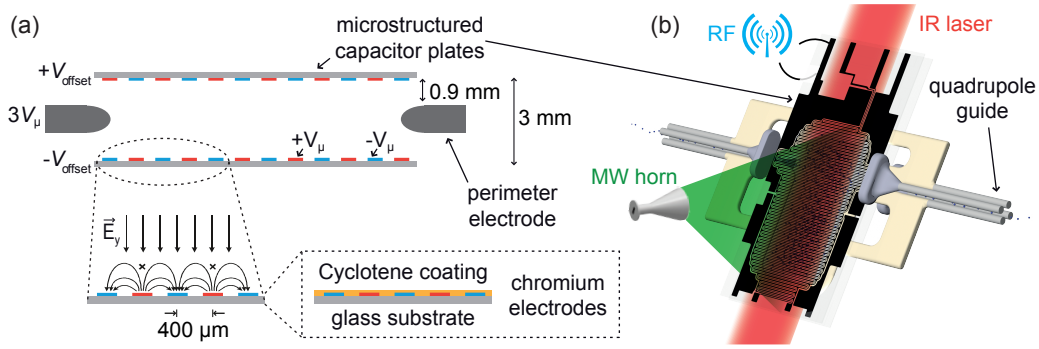

Figure 3.1: Electric trap. The trap consists of two microstructured capacitor plates and a surrounding perimeter electrode which is connected to the input and output quadrupole guides. Its dimensions are $3 \times 20 \times 40\,\mathrm{mm}^3$ [Zep13]. **(a)** Schematic cut through the trap along the longest dimension. The homogeneous offset field is produced by applying a voltage of $2V_{\mathrm{offset}}$ across the capacitor whereas high trapping fields near the surface of the plates are provided by high voltage $\pm V_\mu$ applied to neighboring microstructure electrodes (see first inset). A plate consists of chromium electrodes on a glass substrate coated with the polymer Cyclotene for better high-voltage performance (second inset) [Eng13]. **(b)** 3D drawing of the trap showing the connection to the quadrupole guides and application of the radiation fields for cooling (see also photograph in Fig. A.3).

temperatures would require installation of a new, slightly refined version of the trap. After introducing the general working principle of the trap in Sec. 3.1.1, the improvements and the underlying reasons are discussed in Sec. 3.1.2. A unique feature of the trap is the large low-field region with quasi-homogeneous electric fields in its center. This leads to box-like potentials for low-field-seeking rotational states and spectroscopic separation of rotational M sublevels which is required for cooling. A method to determine the homogeneity of the electric fields in the trap and thus the spectral resolution was introduced by Ref. [Glö16]. In Sec. 3.1.3 it is shown that the homogeneity of electric fields could be improved substantially with the new trap and new parameters of operation. Finally, the lifetime of formaldehyde molecules in the trap is investigated in Sec. 3.1.4.

3.1.1 Design and operation principles

A box-like trapping potential for low-field-seeking molecular states is produced by combining a microstructured plate capacitor with a perimeter electrode surrounding the trapping volume and providing confinement from the side [Zep09, Zep13, Eng11, Eng13]. The geometry of the trap is shown and explained in Fig. 3.1. In particular, the low field in the center of the trap is generated by applying a voltage of $2V_{\mathrm{offset}}$ across the capacitor. The confining electric fields are produced by the electrode microstructure on the plates ($\pm V_\mu$ on neighboring electrodes) and the field between the perimeter electrode ($V_{\mathrm{ring}} = 3V_\mu$) and the capacitor plates ($\pm V_{\mathrm{offset}} \ll V_{\mathrm{ring}}$). The trapping fields decay exponentially towards the trap center [Zep13] but contribute to the field in the low-field region. This results in tunable, quasi-homogeneous offset fields in a large fraction of the trap volume, with a finite roughness owing to $\pm V_\mu$.

The offset electric fields are needed for two reasons. First, a non-zero offset field dramatically reduces losses of trapped molecules due to Majorana flips (transitions

from low-field-seeking to high-field-seeking molecular states). Second, the offset field provides spectroscopic separation of different M sublevels, facilitating internal-state control by, e.g., optical pumping. On the other hand, the trapping signal decreases for too large offset fields (see also Fig. A.2). Optimization measurements [Mie10, Eng13, Kro14] found $V_{\text{offset}} = 0.05 \cdot V_\mu$ as a good compromise. The strength of V_{offset} relative to V_μ is chosen differently only if a particular absolute field strength is needed, e.g., to adjust the offset electric field to molecular properties or transitions.

For the following experiments, different trap voltage configurations are used. If not given explicitly, the preceding relation for V_μ and V_{offset} holds and a single value is quoted to characterize a specific trap voltage configuration. For example,

$$V_{\text{trap}} = \pm 1500\,\text{V}: \; V_\mu = \pm 1500\,\text{V} \text{ and } V_{\text{offset}} = 0.05 \cdot V_\mu = \pm 75\,\text{V} \tag{3.1}$$

is used frequently and results in the offset Stark splittings specified in the detailed cooling scheme in Fig. 2.12, calculated with the measured offset electric field strength (Sec. 3.1.3). Note that the voltage configuration can in principle be chosen independently for the two halves of the trap since the electrode microstructure is cut in half along the longest dimension [Zep13].

The design trap depth [Zep13] is determined by the electric field strength between the perimeter electrode and the capacitor plates, $\mathcal{E}_{\text{trap}} \sim 3V_\mu/0.9\,\text{mm} = 50\,\text{kV/cm}$ for $V_{\text{trap}} = \pm 1500\,\text{V}$. For the state $|0;3,3,3\rangle$ of formaldehyde this would result in a Stark shift of $\mu\mathcal{E}_{\text{trap}}/h \cdot 3/4 = 44\,\text{GHz}$ corresponding to an energy of $3/2 \cdot k_B \cdot 1.4\,\text{K}$. However, molecules with a kinetic energy close to the trap depth are lost from the trap very quickly (see Sec. 3.1.4).

For most of the following experiments, the processes happening in the trap—including optoelectrical Sisyphus cooling and internal-state preparation—are modeled using rate equations to describe population transfer between molecular states [Zep12, Glö16]. Thereby it is assumed that coherences do not play a significant role. This assumption is justified by the experimental parameters. As will be seen, driving rates of vibrational and rotational transitions on the order of or well below 1 kHz compare to a Stark broadening of a few to many MHz for most addressed transitions. Moreover, the RF for cooling has to be applied at very small rates $\sim$ Hz to avoid losses to untrapped states (Sec. 2.5). Considering the trap geometry and the velocity of the molecules, evidently, molecules on average come into resonance with the RF many times before a transition happens justifying the use of rate equation models.

3.1.2 A new trap: technical improvements

Over the years, several ideas were developed to improve the trap characteristics compared to the initial design [Zep13], in particular regarding the trap depth, the homogeneity of the offset electric fields, and the ability to unload molecules at submillikelvin temperatures for detection. In this section, the implemented changes and the underlying reasons and ideas are summarized. Especially the improved homogeneity of the electric fields resulting from these changes was important for the experimental achievements presented in this thesis. In detail, these changes are a rotation of the trap by 90°, installation of a new perimeter electrode with reduced dimension, and use of a fresh set of otherwise unchanged microstructure plates, combined with a reduced maximum voltage ever applied to the new set of plates (see below). Moreover, the reduction of

voltage noise on the trap electrodes also had a small positive effect on the homogeneity of the electric fields. This last technical effect is not discussed here in more detail.

Rotation of the trap. Initially, the trap was mounted in the vacuum chamber with the longest dimension pointing in vertical direction, the direction of gravity, resulting in a distance of 30 mm from the bottom of the trap to the center of the quadrupole guide used for unloading molecules towards the detector [Zep13]. This caused a gravitational sag for the molecules, corresponding to a temperature

$$T_{\mathrm{grav}} = \frac{g \cdot m_{\mathrm{H_2CO}} \cdot 30\,\mathrm{mm}}{\frac{3}{2} k_B} = 709\,\mu\mathrm{K} \tag{3.2}$$

for formaldehyde with mass $m_{\mathrm{H_2CO}}$, gravitational acceleration g, and the Boltzmann constant k_B. Therefore, the trap was rotated such that the longest dimension lies in the plane perpendicular to gravity, eliminating the gravitational sag. There remains a small voltage-dependent potential barrier between the trap and the quadrupole guide [Zep13].

Perimeter electrode with reduced dimensions. For reason which will not be reviewed here[1], the lifetime of molecules with an energy larger than about 1/4 of the nominal trap depth was estimated to be very short, limited to about 2 s at most, too short for significant cooling of the hotter molecules. This effectively decreases the trap depth of the originally designed geometry by a factor of four [Zep13]. To overcome this issue Martin Zeppenfeld designed a new perimeter electrode reaching 1 mm further into the original trapping volume on both sides along the longest dimension. This new electrode was installed during the reconstruction of the trap. However, experiments with the new trap showed no performance improvement or deterioration related to this change so far.

New microstructure plates and operation voltages. From early Sisyphus cooling experiments on [Zep13], there was experimental evidence for the existence of surface charges on the microstructured capacitor plates which alter the electric-field distribution in the trap. The microstructure plates[2] which were recently used in the experiment are completely coated with the polymer Cyclotene (Fig. 3.1). This allows much higher voltages to be applied to the electrodes without flashovers than with uncoated versions of the commercially fabricated microstructure [Eng13] and, thus, increases the maximally reached trap depths[3]. However, due to the insulating property of the polymer, surface charges might easily accumulate in this additional layer and disturb the electric fields. These additional charges manifest in measured electric-field distributions differing substantially from the expected ones (Sec. 3.1.3). Furthermore, even if the trapping voltages were switched off completely, molecules survived in the trapping volume much longer than expected. Additionally, these problems seemed to worsen over time. Investigations showed that very pronounced surface charges could be removed by heating up the entire vacuum chamber hosting the trap to 200 °C for a few days (see Appendix A and Refs. [Kro14, Pre16]).

[1] Explanation of the trap design in full detail [Zep13] would be required.
[2] Fabricated via optical lithography by IMT Masken und Teilungen AG.
[3] Information on the high-voltage performance of microstructure plates differing in electrode material, coating, etc. can be found in Refs. [Mie10, Eng13, Kro14].

To eliminate the unwanted charges completely, at least for some time, a new set of microstructure plates was installed during the reconstruction of the trap and prior to the experiments with formaldehyde. Moreover, the maximally applied trap voltages were reduced from $V_{\text{trap}} = \pm 1800\,\text{V}$ to $V_{\text{trap}} = \pm 1500\,\text{V}$ hoping for less accumulation of surface charges or a longer time for the build-up of disturbing charges. Indeed, hints for surface charges even after two years of operation appeared only at an order of magnitude lower trap voltages.

The changes significantly improved the homogeneity of electric fields (see next section) and reduced the problems experienced with surface charges on the microstructured capacitor plates and thus paved the way to production of molecules at submillikelvin temperatures. Additional data which shows improved trap performance is summarized in Appendix A. Unfortunately, the problem with surface charges persists on a substantially reduced level [Pre16], evidence of which is discussed in Ch. 4.

3.1.3 A tunable box-like trap potential

The trap potential experienced by the molecules, which is given by the distribution of electric fields in the trap, can be investigated by performing spectroscopy on the molecules. Evidently, a box-like potential with a large homogeneous-field region translates to a strongly peaked electric-field distribution, with the width of the peak giving the roughness of the offset. In the following, we discuss the electric-field distribution in the trap and show that the trapping potential indeed is box-like. By comparing the current distribution to the one obtained with the previous trap it is demonstrated that the homogeneity of the offset electric field could be improved substantially with the changes introduced in the preceding section. The reduced roughness of the potential floor is particularly important for cooling to very low temperatures: the regions of low and high electric field needed for Sisyphus cooling are not well-defined any more if the kinetic energy of the molecules is comparable to the roughness of the offset potential energy. Furthermore, the shape of the electric-field distribution determines our ability to selectively drive specific Stark-shifted rovibrational transitions.

A measured electric-field distribution is obtained via Stark spectroscopy on the single rotational transition $|0;3,3,3\rangle \leftrightarrow |0;4,3,4\rangle$ of formaldehyde which shows a linear differential Stark shift (Sec. 2.4 and Fig. 2.11). The line shape of this transition is almost exclusively given by Stark broadening induced by the electric fields in the trap[4]. Therefore, the electric-field distribution can be directly calculated from the spectroscopic measurement. The measurement scheme is investigated in great detail in Ref. [Glö16]. Here, a slightly refined protocol is used which is summarized in Appendix B.

Figure 3.2 displays the measured and calculated electric-field distributions of the current version of the electric trap. Indeed, the offset electric field in the central trapping region is well defined by the peak of the distribution. Compared to the maximum nominal trapping field of $50\,\text{kV/cm}$ for a trap voltage of $V_{\text{trap}} = \pm 1500\,\text{V}$ the peak is very narrow. Consequently, the fields in the center of the trap can be regarded as quasi-homogeneous. The trapping fields are visible as the high-field tail of the distribution. Evidently, fields smaller than the offset electric field exist as well. However,

[4] Other broadening mechanisms like Doppler broadening and the natural line width are at least three orders of magnitude smaller, see also Ch. 5.

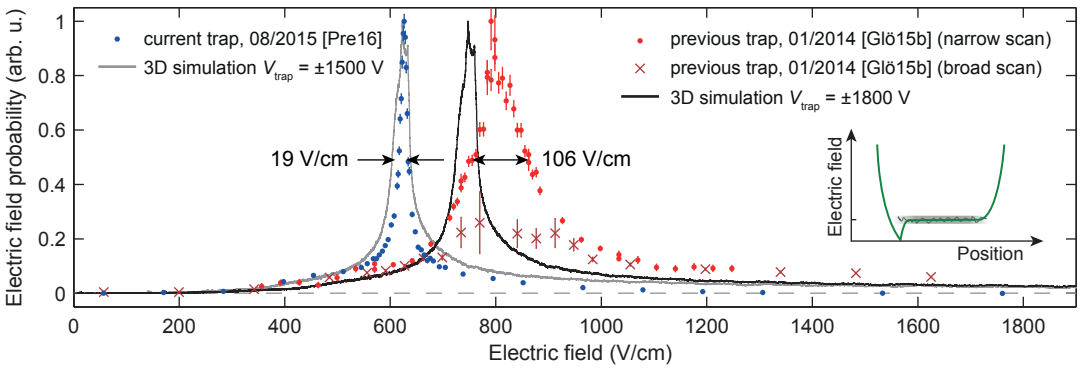

Figure 3.2: Electric-field distributions. Measured (markers) and simulated (lines) data for the current (installed June 2014) and previous (in operation March 2012 to May 2014) trap, all normalized to the maximum signal. The FWHM of the measured distributions are given. The two versions of the trap were operated with different standard voltage configurations for experiments. The month of the measurement is indicated in the legend. The simulation scales with trap voltage V_{trap}. Equally, the measured distributions and their width are expected to scale with V_{trap}. The inset shows a simplified sketch of a potential which serves as an intuitive picture indicating the main features of the actual potential: high trapping fields, a homogeneous offset field with an associated roughness, and regions of smaller electric field.

these small-field dimples occupy only a small fraction of the total trap volume. Note that the measured distribution is convolved with the probability for molecules to be at a given potential energy, which mainly influences the high-field tail of the distribution [Glö15b, Glö16]. Due to the limited kinetic energy[5] of the molecule ensemble used for spectroscopy the measured probability vanishes for high electric fields.

The aspects of the box-like potential which are most relevant to this work can be captured by two parameters of the measured electric-field distribution. First, the center of the peak defines the homogeneous offset electric field which is determined as $\mathcal{E}_{\mathrm{offset}} = 625\,\mathrm{V/cm}$ for the current trap. This allows calculation of the Stark splitting of M sublevels in this region as $f_{\mathrm{offset}} = (\mu\mathcal{E}_{\mathrm{offset}}/h)[K/J(J+1)]$, using the linear approximation for the Stark shift [Eq. (2.16)]. Second, an estimate for the roughness of the offset field is given by the full width at half maximum (FWHM) of the distribution of $\Delta\mathcal{E}_{\mathrm{offset}} = 19\,\mathrm{V/cm}$. For a specific ensemble of cooled molecules, the potential can be treated as box-like, if the kinetic energy of the molecules is much larger than the roughness of the floor of the electric box.

The measured distributions are compared to a simulation performed in April 2015 by Martin Zeppenfeld. The electric fields were simulated on a grid (10 µm × 10 µm × 20 µm grid spacing) considering the entire three-dimensional trap geometry. The simulation predicts the peak position, i.e., the value of the homogeneous offset field, and the shape of the distribution quite well, indicating a good understanding of the trap electric fields. However, the measured peak is even narrower than the simulation. This deviation is attributed to numerical inaccuracies of the simulation.

The electric-field distribution of the previous trap is shown in Fig. 3.2 as well. It was measured with fluoromethane (CH_3F) and $V_{\mathrm{trap}} = \pm 1800\,\mathrm{V}$ [Glö15b]. Although both

[5] Cooling with the standard sequence (Sec. 4.2) was stopped at final $f_{\mathrm{RF}} - f_{\mathrm{offset}} = 189\,\mathrm{MHz}$.

the peak position and the width are expected to scale with V_{trap}, the distribution for the previous trap is much broader which we attribute to the existence of severe surface charges or other experimental imperfections. Consequently, the changes to the trap, in particular the replaced microstructured capacitor plates and the lower maximum trap voltage, led to a better homogeneity of the offset electric field. Most probably, cooling to submillikelvin temperatures would not have been possible with the old trap due to the large roughness of the offset potential (see Sec. 4.2.3). Note that both measurements were performed after each trap was operated for experiments over more than a year.

To selectively drive the rovibrational transitions needed for optoelectrical Sisyphus cooling and rotational-state preparation, the frequencies for the IR or MW radiation are chosen to be resonant to the desired transitions in the offset electric field $\mathcal{E}_{\mathrm{offset}}$. Due to the narrow distribution, the occurrence probability for the field $\mathcal{E}_{\mathrm{offset}}$ is strongly enhanced, giving a good spectroscopic separation of the molecular states. Thus, in the rest of this work, any IR or MW transition specified in, e.g., an optical pumping scheme is meant to be driven in the offset electric field if not stated differently. Nevertheless, other, undesired molecular transitions which might be many MHz away from a target transition can be Stark shifted into resonance when molecules probe different electric fields, especially the high trapping fields. As this can strongly influence the result of, e.g., optical pumping we will come back to this throughout the thesis[6].

We will make use of the tunability of both the magnitude of the offset electric field and its roughness. During optoelectrical Sisyphus cooling the roughness is reduced by scaling the trap voltages to lower values at the expense of smaller trapping fields. Therefore, measured electric-field distributions for three smaller trap voltages are shown in Ch. 4 (Figs. 4.7 and 4.9). The ability to tune $\mathcal{E}_{\mathrm{offset}}$ by adjusting the offset voltage V_{offset} is exploited for precision spectroscopy in a 'magic' electric field as shown in Ch. 5.

3.1.4 Lifetime of molecules in the trap

A very important characteristic of any trap is the lifetime of molecules in that trap, as it sets the timescale on which useful experiments can be performed. For optoelectrical Sisyphus cooling a lifetime on the order of seconds is needed, as a slow vibrational spontaneous decay is used for dissipation. The lifetime in our trap heavily depends on the kinetic energy of the molecules, even if it is much smaller than the trap depth: fast molecules get lost quicker because they probe the regions of small electric field, where Majorana flips can happen, and the entrance and exit holes of the trap a lot more often than slow molecules [Zep13].

For the maximum trap voltage of $V_{\mathrm{trap}} = \pm 1500\,\mathrm{V}$, the hottest uncooled molecules are lost from the trap with a $1/e$ decay time of less than 1 s (see Sec. 4.2.1) whereas for colder uncooled molecules this increases to about 10 s [Eng11]. These numbers can be further improved by cooling the molecules [Zep12]. Figure 3.3 shows the remaining formaldehyde signal versus storage time for two representative cooling sequences. The coldest molecule ensemble produced so far can be stored with a decay constant of 30 s at $V_{\mathrm{trap}} = \pm 100\,\mathrm{V}$ (kinetic energy $\sim 3/2 \cdot k_{\mathrm{B}} \cdot 0.4\,\mathrm{mK}$, experimental sequence described in Ch. 4, final $f_{\mathrm{RF}} - f_{\mathrm{offset}} = 3.1\,\mathrm{MHz}$). This number improves if the trap voltage is increased relative to the molecular kinetic energy. To demonstrate this, a slightly hotter ensemble (with a shorter cooling sequence, final $f_{\mathrm{RF}} - f_{\mathrm{offset}} = 22\,\mathrm{MHz}$) is prepared and

[6] The topic was discussed in great detail in Rosa Glöckner's thesis [Glö16]

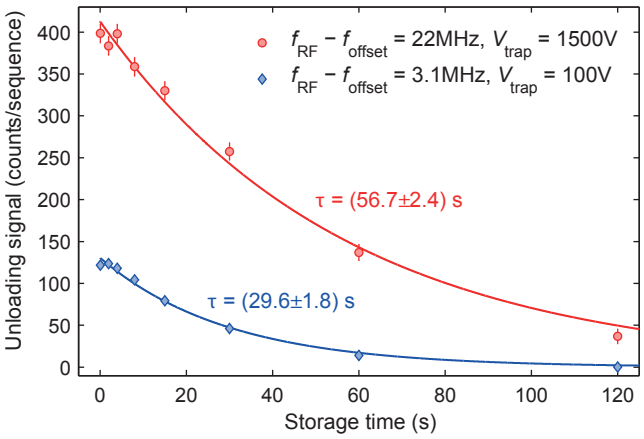

Figure 3.3: Lifetime of cooled molecules in the trap. Molecules are cooled (cooling stopped at the specified value of $f_{\mathrm{RF}} - f_{\mathrm{offset}}$), prepared in the state $|0;3,3,3\rangle$, and stored in the trap for a varying amount of time with the same trap voltage as was applied during the final cooling step (see Ch. 4). The more energetic ensemble has a median energy of $\sim 3/2 \cdot k_{\mathrm{B}} \cdot 2.5\,\mathrm{mK}$, whereas the colder one has $\sim 3/2 \cdot k_{\mathrm{B}} \cdot 0.4\,\mathrm{mK}$. The trap voltage is 15 times smaller for the colder ensemble. State detection for the states $|0;3,3,M\rangle$ was applied prior to storage. The time τ denotes the fitted exponential decay constant.

stored with the maximum trap voltage of $\pm 1500\,\mathrm{V}$. Then, a 1/e decay time of almost a minute is observed.

To obtain the data shown in Fig. 3.3, the molecules were cooled and prepared in the single rotational M sublevel and most strongly trapped state $|0;3,3,3\rangle$ prior to storage. However, state detection (Sec. 3.3.1) was also applied prior to storage allowing for redistribution of the rotational-state population during storage, e.g. by Majorana flips or rovibrational transitions induced by blackbody radiation. In fact, the timescale for rotational redistribution is faster than the timescale of trap loss for molecular ensembles which have been cooled substantially. This was investigated for the hotter of the two ensembles. If state detection is performed after storage, only molecules remaining trapped and staying in the same rotational state are considered in the measured signal. Then, the decay constant is $(32\pm1)\,\mathrm{s}$. Nevertheless, this does not imply any practical limitation. If needed, optical pumping to the initial state $|0;3,3,3\rangle$ (Sec. 3.3.3) can be applied continuously or every couple of seconds for a short time to keep the molecules in that state. If optical pumping is applied continuously and the results are compared to those in Fig. 3.3, the lifetime and the absolute molecule signal does not change for the hotter ensemble [decay constant $(61\pm3)\,\mathrm{s}$], whereas an even longer decay constant of $(45\pm3)\,\mathrm{s}$ is observed for the colder one.

All lifetimes quoted here were obtained with the standard ratio of offset and microstructure electrode voltages, $V_{\mathrm{offset}} = 0.05 \cdot V_{\mu}$. It was noted before that a non-zero offset field is crucial to obtain long lifetimes. A few measurements indicating this fact are found in Appendix A. Although no systematic investigation of molecule trapping times was performed, the data shown here demonstrates the good performance of the trap and indicates how much time is available to perform further experiments after cooling.

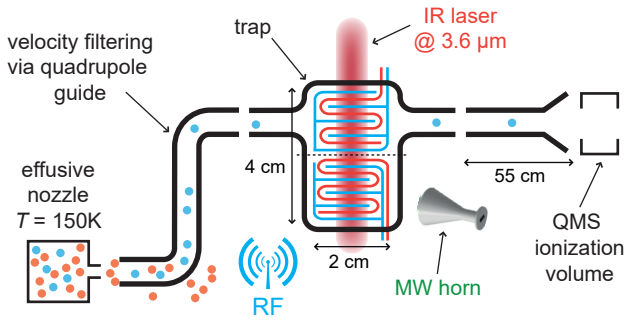

Figure 3.4: Schematic of the experimental setup. The slowest fraction of a thermal molecule sample is loaded from a liquid-nitrogen-cooled source operated at $T = 150\,\mathrm{K}$ into the trap via an electric quadrupole guide. For detection, the molecules are guided to a quadrupole mass spectrometer (QMS).

3.2 The experimental apparatus

In addition to a trap, a molecule source and detection method are also required. Opto-electrical Sisyphus cooling additionally demands IR, MW and RF radiation sources. In this section, the experimental setup and major changes to it are introduced, especially regarding a better data acquisition which dramatically improved the usability and the duty cycle of the setup, allowing more systematic measurements. The section concludes with a description of the building blocks of an experimental sequence.

A schematic of the experiment is shown in Fig. 3.4. The design of the vacuum system, the molecule source, and the initial installation of the trap are described in earlier theses [Mie10, Eng13]. The individual parts and experimental parameters are briefly reviewed below.

The molecule source. The source of formaldehyde molecules for our experiment consists of three parts: an installation to produce gaseous formaldehyde outside the main vacuum chamber, a nozzle with liquid-nitrogen precooling, and a velocity-filtering device inside the vacuum system.

Formaldehyde in the gas phase is produced as described in Ref. [Ibr13] by heating Paraformaldehyde powder[7] to a temperature around 85 °C. Unwanted water and polymer rests are removed from the gas by conducting it through a cold trap at a temperature of $\sim -80\,^{\circ}\mathrm{C}$. The temperature of the cold trap can be maintained with dry ice or more conveniently with an immersion cooler[8]. The reservoir of gaseous formaldehyde is filled by heating the Paraformaldehyde powder up for a few minutes to half an hour. It is large enough to maintain a constant flow of gas into the main vacuum chamber for a couple of days without refilling.

From the reservoir, the formaldehyde is injected into the vacuum system via a ceramic nozzle which is kept at a temperature of about 150 K for precooling of all degrees of freedom [Mie10]. The temperature is chosen as low as possible such that a sufficiently high vapor pressure of formaldehyde still allows continuous operation without ice formation at the nozzle.

[7] Paraformaldehyde, reagent grade, distributed by Sigma-Aldrich.
[8] The immersion cooler Julabo FT902 was used from the beginning of 2016.

From the thermal gas, molecules are velocity filtered and guided to the trap via a bent electric quadrupole guide [Ran03, Jun04] which selects molecules in low-field-seeking rotational states with a translational temperature $\lesssim 1\,\mathrm{K}$. The source is run with a rather small pressure of 4 Pa before the nozzle to ensure operation in the near-effusive regime with a small boosting parameter [Mot09a, Mot09b]. In this way, collisional loss of slow molecules on the way to the trap is suppressed while maintaining a sufficiently high flux of molecules into the trap.

The quadrupole guide influences both the velocity distribution and the rotational-state distribution of the molecular sample. For all experiments, the confining electric field strength of the input quadrupole guide is chosen as $\mathcal{E}_{\mathrm{load}} = 30\,\mathrm{kV/cm}$, smaller than the nominal confining field in the trap $\mathcal{E}_{\mathrm{trap}}$, to increase the guiding probability of slow molecules [Eng13]. This is useful since molecules with an energy close to the nominal trap depth are lost from the trap very fast[9] (see also Sec. 4.2.1). The applied field results in a transverse depth of the guide of $3/2 \cdot k_B \cdot 0.8\,\mathrm{K}$ and a transverse cutoff velocity of $v_{\mathrm{cut}} = 26\,\mathrm{m/s}$ for the state $|0;3,3,3\rangle$ of formaldehyde. The calculated rotational-state distribution of guided, low-field-seeking states in the electric quadrupole guide for the nozzle temperature $T = 150\,\mathrm{K}$ was already shown and discussed in Fig. 2.9. As rotational thermalization is very slow in our setup, the distribution in the trap is initially equal to the distribution in the guide[10].

The detector. For detection, molecules are unloaded from the trap via another quadrupole guide. A quadrupole mass spectrometer (QMS) serves as a time-resolved molecule counter. Although the detection efficiency of the QMS is quite low, on the order of 10^{-4} (see Table 4.4), this simple and robust device facilitates operation of the experimental setup with a high duty cycle. Due to the low detection efficiency, it is crucial to achieve experimental conditions with low background count rates. In particular this requires careful optimization of the QMS parameters and preparation, i.e. baking, of the ultrahigh vacuum chamber. Details on the commercial QMS and the employed settings are summarized in Appendix C.

The fully automated IR laser system. A continuous-wave optical parametric oscillator[11] (OPO) is used to drive vibrational transitions in formaldehyde around a wavelength of 3.6 µm. The OPO is stabilized to an optical frequency comb to sub-MHz precision.

In the course of this thesis a fully automated frequency tuning and stabilization system was developed. Additionally to precise stabilization, it permits fast frequency tuning over more than 60 GHz and an instant relock to the frequency comb, in total on a millisecond timescale. Considering the typical spontaneous vibrational decay rates of polyatomic molecules of 10–100 Hz, the system allows quasi-simultaneous driving of vibrational transitions from different rotational ground states with a single laser source which is very useful for optical pumping (see Sec. 3.3). Furthermore, complex sequences

[9] Detailed considerations on the voltages applied to the quadrupole guide and the trap for trap loading can be found in the appendix of Ref. [Eng13].

[10] Measured and calculated thermal rotational-state distributions of CH_3F in our setup were compared in Ref. [Glö15b] and were found to agree well.

[11] Lockheed Martin Aculight, Argos 2400-SF-15, module C with a wavelength range of 3.2–3.9 µm.

involving many different IR frequencies are executed automatically allowing for around-the-clock, remote-controlled operation of the laser. The complete laser system and the control of its frequency are explained in a detailed article [Pre17] and are therefore not elaborated further here. The developed system was already used before in experiments on rotational cooling of fluoromethane [Glö15a] where vibrational transitions spaced up to 12 GHz at a wavelength of 3.4 µm were driven quasi-simultaneously for optical pumping.

To illuminate a large fraction of the trap, an elliptically shaped IR beam enters the trapping volume between the capacitor plates (Fig. 3.1). About 200 mW of laser power is irradiated onto the vacuum chamber currently. As a result, the addressed vibrational transitions (Fig. 2.10) can be driven with a rate on the order of 1 kHz (see Sec. 3.3.2). The full power is used for optoelectrical Sisyphus cooling. For fast switching of the laser beam an acousto-optic modulator is installed. If a smaller driving rate is desired, the effective driving power is adjusted by lowering the duty cycle.

Microwaves for rotational-state manipulation. At present, we can generate MW with a frequency of $290 - 310$ GHz to couple the rotational states $J = 3$ and $J = 4$ as well as $355 - 375$ GHz to couple $J = 4$ and $J = 5$ in formaldehyde (Fig. 2.10). Up to about 20 mW of MW power can be generated in each frequency band with two independent amplifier-multiplier chains[12] which are seeded by a single MW frequency synthesizer[13]. The ability to switch between different frequencies in ~ 2 µs (currently limited by the control electronics) allows efficient coupling of many rotational M sublevels at essentially the same time, which is required for, e.g., rotational-state detection. The MW radiation is directed onto the trap, passing one microstructured capacitor plate, with horn antennas which are mounted outside the vacuum chamber. The radiation entering the vacuum chamber is polarized linearly, perpendicular to the electrode structure on the capacitor plate.

Incoupling of RF radiation. RF to couple neighboring M sublevels for cooling is applied directly to the contact leads of the trap microstructure. Lower frequencies are coupled in easily, whereas for frequencies higher than 1 GHz naturally occurring electric resonances are exploited [Eng13] (the high-voltage sources and the trap form a complex RC circuit). Due to these resonances, which occur in the entire spectrum, the applied RF power has to be optimized for every used frequency.

Improved data acquisition and automation. Due to the low detection efficiency of the QMS the measured signals are relatively small, even for large ensembles of trapped molecules. As will be seen in the next chapter, the full sequence for cooling of the molecular ensemble to about 400 µK takes approximately a minute owing to the relatively slow vibrational spontaneous decay rate (Sec. 2.1). To reduce the statistical error, the signals obtained from several repetitions of an experiment are averaged. Consequently, systematic investigations require long measurement times. On the other hand, optoelectrical Sisyphus cooling can be realized with a relatively simple setup which has been described above.

[12] Both chains are commercial models: Virginia Diodes, high-power AMC series.
[13] FEI-Elcom Tech, model UFS-1044, 0.5–18 GHz, 250 ns frequency switching time.

Step	Voltages (V)						
	loading guide		trap			unloading guide	
	V_{l1}^{Q}	V_{l2}^{Q}	V_{ring}	V_{μ}	V_{offset}	V_{u1}^{Q}	V_{u2}^{Q}
loading	750	3750	4500	$\pm$1500	$\pm$75	-2260	-2240
storage	-2250	-2250	4500	$\pm$1500	$\pm$75	-2250	-2250
unloading	-2250	-2250	$\frac{3}{2}\lvert V_{\mu}^{(u)}\rvert$	$\pm V_{\mu}^{(u)}$	$\frac{1}{5}V_{\mu}^{(u)}$	0	$V_{\mathrm{ring}}^{(u)}$

Table 3.1: Voltages applied to the quadrupole guides and the trap in a typical experimental sequence (e.g. for the measurements of Figs. 3.2 and 3.3). The two distinct voltages needed for the quadrupole guide (electrode distance 1 mm) are labeled with ($V_{x1,2}^{Q}$). Labels for trap voltages have been introduced in Sec. 3.1.1. The voltages applied during unloading $V^{(u)}$ are discussed in Sec. 4.2.4.

Therefore, the experimental apparatus has been optimized for robust, automated, and remote-controlled operation. Robust means that no part of the setup requires alignments or adjustments on a regular basis. Only the reservoirs of gaseous formaldehyde and liquid nitrogen had to be refilled every couple of days. Moreover, complex parameter scans, spectra, etc. can be performed in automated sequences without physical presence in the lab (see also the paragraph on the IR laser). Finally, data evaluation and definition of the experimental sequences can be accomplished remotely. This was realized with a new experimental control software developed within the first year of the thesis work. It greatly improved the data acquisition and allowed for systematic studies which had not been possible before. In fact, many of the measurements leading to the results presented in Ch. 4 and Ch. 5 could be performed without the need to touch any component of the apparatus for several weeks. This robustness also demonstrates that our method to prepare ultracold molecules can serve as a starting point for new, more complex experiments.

Structure of experimental sequences. All experimental sequences have a similar structure [Eng11]. Firstly, molecules are loaded into the trap for time t_{load} where optoelectrical Sisyphus cooling or another manipulation of the properties of the molecular ensemble inside the trap may already be performed. For most measurements in this thesis it holds $t_{\mathrm{load}} = 18\,\mathrm{s}$. Then, the loading quadrupole guide is switched off and the molecular ensemble is stored in the trap for a varying time t_{store} with further manipulation. Finally, the last guide segment is switched to a guiding configuration and molecules are stochastically unloaded from the trap and counted with the QMS, usually for $t_{\mathrm{unload}} = 12\,\mathrm{s}$. A few time-resolved unloading signals are shown later in Fig. 4.6. Often, the integrated molecule count constitutes the signal of interest. For efficient unloading of molecules from the trap to the detector, the voltages applied to the trap and the guide have to be adjusted to the kinetic energy and internal state of the molecules [Zep13]. This is discussed together with the experimental results in the next chapter (Sec. 4.2.4). Typical voltages used for a standard sequence with $V_{\mathrm{trap}} = \pm 1500\,\mathrm{V}$ are summarized in Table 3.1 (see Refs. [Zep13, Mie10, Eng13] for more details on the choice of voltage settings).

3.3 Internal-state control

The investigation and optimization of optoelectrical Sisyphus cooling greatly benefits from control over the internal molecular states: State detection allows the analysis of rotational-state distributions. Preparation of molecular ensembles in specific internal states is not only interesting in itself but also, e.g., increases control over systematic errors in measurements of the kinetic energy and gives better statistics for many characterization measurements.

The basic techniques for rotational-state detection [Glö15b] and state preparation via optical pumping [Glö15a] were already demonstrated in our experiment with fluoromethane. These methods and results are also described in Rosa Glöckner's thesis [Glö16]. Both state detection and preparation are implemented by manipulating the rotational states of molecules with MW and IR radiation.

In this section, the adaption of the techniques to formaldehyde and their advancement is described. In contrast to previous experiments, rotational-state detection (Sec. 3.3.1) now gives access to population in single J-state manifolds, e.g., $|0; J{=}3, 3, M\rangle$. Moreover, access to the population of all different single M sublevels of, e.g., the rotational state $|0; 3, 3, M\rangle$ enables diagnostic measurements which were not possible before, two of which are described in Sec. 3.3.2. Finally, optical pumping to single rotational states is described with a focus on the target state $|0; 3, 3, 3\rangle$ (Sec. 3.3.3).

3.3.1 Rotational-state detection of formaldehyde

The detector, the QMS, is not sensitive to the internal state of the molecules. For state detection a depletion technique is used: molecules populating certain sets of rotational states are selectively removed from the trap before unloading and detecting the remaining background of molecules. The difference between the total signal without removal and the background signal after removal constitutes the state-selective unloading signal. MW radiation is used to deplete molecules from the chosen states by coupling the states to untrapped states and therefore the method is called microwave depletion (MWD) [Glö15b]. The level scheme in Fig. 2.10 shows the sets of states which can currently be coupled with the available radiation sources.

Using MWD, state-sensitive depletion is performed by coupling trapped M sublevels of at least two neighboring rotational states J to the respective untrapped $M = 0$ states via $\Delta M = \pm 1$ rotational transitions as shown in Fig. 3.5(a). The population in the addressed states is mixed and molecules reaching the $M = 0$ states get lost almost immediately. Two considerations are important in assessing systematic errors and optimizing the process. First, depletion should be saturated to measure all molecules populating the target states. Second, the MWD pulse should not affect other sets of states. In the following, two cases are discussed: detection of population in a manifold of M sublevels, e.g., all trapped states $|0; 3, 3, M\rangle$, and detection of population in a single M sublevel, e.g., $|0; 3, 3, 3\rangle$.

Population in distinct J-states. State detection for a complete manifold of trapped M sublevels $|0; J, 3, M\rangle$ with $J = 3, 4$, or 5 is performed by depleting molecules from all M levels in different combinations of two or three adjacent sets $|0; J, 3, M\rangle$. For example, subtraction of the signal S remaining after depletion of $J = 3, 4, 5$ ($|K| = 3$),

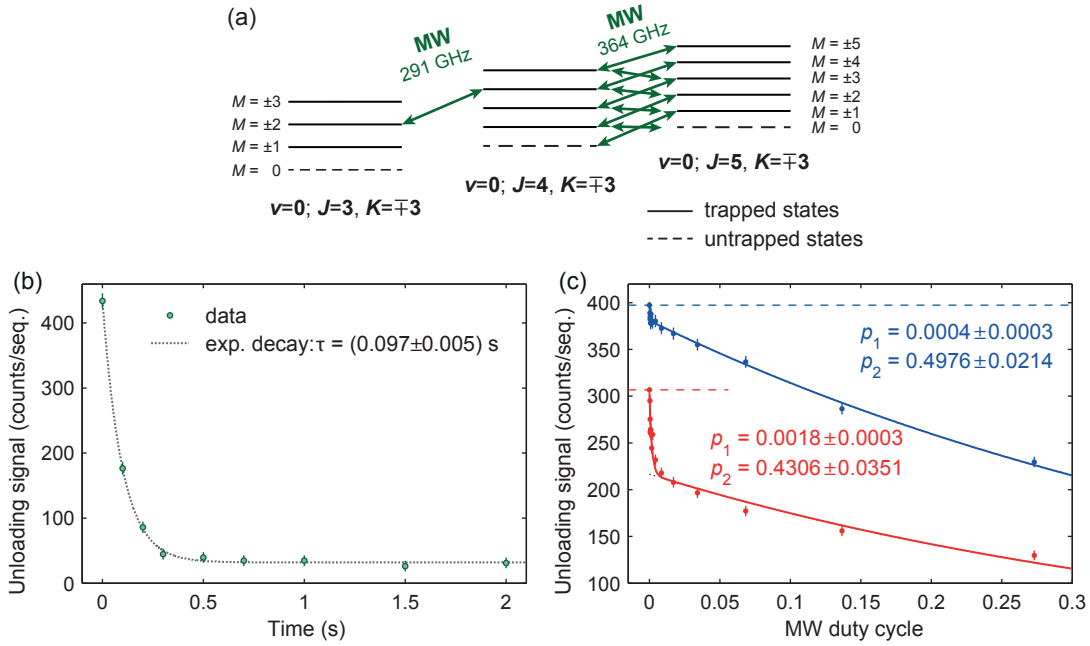

Figure 3.5: State detection of formaldehyde via microwave depletion (MWD). **(a)** Scheme for MWD. Selected or all M sublevels in adjacent rotational states J are coupled with $\Delta M = \pm 1$ transitions to untrapped states to remove molecules in specific rotational states from the trap and, thus, from the detected unloading signal. The population of a rotational state is measured by comparing depletion signals with and without the state being coupled to untrapped $M = 0$ states. **(b)** Saturation of the MWD pulse. The signal remaining after application of the MWD pulse coupling the states $J = 3, 4$ ($|K| = 3$), $S(J{\neq}\{3,4\})$ in the notation of the main text, is plotted as a function of pulse duration (where the storage time was always identical). A depletion time of 0.5–1 s suffices to obtain saturation. **(c)** Optimization of MW duty cycle for the detection of population in single M sublevels. A MWD pulse depleting the states $J = 4, 5$ ($|K| = 3$) is applied for 1 s together with a MW frequency with variable effective power coupling $|0;3,3,2\rangle \leftrightarrow |0;4,3,3\rangle$ to two distinct molecule ensembles (see text for further details). The measurements were conducted at a trap voltage $V_{\mathrm{trap}} = \pm 100\,\mathrm{V}$.

i.e. $S(J{\neq}\{3,4,5\})$, from the signal remaining after removal of $J = 4, 5$ ($|K| = 3$), i.e. $S(J{\neq}\{4,5\})$, yields the state-selected signal for $|0;3,3,M\rangle$, i.e. $S(J{=}3) = S(J{\neq}\{4,5\}) - S(J{\neq}\{3,4,5\})$. Obtaining the population of the states $|0;4,3,M\rangle$, $S(J{=}4)$, is slightly more sophisticated because four individual measurements are required: $S(J{=}4) = S_{\text{no depletion}} + S(J{\neq}\{3,4,5\}) - S(J{\neq}\{3,4\}) - S(J{\neq}\{4,5\})$. Note that the full information about the population distribution in the three J-states which are accessible with MW radiation at present can be acquired by measuring the four individual signals in the preceding equation.

As shown in Fig. 3.5(a), a MWD pulse consists of various frequencies which are all applied quasi-simultaneously with a single source by switching them quickly and cycling through all of them in typically 5 ms. The frequencies of the pulse are chosen to be resonant to the Stark shifted transitions in the offset electric field of the trap. The effective relative MW power is set by adjusting the duty cycle for each frequency. The total MW power for each amplifier-multiplier chain (Sec. 3.2) can be changed by tuning

the duty cycle or the output power of the chain. For fast depletion of entire manifolds of rotational states the full power and duty cycle are used and the relative duty cycles are adjusted such that all applied transitions are driven with roughly the same rate in the homogeneous-field region of the trap. The duty cycles are calculated considering the Clebsch-Gordan coefficient of the transition and Stark broadening (which is proportional to the differential Stark shift) [Eng13, Glö16].

The time needed for saturation of depletion is optimized by observing the unloading signal of molecules while scanning the duration of the MWD pulse. A representative measurement is shown in Fig. 3.5(b) where good saturation is reached after 0.5 s. The saturation timescale depends on the addressed sets of states and the trap voltage (higher trap voltage leads to larger Stark broadening and thus a longer depletion time). In most cases, the MWD pulse is saturated after 1 s of depletion, with 1/e decay times of the aforementioned signal ranging from 0.1 s as seen in Fig. 3.5(b) to 0.3 s (depletion of all states $J = 3, 4, 5$ ($|K| = 3$) at high trap voltage $V_{\mathrm{trap}} = \pm 1500\,\mathrm{V}$). Here, the high MW power provided by the amplifier-multiplier chains comes in handy. Fast depletion not only reduces the measurement time and losses due to the finite lifetime of the molecules in the trap, but also increases the measurement precision. This is the case because the rotational-state distribution of molecules in the trap changes on timescales of several seconds, as we have already seen in the discussion of the lifetime of molecules in the trap (Sec. 3.1.4). Note that the fitted exponential in the data plot only serves as a tool to determine the saturation time. Realistic theory curves can be obtained from rate models as discussed in Refs. [Glö15b, Glö16].

Resolving individual M-sublevels. To measure the population in a single M sublevel of a rotational state a slightly more careful optimization is necessary. Using MW, molecules residing in one M sublevel have to be removed without affecting molecules in other M levels of the same rotational J-state by unwanted driving of respective transitions in electric fields different from the offset field. For example, population in the state $|0; 3, 3, 3\rangle$ is detected as the difference of the following: the molecule signals after MWD for $J = 4, 5$ ($|K| = 3$) with the states $|0; 3, 3, 2\rangle$ and $|0; 3, 3, 1\rangle$ coupled to $|0; 4, 3, M\rangle$ via $\Delta M = +1$ transitions, and after MWD for the complete manifold $J = 3, 4, 5$ ($|K| = 3$). Hence, the effective power of the MW frequencies coupling $|0; 3, 3, 2\rangle \leftrightarrow |0; 4, 3, 3\rangle$ and $|0; 3, 3, 1\rangle \leftrightarrow |0; 4, 3, 2\rangle$ have to be optimized such that they do not affect molecules in $|0; 3, 3, 3\rangle$ while removing all molecules in the two states addressed intentionally.

A typical optimization measurement, which has to be performed for each critical MW frequency and desired trap voltage, is shown in Fig. 3.5(c). The effective power of the frequency applied to couple $|0; 3, 3, 2\rangle \leftrightarrow |0; 4, 3, 3\rangle$ is scanned by varying the duty cycle of this MW while MWD for the states $J = 4, 5$ ($|K| = 3$) is applied at the same time [Fig. 3.5(a) shows all components of this particular MWD pulse]. Data is taken for two experimental sequences: In the first, molecules are prepared in $|0; 3, 3, 3\rangle$ prior to depletion (higher data points). In the second, an additional RF pulse is applied to distribute molecules over the states $|0; 3, 3, M\rangle$ (lower lying data points). In both measurements, depletion occurs with two effective power scales. Resonant driving in the homogeneous offset electric field $\mathcal{E}_{\mathrm{offset}}$ removes molecules from the state $|0; 3, 3, 2\rangle$ already at low power levels as intended. Less probable, unintended driving in other electric fields affects molecules in states $|0; 3, 3, M{\neq}2\rangle$. Owing to the good homogeneity

of electric fields and the choice of transitions the separation of power scales is excellent. Consequently, depletion only from the desired state can be achieved with a small systematic error. The relative population of the state $|0;3,3,2\rangle$ for the two optimization sequences can be inferred from the amplitudes of the double-exponential fits. As expected, the share of molecules in $|0;3,3,2\rangle$ is much larger in the second sequence. Again, the fitted exponentials only serve as a tool to determine the saturation values and rate models can be used to deduce driving rates, etc. [Glö16].

The measured effective power scales for depletion can also be compared to quantitative expectations. The MW frequency is chosen such that it is resonant to the transition $|0;3,3,2\rangle \leftrightarrow |0;4,3,3\rangle$ for $\mathcal{E}_{\text{offset}}$. The same frequency is resonant to the transition $|0;3,3,3\rangle \leftrightarrow |0;4,3,4\rangle$, which has to be avoided, in an electric field three times smaller than $\mathcal{E}_{\text{offset}}$. From the simulated electric-field distribution one can extract that this field is 250 times less probable. Considering the Clebsch-Gordan coefficient and the larger differential Stark shift the unwanted transition is attenuated by another factor of two. Within the experimental uncertainty this estimate agrees with the observed separation of effective power scales.

Potentially, unwanted depletion could also occur via $\Delta M = -1$ or $\Delta M = 0$ transitions. Fortunately, these are suppressed even stronger. Particularly the former are a lot weaker than $\Delta M = +1$ transitions at a given electric field strength, e.g., $\mathcal{E}_{\text{offset}}$, due to small Clebsch-Gordan coefficients and large differential Stark shifts. For example, the $\Delta M = -1$ transition $|0;3,3,3\rangle \leftrightarrow |0;4,3,2\rangle$ would have to be driven with 80 times larger effective power than the $\Delta M = +1$ transition $|0;3,3,3\rangle \leftrightarrow |0;4,3,4\rangle$ to achieve equal transition rates. Unintended driving in other electric fields is further attenuated by the strongly peaked electric-field distribution. In addition to that, $\Delta M = 0$ transitions are suppressed even more by geometry arguments[14], which was verified with spectroscopic measurements. For these reasons, $\Delta M = +1$ transitions are used, if single M sublevels have to be resolved with MW.

State selectivity. So far, state selectivity was only considered within the manifold of the used $|K| = 3$ states. Additionally, transitions coupling states with other $K = K_A$ could lie close enough to play a role for depletion measurements [Glö16], especially when applied to uncooled molecules. In this thesis, state detection is applied to ensembles of cooled molecules. Molecules in states not addressed by the cooling scheme, i.e. not subject to continuous optical pumping to strongly trapped states, are almost completely lost from the trap during cooling because of too small lifetimes in the trap for uncooled molecules (Sec. 3.1.4) or depletion by the RF which is applied for Sisyphus cooling [Zep12, Glö15a]. Unintended driving of molecules in states with other $|K| = K_A \neq 3$ can therefore be neglected[15].

[14] The MW radiation is polarized linearly parallel to the capacitor plates of the trap and perpendicular to the electrodes of the microstructure such that it is not attenuated strongly by the grating-like microstructure. In the central trap region with electric field $\mathcal{E}_{\text{offset}}$, the electric field component in the direction of the MW polarization is negligible. In the outer regions it is weaker than the other components [Zep13]. Hence, $\Delta M = 0$ transitions cannot be driven efficiently.

[15] The transitions coupling the manifolds $|0;3,2,M\rangle \leftrightarrow |0;4,2,M\rangle$ (291.6 GHz) and $|0;4,4,M\rangle \leftrightarrow |0;5,4,M\rangle$ (364.1 GHz) are close to the transitions driven in this thesis [Cor80]. They should be considered if the goal is to measure accurate rotational-state distributions of uncooled molecules.

3.3.2 Diagnostic applications of internal state control

The improved control over the internal state can be utilized to investigate molecular properties or experimental performance. In this section two diagnostic measurements are presented as examples of improved experimental control. With one measurement, the IR driving rate in the trap is determined and the spontaneous vibrational decay rate from the used excited state is verified. In addition, IR spectroscopy on narrow $\Delta M = 0$ transitions yields the electric dipole moment in the excited vibrational state.

Measurement of IR driving and spontaneous vibrational decay rates. In earlier experiments with the electric trap, the rate with which molecular vibrational transitions were driven by the IR laser could not be determined very well [Eng13, Glö16]. Moreover, in contrast to before, an elliptical IR beam is now used to illuminate a large fraction of the trap volume with the available laser power. However, the exact amount of power seen by the molecules in the trap cannot be measured easily and the perimeter electrode might cause shadows. It is therefore of interest to verify good coupling of the IR laser to the trapped molecules. A method to measure the IR driving rate and the spontaneous decay rate via state-selective depletion after laser excitation for varying time is presented in the following.

In particular, a two-level system of the vibrational ground state $|0;3,3,3\rangle$ and the excited state $|1;3,3,2\rangle$ is considered. Initially, all molecules are prepared in $|0;3,3,3\rangle$ (see Sec. 3.3.3). Laser excitation and subsequent spontaneous decay leads to losses from this two-level system, because the electric-dipole selection rules also permit decay to the states $|0;3,3,2\rangle$, $|0;3,3,1\rangle$, and $|0;4,3,M\rangle$ with $M = 1,2,3$. Measuring the remaining population in $|0;3,3,3\rangle$ for different durations of the laser pulse and after a suitable waiting time to allow for complete decay of the excited state population gives access to the IR driving rate B and the spontaneous decay rate A. Here, the signal of molecules in $|0;3,3,3\rangle$ is measured as described in the preceding section.

Figure 3.6 shows the remaining signal of molecules in $|0;3,3,3\rangle$ for varying laser pulse duration Δt and the fit of a theory curve to the data. Rate equations of the usual form

$$\dot{P}_i = \sum_j M_{ij} P_j \tag{3.3}$$

are used to model the population P_i in a state i with the matrix M containing the coupling rates A and B. The state vector P_{state} for the considered two-level system and the two coupling matrices for laser driving, M_{driving}, and subsequent waiting and decay time, M_{decay}, are summarized in an inset of the figure. Assuming that all molecules populate $|0;3,3,3\rangle$ initially, the dependence on Δt is given by[16]

$$\begin{pmatrix} P_{|0;3,3,3\rangle}(\Delta t) \\ P_{|1;3,3,2\rangle}(\Delta t) \end{pmatrix} = \exp\left(M_{\text{decay}} \cdot 1\,\text{s}\right) \exp\left(M_{\text{driving}} \cdot \Delta t\right) \begin{pmatrix} 1 \\ 0 \end{pmatrix}. \tag{3.4}$$

Scaling $P_{|0;3,3,3\rangle}(\Delta t)$ to the measured signal for $\Delta t = 0$ and fitting it to the data yields the two desired rates (Fig. 3.6). Except for very short pulse durations, the agreement of theory and data is excellent. The small deviation for short driving (leftmost inset) might be due to a slightly inhomogeneous illumination of the trapping volume.

[16] In the experimental sequence, there is enough time for a complete decay of the excited state population. In the rate model this time is fixed to $1\,\text{s} \gg 1/A$, as specified after M_{decay} in the equation.

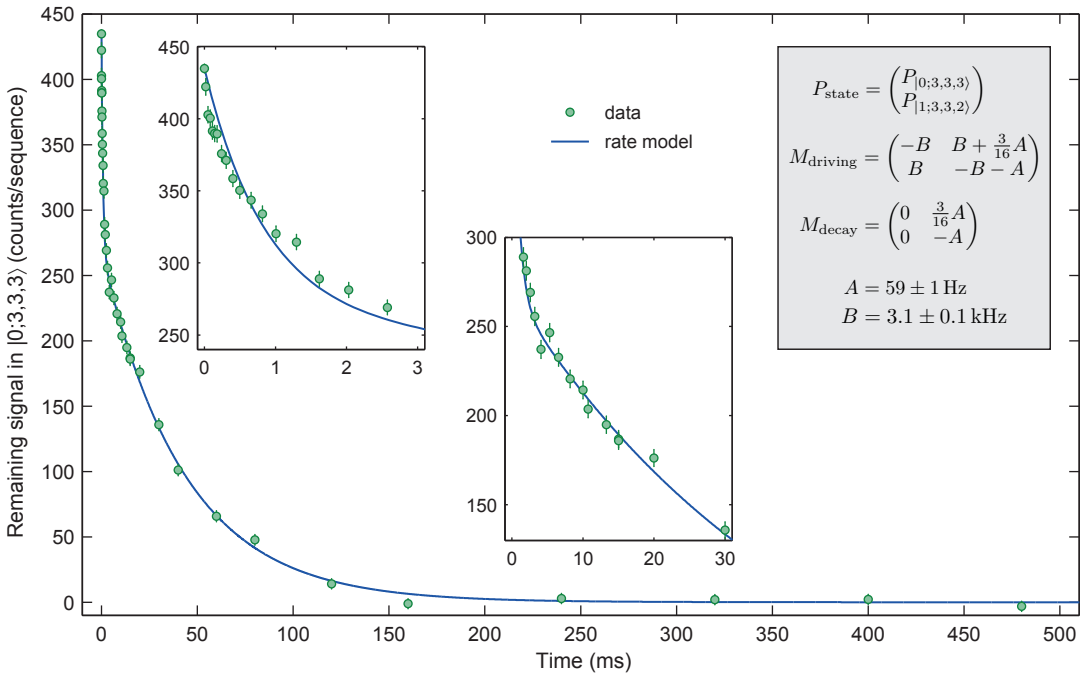

Figure 3.6: Measurement of the IR driving and spontaneous decay rates. Cooled molecules (final $f_{\mathrm{RF}} - f_{\mathrm{offset}} = 134\,\mathrm{MHz}$, kinetic energy $\sim 3/2 \cdot k_B \cdot 14\,\mathrm{mK}$) are prepared in $|0;3,3,3\rangle$ (see Sec. 3.3.3) and stored 1 s for laser excitation to $|1;3,3,2\rangle$ with pulse durations ranging from 16 µs to ∼1 s (IR frequency 83373136 MHz). From the excited state, spontaneous decay to the initial state or other ground states is possible. The state-selected signal of molecules remaining in $|0;3,3,3\rangle$ is plotted versus the length of the laser pulse (two insets show the same data for short times). A simple rate model (solid line) is fitted to the data to extract the spontaneous decay rate A from the excited vibrational state and the IR coupling rate B. The coupling matrices M for the rate model (see main text) and the corresponding state vector P_{state} are summarized together with the fit result in the rightmost inset. The kink in the curve (see central inset) is a signature of the two distinct rates involved in the depletion process. As a result, both rates can be deduced relatively precisely.

The measured driving rate of $B \approx 3\,\mathrm{kHz}$ holds if the laser frequency is chosen to be resonant to a molecular transition in the offset electric field as it was the case here. Then, the driving rate depends only weakly on the temperature of the molecules, because under normal conditions all molecules probe the offset field in the box-like potential. The data was taken with substantially cooled molecules (kinetic energy $\sim 3/2 \cdot k_B \cdot 14\,\mathrm{mK}$) and shows that even these are driven with a high rate by the IR laser. This is important for fast optical pumping to strongly trapped states during Sisyphus cooling. By detuning the laser slightly, one could probe driving rates in other regions of the box-like trapping potential. From the data, also the spontaneous decay rate $A = (59 \pm 1)\,\mathrm{Hz}$ from the state $|1;3,3,2\rangle$ is extracted. The measurement agrees with the value published in the HITRAN database [Rot13] for this state, 61.3 Hz.

Note that a similar measurement could be performed without control over single M sublevels by measuring loss from the entire set $|0;3,3,M\rangle$ after laser excitation via a $\Delta M = -1$ transition. Then, however, systematic effects arising from rotational-state

dependent trap unloading efficiencies would have to be considered—demanding more measurements and a more sophisticated evaluation to extract the same parameters.

Dipole moment in the $v_1 = 1$ excited state. The electric dipole moment which is used to calculate the Stark shift in linear approximation [Eq. (2.16)] depends on the internal molecular state. The dependence on the rotational state is on the 10^{-3} level for formaldehyde [Fab77] and can therefore be neglected in the experiments presented in this thesis. The dipole moment in the excited vibrational state, however, varies measurably from the ground state value. As a consequence of the distinct dipole moments, infrared transitions between identical rotational states in the ground and excited vibrational state have a non-zero differential Stark shift even in linear approximation. This shift needs to be considered in calculations of transition frequencies and can hence be used to determine the excited-state dipole moment.

Infrared transitions with equal rotational quanta in ground and excited state are best suited for this investigation, because they feature a small differential Stark shift and thus small Stark broadening in the electric trap. To perform accurate spectroscopy on a single of these transitions, namely $|0;3,3,3\rangle \leftrightarrow |1;3,3,3\rangle$, the molecular ensemble has to be prepared in a single M sublevel. The following sequence is used: Cooled molecules (kinetic energy $\sim 3/2 \cdot k_B \cdot 14\,\mathrm{mK}$) are optically pumped to $|0;3,3,3\rangle$ (see Sec. 3.3.3). Then, MWD is applied as explained in the preceding section to remove molecules which might be left in other states than $|0;3,3,3\rangle$ due to imperfect optical pumping [driven MW transitions are sketched in Fig. 3.7(a) as solid and dotted green lines]. Subsequently, molecules are excited with the IR laser to $|1;3,3,3\rangle$ (dotted red line in the figure) and MWD is applied again to measure only the molecules which are left in the initial state $|0;3,3,3\rangle$ after laser excitation and the following spontaneous decay. By scanning the frequency of the IR laser, the depletion spectrum plotted in Fig. 3.7(b) is recorded.

From the fitted detuning $\Delta f_{|0\leftrightarrow 1;3,3,3\rangle}$ of the spectral line from the known zero-field frequency, i.e. the differential Stark shift of the transition, the dipole moment in the excited state $\mu_{|1;3,3,3\rangle}$ is deduced via the relation

$$\Delta f_{|0\leftrightarrow 1;3,3,3\rangle} = \left(\mu_{|1;3,3,3\rangle} - \mu_{|0;3,3,3\rangle}\right) \frac{\mathcal{E}_{\mathrm{offset}}}{h} \frac{3}{4}. \tag{3.5}$$

Thereby a linear Stark shift is assumed ($\nu_s = -\frac{\mu\mathcal{E}}{h}\frac{KM}{J(J+1)}$, see Sec. 2.3) and the measured value of the offset electric field $\mathcal{E}_{\mathrm{offset}}$ (Sec. 3.1.3) is used. With the ground state dipole moment $\mu_{|0;3,3,3\rangle} = 2.33\,\mathrm{Debye}$ [Fab77] one finds $\mu_{|1;3,3,3\rangle} = 2.29\,\mathrm{Debye}$ for the excited vibrational state. As a consistency check, the same measurement[17] was performed for the transition $|0;3,3,2\rangle \leftrightarrow |1;3,3,2\rangle$. It is shown in Fig. 3.7(c) and, as expected, yields a differential Stark shift $\Delta f_{|0\leftrightarrow 1;3,3,2\rangle}$ a factor of $\Delta f_{|0\leftrightarrow 1;3,3,2\rangle}/\Delta f_{|0\leftrightarrow 1;3,3,3\rangle} = 0.64 \approx 2/3$ smaller. Note that the laser frequency is stabilized to a precision of only a couple of hundred kHz. This uncertainty is not included in the fit and, apart from the small dependence on the rotational state, is the second reason for specifying the dipole moment only with an accuracy of two digits.

[17] After preparation of the molecular ensemble in the state $|0;3,3,3\rangle$, the molecules were distributed over the states $|0;3,3,M\rangle$ with an RF pulse. As needed, MWD for the states $J = 3,4,5$ ($|K| = 3$) except for $|0;3,3,2\rangle$ leaves a reduced number of molecules prepared in the single rotational state $|0;3,3,2\rangle$ [the dashed transitions in Fig. 3.7(a) are driven instead of the dotted ones].

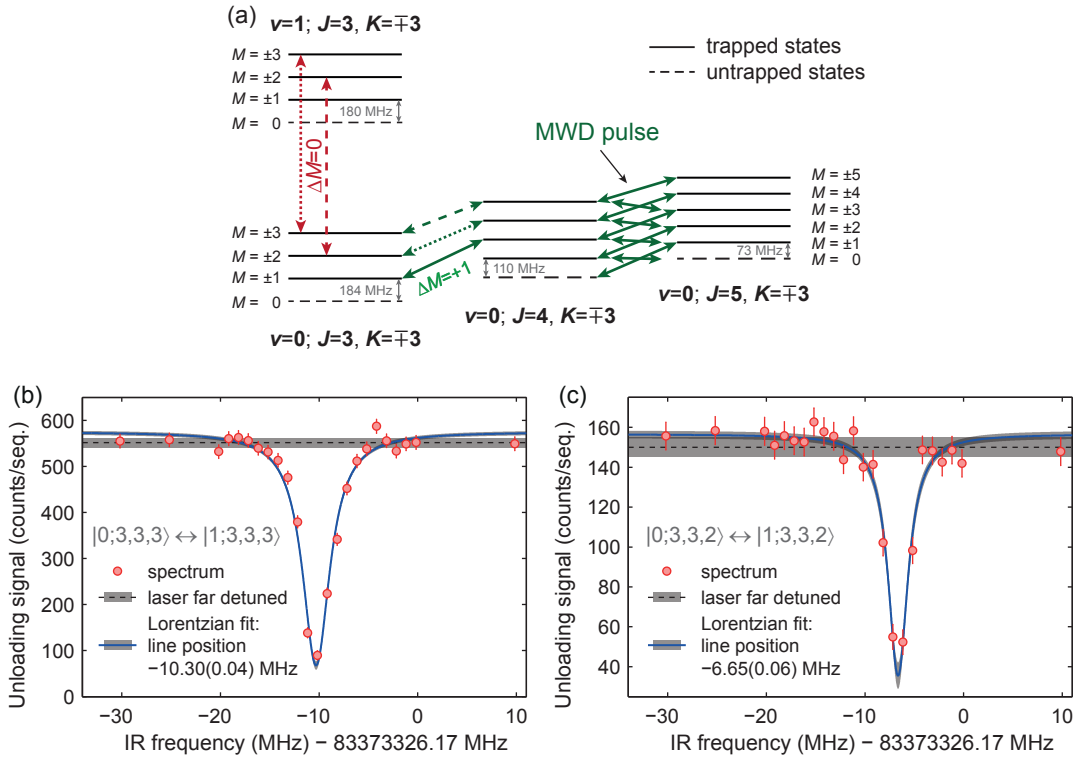

Figure 3.7: Determination of the dipole moment in the vibrational excited state $v_1 = 1$ via IR spectroscopy on state-selected molecules. (a) Level scheme with driven transitions for state-selection via MWD (green) and IR spectroscopy (red). Only the dotted or dashed transitions are applied (in addition to the solid ones) to obtain the data in (b) or (c), respectively. The splitting of M sublevels is specified for $V_{\mathrm{trap}} = \pm 1500\,\mathrm{V}$, the trap voltage used for spectroscopy. **(b), (c)** Depletion spectra of the transitions $|0;3,3,3\rangle \leftrightarrow |1;3,3,3\rangle$ and $|0;3,3,2\rangle \leftrightarrow |1;3,3,2\rangle$. Extremely low laser power is used to obtain narrow spectra of the two transitions with equal rotational quanta. The error bars and the shaded regions specify the statistical error. The uncertainty of the stabilized laser frequency is a couple of hundred kHz and is not included in the fit.

With the deduced dipole moment in the excited vibrational state, 2.29 Debye, Stark-shifted IR transition frequencies in the regime of linear Stark shifts can now be calculated accurately. The effect of the reduced excited state dipole moment on optical pumping of the trapped molecules is the following: By choosing the IR frequency, one can select from which M sublevel of a rotational ground state IR transitions are driven with the highest rate. For example, for Sisyphus cooling both $\Delta M = +1$ transitions from states $|0;3,3,M{<}3\rangle$ have to be driven (Fig. 2.12). For the offset electric field at a trap voltage of $V_{\mathrm{trap}} = \pm 1500\,\mathrm{V}$ the two transitions $|0;3,3,2\rangle \leftrightarrow |1;3,3,3\rangle$ and $|0;3,3,1\rangle \leftrightarrow |1;3,3,2\rangle$ are spaced 3.4 MHz. This compares to a FWHM of 5.6 MHz of the peaked distribution of Stark shifts obtained from the electric-field distribution for this trap voltage. As only one IR frequency resonant to the first transition is applied, the second one is driven with a slightly reduced rate in the flank of the peak of the distribution. Due to the high IR driving rates in the low-field region of the trap this detail does not restrict optoelectrical Sisyphus cooling. It should, however, be taken into account in detailed rate models of the optical pumping process.

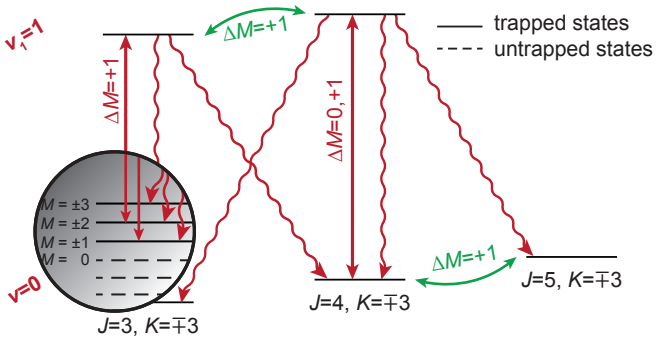

Figure 3.8: Optical pumping scheme for preparation of molecules in the single M sublevel $|0;3,3,3\rangle$. The M levels are only sketched for $J = 3$. Three IR frequencies are applied quasi-simultaneously with a single laser by cycling through them every 25 ms. In total, seven $\Delta M = +1$ MW transitions are driven (reduced duty cycle, 10 ms total cycle duration including waiting time). Solid arrows represent the driven transitions, whereas wavy arrows indicate the spontaneous decay channels.

3.3.3 Rotational-state preparation via optical pumping

The preparation of the molecular ensemble in the single rotational state $|0;3,3,3\rangle$ was already used for some of the measurements presented previously. It will also be important for the correct determination of the molecular kinetic energy after cooling (Secs. 4.1 and 4.3). Similar to Sisyphus cooling and previous work [Glö15a], optical pumping via the vibrational mode in conjunction with MW coupling of rotational states is used for preparation of molecules in specific rotational states. In this section, the process is finally explained, using results obtained in previous sections. First, the optical pumping scheme is introduced. Then, we show how losses to untrapped states can be avoided with a correct choice of parameters.

Optical pumping to $|0;3,3,3\rangle$. The driven transitions are sketched in Fig. 3.8. In particular, three IR transitions are addressed quasi-simultaneously[18]: $|0;3,3,M\rangle \leftrightarrow |1;3,3,M{+}1\rangle$, $|0;4,3,M\rangle \leftrightarrow |1;4,3,M{+}1\rangle$, and (with reduced duty cycle) $|0;4,3,M\rangle \leftrightarrow |1;4,3,M\rangle$. To achieve this, the IR frequency is quickly ramped between the three mentioned transitions every 10 ms, 10 ms, and 5 ms, respectively (Sec. 3.2 and Ref. [Pre17]). For all three cases, the IR frequencies are calculated to be resonant to the specified transition with the highest possible value of M (in the offset electric field). Nevertheless, the remaining transitions addressing lower M are also driven by the same laser frequency with a reduced rate (Sec. 3.3.2). Furthermore, the levels $|0;4,3,M{>}0\rangle \leftrightarrow |0;5,3,M{+}1\rangle$ are coupled in the ground state and $|1;3,3,M{>}0\rangle \leftrightarrow |1;4,3,M{+}1\rangle$ in the vibrational excited state with MW (see Fig. 2.10 for transition frequencies). Here, the MW in the excited state are applied to increase the decay probability to the $J = 3$ states [Glö16]. As a result, the state $|0;3,3,3\rangle$ is the only dark state in the manifold of addressed vibrational ground states $|0;J,3,M\rangle$ for $J = 3,4,5$. With this scheme, 1.5 s of optical pumping suffice to accumulate cooled molecules in the target state with high efficiency.

[18] The rate of switching between the different IR frequencies is on the order of or larger than the spontaneous vibrational decay rate.

Avoiding losses to untrapped states. Losses during state preparation can occur, if the applied IR and MW frequencies drive unwanted transitions out of the target dark state or to untrapped states, which come into resonance when molecules probe electric fields in the wings of the electric-field distribution in the trap. To minimize these losses, the molecular structure as well as the influence of the electric-field distribution and the temperature of the molecules have to be considered.

Unwanted driving of rotational (MW) transitions is eliminated by choosing only $\Delta M = +1$ transitions, which generally possess large Clebsch-Gordan coefficients and small Stark broadening, and adjusting the effective driving power (see also Sec. 3.3.1 and Ref. [Glö15b]). In the described scheme, driving from the target dark state $|0;3,3,3\rangle$ to any unwanted state is further reduced by not applying MW to any transitions connected to the states $|0;3,3,M\rangle$. Therefore, the MW couplings between $J = 3$ and $J = 4$ are applied in the excited state, detuned $\sim 490\,\mathrm{MHz}$ from the ground-state frequencies.

For formaldehyde, the vibrational transitions have to be examined more closely because the Q-branch IR transitions of the v_1 mode lie close together in frequency space. In particular, the zero-field frequency of the $\Delta J = 0$ IR transition from $|0;4,3,M\rangle$ is only 493 MHz red-detuned from the transition from $|0;3,3,M\rangle$ (Fig. 2.10 and Table 2.3). Consequently, intentional driving of the $\Delta M = +1$ transitions from the states $|0;4,3,M\rangle$ in the offset electric field can lead to unwanted driving of the $\Delta M = -1$ transitions from the states $|0;3,3,M\rangle$ in higher electric fields in the edge region of the trap. Potentially, this results in loss from the target state and to untrapped states and is investigated in Fig. 3.9. The plot displays calculated Stark shifted transition frequencies for two trap voltages in the lower panel and the spectroscopic verification for the higher trap voltage in the upper panel. As explained in the figure caption, the described loss channel disappears completely for colder molecules. It can be suppressed for hotter molecules by driving the $J = 4$ transitions with a lower effective power. Further, losses are less probable at low trap voltages. Therefore, optical pumping is usually performed at $V_{\mathrm{trap}} = \pm 400\,\mathrm{V}$ or $V_{\mathrm{trap}} = \pm 100\,\mathrm{V}$, even for molecules with intermediate temperatures. Note that unintended driving does not occur during optoelectrical Sisyphus cooling which relies on driving the transitions $|0;3,3,M\rangle \leftrightarrow |1;3,3,M{+}1\rangle$ because there are no other relevant transitions close to and blue detuned from the driven one.

Efficiency and losses. The efficiency of state preparation can be defined as the fraction of molecules populating the target state after optical pumping with respect to all molecules in the addressed states $|0;J,3,M\rangle$ for $J = 3,4,5$. For hotter molecules it is difficult to reach efficiencies close to one owing to the loss channel discussed above. For the coldest molecule ensemble (kinetic energy $\sim 3/2 \cdot k_B \cdot 0.4\,\mathrm{mK}$) the efficiency is close to 90 % for 1.5 s of optical pumping at $V_{\mathrm{trap}} = \pm 100\,\mathrm{V}$. A longer pumping time does not increase this value, most probably because Majorana flips to less strongly trapped states occur at a slow rate (cf. Secs. 3.1.4 and 4.3.5). With these parameters, losses to untrapped states of $(2 \pm 1)\,\%$ are negligible. The measured rotational-state distribution for this sequence is discussed with the cooling results in Sec. 4.3.5. Despite these imperfections molecule ensembles populating a specific internal state with high purity can be obtained even for hotter molecules by combining optical pumping with state-selective depletion. This was discussed in Sec. 3.3.1 and was utilized for obtaining the spectrum in Fig. 3.7(c).

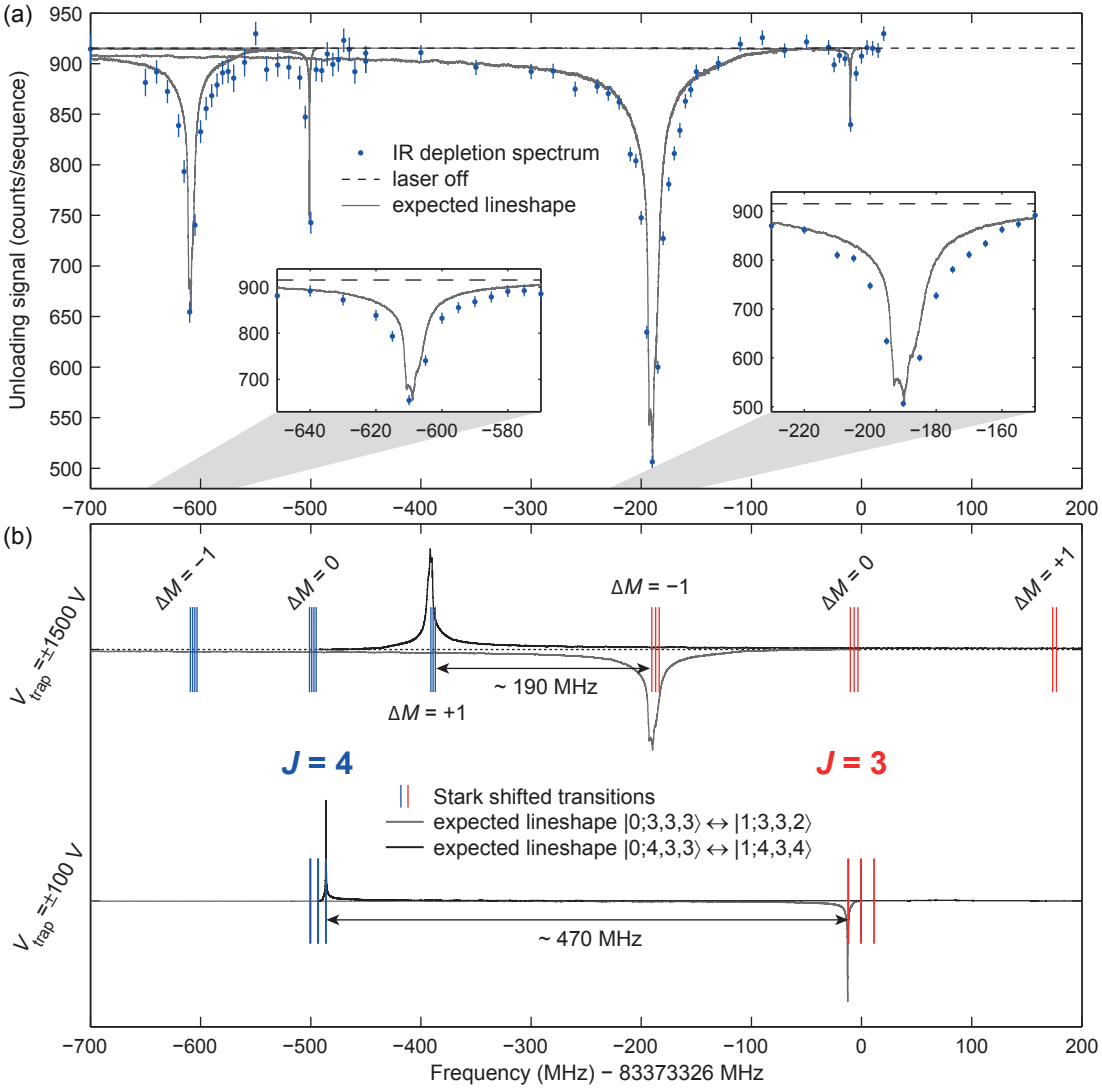

Figure 3.9: Stark shifted $\Delta J = 0$ vibrational transitions addressing the states $|0;3,3,M\rangle$ and $|0;4,3,M\rangle$. **(a)** IR depletion spectrum showing the corresponding $\Delta M = -1$ and $\Delta M = 0$ transitions, measured at $V_{\mathrm{trap}} = \pm 1500\,\mathrm{V}$. Laser excitation via these transitions and subsequent spontaneous decay leads to population transfer to untrapped states and, thus, a reduced signal of molecules at resonance. The expected line shapes (vertically scaled to the data) are calculated from the simulated electric-field distribution (Sec. 3.1.3) and the differential Stark shift (with the excited-state electric dipole moment determined in the previous section). Here, the measured spectrum is broader than the simulated one, most probably due to saturation effects. $\Delta M = +1$ transitions are not observed because driving of these does not cause losses. **(b)** Stark shifted transition frequencies for high trap voltage, $V_{\mathrm{trap}} = \pm 1500\,\mathrm{V}$, and low trap voltage, $V_{\mathrm{trap}} = \pm 100\,\mathrm{V}$. Additionally, the expected line shapes are plotted for the $\Delta M = +1$ transition $|0;4,3,3\rangle \leftrightarrow |1;4,3,4\rangle$ (upward) needed for state preparation and the $\Delta M = -1$ transition $|0;3,3,3\rangle \leftrightarrow |1;3,3,2\rangle$ (downward) which has to be avoided. Evidently, parasitic driving of the unwanted $\Delta M = -1$ transition is much more likely at higher trap voltage. If the kinetic energy of the molecules is low enough ($\ll 3/2 \cdot k_B \cdot 18\,\mathrm{mK}$ for $V_{\mathrm{trap}} = \pm 1500\,\mathrm{V}$, $\ll 3/2 \cdot k_B \cdot 45\,\mathrm{mK}$ for $V_{\mathrm{trap}} = \pm 100\,\mathrm{V}$), molecules no longer reach the high electric-field strengths where unwanted driving can occur.

Optical pumping to other states. Although we focused on the state $|0;3,3,3\rangle$, molecules can also be prepared in other target rotational states with this method. To date, this works with good efficiency only when choosing the highest M sublevel as a target state, $|0;J,3,M{=}J\rangle$. In principle, the distinct dipole moments in the ground and excited vibrational states could also allow optical pumping to other states.

3.4 Summary

In this chapter, the experimental apparatus and important techniques were introduced. Both the setup and experimental methods have been adapted to formaldehyde and improved substantially over previous results. Characterization measurements of the electric trap with formaldehyde showed increased performance of the refined trap. In particular, the homogeneity of the offset electric field of the box-like trapping potential has been improved dramatically. Moreover, record storage times were observed for cooled molecules held in our electric trap. Thus, the 1/e trap decay time can be as long as one minute.

In addition, we presented the key parts of the experimental setup. The setup is robust, remote-controllable and can be operated with a high duty cycle essentially around-the-clock. Together with the results of Ch. 4 this shows that the method of optoelectrical Sisyphus cooling can serve as a starting point for more complicated experiments.

In the last section, precise control over the rotational state of the formaldehyde molecules was demonstrated. It is achieved with optical pumping and state-selective depletion methods. Especially for electrically trapped molecules, rotational-state control is important because the trapping potentials strongly depend on the rotational state the molecules populate. Hence, these techniques greatly improve control over systematic effects caused by electric trapping. Moreover, two applications of improved rotational-state control were outlined, with one measurement yielding the electric dipole moment in the $v_1 = 1$ excited vibrational state, $\mu_{(v_1=1)} = 2.29\,\mathrm{Debye}$, allowing for a precise calculation of Stark-shifted IR transition frequencies. It will become evident in the next chapter that the presented changes to the setup and the advancement of the experimental methods were crucial to allowing optoelectrical cooling of formaldehyde to submillikelvin temperatures.

4 Sisyphus cooling to submillikelvin temperatures

The main experimental result of this thesis is the demonstration of direct cooling of electrically trapped, gaseous formaldehyde (H_2CO) to the microkelvin temperature regime. The temperature was reduced by a factor of thousand and the phase-space density was increased by a factor of $\sim 10^4$ to produce an ensemble of 300,000 molecules with a temperature of about 420 µK. Additionally, the molecules populate a single rotational state with more than 80 % purity. With these results, our group was among the first two to show direct cooling of molecules to below 1 mK (see Ch. 1). To date, our ensembles of cooled formaldehyde molecules are still the largest ensembles of ultracold ($T < 1\,\mathrm{mK}$) molecules produced so far in laboratories.

The most important results are published in a short article [Pre16] and some parts of this chapter are presented in close relation to the paper. Here, optoelectrical Sisyphus cooling of formaldehyde is demonstrated in more detail and with additional experimental data. Especially the experimental sequence, optimization procedures, and the method to measure the kinetic energy of the trapped molecules are discussed thoroughly. The latter requires the asymmetric rotor structure of formaldehyde to be taken into account, as was already discussed in Ch. 2. After the presentation of the key results, current technical limitations and possible solutions are summarized.

The chapter is structured as follows. Firstly, the method to measure the kinetic energy of the molecular ensemble, RF knife-edge filters, is explained in Sec. 4.1. This tool was used frequently for characterization measurements and the development of the experimental sequence. Then, the sequence is described in Sec. 4.2 with an emphasis on aspects which are different from the initial proof-of-principle demonstration of Sisyphus cooling of fluoromethane [Zep12, Zep13, Eng13, Pre12]. The molecular ensemble produced by optoelectrical Sisyphus cooling is characterized in Sec. 4.3. The experimental data yields the key numbers mentioned above. Additionally, we discuss the influence of systematic effects originating in the trapping potential on the measured kinetic energy. Finally, the obtained results and current technical limitations as well as possible solutions are summarized in Sec. 4.4.

4.1 Measuring the kinetic energy of trapped molecules

For any demonstration of cooling, the molecular kinetic energy or temperature has to be measured. To minimize systematic effects arising from unloading the molecules from the trap (see Sec. 4.2.4), the method should preferably probe the molecules in the electric trap. The tool of choice is a strong RF field which acts as a knife-edge filter and only eliminates hotter molecules from the trap. It can be used to measure energy distributions of trapped molecules or select molecules by energy.

As the energy threshold for depletion by RF radiation with a specific frequency

depends on the internal molecular state, the ensemble is prepared in a defined rotational state (or set of states) before application of the knife-edge filter. For the final energy measurement and many optimization procedures molecules are optically pumped to the state $|0;3,3,3\rangle$ as explained in Sec. 3.3.3. Accordingly, the RF knife is discussed in relation to the rotational states $|0;3,3,M\rangle$.

The principle of the knife-edge filter and its optimization for asymmetric rotor molecules is introduced in Sec. 4.1.1. Then, the unwanted K-flip transitions which are induced in asymmetric rotor molecules by very strong RF fields (Sec. 2.3.3) are experimentally investigated in Sec. 4.1.2. In the last Sec. 4.1.3, the terms total energy, kinetic energy and offset potential energy are differentiated for further use.

4.1.1 RF knife-edge filters for asymmetric rotor molecules

In this section, two depletion processes caused by the RF knife are distinguished. The use of RF radiation as a tool to measure the energy of a molecular ensemble in the trap relies on the fact that RF can couple successive M sublevels of rotational states and induce $\Delta M = -1$, $\Delta K = 0$ transitions to untrapped states within the low-field-seeking manifold of states. Molecules reaching the $M = 0$ states are lost from the trap almost immediately. The frequency f_{knife} can be chosen such that molecules need a certain total energy to reach the regions of high electric field where the RF is resonant. This is illustrated in the left part of Fig. 4.1(a). As all molecules populate the same internal state $|0;3,3,3\rangle$ initially, a sufficiently strong RF pulse truncates the energy distribution of the ensemble at a defined value by depleting all hotter molecules from the trap.

Due to formaldehyde being a slightly asymmetric rotor (Sec. 2.2) and the small but not negligible inversion splitting $\Delta = 0.65\,\text{MHz}$ of the states $|0;3,3,M\rangle$ (Sec. 2.4), a second depletion process can occur. It is caused by the strongly suppressed K-flip transitions (discussed in Sec. 2.3.3) which bring molecules directly from low-field-seeking to high-field-seeking states via $\mp K$ to $\pm K$ transitions (with $\Delta M = 0, \pm 1$). For a given frequency f_{knife}, these unwanted K-flip transitions occur in lower electric fields where f_{knife} equals approximately five or six times the splitting of M sublevels [Fig. 4.1(a)]. Therefore, this process commonly depletes molecules independent of their energy. We have seen in the theoretical discussion that the matrix elements for the unwanted K-flip transitions are suppressed by at least a factor of 10^2 for our experimental parameters. However, for the knife-edge filters large RF power is applied to saturate the filtering process in a short time. Consequently, K-flips have to be taken into account during the experimental optimization of the RF knife.

The largely different matrix elements for the wanted transitions of the RF knife and the unwanted K-flip transitions manifest themselves, when the RF power used for the knife-edge filter is scanned. Such a power scan is performed for two experimental sequences producing molecular ensembles with about a factor of four difference in kinetic energy [cooling stopped at $f_{\text{RF}} - f_{\text{offset}} = 20\,\text{MHz}$ or $3.1\,\text{MHz}$, corresponding to a median kinetic energy of $\sim 3/2 \cdot k_B \cdot 1.8\,\text{mK}$ or $0.4\,\text{mK}$, see Fig. 4.1(b)]. A knife-edge filter with $f_{\text{knife}} = 16.5\,\text{MHz}$ is applied at a trap voltage of $V_{\text{trap}} = \pm 100\,\text{V}$ ($f_{\text{offset}} = 11.9\,\text{MHz}$). The hotter ensemble is depleted completely with low power filters. In the colder ensemble, depletion of molecules occurs with two power scales. The rapid decay at low powers is due to the RF knife. Depletion at high RF power, on the other hand, is caused by K-flip transitions.

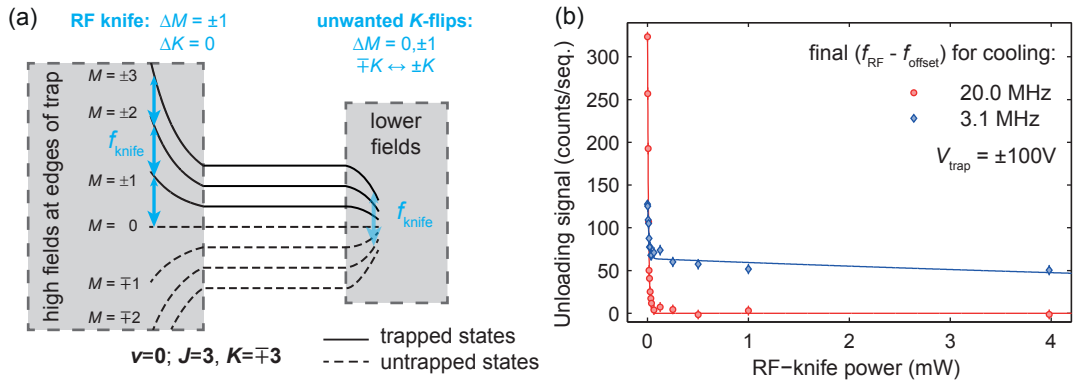

Figure 4.1: RF knife-edge filters. **(a)** Scheme of the Stark shifted energy levels of the states $|0;3,3,M\rangle$ for different electric-field regions in the trap. RF applied with a frequency f_{knife} induces strongly allowed transitions in the edge region of the trap, quickly depleting hot molecules which are able to reach the higher electric fields. This process acts as the RF knife. Additionally, K-flip transitions can occur in regions with lower electric field leading to unwanted depletion of hot *and* cold molecules. The latter process is forbidden in first approximation and thus requires dramatically larger RF power. **(b)** Scan of the RF power applied as a knife-edge filter ($f_{\text{knife}} = 16.5\,\text{MHz}$, 1 s depletion time) for two cooling sequences producing molecular ensembles with different energies. The molecules were prepared in $|0;3,3,3\rangle$ prior to depletion. The data for the hotter ensemble is well-fitted with an exponential model as shown because all molecules are depleted by the RF knife. The scan for the colder ensemble is fitted with a double-exponential model to account for the additional decay of signal at high RF powers due to induced K-flip transitions.

Optimization procedure. The following recipe is used to chose an adequate RF power for energy-dependent filtering without significant depletion via K-flips. For every desired combination of knife frequency f_{knife} and trap voltage an RF power scan[1] is performed with a molecular ensemble having a suitable energy to allow both depletion processes to be resolved. The appropriate power for a knife-edge filter is then chosen such that the low-power process is clearly saturated (power at least five times the fitted decay constant) but depletion due to K-flips is still suppressed. From the calculations of Sec. 2.3.3 we know that the two energy scales differ by at least two orders of magnitude for our experimental parameters, as will be demonstrated more thoroughly in the next section. Note again that during Sisyphus cooling K-flip transitions are not an issue, because the RF is applied with dramatically reduced power.

4.1.2 Experimental investigation of K-flip RF transitions

In this section, K-flip transitions in formaldehyde are investigated experimentally in more detail. A closer look is instructive for several reasons. Foremost, the observation of RF depletion with two power scales was a mystery initially because it contradicts the intuitive notion that the chosen states of formaldehyde are like symmetric-top rotational states for which this behavior is not anticipated. Of course, the effect, caused by the finite inversion splitting of the states, is expected, as was demonstrated theo-

[1] For $f_{\text{knife}} \lessapprox 500\,\text{MHz}$ a depletion time of 1 s suffices. For much higher frequencies more time is required because the RF is coupled into the system less efficiently.

retically in Sec. 2.3.3. Thus, depletion via K-flips is—at the moment—the only aspect of the experiment where the asymmetric-rotor structure of formaldehyde manifests itself. Finally, a systematic investigation of the two depletion processes is a test of the simple analytical model presented in Sec. 2.3 for inversion-doublet states in a static electric field. Confirmation of this model also supports the conclusions drawn from it for Sisyphus cooling, namely that K-flip transitions can be ignored during cooling.

Depletion due to the high-power K-flip process should happen at an electric field where the knife frequency f_{knife} equals five or six times the splitting of M sublevels. Consequently, the process should start at lower power levels, if the resonance condition is fulfilled in the offset electric field because this field is much more probable than lower or higher electric fields owing to the strongly peaked electric-field distribution (Sec. 3.1.3). The hypothesis was tested by performing RF power scans resolving both depletion processes with a fixed f_{knife} while changing the trap voltage V_{trap}. The measurement is shown, explained, and compared to calculations in Fig. 4.2.

The data in Fig. 4.2(a) clearly reveals the influence of the electric-field distribution on the fitted power constants and, thus, the observed transition probabilities. In particular, the constants of the high-power, K-flip process vary significantly. In contrast, the low-power, $\Delta K = 0$ RF knife process happens in the high-field region and, consequently, the variation with trap voltage is almost negligible. The fitted relative RF power constants directly relate to the relative transition rates of the two processes and can therefore be compared with theory. Towards this end, the relative transition probabilities obtained with the analytical model considering pairs of inversion-doublet states (Sec. 2.3.3, Fig. 2.8) have to be weighted with the occurrence probability of the electric-field strength where the transition is resonant. The electric-field probabilities are extracted from the measured[2] (and scaled) electric-field distribution for $V_{\text{trap}} = \pm 100\,\text{V}$. Figure 4.2(c) demonstrates that RF depletion in the trap is well-understood with this model and the calculated relative transition probabilities match experimental observations remarkably well[3]. Hence, the data supports the given explanation that at high power, K-flip depletion is occurring. It also shows that for the relevant $|0;3,3,M\rangle$ states the power scales can be clearly distinguished and are separated by about a factor of 100, if the K-flip process is not resonant in the offset electric field. For RF-knife measurements the frequency f_{knife} is usually chosen such that this condition is fulfilled.

The separation factor depends on the rotational state, i.e. the inversion splitting, and on the applied electrostatic field, as discussed in Sec. 2.3. Both effects were observed in experiments. For example, K-flip transitions are stronger and the separation factor is smaller for the states $|0;4,3,M\rangle$ because the inversion splitting is a factor of seven larger. Yet, the separation factor is much larger for higher trap voltages.

[2] For the relevant small trap voltages, the measured distribution deviates slightly from the simulated one as will be discussed in Sec. 4.2.3. To model the RF depletion data correctly, the measured distribution has to be used (see also the next footnote).

[3] The remaining discrepancy is most probably explained by the following effect. The RF-knife process is resonant in higher electric fields. Moreover, the energy of the molecular ensemble is chosen such that not all molecules reach the high electric fields where the RF knife is resonant. Otherwise, the K-flip process could not have been resolved. Therefore, the probability that molecules actually probe the high electric field is slightly reduced due to their limited kinetic energy. One could account for this effect by measuring the electric-field distribution with a molecule sample of equal energy and for every trap voltage configuration. However, the electric-field distribution used for the calculation was only measured once, with molecules having about twice the kinetic energy.

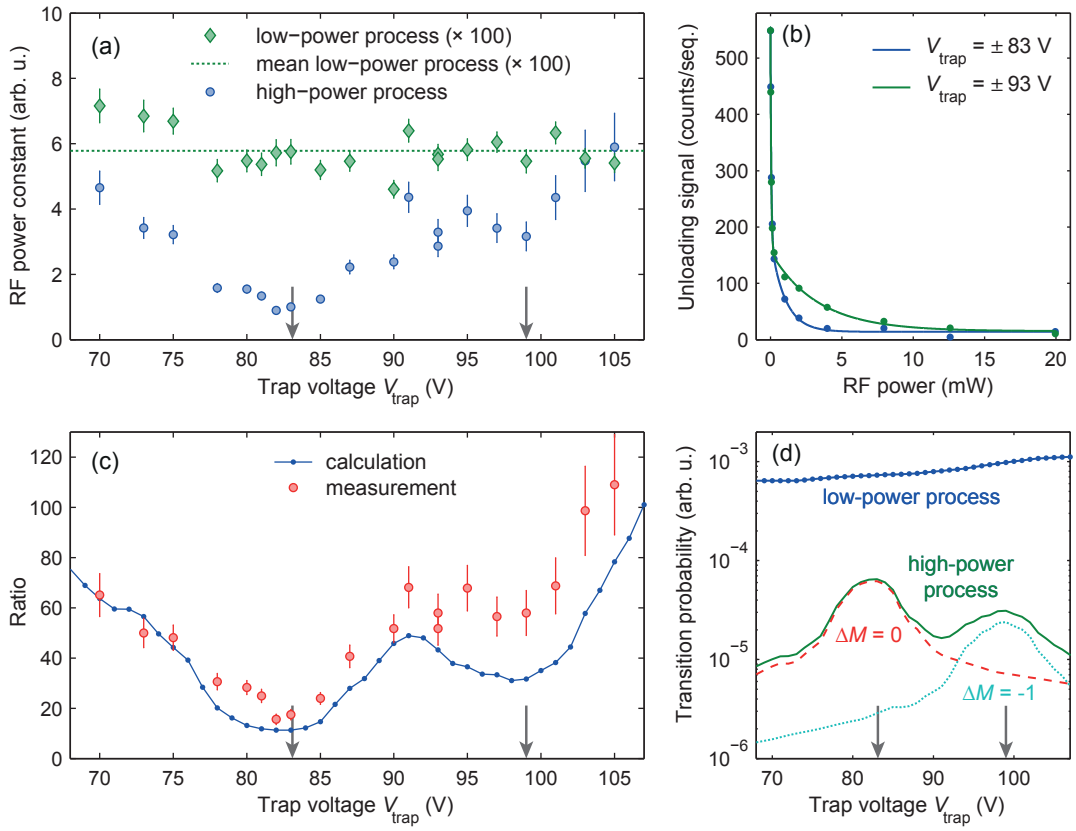

Figure 4.2: Experimental investigation of RF depletion processes. Cooled molecules (final $f_{\mathrm{RF}} - f_{\mathrm{offset}} = 78\,\mathrm{MHz}$) were prepared in $|0;3,3,3\rangle$ and the remaining signal vs. RF power was recorded for $f_{\mathrm{knife}} = 58.5\,\mathrm{MHz}$ and with varying trap voltage V_{trap} (1 s RF depletion time). Both the $\Delta K = 0$ and the K-flip depletion processes were resolved and the data was fitted with a double-exponential model. **(a)** Fitted power constants for the low- and high-power processes vs. trap voltage (the low-power constants are scaled by a factor of 100). The arrows mark the voltage configurations where f_{knife} is resonant to the K-flip transition in the offset electric field, i.e. where $f_{\mathrm{knife}} = 6 \cdot f_{\mathrm{offset}}$ ($\mp K \leftrightarrow \pm K$, $\Delta M = 0$ transition resonant) or $5 \cdot f_{\mathrm{offset}}$. As before, f_{offset} is the splitting of M sublevels of the states $|0;3,3,M\rangle$ in the offset electric field and varies from 8 to 13 MHz across the horizontal voltage scale. **(b)** Remaining signal of molecules vs. RF power for two representative trap voltages, $V_{\mathrm{trap}} = \pm 83\,\mathrm{V}$ and $\pm 93\,\mathrm{V}$. The power constants plotted in part (a) were extracted from fits to such individual measurements. **(c)** Ratio of fitted power constants of the two processes compared to the ratio of calculated transition probabilities. The calculation is based on the model developed in Sec. 2.3.3 and takes into account the measured electric-field distribution in the trap, i.e. the probability to find the electric-field strength where the respective depletion process is resonant. Here, the field distribution was not recorded for every trap voltage, but the measured (and interpolated) distribution for $V_{\mathrm{trap}} = \pm 100\,\mathrm{V}$ [Fig. 4.7(c)] was scaled accordingly. **(d)** Calculated, relative RF transition probabilities for the low- and high-power processes. The contribution of the $\Delta M = 0$ and $\Delta M = -1$ K-flip transitions is resolved. The calculated curve in panel (c) is the ratio of the blue and green lines.

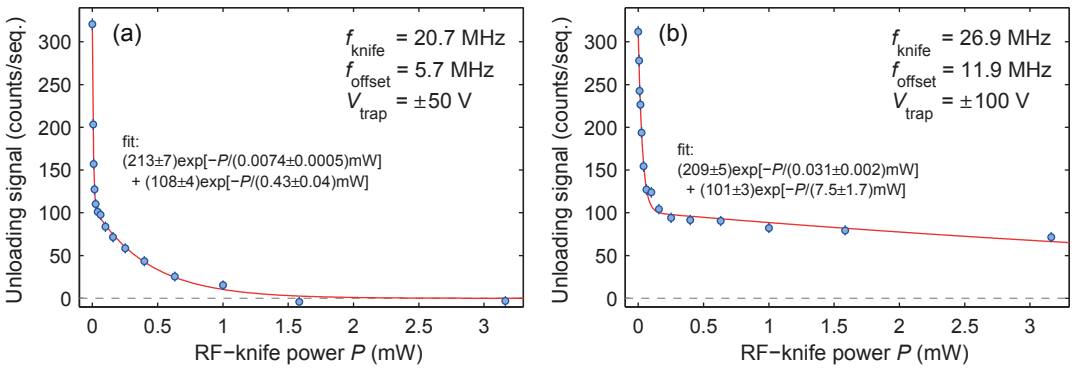

Figure 4.3: RF knife-edge filters for different offset electric fields. Cooled molecules ($f_{\mathrm{RF}} - f_{\mathrm{offset}} = 20\,\mathrm{MHz}$) are prepared in $|0;3,3,3\rangle$ and probed with an RF knife with frequency $f_{\mathrm{knife}} = f_{\mathrm{offset}} + 15\,\mathrm{MHz}$. The remaining signal is recorded vs. RF power and fitted with a double-exponential model. The experiment is performed for two trap voltages: $V_{\mathrm{trap}} = \pm 50\,\mathrm{V}$ **(a)** and $V_{\mathrm{trap}} = \pm 100\,\mathrm{V}$ **(b)**. In both cases, the low-power, RF-knife process filters out the same fraction of the molecular ensemble. The electric-field distributions corresponding to these V_{trap} are shown in Fig. 4.9(b). Note that the separation of power scales is better for higher trap voltage as expected from the theoretical discussions of RF depletion.

4.1.3 Total energy, kinetic energy and offset potential energy

It remains to be discussed how the molecules' kinetic energy is deduced from RF-knife measurements. An optimized RF knife-edge filter probes the total, that is the kinetic and potential energy of the molecules. Given that all molecules populate the same internal state, a filter with frequency f_{knife} truncates the energy distribution of a molecular ensemble at a known total energy and leaves only less energetic molecules in the trap. By scanning f_{knife} and observing the remaining signal of molecules, an integrated energy distribution is obtained.

As all molecules populate the single internal state $|0;3,3,3\rangle$ during energy measurements and are trapped in a box-like potential, the kinetic energy can be calculated from such a measurement by subtracting the known offset potential energy which is given by Mhf_{offset}. To this end, f_{offset} for the states $|0;3,3,M\rangle$ is deduced from measured electric-field distributions (Sec. 3.1.3) and is specified wherever it is used. The threshold kinetic energy for depletion with an RF knife of frequency f_{knife} is then given by $E_{\mathrm{kin}} = Mh\,(f_{\mathrm{knife}} - f_{\mathrm{offset}})$. For a given molecular ensemble and a fixed difference $f_{\mathrm{knife}} - f_{\mathrm{offset}}$, the optimized RF knife should thus remove an equal fraction of molecules from the trap independent of f_{offset}, i.e., the trap voltage configuration. This is indeed observed in the experiment as shown in Fig. 4.3.

The investigation of the electric-field distribution in the trap (Sec. 3.1.3) showed that the trap potential deviates slightly from a perfect box potential. Nevertheless, considering the uncertainty of our measurements, the assumption of a box-like potential is valid for the purpose of the energy measurement. This will be further investigated in Sec. 4.3.2 together with the presentation of the main cooling results.

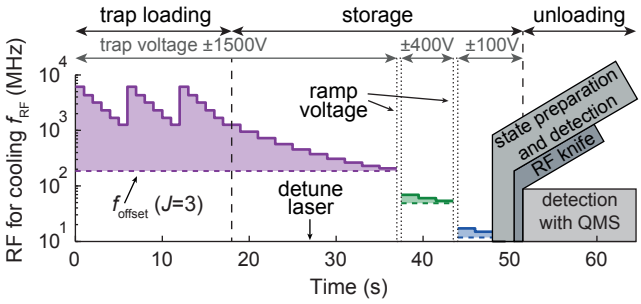

Figure 4.4: Full experimental cooling sequence. The RF applied for cooling is plotted together with the trapping sequence vs. time. The dashed horizontal lines mark the offset Stark splitting f_{offset} in the homogeneous-field region of the trap for the states $|0;3,3,M\rangle$. The steps performed after cooling are explained in the text.

4.2 The cooling sequence

In this section, the experimental sequence to cool and detect a sample of formaldehyde molecules is described. Many parameters cannot be determined from theoretical considerations of the cooling scheme (Sec. 2.5) but have to be optimized in the laboratory. Before describing a few aspects in more detail, the complete sequence is introduced. It consists of six parts, as depicted in Fig. 4.4.

First, molecules are continuously loaded into the trap for 18 s, with cooling already applied (see Fig. 2.12 for the state-transition scheme and Table 3.1 for voltages applied to the trap and the quadrupole guides). As cooling increases the lifetime of molecules in the trap substantially, cooling as many hot molecules entering the trap at different times and with varying energy as fast as possible to an energy with a decent trap lifetime is desirable. Therefore, six f_{RF} for cooling are applied and cycled during trap loading as discussed in Sec. 4.2.1. Then, the ensemble is stored and further cooled while reducing f_{RF} stepwise. The choice of IR and RF frequencies for efficient cooling is outlined in Sec. 4.2.2. It turns out that the kinetic energy of amply cooled molecules becomes comparable to the roughness of the offset electric field of the box-like trapping potential. To avoid complications, the trapping potential is lowered two times during cooling (Sec. 4.2.3).

After cooling, the molecules are prepared in the single rotational state $|0;3,3,3\rangle$ as already described in Sec. 3.3.3. Optical pumping is applied for 1.5 s. Thus, the trap potential is identical for all observed molecules which is important for the determination of their kinetic energy. For state detection, microwave depletion (MWD) is utilized to only measure molecules in the states $|0;3,3,M\rangle$ (1 s of depletion time, see Sec. 3.3.1). Next, the energy of the molecular ensemble is probed by applying RF knife-edge filters as already introduced in the preceding section. Finally, the molecules are unloaded from the trap and counted with the QMS (Sec. 4.2.4).

4.2.1 Trap loading

A carefully optimized trap loading sequence is extremely important, because it determines the size of the molecular ensemble which is available for further cooling. As both the trap and optoelectrical Sisyphus cooling itself induce losses, a larger initial ensem-

ble allows for cooling to lower temperatures. The most important parameter to choose is the frequency of the RF for cooling, f_{RF}, which is determined from characteristics of the molecules loaded into the trap[4]. The resulting ensemble of cooled molecules after trap loading is then compared to uncooled ensembles.

The hottest molecules loaded into the trap in state $|0;3,3,3\rangle$ reach electric fields of 30 kV/cm, determined by the loading quadrupole guide (Sec. 3.2), which translates to a maximum Stark shift of 26 GHz. However, the most energetic fraction is lost from the trap very quickly and is thus unlikely to be cooled. Furthermore, the trap is loaded continuously with molecules having different energies and populating many internal states with differing Stark interaction. Therefore, on one hand, the initial RF for cooling should be large enough to extract a lot of energy from the hottest molecules one could hope to cool. On the other hand, it should be small enough to allow many, also less energetic molecules to reach the higher point in the potential where the RF is resonant and hence to be cooled.

A single or very few cooling cycles are sufficient to increase the lifetime in the trap to more than 10 s and allow cooling to much lower temperatures in many sequential cooling cycles. However, RF transitions have to happen at a slow rate $\sim$ Hz (Sec. 2.5). Therefore, molecules with a 1/e trap lifetime shorter than 1 s will most probably be lost already during trap loading.

Suitable f_{RF} for trap loading are determined with the following measurement on molecules populating $|0;\{3,4\},3,M\rangle$, the rotational states on which Sisyphus cooling acts. With a simplified and short sequence, an estimate for the energy-dependent lifetime of molecules in the trap is acquired by recording the molecule signal with the QMS under conditions usually applied for trap loading and storage, i.e. with $V_{\mathrm{trap}} = \pm 1500$ V. Despite the high trap voltage[5], a decaying signal of molecules leaking through the quadrupole guide is obtained and allows deduction of the lifetime in the trap. Energy selection is accomplished with RF knife-edge filters (Sec. 4.1.1). More specifically, molecules are loaded into the trap for 6 s or 3 s with only optical pumping to the highest M sublevels $|0;3,3,3\rangle$ and $|0;4,3,4\rangle$, which is part of Sisyphus cooling, applied. Due to the high driving rate of IR vibrational transitions (Sec. 3.3.2) and the spontaneous decay rate of ~ 60 Hz, optical pumping to—and accumulation of molecules in—the strongly trapped states saturates in a time $\ll 1$ s. Then, molecules are stored for 2 s allowing for 0.5 s of continued optical pumping to the highest M sublevels, 1 s for the application of the RF knife, and 0.5 s for state detection via MWD (Sec. 3.3.1). Finally, the trap decay signal is recorded for 8 s or 4 s. By analyzing signal differences, one obtains the results presented in Fig. 4.5. The findings can be transferred to the selection of cooling frequencies, because the strong RF knife and a weak RF for cooling, f_{RF}, address the same molecules, but with distinct effects: removal from the trap by transitions to untrapped states in the case of the strong filter or extraction of kinetic energy when combined with optical pumping to a full Sisyphus cooling cycle.

Clearly, molecules which reach RF larger than 5 GHz still have a 1/e lifetime in the trap of more than one second. Consequently, the initial f_{RF} for cooling should be

[4] A note on the trap electric fields: In principle, it holds the higher the trapping fields, the more molecules can be captured from the thermal source. However, the maximum voltages applied to the trap were chosen even lower than in previous experiments for technical reasons (Sec. 3.1.2).

[5] The trap voltage $V_{\mathrm{trap}} = \pm 1500$ V is higher than the appropriate voltage one would apply to efficiently unload molecules from the trap and observe the largest unloading signals (see Sec. 4.2.4).

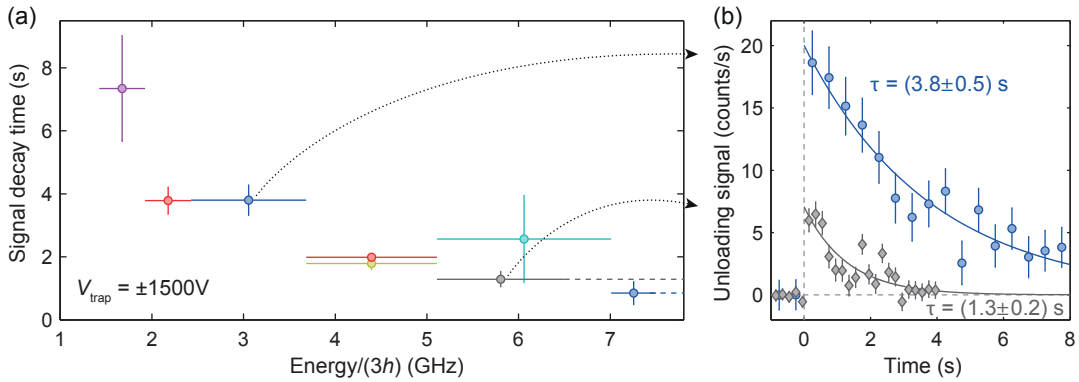

Figure 4.5: Estimate for the lifetime of uncooled molecules in the trap by energy class for the rotational states $|0;\{3,4\},3,M\rangle$. The estimate is obtained by measuring the decay of the molecule signal from the trap with the QMS and fitting it with an exponential. The simplified experimental sequence used here is explained in the text. RF knife-edge filters are employed to discriminate molecules by energy class. The difference of two molecule unloading signals for two distinct filter frequencies gives the estimated lifetime in the trap for molecule energies limited by the two frequencies. **(a)** Estimated lifetime vs. total energy of the molecules. Vertical bars specify the statistical error of the fitted decay time. Horizontal lines mark the range of energy encompassed by the measurement (lower and upper filter frequencies). The dashed lines towards high energy indicate that no upper knife-edge filter was applied for the respective data points. **(b)** Trap unloading signal and fit for two representative energy classes.

on that order. The lifetime gradually increases for less energetic molecules. Even for molecules addressed by frequencies in the range of 1.5 to 2 GHz the 1/e decay time is only ~ 7 s. To make sure that these molecules have a chance to survive trap loading, a frequency in that range has to be used during loading as well.

A separate measurement yields the total duration of trap loading. When the loading time is varied, the measured signal of molecules trapped after loading exponentially approaches a saturation value with a certain time constant. The rising time was determined as ~ 6 s by scanning the time for trap loading while the $f_{\mathrm{RF}} = [5.1, 3.6, 1.9]$ GHz were applied sequentially for cooling. The trap loading duration was fixed to 18 s for further experiments, a reasonable trade-off between large signals and short sequences.

A suitable scaling factor between subsequent effective cooling frequencies ($f_{\mathrm{RF}} - f_{\mathrm{offset}}$) of about $1/\sqrt{2}$ was determined in earlier experiments [Zep12] and is further motivated in Sec. 4.2.2. By trying different sets of f_{RF} and considering that naturally occurring resonances have to be exploited to couple sufficient RF power to the molecules for frequencies >1 GHz (Sec. 3.2), the final sequence was found: the six $f_{\mathrm{RF}} = [6.1, 4.3, 3.2, 2.3, 1.7, 1.3]$ GHz are applied sequentially three times during trap loading for 1 s each as shown in Fig. 4.4.

The state-selected molecular ensemble generated after trap loading with the optimized sequence is now characterized and compared to two uncooled ensembles: one with only optical pumping to strongly trapped states applied (accumulated molecules) and one without any manipulation at all (reference). The measurement is shown and explained in Figs. 4.6(a) and (b). Both accumulation in the highest M sublevels and cooling increase the signal substantially which is mainly attributed to better trapping.

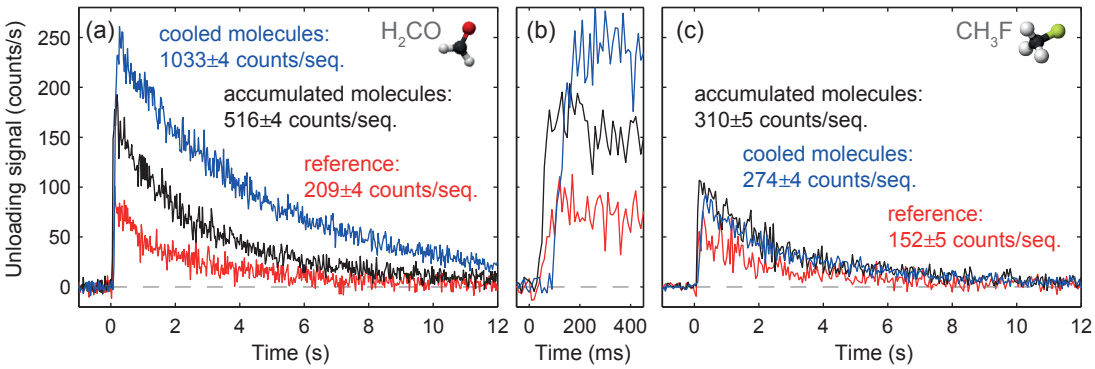

Figure 4.6: Molecule signal in the rotational states $|0;\{3,4\},3,M\rangle$ after varying trap loading sequences. (a) Trap unloading signal of formaldehyde. Molecules are loaded (and cooled) for 18 s with another second of storage (and cooling) appended (first 19 s of sequence in Fig. 4.4). MWD for state detection is applied for 2 s. Then, molecules are unloaded and detected for 12 s with the unloading voltage optimized for each sequence as described in Sec. 4.2.4. The ensemble of cooled molecules is compared to two other ones: leaving only the RF for cooling off results in accumulation of molecules in the highest M sublevels of the involved states, $|0;3,3,3\rangle$ and $|0;4,3,4\rangle$. This already increases the signal compared to the reference sequence, where all radiation fields (except for the MW for state detection) were left off and thus no manipulation of the molecular ensemble takes place. The central panel **(b)** shows the same data with higher resolution for short times after unloading begins. Evidently, the cooled molecules arrive at the QMS later. **(c)** Trap unloading signal of fluoromethane. For comparison, a very similar measurement from earlier experiments with CH_3F is shown [Eng13, Pre12]. Cooling here leads to a smaller increase in signal. Note that the cooling sequence optimized for CH_3F at the time differs from the one explained in this section. However, the resulting cooled molecular ensemble was approximately equally cold.

One of the main reasons for the choice of formaldehyde for these experiments is the four times faster vibrational decay rate in comparison to fluoromethane allowing faster cooling (Sec. 2.1). Cooling is particularly time-critical during trap loading. Therefore, the performance of formaldehyde is compared to fluoromethane here. Although absolute signals for the two species cannot be related to each other easily, the increase of the state-selected signal of cooled and accumulated molecules relative to the reference shows better cooling of formaldehyde. Here, the ratio of signals for the cooled, accumulated, and non-manipulated ensembles is $1033/516/209 = 4.9/2.5/1$. For fluoromethane, in contrast, only a much smaller increase was observed: $274/310/152 = 1.8/2/1$ [Fig. 4.6(c)]. In both cases, it holds for the cooled sample $(f_{\mathrm{RF}} - f_{\mathrm{offset}}) \approx 1\,\mathrm{GHz}$.

The 1/e lifetime of cooled molecules after trap loading, which populate mainly the states $|0;3,3,3\rangle$ and $|0;4,3,4\rangle$ (see Sec. 4.3.5) was determined as (22 ± 1) s giving plenty of time for further cooling. When allowing new uncooled molecules to enter the trap via the loading quadrupole guide during storage, which simulates the conditions present during trap loading, the decay constant drops to about half. This might explain why longer trap loading does not increase the molecule signal, although the observed 1/e lifetime for a closed trap is already larger than the trap loading duration. Possibly, cooled molecules are lost in collisions with uncooled molecules. However, this was not further investigated experimentally.

Step	V_{trap} (V)	Frequencies (MHz)			
		f_{offset}	f_{RF}	Δf_v	Δf_{IR}
loading	±1500	183.7	6090, 4316, 3160, 2288, 1686, 1258	173.5	174
storage	±1500	183.7	946, 726, 564, 452	173.5	174
	±1500	183.7	373, 308, 262, 229, 206	173.5	140
	±400	48.6	69, 60, 54	45.8	36
	±100	11.9	17.2, 15	11.2	9

Table 4.1: Frequencies involved in the cooling sequence. f_{offset} specifies the offset splitting of M sublevels of the states $|0;3,3,M\rangle$ determined from the measured electric-field distributions (Fig. 4.7) for the corresponding trap voltage V_{trap}. Each RF for cooling, f_{RF}, is applied for 1 s during trap loading and for 2 s during storage (Fig. 4.4). Δf_v denotes the differential Stark shift (for $\mathcal{E}_{\mathrm{offset}}$) of the vibrational transition $|0;3,3,2\rangle \leftrightarrow |1;3,3,3\rangle$ relative to the zero-field frequency 83373326 MHz. Δf_{IR} is the actual detuning of the IR laser from the zero-field frequency during cooling, as explained in the text.

4.2.2 Choice of laser and radio frequency for efficient cooling

In this section, the choice of the RF and IR frequencies for cooling are described. Together with the offset electric field $\mathcal{E}_{\mathrm{offset}}$ in the trap both frequencies determine the amount of kinetic energy which is extracted from the molecules in one complete Sisyphus cooling cycle (Fig. 2.12 and Secs. 2.1 and 2.5). In the following, we first specify how consecutive f_{RF} are calculated and the IR detuning is chosen. Then, the approach is motivated and related quantities like the amount of extracted energy and the resulting kinetic energy of the molecular ensemble are discussed.

For a given trap potential, successive f_{RF} for cooling are calculated as follows:

$$\begin{aligned} f_{\mathrm{RF},i+1} &\approx \frac{f_{\mathrm{RF},i} - f^*_{\mathrm{offset}}}{\sqrt{2}} + f^*_{\mathrm{offset}}, \\ f^*_{\mathrm{offset}} &= \begin{cases} f_{\mathrm{offset}} & \text{for } f_{\mathrm{RF},i} > 400\,\mathrm{MHz} \\ f_{\mathrm{offset}} - (\Delta f_v - \Delta f_{\mathrm{IR}}) & \text{for } f_{\mathrm{RF},i} < 400\,\mathrm{MHz} \end{cases} \end{aligned} \tag{4.1}$$

Here, f_{offset} denotes the splitting of M sublevels of the states $|0;3,3,M\rangle$ in the offset electric field $\mathcal{E}_{\mathrm{offset}}$ as specified in Sec. 3.1.3. For colder molecules, i.e. for later cooling steps, the IR frequency for optical pumping to strongly trapped states is changed [second case in Eq. (4.1)], modifying the subtracted offset and increasing the amount of extracted energy as explained below. The resulting f_{RF} were already plotted in Fig. 4.4 and are summarized in Table 4.1, where also the remaining symbols are defined. The selection of the first f_{RF} after a reduction of the trapping fields is discussed in the following Sec. 4.2.3.

Scaling of the effective cooling frequency. The sequence of f_{RF} was determined with the following reasoning [Zep12]. An RF transition leading to cooling can take place, if a molecule in the box-like potential has sufficient kinetic energy to reach resonance with f_{RF}: $E_{\mathrm{kin}} \geq Mh(f_{\mathrm{RF}} - f_{\mathrm{offset}})$. After the RF transition, the molecule's energy is reduced by a factor $E_{\mathrm{kin}}/\left[E_{\mathrm{kin}} - h\left(f_{\mathrm{RF}} - f_{\mathrm{offset}}\right)\right]$. For efficient cooling, f_{RF} should be

as large as possible and molecules with a range of energies should be able to perform one final RF transition in the cooling step. As cooling mainly takes place in the uppermost M levels of the rotational states $|0;3,3,M\rangle$, $M = 3$ and $3h\,(f_{\mathrm{RF}} - f_{\mathrm{offset}}) \leq E_{\mathrm{kin}} \leq 4h\,(f_{\mathrm{RF}} - f_{\mathrm{offset}})$. On average, the reduction in kinetic energy then is on the order of $3.5/2.5 \simeq \sqrt{2}$ per step and thus the subsequent frequencies are chosen according to the above equation. As a consequence of this choice, the molecules perform about one induced RF transition per applied frequency or per 2 s of cooling and their kinetic energy is approximately halved every 4 s.

Red-detuning the laser. To increase the efficiency of cooling, i.e. to remove a larger fraction of the total molecular energy per Sisyphus cycle, the IR frequency needed for optical pumping is changed for later cooling steps. In particular, the transition $|0;3,3,2\rangle \leftrightarrow |1;3,3,3\rangle$ is driven in lower electric fields $\mathcal{E} < \mathcal{E}_{\mathrm{offset}}$ at the expense of a reduced driving rate. In the equation and the table the differential Stark shift of the transition for $\mathcal{E}_{\mathrm{offset}}$ is denoted by Δf_v. To extract more energy per Sisyphus cycle, the laser is detuned $\Delta f_{\mathrm{IR}} < \Delta f_v$ from the zero-field frequency of the transition [second case in Eq. (4.1)]. The detuning specified in the table was optimized experimentally by maximizing the signal of cooled molecules. The smaller fields where the transition is resonant in this case are less probable. Considering the simulated and measured electric-field distributions for the used trapping configurations, one finds that the electric-field probability is reduced to approximately 8 % of the value measured for the offset electric field (see also Fig. 4.7, where the respective electric fields are marked). Therefore, the IR driving rate is lowered from about 3 kHz (Sec. 3.3.2) to $\sim$240 Hz which is still four times faster than the spontaneous decay rate and ensures sufficiently fast optical pumping to strongly trapped states. In the beginning of the sequence, the modified detuning is not applied because the increased energy extraction is small relative to the large f_{RF} and quick optical pumping is more important.

Amount of extracted energy. Keeping in mind the level scheme and the fact that cooling mostly takes place in the highest M sublevels after initial optical pumping, the portion of energy which is extracted in each Sisyphus cycle is found to be roughly

$$\Delta E_{\mathrm{kin}} \simeq h\,[f_{\mathrm{RF}} - f_{\mathrm{offset}} + (\Delta f_v - \Delta f_{\mathrm{IR}})]\,. \tag{4.2}$$

For this relation it is assumed that the spontaneous decay takes place when the molecule is in the offset electric field, the most probable electric-field strength. However, this does not always have to be the case. Evidently, the detuning of the laser increases the amount of extracted energy and its relative effect is larger for smaller f_{RF}.

Estimate of the resulting kinetic energy. For an optimized[6] cooling sequence down to a final f_{RF}, the order of magnitude of the molecules' kinetic energy can be estimated from the final cooling frequency as

$$E_{\mathrm{kin,final}} \simeq 3h\,(f_{\mathrm{RF}} - f_{\mathrm{offset}}) \simeq \frac{3}{2} k_B T_{\mathrm{final}}. \tag{4.3}$$

[6] The RF power has to be adjusted for every frequency (Sec. 3.2). The procedure making use of RF knife-edge filters is explained in Ref. [Eng13].

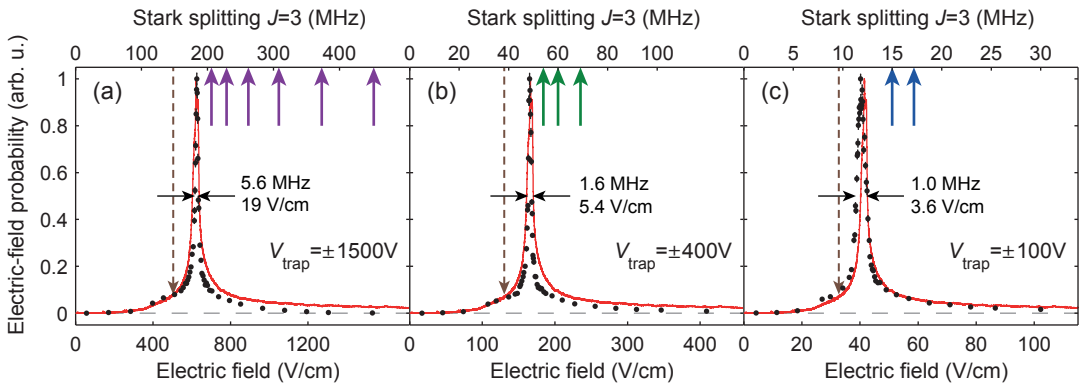

Figure 4.7: Measured (dots) and simulated (solid line) electric-field distributions for the trap voltage configurations used during cooling (cf. Sec. 3.1.3, the data shown in (a) is identical to Fig. 3.2). The FWHM is given for the measured distributions. The applied trap voltages varied over a factor of 15 (see the lower right corner of the panels). The upper horizontal axes show the Stark splitting of the states $|0;3,3,M\rangle$ in frequency units and arrows pointing to these axes indicate the frequencies of the RF coupling (f_{RF}) applied sequentially for cooling. The long dashed arrows point to the electric field strengths to which the red-detuned IR frequency for cooling is resonant (Sec. 4.2.2).

This follows from the notion that most of the molecules performed a Sisyphus cycle with the specified final f_{RF} and are now cold enough to not reach resonance with f_{RF} in high electric fields any more. The factor 3 stems from $M = 3$ for the initial and final state of the Sisyphus cycle, $|0;3,3,3\rangle$. With the discussion of the final results this order-of-magnitude estimate will be substantiated.

The estimate shows that the final kinetic energy of a molecular ensemble is tunable over a large range by adjusting the cooling sequence. Furthermore, distinct sequences are easily distinguishable by specifying the final cooling frequency. This was already used previously and will continue to be helpful. Different cooling sequences and the resulting molecular ensembles are simply labeled with the frequency difference $f_{\mathrm{RF}} - f_{\mathrm{offset}}$ applied in the final cooling step.

4.2.3 Ramping to lower trapping potentials

The potential produced by our electrostatic trap was investigated in Sec. 3.1.3. It is mainly characterized by the offset electric field $\mathcal{E}_{\mathrm{offset}}$ determined by the sharp peak of the electric-field distribution and an associated roughness of the potential floor given by the width of the peak. We regard it as box-like for molecules in low-field-seeking states, if the kinetic energy of the molecules is sufficiently larger than the roughness of the offset field. In this section, it is shown that we have to reduce the electric potential in the course of cooling to fulfill this condition. Besides, characteristics of the reduced potential are discussed.

As cooling progresses, f_{RF} approaches f_{offset} and $(f_{\mathrm{RF}} - f_{\mathrm{offset}})$ becomes comparable to the width of the electric-field distribution. This can be seen in Fig. 4.7(a), where vertical arrows denote the last six f_{RF} applied with the initial trap-voltage configuration $V_{\mathrm{trap}} = \pm 1500\,\mathrm{V}$. Thus, the molecules do not move in a well-defined box potential anymore and spend significant time in not very well-defined isolated regions of low

electric field which we call dimples. Moreover, with continued cooling with the same trapping potential and the red-detuned IR frequency the molecules would accumulate in these low-field dimples. To maintain a simple box-like potential, the trap voltages are ramped down adiabatically (0.5 s ramp time) twice during cooling to $V_{\mathrm{trap}} = \pm 400\,\mathrm{V}$ and $V_{\mathrm{trap}} = \pm 100\,\mathrm{V}$. This shifts the offset of the potential, f_{offset}, and reduces the width of the field distribution as intended. In total, five more cooling steps are performed in a reduced potential as shown in Figs. 4.7(b) and (c) as well as Table 4.1.

After a ramp to a lower trapping potential, a suitable f''_{RF} for further cooling in the reduced potential has to be selected. The following phase-space arguments are applied. The available phase space volume for a molecule with exactly enough energy to come into resonance with f''_{RF} in the reduced potential, i.e. with total energy $E_0 = 3hf''_{\mathrm{RF}}$, should be about half as large as the phase space volume corresponding to the f'_{RF} of the previous cooling step in higher trapping fields. The phase space volume Ω available to a molecule with total energy E_0 in a potential $V(E)$ is given in energy space by

$$\Omega \propto \int_0^{E_0} V(E)(E_0 - E)\sqrt{E_0 - E}\mathrm{d}E. \tag{4.4}$$

Here, $V(E)$ is the trapping potential given by the electric-field distribution, the factor $(E_0 - E)$ is the kinetic energy of the molecule, and $\sqrt{E_0 - E}\mathrm{d}E$ the phase-space element. For the numerical calculation of f''_{RF}, Eq. (4.4) and the simulated electric-field distributions are used and yield the frequencies specified in the above table. Note that due to some adiabatic cooling during the ramp to lower potentials the f''_{RF} calculated from phase-space considerations is smaller than what would be obtained with a modified version of Eq. (4.1), accounting for the changed trapping potential, $f_{\mathrm{RF},i+1} \approx (f_{\mathrm{RF},i} - f^*_{\mathrm{offset,high\ potential}})/\sqrt{2} + f^*_{\mathrm{offset,low\ potential}} > f''_{\mathrm{RF}}$.

Disturbed electric fields for very low trap voltages. Before continuing with the description of the cooling sequence, the electric-field distributions in Fig. 4.7 are discussed more closely because the ones for smaller trap voltages deviate from the expectation and show hints for the existence of surface charges on the microstructured capacitor plates, as already mentioned in Sec. 3.1. As one can see from the simulated distributions, the curves are expected to scale with the applied trap voltage. However, the relative widths of the distributions increase and a slight shift of the peak is observable for small voltages. In particular, reducing the voltage by a factor of four from $V_{\mathrm{trap}} = \pm 400\,\mathrm{V}$ to $V_{\mathrm{trap}} = \pm 100\,\mathrm{V}$ [Figs. 4.7(b) and (c)] still reduces the strength of the homogeneous field by the same factor, but it narrows the width only by a factor < 2. This effect is even more pronounced when the voltage is halved once more to $V_{\mathrm{trap}} = \pm 50\,\mathrm{V}$ [see also Fig. 4.9(b)]: While f_{offset} scales as expected, the width is not compressed noticeably anymore. This is attributed to surface charges on the electrode microstructure. Thanks to the installation of the new trap (Sec. 3.1.2) these hints for surface charges appeared at a substantially reduced voltage in the experiments with formaldehyde facilitating cooling to much lower temperatures. Nevertheless, the observations were one of the reasons for not attempting to cool formaldehyde molecules to even lower temperatures with the present setup.

Lifetime of cooled molecules in the trap. The section on the trapping potential is a suitable place to list the measured values for the lifetime of cooled molecules in different

V_{trap} (V)	final ($f_{\mathrm{RF}} - f_{\mathrm{offset}}$)	1/e decay time (s)
±1500	1074 MHz	26 ± 1
	189 MHz	34 ± 1
	22 MHz	57 ± 2 [61 ± 3]
±400	5.4 MHz	21 ± 1 [57 ± 2]
±100	3.1 MHz	30 ± 2 [45 ± 3]

Table 4.2: Lifetime of molecules in the trap after different cooling sequences. Molecules are prepared in the state $|0;3,3,3\rangle$ and stored with the voltage configuration which was used in the final cooling step. The measurement sequence is identical to the one used for Fig. 3.3 (third and fifth data set in the table). Continuous optical pumping to $|0;3,3,3\rangle$ increases the decay time for low trap voltages (decay constants in parentheses, see Sec. 3.1.4).

trapping potentials (see Table 4.2). The measurement procedure and important effects determining the lifetime were already discussed in Sec. 3.1.4. In particular, it was noted before that the lifetime of molecules in the trap depends non-trivially on their kinetic energy and the trap voltage applied for storage, as seen here as well.

4.2.4 Unloading cooled molecules from the trap

As a final step of the experimental sequence molecules have to be unloaded from the trap and counted with the QMS. In general, this requires optimization of the trapping voltages during unloading. Apart from that, presently, very cold molecules can only be detected with the QMS, if the ensemble is parametrically heated before unloading. In this section, both aspects are discussed.

In order to efficiently extract the molecules from the trap and guide them to the ionization volume of the QMS, the electric fields in the trap and the quadrupole guide have to be adjusted to the kinetic energy of the molecules and to the Stark shift of the rotational state or set of states [Zep12, Glö15b] (detailed description in Ref. [Eng13]). On one hand, a small confining electric field strength leads to losses of hotter molecules. On the other hand, a higher electric field strength reduces the probability for colder molecules to find the trap exit hole to the QMS.

To optimize the trap voltage applied during unloading we usually measure the integrated unloading signal with varying voltages applied. For unloading, a higher offset electric field between the capacitor plates, i.e., $V_{\mathrm{offset}} = \frac{1}{5} V_{\mu}^{(u)}$ is applied because it was found that during molecule extraction (as opposed to storage) a higher offset electric field increases the molecule signal.

Data for optimizing the unloading voltage for a few cooling sequences is shown in Fig. 4.8. Looking at the more energetic molecular ensembles at first (cooling stopped at higher frequency $f_{\mathrm{RF}} - f_{\mathrm{offset}}$), we note that the optimal unloading voltage shifts towards lower values as the molecules are cooled further, satisfying the expectation. In particular, both the left and right flanks of the curves are shifted. For the three coldest ensembles, however, where the optimal unloading voltage based on scaling should be considerably smaller than 200 V, only the right flank of the curve shifts and we observe a dramatic decrease in signal. Apparently, the unloading efficiency drops abruptly if molecules are cooled further.

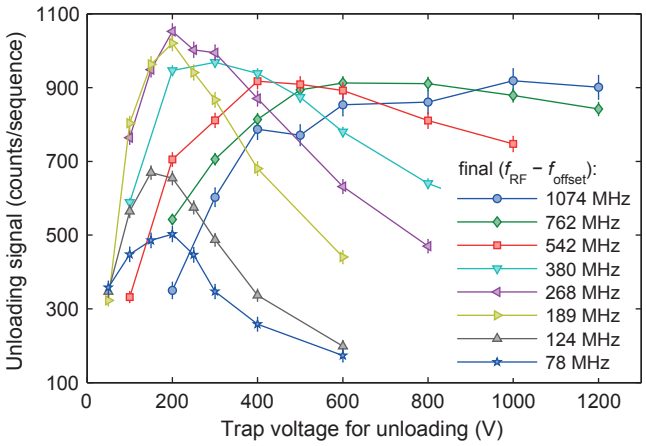

Figure 4.8: Unloading molecules from the trap. Molecule signal vs. trap voltage $\pm V_\mu^{(u)}$ (with $V_{\text{offset}} = \frac{1}{5} V_\mu^{(u)}$, cf. Table 3.1) applied during unloading for various cooling sequences. Here, the molecules were not prepared in $|0;3,3,3\rangle$. Instead, we measured the signal of molecules populating the states $|0;\{3,4\},3,M\rangle$. Solid lines are guides to the eye and keys specify when cooling was stopped.

The reason for this drop in efficiency lies in the QMS itself. In the QMS, molecules are ionized by bombardment with an electron beam and the emerging molecular ions are guided, filtered, and counted. For electron acceleration and ion collection static voltages are applied in or around the ionization volume. There is strong experimental evidence that very cold and thus slow molecular beams are deflected from the ionization volume by the resulting electric fields inhibiting molecule detection. The measurements leading to this conclusion are summarized in Appendix C.2. Unfortunately, the present setup does not allow adjustment of the QMS electric fields in a way which permits efficient electron-impact ionization and detection of slow molecular beams at the same time.

Efficient unloading and detection of colder ensembles in the trap is possible by parametrically heating the molecules directly before trap unloading, using the following sequence. Rapidly ramping to an increased offset electric field in one half of the trap [Eng11] with the other half remaining at the usual offset allows molecules residing in the region with higher field to roll down an electric field gradient and be accelerated. After a hold time of 50 ms, the configuration of offset electric fields in the two halves of the trap is reversed. In total, we switch the offset electric fields 20 times during 1 s, with the ramps performed in about 1 ms. Molecules which were sufficiently cold initially thereby gain enough kinetic energy to be optimally unloaded from the trap at a voltage of $V_\mu^{(u)} = \pm 200\,\text{V}$. With parametric heating applied, a dramatic loss in signal for a final cooling frequency of $(f_{\text{RF}} - f_{\text{offset}}) < 189\,\text{MHz}$ is no longer observed, showing that the severe losses without heating are caused during unloading and not during cooling. However, the heating also causes some losses.

Parametric heating is applied for sequences with final $(f_{\text{RF}} - f_{\text{offset}}) < 189\,\text{MHz}$. After heating, all molecular ensembles have approximately the same energy distribution, independent of how far they have been cooled before. This was verified by recording energy distributions for different cooling sequences after heating (Appendix C.3).

Therefore, all ensembles can be unloaded with a fixed set of unloading voltages after heating.

Note that the deflection of slow molecular beams from the QMS ionization volume might explain why higher molecule signals have been observed with a larger offset voltage $V_{\text{offset}} = \frac{1}{5}V_{\mu}^{(u)}$. Due to the higher offset field in the trap molecules are slightly accelerated while they transition from the trap to the quadrupole guide, increasing the chances of the molecules to overcome the potential barrier around the ionization volume of the QMS.

A final interesting feature in Fig. 4.8 is the fact that from $(f_{\text{RF}} - f_{\text{offset}}) = 1074\,\text{MHz}$ to $(f_{\text{RF}} - f_{\text{offset}}) = 268\,\text{MHz}$, we observe an increase in signal for optimal unloading voltage. This is observed despite an expected decrease in molecule number due to losses during additional cooling. However, the increased signal can be explained by a higher detection efficiency in the QMS for slower molecules since the ionization probability is proportional to the inverse velocity (see also Sec. 4.3.3).

4.3 Experimental cooling results

This section is devoted to the characterization of the molecular ensemble produced after the full optoelectrical Sisyphus cooling sequence shown in Fig. 4.4. The obtained data represents the key experimental achievements of this thesis work. Comparison of the fully cooled ensemble with molecules produced with modified experimental sequences will reveal some characteristics of the cooling method and numbers for the cooling factor and the increase in phase-space density.

The results are presented in the following order: At first, the energy distribution of the molecules (Sec. 4.3.1) and the influence of the offset potential energy on it (Sec. 4.3.2) are examined. In order to measure the number of molecules unloaded from the trap, the sensitivity of the QMS used for detection has to be calibrated (Sec. 4.3.3). Then, the cooled molecular ensemble is compared to an uncooled reference in Sec. 4.3.4. Finally, we investigate the internal-state purity in Sec. 4.3.5.

4.3.1 Final temperature

Optoelectrical Sisyphus cooling is not expected to produce a thermal ensemble of molecules. Furthermore, the trapped gas is dilute, inhibiting quick thermalization (see also outlook, Ch. 6). Therefore, the temperature of the ensemble is not defined strictly. To assign a number to the cooled gas nonetheless, the energy distribution is measured using RF knife-edge filters as explained in Sec. 4.1. Scanning the filter frequency f_{knife} and recording the remaining signal of trapped molecules yields an integrated distribution of the total molecular energy. After careful consideration of the offset potential energy, a value for the median kinetic energy energy is extracted from the data.

The inset of Fig. 4.9(a) shows the remaining signal in the state $|0;3,3,3\rangle$ vs. f_{knife}. To address the issue of offset subtraction, the energy distribution is measured for two distinct trap voltages: $V_{\text{trap}} = \pm 100\,\text{V}$, the trap potential present in the final two cooling steps, and $V_{\text{trap}} = \pm 50\,\text{V}$. In both cases, a knife with $f_{\text{knife}} \approx f_{\text{offset}}$, resonant to the offset of the box-like potential, depletes all molecules from the trap as expected. With rising knife frequency we observe steeply rising flanks which are clearly separated due to the different potential energy offsets. At higher frequencies a slight further

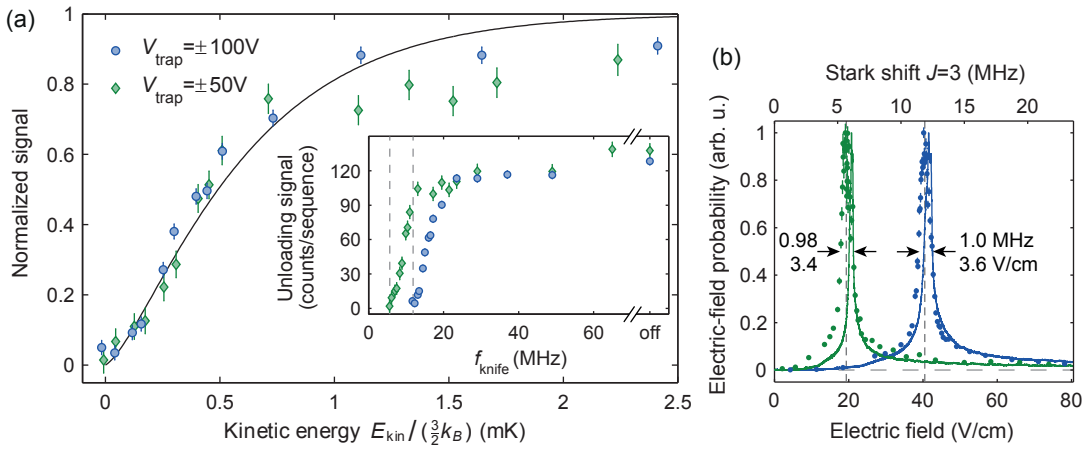

Figure 4.9: Measurement of the kinetic energy via RF knife-edge filters. (a) Integrated energy distribution of the fully cooled molecules. The inset shows the signal of molecules remaining in the state $|0;3,3,3\rangle$ vs. f_{knife}, with the filter applied with two distinct trap voltages. The dashed lines mark the potential energy offset f_{offset}, which is 11.9 MHz (5.7 MHz) for $V_{\mathrm{trap}} = \pm 100\,\mathrm{V}$ ($V_{\mathrm{trap}} = \pm 50\,\mathrm{V}$). The main panel shows the same data vs. kinetic energy, normalized to the signal without an RF knife and on a narrower horizontal scale. The solid line represents an integrated Boltzmann distribution for a temperature of 420 µK. **(b)** Measured and simulated electric-field distributions for the two relevant trap voltages used to determine f_{offset} (cf. distributions for higher voltages in Figs. 3.2 and 4.7).

increase towards the data point without RF knife is visible. Those molecules, about 10 % of the ensemble, were not cooled efficiently in the last cooling steps and therefore have a much higher kinetic energy than the vast majority of the fully cooled ones. If necessary, this high-energy part of the molecular ensemble could be removed from the trap by applying a suitable RF knife.

To obtain a kinetic energy distribution from the measurement, the contribution of potential energy has to be considered. To this end, the trap potential is treated as box-like. Systematic errors caused by this simple approach will be investigated in the subsequent section. They are smaller than the statistical uncertainty of the data. The offset potential energy, Mhf_{offset}, extracted from the measured electric-field distributions [Fig. 4.9(b)], is subtracted. Consequently, we find for the kinetic energy $E_{\mathrm{kin}} = Mh\,(f_{\mathrm{knife}} - f_{\mathrm{offset}})$. The measured data with the offset potential energy subtracted is shown in the main panel of Fig. 4.9(a). Normalized to the signal without RF knife, the two curves obtained with different trap voltages show a good overlap. This is expected from the fact that the subtraction of a well-defined offset potential energy should not influence the kinetic energy distribution.

From the data, a median kinetic energy of $E_{\mathrm{kin}} = \frac{3}{2}k_B\,(420 \pm 90)\,\mu\mathrm{K}$ is computed, with the factor of 3 accounting for the three translational degrees of freedom in a box potential. The energy at which half of the molecular ensemble is depleted was determined by fitting the curve for $V_{\mathrm{trap}} = \pm 100\,\mathrm{V}$ with a linear slope in the vicinity of this kinetic energy. As a comparison, we additionally plot a Boltzmann distribution for a temperature of 420 µK. The good agreement of thermal distribution and measured data supports the interpretation of $E_{\mathrm{kin}}/\left(\frac{3}{2}k_B\right)$ as an approximate temperature.

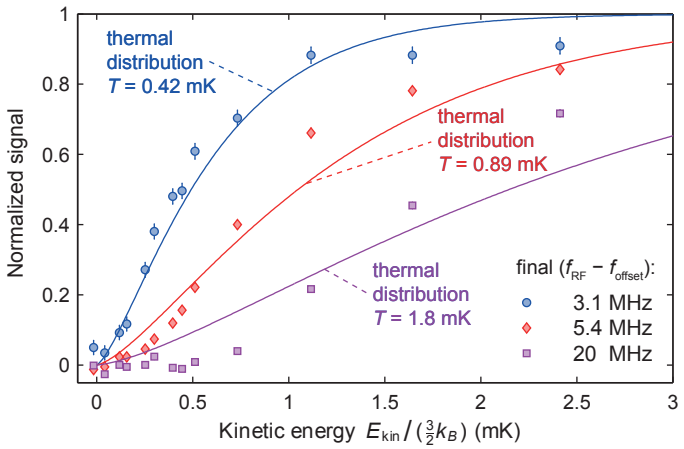

Figure 4.10: Kinetic energy distributions for three cooling sequences. The integrated energy distributions were measured with RF knife-edge filters at a trap voltage of $V_{\mathrm{trap}} = \pm 100\,\mathrm{V}$ [cf. Fig. 4.9(a)]. The experimental sequence is equal to the one summarized in Fig. 4.4, with cooling stopped two and four steps earlier for two of the data sets. The data for the coldest ensemble is identical to Fig. 4.9(a). Again, the solid lines show integrated Boltzmann distributions for the specified temperatures which correspond to the determined median kinetic energy for the respective molecule sample (see Table 4.3).

The same procedure was carried out for three shorter cooling sequences producing molecular ensembles with higher energy. For these, the frequency $f_{\mathrm{knife,median}}$ of the RF knife removing the more energetic half of the molecules and the deduced median kinetic energy in units of mK are given in Table 4.3. The results confirm the order-of-magnitude estimate for the final kinetic energy after cooling made in Sec. 4.2.2: $E_{\mathrm{final}} \simeq 3h\,(f_{\mathrm{RF}} - f_{\mathrm{offset}})$. Furthermore, the data shows that the molecular kinetic energy is approximately halved every two cooling steps. Note that the deviation of the measured energy distribution from a Boltzmann distribution is larger for more energetic ensembles. In fact, the measured distributions are narrower than a thermal distribution for molecules cooled to intermediate energies, as shown in Fig. 4.10 for two of the ensembles with larger energy.

final $(f_{\mathrm{RF}} - f_{\mathrm{offset}})$	$f_{\mathrm{knife,median}} - f_{\mathrm{offset}}$	median E_{kin}
(MHz)	(MHz)	$(3/2 \cdot k_B\,\mathrm{mK})$
45	37 ± 6	3.5 ± 0.6
20	19 ± 1	1.8 ± 0.1
5.4	9.2 ± 0.6	0.89 ± 0.05
3.1	4.4 ± 1.0	0.42 ± 0.09

Table 4.3: Median kinetic energy after a varying amount of cooling. The experimental sequence is identical to the one summarized in Fig. 4.4, with cooling stopped earlier for the three uppermost data sets. From top to bottom, each measurement probes a cooling sequence prolonged by two cooling steps at a time.

4.3.2 Subtraction of the offset potential energy

For the previously presented energy measurements the simple assumption of a box potential was used to subtract a large amount of offset potential energy. In this section, the validity of the approach is investigated considering also the measured, actual trap potential which deviates slightly from a perfect box (Sec. 3.1.3).

First, we assume a molecular temperature of $T = 420\,\mu\mathrm{K}$ and calculate thermal energy distributions for the two trap voltage configurations relevant to the measurement and compare the result to the case of a simple box potential. A Boltzmann distribution $p(E)\,\mathrm{d}E$ in a given potential $V(E)$ is calculated as

$$p(E)\,\mathrm{d}E = a\int_0^E V\left(E'\right)\exp\left(-\frac{E}{k_B T}\right)\sqrt{E-E'}\mathrm{d}E'. \tag{4.5}$$

Here, $V(E)$ is given by the measured electric-field distribution in the trap and a is a normalization factor. The exponent is the Boltzmann factor and $\sqrt{E-E'}\mathrm{d}E'$ the phase-space element in units of energy [cf. Eq. (4.4)]. To simplify comparison with the measured data, the integrated Boltzmann distribution

$$f(E) = \int_0^E p\left(E'\right)\mathrm{d}E' \tag{4.6}$$

is investigated. The resulting distributions for $V_{\mathrm{trap}} = \pm 100\,\mathrm{V}$, $V_{\mathrm{trap}} = \pm 50\,\mathrm{V}$, and a box potential with a perfectly defined offset are plotted in Fig. 4.11(a). The close proximity of the curves already indicates that the simple assumption of a box potential is useful. The deviation from the curve assuming a box potential is smaller for the lower trap voltage, because the offset potential energy accounts for a smaller fraction of the total molecular energy.

With the RF knife-edge filter the total molecular energy is probed. Therefore, as a second consideration, we calculate the mean kinetic energy $\langle E_{\mathrm{kin}}\rangle$ for a given total energy E_0 and potential shape $V(E)$. It is given by

$$\langle E_{\mathrm{kin}}\rangle(E_0) = \frac{\int V(E)\,(E_0-E)^{\frac{3}{2}}\,\mathrm{d}E}{\int V(E)\sqrt{E_0-E}\mathrm{d}E}. \tag{4.7}$$

In this relation, the enumerator is proportional to the phase-space volume Ω of a particle with total energy E_0 and kinetic energy $(E_0 - E)$ [Eq. (4.4)]. Dividing Ω by the contribution of the potential alone, the denominator in Eq. (4.7), yields the mean kinetic energy as specified. The resulting dependency $\langle E_{\mathrm{kin}}\rangle(E_0)$ is shown in Fig. 4.11(b) for $V_{\mathrm{trap}} = \pm 100\,\mathrm{V}$ and a simple box potential. The two lines basically overlap for larger total energies (large f_{knife}). As expected, deviations are visible for energies close to or below the offset potential energy given by the peak of the electric-field distribution. The function $\langle E_{\mathrm{kin}}\rangle(E_0)$ for $V_{\mathrm{trap}} = \pm 100\,\mathrm{V}$ is not monotonically increasing close to the offset region because compression of the gas to a total energy below f_{offset} would lead to adiabatic heating. The molecules are faster in the small-field dimples than they are above the offset potential where an ample volume with constant potential energy is available.

Nevertheless, these details only slightly affect the determination of the molecular kinetic energy as performed in the previous section. For the median total energy of the

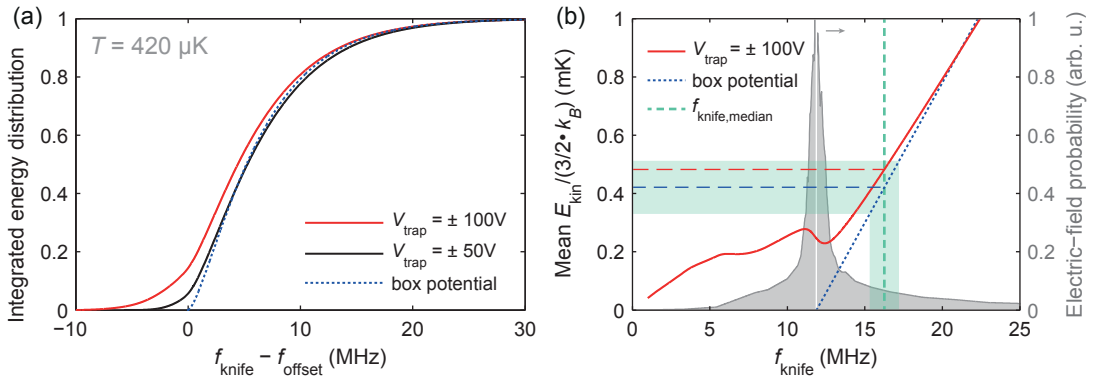

Figure 4.11: Influence of the trapping potential on the measured kinetic energy. (a) Integrated Boltzmann distributions (in frequency units for the state $|0;3,3,3\rangle$) for a temperature of 420 µK in different potential landscapes, namely the actual trap potentials given by the measured electric-field distributions for the respective trap voltage [Fig. 4.9(b)], and a perfect box potential. The latter curve is equal to the distribution plotted in Fig. 4.9(a). **(b)** Mean kinetic energy for a given total energy for $V_{\mathrm{trap}} = \pm 100\,\mathrm{V}$ and a box potential. To simplify comparison to the knife-edge filters, the horizontal energy axis is chosen in units of frequency (for the molecular state $|0;3,3,3\rangle$). $f_{\mathrm{knife,median}}$ for the coldest molecular ensemble is marked with the corresponding statistical error (shaded area). The mean kinetic energies one obtains for a total energy given by $f_{\mathrm{knife,median}}$ with different assumed potentials are specified by the horizontal lines. The gray curve shows the measured electric-field distribution for $V_{\mathrm{trap}} = \pm 100\,\mathrm{V}$ (right vertical axis) with the white line specifying f_{offset}.

coldest produced molecular ensemble one obtains values for the mean kinetic energy which lie within each others statistical measurement uncertainty (see figure). The situation plotted in Fig. 4.11(b), i.e. consideration of a sample of molecules with a kinetic energy substantially smaller than the offset potential energy, is the one in which the assumption of a perfect box potential induces the largest systematic error for a kinetic energy measurement. The error is smaller for smaller trap voltages, i.e. smaller offset potential energies, as well as for larger molecule energies with an unchanged potential. The results of this section show that the simplified subtraction of the offset potential energy and the assumption of a box potential is acceptable.

4.3.3 Counting trapped molecules: calibration of the detector

To determine the number of cooled molecules, the sensitivity of our detector, the QMS, has to be calibrated. With the procedure described here, the number of molecules unloaded from the trap can be determined. The result is estimated to be accurate to within a factor of 2.

For the calibration, the following parameters of the molecular beam exiting the trap have to be determined. A given molecule traversing the ionization region of the QMS has a low ionization probability. Therefore, the QMS count rate s is proportional to the number density of molecules in the ionization region, n, independent of molecule velocity, i.e. $s = C \cdot n$. The coefficient C quantifies the sensitivity of the QMS. The

number of molecules N leaving the trap is then equal to

$$N = S \cdot A \cdot v \cdot \frac{1}{C}. \tag{4.8}$$

Here, S is the background subtracted signal (counts) measured by the QMS and integrated over the time of unloading. A is the area of the molecular beam at the QMS and v is the velocity of molecules in the QMS.

Most of the quantities in Eq. (4.8) can be obtained easily and relatively accurately. The integrated signal S is measured directly and the beam area A is measured by varying the position of the QMS [Mie10]. The velocity v is extracted from the median energy of molecules in the trap measured via RF knife-edge filters after heating them for efficient unloading and based on the fact that the potential energy of molecules is entirely converted to forward kinetic energy before molecules enter the QMS.

The greatest difficulty in measuring the number of molecules exiting the trap originates from the need to determine the sensitivity coefficient C of the QMS. In principle, this is measured by applying a constant pressure of gas at room temperature to the QMS vacuum chamber, and measuring the QMS count rate while monitoring the pressure with a Bayard-Alpert gauge. This procedure suffers from several problems. First, even taking into account gas correction factors, the specified accuracy of our Bayard-Alpert gauge is at best 20 %. Second, since a titanium sublimation pump attached to the system cannot easily be turned off, a constant input stream of gas is needed to maintain a constant pressure. It is thus not clear if the pressure at the QMS is equal to the pressure at the Bayard-Alpert gauge. Finally, depending on the molecule, fragmentation in the QMS and in the Bayard-Alpert gauge can lead to a substantial partial pressure of fragments in the vacuum chamber which distorts the result. To reduce the third effect, the sensitivity coefficient of the QMS was measured for oxygen and nitrogen and the value for formaldehyde was extrapolated based on ionization cross sections and fragmentation probabilities for electron impact ionization from the literature [Kim04, Lin15]. The sensitivity coefficient for formaldehyde obtained from nitrogen differs from the one obtained from oxygen by about 15 %, which we attribute to the sources of error identified above. The exact procedure and data used to determine the sensitivity coefficients are summarized in Appendix C.4.

Obtaining the overall error for the molecule number N is difficult since the main source of error, from the sensitivity coefficient C of the QMS, is hard to quantify, as discussed above. As a conservative value, it is estimated that the number of molecules exiting the trap is determined to within at least a factor of two. Note that when comparing different ensembles in the trap, the effect of the sensitivity coefficient cancels, so that relative populations can be determined much more accurately.

The calibration of the molecule number N was performed twice—for the ensemble generated with the full cooling sequence and for an uncooled reference ensemble. The key results are discussed in the next section.

4.3.4 Number of molecules and cooling factor

Optoelectrical Sisyphus cooling can deliver large numbers of cooled molecules as will be shown now. Then, key figures of the ensemble of cooled molecules are compared to a reference of uncooled molecules in order to quantify the amount of cooling observed in the presented experiments.

	Cooled molecules	Reference ensemble
Temperature (mK)	0.42 ± 0.09	460 ± 23
Number of molecules N	3×10^5	1×10^6
Rotational states	$\|0;3,3,3\rangle$	$\|0;3,3,M\rangle$
Number density n (cm^{-3})	1×10^5	4×10^5
Phase-space density	5×10^{-13}	4×10^{-17}
Velocity in QMS (m/s)	5.1 ± 0.9	19.5 ± 0.5
Integrated signal S (counts)	131 ± 5	108 ± 2
Detection efficiency N/S	4×10^{-4}	1×10^{-4}

Table 4.4: Comparison of cooled molecules to a reference ensemble. The cooled molecules are produced according to the sequence of Fig. 4.4. The uncooled reference ensemble consists of molecules unloaded from the trap after 18 s of trap loading and 2 s of storage without any manipulation (except for state detection via MWD). Temperature and velocity of the cooled molecules were determined with RF knife-edge filters, whereas a time-of-flight measurement [Eng13, Pre12] was used for the reference ensemble for technical reasons.

We find that 3×10^5 molecules are unloaded from the trap at the end of the full cooling sequence. From this number and the previously determined approximate temperature of 420 µK, the phase-space density can be calculated as $\rho = n\Lambda^3$, with the number density n and the thermal de-Broglie wavelength $\Lambda = h/\sqrt{2\pi m_{\mathrm{H_2CO}} k_B T}$. Here, the volume of the trap is $0.3 \times 2 \times 4\,\mathrm{cm}^3$ (Sec. 3.1.1). The outcome and other characteristic quantities of the cooled molecular ensemble are listed in Table 4.4 and compared to the following reference. Unloading molecules from the trap after 18 s of trap loading and 2 s of storage without any manipulation, results in detection of 10^6 molecules with a temperature of about 460 mK in the rotational states $|0;3,3,M\rangle$. The comparison yields a reduction of kinetic energy by a factor of 1000 and an increase in phase-space density (neglecting internal molecular states, i.e. the M sublevels of $|0;3,3,M\rangle$) of about 10^4 caused by optoelectrical Sisyphus cooling.

With cooling to intermediate temperatures much larger ensembles can be produced. This is shown in Fig. 4.12 where the integrated unloading signal is plotted vs. the final effective RF for cooling of the last ten cooling steps. The relative signals can be approximately related to molecule numbers using the sensitivity calibration for the coldest molecular ensemble (lowest data point) because the unloading procedure involving parametric heating (Sec. 4.2.4) creates identical unloading and detection conditions for all ensembles shown in the figure (Appendix C.3).

From the data one can also see that per decrease of the kinetic energy by a factor of two (two cooling steps, two data points in the figure), a loss of signal of about 20 to 30 % is observed. These losses are caused by a prolonged trapping time and by cooling itself. During the very last cooling step (lowest data point), larger losses are seen. Attempts to add another step of Sisyphus cooling confirmed this trend making further cooling with the present setup increasingly difficult. These losses at very low molecule energies are attributed to technical imperfections which are discussed in the final Sec. 4.4 of this chapter.

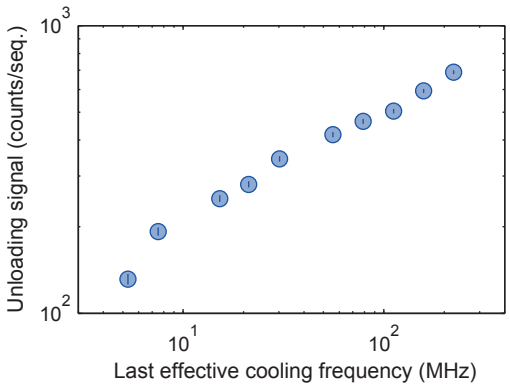

Figure 4.12: Molecule signal in the state $|0;3,3,3\rangle$ vs. final effective cooling frequency. The effective cooling frequency is given by $f_{\mathrm{RF}} - f_{\mathrm{offset}} + (\Delta f_v - \Delta f_{\mathrm{IR}})$ [cf. Eq. (4.2)]. The experimental sequence is equal to the one shown in Fig. 4.4 except that cooling was stopped earlier for the higher data points.

4.3.5 Internal-state purity

As a final characterization, the internal-state distribution after optoelectrical Sisyphus cooling is investigated now. Therefore, state detection via MWD is applied (Sec. 3.3.1) directly after Sisyphus cooling or after subsequent optical pumping to the state $|0;3,3,3\rangle$. The obtained data is presented in Fig. 4.13 and discussed in the following.

Although molecules enter the trap in many different rotational states initially, after Sisyphus cooling the majority of molecules populate only the highest ground-state M sublevels involved in the cooling scheme, namely $|0;3,3,3\rangle$ and $|0;4,3,4\rangle$, owing to two filtering effects. First, the lifetime of uncooled molecules is a lot shorter than the duration of the cooling sequence such that molecules not being cooled get lost quickly. Second, the RF for cooling which slowly drives transitions to lower lying M sublevels acts on molecules in all rotational states. Molecules not addressed by the IR laser will be lost due to induced RF transitions to untrapped states and the lack of optical pumping to strongly trapped states. This is also observed in the rotational-state distribution shown in Fig. 4.13(a): about 90 % of the trapped molecules populate the states $|0;\{3,4\},3,M\rangle$.

By appending the optical pumping scheme for preparation in $|0;3,3,3\rangle$ (Sec. 3.3.3), the molecules can be prepared in a single rotational M sublevel with high purity as shown in Figs. 4.13(b) and (c). Some molecules remain in other rotational states addressed by the state preparation scheme, $|0;\{4,5\},3,M\rangle$, whereas (5 ± 1) % are in states which are not addressed by optical pumping at all. Combining the J and M distributions, (83 ± 3) % of the ultracold molecules are measured in the target state $|0;3,3,3\rangle$. It is noted that with a careful combination of optical pumping and state-selective depletion it should be possible to obtain even higher purities (cf. Sec. 3.3).

Majorana flips to lower M sublevels. The state detection techniques employed here allow a detailed investigation of loss mechanisms from the trap and the time evolution of rotational-state distributions. While no systematic studies in these directions were performed, a final experimental observation indicating Majorana flips to lower M sub-

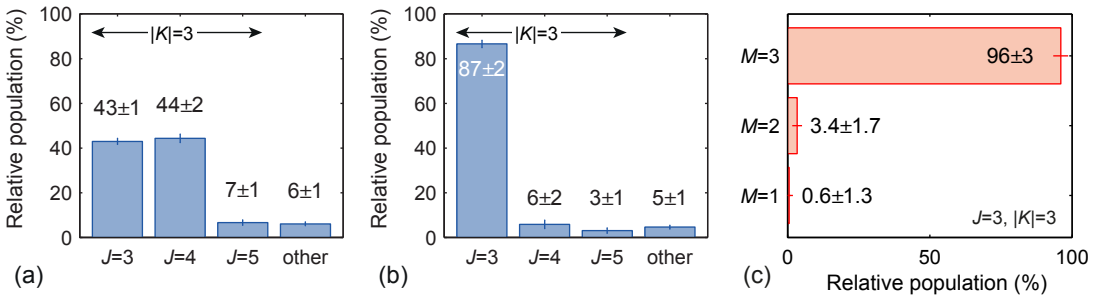

Figure 4.13: Rotational-state distribution after optoelectrical Sisyphus cooling and state preparation. State detection is performed via microwave depletion (MWD, Sec. 3.3.1) after the full cooling sequence excluding RF knife-edge filters. **(a)** J distribution directly after cooling. Molecules in the set of states $|0; J{=}\{3,4\}, 3, M\rangle$ populate mainly the highest M sublevels of the two J states due to optical pumping to strongly trapped states which is part of Sisyphus cooling. **(b)** J distribution after Sisyphus cooling and state preparation in $|0;3,3,3\rangle$ as explained in Sec. 3.3.3. **(c)** Distribution over the M sublevels of $|0;3,3,M\rangle$ after Sisyphus cooling and state preparation: the vast majority of molecules populates the highest M sublevel. In combination, (83 ± 3) % of the molecules are measured in the single rotational state $|0;3,3,3\rangle$.

levels is discussed. The population of M sublevels of the rotational state $|0;3,3,M\rangle$ which is plotted in Fig. 4.13(c) was measured directly after state preparation. If the measurement is performed after 5 s of storage and waiting time, the distribution already has changed: only (80 ± 3) % of the signal originates from the highest $M = 3$ level, whereas (16 ± 2) % and (4 ± 2) % of the molecules are measured in $M = 2$ and $M = 1$, respectively. At the same time, about 20 % of the molecules were lost from all the states $|0;3,3,M\rangle$. At least part of the Majorana transitions and losses can be suppressed by continuous optical pumping to a strongly trapped state as indicated in Sec. 3.1.4. This demonstrates once more that optical pumping, and in general control over the internal molecular state is useful for electric trapping of molecules.

4.4 Discussion and outlook

It was demonstrated that optoelectrical Sisyphus cooling is capable of producing large ensembles of ultracold ($T < 1$ mK) polar molecules. By applying the method to formaldehyde (H_2CO) it was shown that even simple species of the most general class of molecules, asymmetric rotors, can be cooled to low temperatures and controlled to a very high degree: 300,000 molecules are held in the trap, with a temperature of about 420 µK and populating a single rotational state with a purity of over 80 %. Moreover, the method relies on rather general properties of polar molecules and should therefore be applicable to other species [Zep09].

The results were achieved with a simple and robust technique and, thus, should also be usable in other experiments. The method is simple because it requires only a single laser, a single microwave, a single RF source and an electric trap which can be reproduced easily. The scheme was implemented in a robust experimental setup which was routinely operated 24 hours a day and where the experimental sequences are remote-controlled.

At present, the achieved temperature is limited by technical imperfections which was suggested by increasing losses in the last cooling step and characterization measurements of the trap electric fields. First, the roughness of the offset electric field is larger than expected for low trap voltages and does not further decrease when lowering the applied voltages. There are strong experimental hints that the disturbed electric fields are caused by surface charges on the microstructured capacitor plates of the trap. These imperfections, however, now appear at considerably lower voltages than before and hence could be reduced substantially. The issues could be overcome with an improved manufacturing process for the microstructured electrodes which delivers good high-voltage performance without a dielectric coating on the electrodes. Investigations in this direction are ongoing in our group [Kro14]. Second, measurements suggested that the coldest molecules are heated in the trap at a slow rate, possibly due to imperfect voltage sources. New devices with better specifications are already available in the laboratory and are awaiting tests. Furthermore, a different detection setup (see outlook, Ch. 6) would eliminate the need for parametric heating and, thus, a technical source of molecule losses.

More fundamentally, cooling can be improved in the following ways. The experimental tools explained in this and the preceding chapter allow for detailed characterization measurements. Developing a full simulation of the optoelectrical cooling process in the electric trap in close relation to experimental observations could yield a quantitative understanding of losses during cooling and might allow a reduction of the very same. Additionally, the electric trap itself causes losses. Despite the observation of record trapping times with 1/e decay times up to one minute, promising ideas for an improved design of the microstructured electrodes already exist [Zep13] and could lead to even better trapping and thus larger ensembles of molecules. Although a number of new characterization measurements for trap loading were presented in this chapter, the process is not entirely understood yet. In particular, it is still unclear whether the number of molecules loaded into the trap is limited by technical effects or by physical properties of the molecules, e.g., by collisions. Systematic measurements could provide a deeper understanding of this part of the sequence and open up ways to enlarge the initial sample of molecules available for cooling. Note that the temperature limit T_{grav} below which formaldehyde molecules do not possess enough kinetic energy to cover the height of 3 mm in gravity any more is close: $T_{\mathrm{grav}} = 71\,\mu\mathrm{K}$ [cf. Eq. (3.2)]. The microstructured capacitor plates of the trap are separated by this distance in the present setup. Well below that temperature it is likely that slow diffusion of molecules between different regions of the trap will make optoelectrical Sisyphus cooling to even lower temperatures hard with the current apparatus, demanding an extension of the setup (Ch. 6).

Despite the imperfections and possible improvements, the achieved temperatures and molecule numbers enable further experiments already now. For example, the low velocity of the cooled molecules of $\sim 0.6\,\mathrm{m/s}$ is ideal for high-resolution spectroscopy. In this direction, a first proof-of-principle experiment on precision spectroscopy in the electric trap is presented in the next chapter. Further exciting research possibilities for our experiment and ultracold formaldehyde molecules are discussed in the outlook of this thesis (Ch. 6).

5 Doppler-limited high-resolution spectroscopy on trapped molecules

The majority of this thesis work and the preceding chapters of this text focused on the development of cooling and control techniques for electrically trapped, polyatomic molecules. The final experimental part of the thesis presents a technique and first results for high-precision spectroscopy on electrically trapped molecules. On the one hand, this project is closely connected to the remaining experiments because it makes use of the same setup and all of the previously developed techniques. On the other hand, it also stands on its own to some extent since it tackles a separate problem, namely measuring a spectral line very accurately, which can in principle be approached from many different directions. Therefore, this chapter begins with an introduction to precise spectroscopy with molecules and its applications, as it was promised back in Ch. 1, before reporting on the results obtained in this thesis.

5.1 Introduction

Precise measurements of atomic transition frequencies, which now reach relative accuracies below 10^{-17} [Ros08], have enabled groundbreaking progress in science and technology, ranging from optical atomic clocks [Lud15] to tests of fundamental physical theories [Gri09]. Despite the lower accuracy achieved with spectroscopic investigations of molecules so far, the structure and symmetry of molecular systems can often provide a more sensitive probe of fundamental physics [Ste14, DeM17]. For example, in the search for physics beyond the standard model and time-symmetry violating interactions, experiments on ThO molecules [Bar14a, Bar17] and $^{180}Hf^{19}F^{+}$ molecular ions [Cai17] now provide the most precise upper limit for a permanent electric dipole moment (EDM) of the electron. Molecules are also used to test parity violation [Dau99, DeM08, Qua11, Cah14, Die15, Tok17], measure fundamental constants [Dau07, Mej15, Bie16], as well as their possible time variation [Hud06b, She08, Bag13, Tru13]. Moreover, precise knowledge of molecular constants is required in, among other fields, cold chemistry and collision studies, and for the interpretation of astrophysical spectra, a research area where formaldehyde is of immense importance (Sec. 1.1).

In order to achieve the demanded accuracy, isolation from the environment as well as cooling and control of all degrees of freedom of the molecules, internal and external, is often required. So far, the lowest temperatures and the highest level of control of ensembles of molecules have been achieved with 'indirect' production methods (Sec. 1.2), i.e. by forming molecules from laser-cooled atoms via photoassociation or magneto-association. From this active field of research two recent results demonstrate the potential for performing precise spectroscopy with such molecules. By driving Rabi oscillations between different vibrational states of photoassociated Sr_2 molecules confined in an optical lattice, line widths on the order of 100 Hz were measured [McG15].

With ground-state $^{23}Na^{40}K$ molecules produced via magneto-association and held in a crossed-beam dipole trap, a coherence time on the order of one second was observed for nuclear spin states [Par17]. However, the range of molecular species to which these techniques are applicable is limited, mostly to bialkali dimers and related constituent atoms, and for most of the applications introduced above other species are more suitable. Therefore, 'direct' cooling techniques (Sec. 1.3) are more relevant for the preparation of molecule ensembles for spectroscopy and potentially applicable to a much larger range of species. These 'direct' cooling and preparation techniques for high-resolution spectroscopy, their current status, and representative spectroscopic results are summarized in a recent review article [Wal16].

So far, most spectroscopic experiments with neutral molecules probing fundamental physics or measuring transition frequencies with high resolution use beams of cold particles, limiting the interrogation time to $\sim$ milliseconds as, for instance, in Refs. [Vel04, Hud06b, Tru13, Bar14a, Nij14, Cah14]. Longer interaction times can be achieved by launching cooled or decelerated molecules in a fountain geometry [Bet08, Tar13]. A molecular fountain of ammonia ($^{14}NH_3$) molecules with a free fall time of 266 ms was demonstrated experimentally [Che16] but not yet used for spectroscopy. Ultimately, for very long interaction times and hence high accuracy, however, spectroscopic experiments with directly cooled and trapped molecules are desired [Wal16, Koz17b]. The possibly very long interrogation time comes at the expense of Stark or Zeeman shifts of the molecular energy levels, broadening spectral lines if no additional measures are taken. Therefore, up to the year 2016 no precision spectroscopy had been performed on trapped molecules produced with 'direct' methods [Wal16].

In this chapter, we combine techniques well-known from atomic clocks [Ye08], i.e. the choice of a 'clock' transition with vanishing first-order differential Stark shift and measurement at a 'magic' electric field with minimal residual Stark broadening, with the experimental toolbox developed throughout this thesis to accurately investigate a rotational microwave (MW) transition of formaldehyde. Our box-like electric trap, the low temperatures achieved with optoelectrical Sisyphus cooling, and the high level of rotational-state control give ideal conditions for precise spectroscopy. Here, the primary motivation for this work is to find out how accurately we can probe molecular transition frequencies with the current experimental apparatus.

In particular, Doppler-limited precision spectroscopy on electrically trapped and cooled formaldehyde molecules is shown as a first application of optoelectrical Sisyphus cooling. By choosing the rotational 'clock' transition $|0;4,3,2\rangle \leftrightarrow |0;5,3,3\rangle$ and tuning the trapping fields to a 'magic' offset electric field, line widths down to 3.8 kHz are observed. The developed simulations fit the observed spectra and explain their shape. Experimentally, the line position can be determined with sub-kHz statistical uncertainty. However, the calculations of the differential Stark shift are less accurate, limited by the precision of the rotational constants [Brü03]. Nevertheless, a relative uncertainty of 10^{-8} is reached for both line width and position. The observed precision is not yet better than what is achieved with conventional techniques employing molecular beams. Nevertheless, this proof-of-principle experiment for the first time transferred successful techniques for precision spectroscopy in traps from atoms and simple diatomic molecules to cooled and electrically trapped polyatomic molecules. Furthermore, a clear path towards narrower spectra opens up a way towards spectroscopy experiments of unprecedented precision for this class of molecules.

The remaining chapter is structured as follows. In Sec. 5.2 it is shown how Stark broadening is reduced to the sub-kHz level for the chosen transition by adjusting the offset electric field in the trap. A numerical simulation of the spectral shape, given by Stark broadening and the energy distribution of the trapped molecules, is developed in Sec. 5.3. Then, Doppler-limited spectroscopy results for trapped formaldehyde are presented in Sec. 5.4. Fits of the simulated spectra to the data demonstrate a good understanding of the experiments. We also discuss technical effects which inhibit spectroscopy measurements on the coldest molecular ensembles at the 'magic' electric field with the current experimental sequence. Finally, prospects for obtaining narrower spectra are examined in Sec. 5.5.

5.2 Eliminating Stark broadening

Electric or magnetic traps by definition rely on inhomogeneous electromagnetic fields in order to confine the molecules. Hence, spectroscopic lines of trapped molecules are usually broadened by Stark or Zeeman shifts and a reduction or the elimination of such a line broadening is a major challenge on the way towards precise spectroscopy. To achieve good trapping conditions in our electric trap, we prefer to work with molecules in internal states with a large (linear) Stark shift. Therefore, the differential Stark shifts usually depend linearly on the electric-field strength and line widths are dominated by Stark broadening. In fact, this feature has been exploited to measure the electric-field distribution in the trap (Sec. 3.1.3 and Appendix B). Thus, even in our box-like trap, Stark broadening amounts to several MHz for most transitions and scales with the differential Stark shift. To measure a narrow spectral line with trapped molecules, the differential Stark shift of the chosen transition should be small, while the initial and final states should, of course, be trapped, i.e. have sizable individual Stark shifts. In our approach, Stark broadening is essentially eliminated with two measures: by selecting a transition with vanishing first-order differential Stark shift and by tuning the offset electric field in the trap to a 'magic' value where the remaining (quadratic) differential Stark shift is minimal and hence the residual Stark broadening is minimized.

First, the conditions for vanishing first-order differential Stark shift $\Delta\nu_s^{(1)}$ are examined.

$$\Delta\nu_s^{(1)} = \frac{\mathcal{E}}{h}\left(\mu' \frac{K'M'}{J'\,(J'+1)} - \mu \frac{KM}{J\,(J+1)}\right) \tag{5.1}$$

is obtained from the formula for the linear Stark shift emerging from first-order perturbation theory for symmetric-top-like rotational states [Eq. (2.16)], with the electric-field strength $\mathcal{E}$, the potentially state-dependent electric-dipole moment μ, and the rotational quantum numbers of the initial and final rotational states. Evidently, a $M = 0 \leftrightarrow M' = 0$ transition would trivially eliminate $\Delta\nu_s^{(1)}$. However, the initial and final molecular states would not be trapped then. Small differential Stark shifts can be observed for $\Delta J, \Delta K, \Delta M = 0$ vibrational transitions connecting trapped states, as we have already seen in Sec. 3.3.2. Yet, for the vibrational mode we are presently able to excite in formaldehyde, the dipole moments of the ground and excited vibrational states differ significantly, causing a reduced but still linear Stark shift. Moreover, very precise vibrational spectroscopy would require a more accurate frequency stabilization of our infrared laser. Restricting ourselves to purely rotational, electric-dipole-allowed

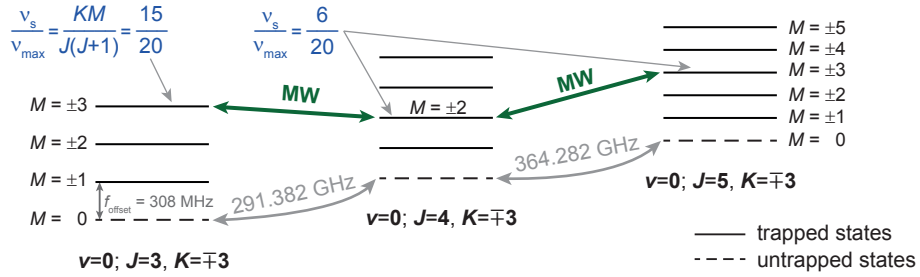

Figure 5.1: Level scheme for precision spectroscopy. The transition $|0;4,3,2\rangle \leftrightarrow |0;5,3,3\rangle$ fulfills the condition for vanishing first-order Stark shift. This is seen from the fractional first-order Stark shifts $\nu_s/\nu_{\max} = \nu_s/(\mu\mathcal{E}/h)$ which are specified for the involved states [cf. Eq. (2.16)]. After optoelectrical Sisyphus cooling and state preparation, the molecules populate the state $|0;3,3,3\rangle$ with high purity (Sec. 4.3.5). The spectroscopy signal is obtained by coupling the states $|0;3,3,3\rangle$, $|0;4,3,2\rangle$, and $|0;5,3,3\rangle$ with microwaves (MW) as shown and measuring the signal of molecules originating from the states $|0;5,3,M\rangle$ after application of the MW.

transitions between trapped, low-field-seeking states, $\Delta\nu_s^{(1)}$ can also be eliminated by choosing a $J \leftrightarrow J' = J+1$, $M \leftrightarrow M' = M+1$ transition with the additional condition

$$\frac{K(M+1)}{(J+1)(J+2)} - \frac{KM}{J(J+1)} = 0 \tag{5.2}$$

which translates to J being even and $M = J/2$. Many of these $|0;J,K,J/2\rangle \leftrightarrow |0;J{+}1,K,J/2{+}1\rangle$ transitions with even J exist and one of them, $|0;4,3,2\rangle \leftrightarrow |0;5,3,3\rangle$, is already part of our state-detection and state-preparation schemes (cf. Fig. 2.10). We pick this 'clock' transition with vanishing $\Delta\nu_s^{(1)}$ for further investigations.

Spectroscopic measurements of the selected transition with cooled molecules can be performed with the scheme shown in Fig. 5.1. Starting with the molecules prepared in the state $|0;3,3,3\rangle$, two MW frequencies transfer population to $|0;5,3,3\rangle$ via the transition under investigation. State detection is applied to measure the signal originating from molecules in $|0;5,3,M\rangle$. Spectroscopy on molecules cooled with the present level scheme (Sec. 2.5) can only be conveniently performed in the $|K| = 3$ manifold of states since transitions with $\Delta K \neq 0$ are strongly suppressed (Sec. 2.2), making a transfer of cooled molecules to other K-manifolds difficult.

In order to find the optimal electric-field configuration for the measurement, the remaining higher-order differential Stark shift of the chosen transition is investigated. It is plotted in Fig. 5.2(a) and was calculated by numerically diagonalizing the full rotational Hamiltonian in a static electric field using the rotational constants of Ref. [Brü03] and the vibronic-ground-state electric dipole moment of 2.3321 Debye [Fab77]. As expected, the Stark shift is comparably small and features a minimum around which the calculated shift varies only slightly even for big variations of the electric field. The 'magic' electric field for minimal Stark shift is 1.05 kV/cm. Tuning the trapping potential such that the offset electric field $\mathcal{E}_{\text{offset}}$ of the box-like potential is exactly at this value minimizes the residual Stark broadening. The required trap voltage configuration and the resulting simulated electric-field distribution are shown in Fig. 5.2(b). The desired $\mathcal{E}_{\text{offset}}$ is higher than what is usually used for trapping and cooling, but it is

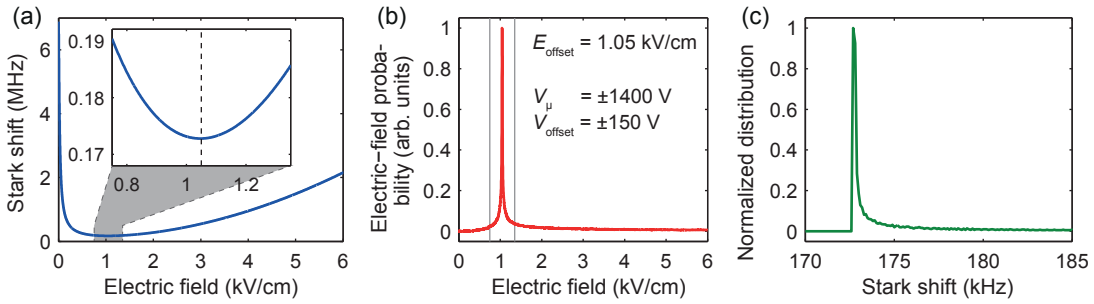

Figure 5.2: Differential Stark shift of the transition $|0;4,3,2\rangle \leftrightarrow |0;5,3,3\rangle$ in the 'magic' electric field. **(a)** Stark shift vs. electric field. The minimum is marked with a dashed line in the inset. Around the minimum, the Stark shift varies only slightly even for largely different electric field strengths. The differential Stark shift was calculated by numerical diagonalization of the full rotational Hamiltonian with electric-field interaction using the rotational constants of Ref. [Brü03] and the electric dipole moment of Ref. [Fab77]. Note that the shift is specified relative to the zero-field center frequency 364282.0125 MHz coupling the two inversion doublets in question (cf. Table 5.2 and Sec. 2.4.3). **(b)** Simulated electric-field distribution with the desired offset electric field (see also Sec. 3.1.3). The gray lines mark the electric-field range of the inset of part (a). The applied trap-electrode voltages are specified. **(c)** Distribution of differential Stark shifts in the trap for the chosen voltage configuration. Stark broadening in the trap is reduced to well below 1 kHz for optimal experimental parameters.

accessible with the current trap (cf. Sec. 3.1). From the differential Stark shift and the field distribution, the distribution of Stark shifts in the trap is calculated for the 'clock' transition in the 'magic' trapping configuration [see Fig. 5.2(c)]. Evidently, the choice of parameters results in a very narrow distribution and Stark broadening is reduced to the sub-kHz level. Furthermore, the asymmetry of the distribution of Stark shifts and hence of the expected spectral line shape, with the steep cutoff due to the minimum of the differential Stark shift, allows for a precise measurement of this minimal shift. The minimum originates in the interplay of two effects: the inversion splitting which dominates the differential Stark shift for small electric fields and the quadratic, second-order Stark shift observed at high electric fields. Thus, the 'magic' electric field for minimal Stark shift strongly depends on the specific 'clock' transition, while the behavior shown in Fig. 5.2 is qualitatively similar for other such transitions with vanishing first-order differential Stark shift (see also the discussion of future prospects in Sec. 5.5).

The Stark broadening is now small enough to allow hyperfine structure to be resolved (Sec. 2.2) if other broadening mechanisms are reduced to the same level. For the chosen transition and the high offset electric field the hyperfine components are split ~ 0.6 kHz [Fab77]. However, in the first proof-of-principle experiments on precision spectroscopy presented here, the required resolution could not be achieved and hyperfine structure is still covered by Doppler broadening, mostly for technical reasons as will be seen throughout the chapter.

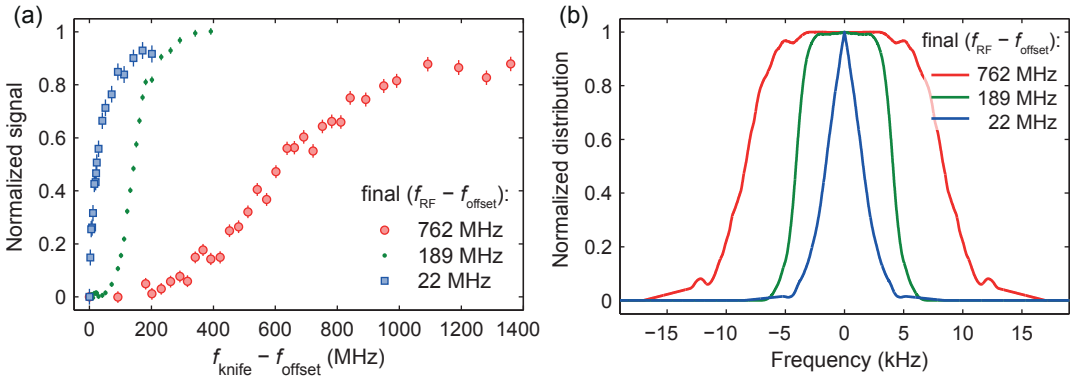

Figure 5.3: Doppler broadening resulting from the velocity distribution of the molecules. (a) Measured, integrated energy distribution for three molecule ensembles in frequency units $[E_{\mathrm{kin}} = 3h\,(f_{\mathrm{knife}} - f_{\mathrm{offset}})]$. The distributions were recorded with RF knife-edge filters (Secs. 4.1 and 4.3.1) at the 'magic' offset electric field desired for spectroscopy. Molecules were prepared in the state $|0;3,3,3\rangle$ and only those with a total energy exceeding the offset potential energy are considered (see text). The extracted median kinetic energies are summarized in Table 5.1. **(b)** Doppler broadening calculated from the measured energy distributions for the three investigated molecule ensembles.

5.3 Understanding the spectral shape

In general, a spectral line has a non-zero line width due to a number of possible broadening mechanisms [Tow75]. For purely rotational MW transitions, the natural line width is in the range of mHz or below and can therefore be safely neglected [Tow75]. Stark broadening caused by the distribution of electric fields in the trap was already discussed in the previous section and has to be considered. A line broadening can also be caused by collisions between molecules and by Doppler shifts brought about by the finite velocity of the molecules relative to the MW. As we have seen in Ch. 4, the gas of trapped and cooled molecules is dilute which is why collisional broadening can be neglected for our experimental parameters. Doppler broadening is significant and is explored in this section. Broadening of the spectral line owing to a limited interaction time of the molecules with the MW pulse or saturation of the molecular transition is avoided by choosing the length and power of the MW pulse appropriately (see Sec. 5.4.1). Consequently, the latter effects are ignored in the following, where a numerical simulation of the spectral shape is developed, considering the trapping electric fields and the Stark shift (Fig. 5.2) as well as Doppler broadening calculated from the measured energy distribution of the molecule ensemble.

Measured energy distributions. First, the energy distribution of the trapped molecules is investigated with RF knife-edge filters (Sec. 4.1). The ideal offset electric field for spectroscopy, $\mathcal{E}_{\mathrm{offset}} = 1.05\,\mathrm{kV/cm}$, is larger than the offset electric fields present during cooling, ranging from about $625\,\mathrm{V/cm}$ to $40\,\mathrm{V/cm}$, depending on the final cooling step (cf. Fig. 4.7). Therefore, the trapping potential is ramped to high offset fields adiabatically for spectroscopy after cooling with the standard sequence (Fig. 4.4). As the adjustment of the electric fields may influence the energy distribution of the molecules, the energy was measured at the target electric field with conditions identical to those

final $(f_{\mathrm{RF}} - f_{\mathrm{offset}})$	$f_{\mathrm{knife,median}} - f_{\mathrm{offset}}$	median E_{kin}
(MHz)	(MHz)	$(3/2 \cdot k_B\,\mathrm{mK})$
762	638 ± 3	61.2 ± 0.3
189	143 ± 3	13.7 ± 0.3
22	27 ± 3	2.6 ± 0.3

Table 5.1: Median kinetic energy of the molecule ensembles prepared for spectroscopy. For cooling, the sequence of Fig. 4.4 was used, with cooling stopped at the specified final f_{RF} ($f_{\mathrm{offset}} = 183.7\,\mathrm{MHz}$ for $|0;3,3,M\rangle$). The energy distributions [Fig. 5.3(a)] were measured at a high offset electric field, $\mathcal{E}_{\mathrm{offset}} = 1.05\,\mathrm{kV/cm}$, where $f_{\mathrm{offset}} = 308.4\,\mathrm{MHz}$ (see also Sec. 5.4.2). In contrast to the measurements of Ch. 4, here all molecules with a total energy smaller than the offset potential energy are not considered for the distribution and the calculation of the median kinetic energy.

used for spectroscopy. As before, the molecules are prepared in the state $|0;3,3,3\rangle$ after cooling and prior to application of the RF knife.

Integrated energy distributions for three representative molecule ensembles are shown in Fig. 5.3(a). Only molecules whose total energy $E = 3hf_{\mathrm{knife}}$ exceeds the offset potential energy $E_{\mathrm{pot}} = 3hf_{\mathrm{offset}}$ are considered in the plotted distribution because only those contribute significantly to the spectroscopy signal. To this end, the signal measured for $f_{\mathrm{knife}} = f_{\mathrm{offset}}$ is subtracted from the data and the curve is normalized to the measured signal without application of the RF knife, yielding the displayed graphs. In the two more energetic ensembles, all molecules have energies exceeding E_{pot}. However, in the case of the coldest ensemble, about 30 % of the molecules do not possess enough energy to reach the high offset electric field and are therefore discarded in the evaluation. As a characteristic number, the median kinetic energy was extracted from each distribution as previously described in Sec. 4.3.1. The values are summarized in Table 5.1. Note here that the median kinetic energy of the coldest ensemble is a factor of ten smaller than the molecules' offset potential energy.

Doppler broadening. The measured energy distributions are used to numerically calculate the expected spectral profiles resulting from Doppler broadening. To this end, a distribution of the molecular velocity $|v|$ is computed by interpolating and differentiating the measured data which represents an integrated distribution of the kinetic energy $E_{\mathrm{kin}} = \frac{1}{2} m_{\mathrm{H_2CO}} |v|^2$. Then, for every point of the velocity distribution a Doppler profile is calculated as described below. These individual spectral profiles are finally summed up, weighted with the probability to find the absolute velocity $|v|$ in the ensemble.

The measured data yields the distribution of the absolute value $|v|$ of the molecular velocity. For the calculation of the Doppler shift, however, the velocity component v_z parallel to the propagation direction of the microwave is relevant. Assuming an isotropic velocity distribution in the trap, we account for this fact in the following way. For a MW frequency f_0 and a molecular velocity component v_z, the Doppler shift is $\delta f = f_0 v_z / c$, with the speed of light c. The probability distribution $p_D(\delta f)$ of Doppler shifts for a particular total molecule velocity $|v|$ is then given by the distribution $p(v_z)\mathrm{d}v_z$ for that velocity which is constant for $-|v| \leq v_z \leq |v|$ and zero everywhere else. Using spherical coordinates and $v_z = |v| \cos\theta$ as well as $\mathrm{d}v_z = |v| \sin\theta \mathrm{d}\theta$, this can be understood as

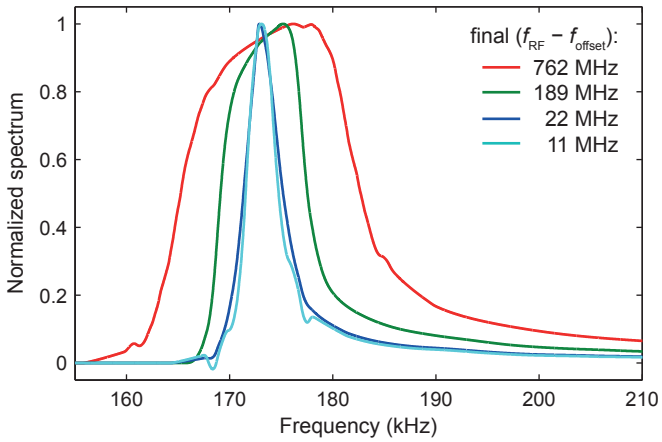

Figure 5.4: Simulated Doppler-limited spectra in the 'magic' electric field. The shape is given by the energy distribution of the molecules prepared for spectroscopy and the small residual differential Stark shift. The simulation for cooling to a final $f_{\mathrm{RF}} - f_{\mathrm{offset}} = 11\,\mathrm{MHz}$ is discussed later in Sec. 5.4.4.

follows. The probability to find v_z for a given $|v|$ is

$$p(v_z)\mathrm{d}v_z = \frac{\int_0^{2\pi} \mathrm{d}\phi |v|^2 \sin\theta \mathrm{d}\theta}{\int_0^{2\pi} \mathrm{d}\phi \int_0^{\pi} \sin\theta \mathrm{d}\theta |v|^2} = \frac{2\pi |v|^2 \sin\theta \mathrm{d}\theta}{4\pi |v|^2} = \frac{1}{2|v|}\mathrm{d}v_z. \tag{5.3}$$

Hence, we find the constant Doppler profile for a single $|v|$,

$$p_D(\delta f) = \begin{cases} \text{const.}, & \text{for } |\delta f| \leq f_0 \frac{|v|}{c} \\ 0, & \text{for } |\delta f| > f_0 \frac{|v|}{c} \end{cases}. \tag{5.4}$$

Summation over the individual $p_D(\delta f)$ for all velocities $|v|$ yields the expected Doppler broadening for a given molecule ensemble. The results of the calculation are shown in Fig. 5.3(b). For the three investigated ensembles Doppler broadening exceeds Stark broadening by far. Nevertheless, we have to work with one of these ensembles in this spectroscopy project, because colder ensembles of molecules cannot be produced at the high 'magic' electric field easily with the present sequence, as will be elaborated in Sec. 5.4.4.

Simulated spectral shape. Simulated line shapes for the transition $|0;4,3,2\rangle \leftrightarrow |0;5,3,3\rangle$ in the magic offset electric field $\mathcal{E}_{\mathrm{offset}} = 1.05\,\mathrm{kV/cm}$ are obtained by combining the calculated Doppler profiles [Fig. 5.3(b)] and the distribution of differential Stark shifts [Fig. 5.2(c)]. The resulting expected spectra are displayed in Fig. 5.4. Unsurprisingly, the form is dominated by Doppler broadening, with the asymmetry being due to the minimum of the differential Stark shift. Comparison with experimental data will show that the line shapes calculated with the presented model match the observation within the present experimental accuracy.

5.4 Experimental results

In this section, measured spectra of the transition $|0;4,3,2\rangle \leftrightarrow |0;5,3,3\rangle$ of formaldehyde are presented, showing high-resolution rotational spectroscopy on trapped polyatomic molecules and demonstrating a high level of control over all experimental parameters. After specifying the experimental sequence (Sec. 5.4.1), we investigate the influence of the trapping field on the observed line shape (Sec. 5.4.2) by comparing measurements in distinct offset electric fields including the 'magic' field. Doppler-limited spectra in the optimal electric-field configuration for different molecule energies, the main result of this chapter, are presented in Sec. 5.4.3. Finally, practical limitations of the achieved precision resulting from the current experimental sequence and the choice of internal molecular states are discussed in Sec. 5.4.4.

5.4.1 Experimental sequence

The following experimental sequence is used to record the spectra presented in this section. Formaldehyde molecules are cooled according to the standard optoelectrical Sisyphus cooling sequence of Fig. 4.4, with cooling stopped at $f_{\mathrm{RF}} - f_{\mathrm{offset}} = 726\,\mathrm{MHz}$, 189 MHz, or 22 MHz. The entire cooling process takes place at a trap voltage $V_{\mathrm{trap}} = \pm 1500\,\mathrm{V}$ with an offset electric field $\mathcal{E}_{\mathrm{offset}} = 625\,\mathrm{V/cm}$ (Sec. 3.1.3). Thereafter, the ensemble is optically pumped to the state $|0;3,3,3\rangle$ (Sec. 3.3.3). Then, the box-like trapping potential is adiabatically ramped to $\mathcal{E}_{\mathrm{offset}} = 1.05\,\mathrm{kV/cm}$ in 250 ms. The MW coupling for the spectrum is applied for 500 ms, as depicted in Fig. 5.1 and detailed below. Next, the trapping potential is ramped down again and MWD is applied for 1.5 s for state selection (Sec. 3.3.1), removing all molecules from the trap which still populate the states $|0;\{3,4\},3,M\rangle$. Finally, the molecules remaining in $|0;5,3,M\rangle$ are unloaded from the trap[1] and detected with the QMS. Thus, the spectroscopic signal consists of an increased number of molecules detected in the state manifold $|0;5,3,M\rangle$.

Microwave coupling. To record the spectrum, two MW are applied for 500 ms, coupling the states $|0;3,3,3\rangle \leftrightarrow |0;4,3,2\rangle$ and $|0;4,3,2\rangle \leftrightarrow |0;5,3,3\rangle$ with the frequency of the latter MW being scanned. For quasi-simultaneous driving, the two frequencies are cycled with a total period of 10 ms. The transition $|0;3,3,3\rangle \leftrightarrow |0;4,3,2\rangle$ has a large differential Stark shift of $-555\,\mathrm{MHz}$ at the 'magic' electric field and requires large power because of the substantial Stark broadening and a small Clebsch-Gordan coefficient. In every cycle, the corresponding MW is applied for 4 ms. For the remaining time, the MW coupling for the transition under investigation is applied. Due to the tiny Stark broadening, the radiation source, an amplifier multiplier chain (Sec. 3.2), has to be attenuated dramatically to drive the transition well below saturation. This was accomplished by using the built-in voltage-controlled attenuator of the chain and by placing additional attenuating material[2] between the microwave horn antenna and the vacuum chamber. The applied power was optimized experimentally by scanning the

[1] The signal consists mainly of molecules in the state $|0;5,3,3\rangle$ having a smaller Stark shift than the state $|0;3,3,3\rangle$. Therefore, a higher unloading electric field strength than in previous experiments (Sec. 4.2.4) is required for optimal trap unloading. The coldest of the three molecule ensembles is parametrically heated directly before unloading, as explained in Sec. 4.2.4.

[2] The custom-built attenuator consists of (part of) an old trap microstructure plate with rotatable orientation, placed between cardboard.

attenuator control voltage. In this way, power broadening of the spectral line due to saturation of the molecular transition was eliminated and does not have to be considered in the numerical simulation. To allow precise frequency measurements, the MW synthesizer was phase-locked to a stable 10 MHz frequency reference derived from the H_2-maser which is operated at the institute.

5.4.2 Influence of the trap electric fields

The specific electric-field distribution in the trap strongly influences the shape of the investigated spectrum. Therefore, the field distribution was measured for the desired offset electric field. Moreover, the spectral shape of the transition $|0;4,3,2\rangle \leftrightarrow |0;5,3,3\rangle$ was investigated for different electric-field configurations in order to verify the previous calculations, e.g., of the differential Stark shift (Fig. 5.2) and the expected spectral line shape (Fig. 5.4).

Measured electric-field distributions[3] for three offset electric fields, including the 'magic' field $\mathcal{E}_{\text{offset}} = 1.05\,\text{kV/cm}$, are shown in Fig. 5.5(a). The simulation of the electric-field distribution describes the observed data well enough to serve as useful input for the previously discussed simulations of the spectrum of interest. Furthermore, the applied voltages indeed produce the desired offset electric field and the distribution is narrow, with the relative full width at half maximum being only 1.4 % at the 'magic' trapping configuration. Note that the simulated curves are scaled with a factor 1.005 in horizontal direction to achieve good overlap with the data. This small discrepancy could be due to, e.g., a slight deviation of the separation of the microstructured capacitor plates of the trap from the specified value (cf. Sec. 3.1.1) or a tiny—and neglected—dependence of the electric dipole moment of formaldehyde on the rotational state.

For the three offset electric fields, the distribution of differential Stark shifts of the transition $|0;4,3,2\rangle \leftrightarrow |0;5,3,3\rangle$ was calculated. The benefit of the 'magic' offset electric field is apparent in Fig. 5.5(b). The two remaining trap voltage configurations were chosen such that the Stark shift in the corresponding offset electric field is approximately 10 kHz larger, with one offset field being smaller than the 'magic' field and the other one larger. The two distributions with the double-peak structure are very similar but deviate slightly due to the exact form of the differential Stark shift and specific electric-field distributions. Common to all three distributions is the sharp cutoff at their left sides due to the minimum of the differential Stark shift.

Following the recipe outlined in Sec. 5.3, the expected Doppler-broadened spectra were calculated for the molecule ensemble with intermediate kinetic energy and the three trapping configurations. The measured spectra and the simulations fitted to them are displayed in Fig. 5.5(c). The good overlap of experiment and theory demonstrates decent control over all relevant parameters. As expected, the narrowest spectrum is observed at the 'magic' offset electric field. Note that the small differences observed in the (double-peaked) distribution of Stark shifts for the remaining two trapping configurations are also visible in the measured spectra.

[3] See Sec. 3.1.3 and Appendix B for details on the measurement procedure and the simulation.

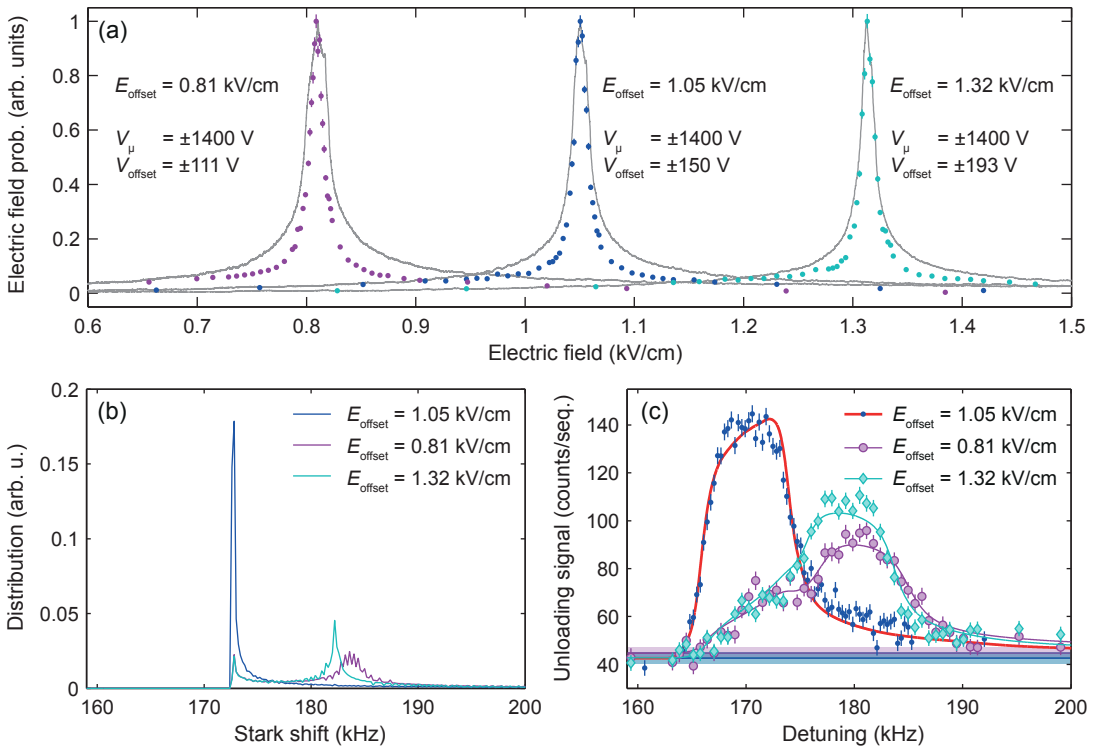

Figure 5.5: Spectral shape for different electric-field distributions in the trap. **(a)** Measured and simulated electric-field distributions for three offset electric fields. The simulated distributions were scaled with a factor 1.005 in horizontal direction. **(b)** Distribution of differential Stark shifts of the transition $|0;4,3,2\rangle \leftrightarrow |0;5,3,3\rangle$ for the three trap voltage configurations. The curves are normalized to equal areas under the curves. The data for $\mathcal{E}_{\text{offset}} = 1.05\,\text{kV/cm}$ is identical to Fig. 5.2(c). **(c)** Measured and simulated MW spectra (final cooling frequency $f_{\text{RF}} - f_{\text{offset}} = 189\,\text{MHz}$, $E_{\text{kin}} \sim \frac{3}{2}k_B \cdot 14\,\text{mK}$). The vertical scaling and the horizontal position of the simulated spectra was fit to the data (see also Fig. 5.6). The calculated shape of the spectra is solely determined by the Stark shift, the electric-field distribution, and the measured velocity distribution of the probed molecules (Sec. 5.3).

5.4.3 Doppler-limited spectra in a 'magic' electric field

Finally, spectra in the 'magic' field are investigated for different molecular kinetic energies, showing that the line width is indeed limited by Doppler broadening. We discuss the effects limiting the accuracy with which the line position can be determined.

The measured and simulated spectra are shown in Fig. 5.6. The measurement was performed for the three molecule ensembles already investigated in Sec. 5.3. The agreement of the observed shape with the numerical calculation is excellent in all cases, demonstrating a good understanding of the performed experiment. The simulated spectra have three free parameters, the baseline in vertical direction which is defined by the measured signal with the MW coupling $|0;4,3,2\rangle \leftrightarrow |0;5,3,3\rangle$ left off, a vertical scaling factor, and a frequency shift Δf_{shift} in horizontal direction. The latter two parameters were determined with a least-χ^2 fit.

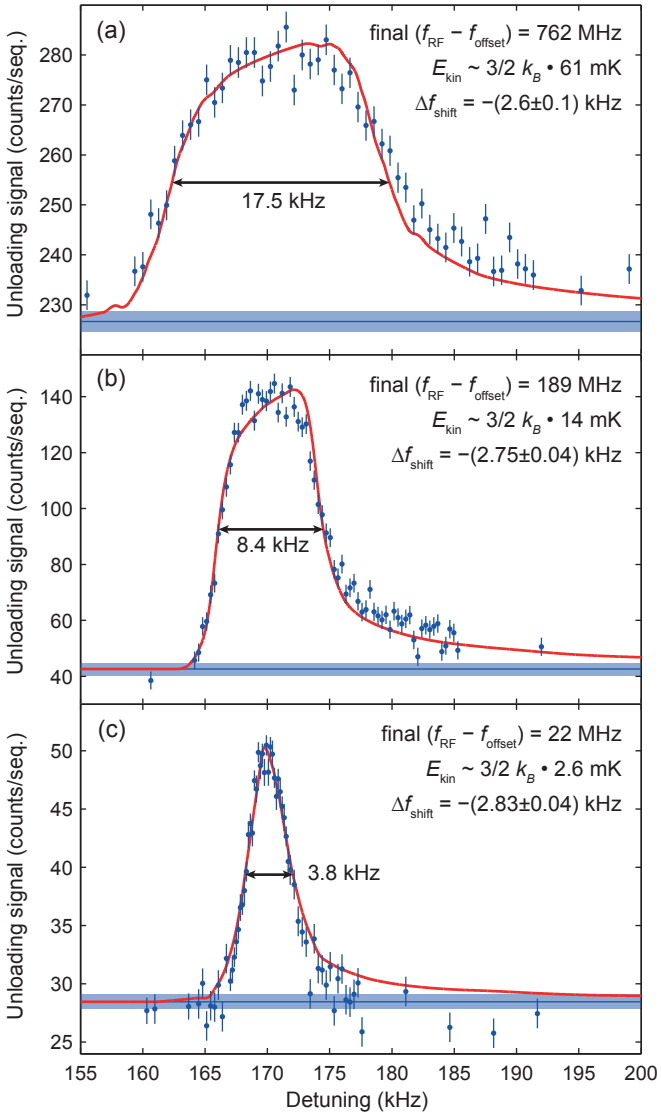

Figure 5.6: Measured and simulated Doppler-limited spectra of formaldehyde's MW transition $|0;4,3,2\rangle \leftrightarrow |0;5,3,3\rangle$. The detuning of the measured data and the theory curves is specified relative to the frequency 364282.0128 MHz (the zero-field center frequency coupling the two inversion doublets $|0;4,3,M\rangle$ and $|0;5,3,M\rangle$, calculated from literature data [Cor80], see Table 5.2 and Sec. 2.4.3). The vertical scaling and the horizontal position ($\Delta f_{\mathrm{shift}}$) of the simulated spectra (Fig. 5.4) were fit to the data. The horizontal line marks the signal measured with the MW left off (shaded region specifies the statistical error). The spectra were recorded with the three molecule ensembles discussed in Sec. 5.3, with the molecular kinetic energy varying by a factor of ~ 20 from panel **(a)** to panel **(c)**.

Transition	Frequency (kHz)	Reference
$\lvert v; J, K_A, K_C\rangle = \lvert 0; 4, 3, 2\rangle \leftrightarrow \lvert 0; 5, 3, 3\rangle$	$364\,275\,141 \pm 30$	[Cor80]
$\lvert v; J, K_A, K_C\rangle = \lvert 0; 4, 3, 1\rangle \leftrightarrow \lvert 0; 5, 3, 2\rangle$	$364\,288\,884 \pm 30$	
$\lvert v; J, K_A, K_C\rangle = \lvert 0; 4, 3, 1\rangle \leftrightarrow \lvert 0; 4, 3, 2\rangle$	$4\,572.8 \pm 0.2$	[Cha73]
$\lvert v; J, K_A, K_C\rangle = \lvert 0; 5, 3, 2\rangle \leftrightarrow \lvert 0; 5, 3, 3\rangle$	$18\,283.4 \pm 0.2$	
$\lvert v; J, K, M\rangle = \lvert 0; 4, 3, M\rangle \leftrightarrow \lvert 0; 5, 3, M\rangle$	$364\,282\,013 \pm 21$	[Cor80]
$\lvert v; J, K, M\rangle = \lvert 0; 4, 3, M\rangle \leftrightarrow \lvert 0; 5, 3, M\rangle$	$364\,282\,010 \pm 3.1$	

Table 5.2: Frequency of the investigated transition. The upper four lines of the table summarize literature values of the transitions connecting the two inversion-doublet state manifolds under investigation (no external electric fields), with asymmetric-top rotational quantum numbers as state labels. For experimental purposes, a zero-field center frequency coupling the two inversion doublets is calculated because the relevant states are strongly coupled by the electric field (Sec. 2.4). All detunings are specified relative to this frequency (fifth line). From our measured data and simulated spectrum a new zero-field center frequency is calculated with smaller experimental error (last line), limited by the accuracy of the calculated minimum of the differential Stark shift, that is the accuracy of the rotational constants [Brü03] (see text).

Line width. By performing spectroscopy with cooled molecules in a low-millikelvin temperature range Doppler broadening is reduced and line widths down to 3.8 kHz are observed. This corresponds to a relative precision of 10^{-8}. Doppler broadening can be decreased further by using colder molecules. However, for this particular measurement sequence with a relatively high 'magic' electric field, a further reduction of the molecular temperature cannot be achieved easily as will be discussed in the following subsection. Despite this limitation, the observed line width sets a new record for spectroscopy on trapped polyatomic molecules.

Line position. To assess the precision with which the position of the spectral line is measured, two cases can be distinguished. First, the position of the Stark-shifted line can be determined with high accuracy, due to the sharp cutoff on the left side of the spectrum, caused by the minimum of the differential Stark shift. From the fit of the theory curve to the data, the position is determined with sub-kHz statistical uncertainty (see fitted parameter Δf_{shift}). As the spectrum was simulated with a simplified model and hyperfine structure was neglected, we estimate as a conservative value that the Stark-shifted line position of the transition $\lvert 0; 4, 3, 2\rangle \leftrightarrow \lvert 0; 5, 3, 3\rangle$ is measured with an accuracy of at least a couple of hundred Hz.

Often, the transition frequency without electric field is of interest. It can be computed from the measurement considering the calculated minimum of the differential Stark shift, (172.5 ± 3.1) kHz. This value depends on the rotational constants and is thus limited by their accuracy [Brü03]. Consequently, the zero-field center frequency of the investigated transition can be deduced with a systematic uncertainty of 3.1 kHz. The extracted frequency with marginally increased precision and measured values from the literature are summarized in Table 5.2.

While we could measure the investigated transition with higher accuracy, the primary goal of the evaluation was not the precise specification of a particular transition

frequency in formaldehyde. Rather, the aim was the demonstration of high-resolution spectroscopy of a 'clock' transition of a polyatomic molecule in a 'magic' electric field and the identification of general limitations and future possibilities for precision spectroscopy of trapped molecules in our experimental apparatus.

5.4.4 Experimental limitations

Although this thesis work demonstrated that optoelectrical Sisyphus cooling can produce molecules with an approximate temperature of 400 µK in our trap, spectroscopy in the 'magic' field was not performed with molecules cooled that far. The underlying reasons will be explained now.

For cooling, the trap electric fields are ramped down twice to reduce the roughness of the floor of the box-like potential (Sec. 4.2.3). Thus, the coldest molecules are produced in an offset electric field of only about 40 V/cm. On the other hand, the 'magic' offset electric field for spectroscopy of the chosen transition is 1.05 kV/cm, even higher than the offset field applied during trap loading ($\mathcal{E}_{\mathrm{offset}} = 625\,\mathrm{V/cm}$). It turns out that the coldest ensembles of molecules are either heated or accumulated in the low-field dimples ($\mathcal{E} < \mathcal{E}_{\mathrm{offset}}$) during the inevitable adjustment of the offset electric field to high values. Consequently, the coldest molecules produced during this thesis work cannot be probed at high offset electric fields at the moment.

The difficulty of such an attempt can already be seen by inspecting the involved energy scales. For the coldest ensemble for which spectroscopy results were shown in this chapter [final $(f_{\mathrm{RF}} - f_{\mathrm{offset}}) = 22\,\mathrm{MHz}$], the median kinetic energy of the molecules ($f_{\mathrm{knife,median}} - f_{\mathrm{offset}} = 27\,\mathrm{MHz}$) is already a factor of ten smaller than their offset potential energy in the 'magic' trapping configuration ($f_{\mathrm{offset}} = 308\,\mathrm{MHz}$). Moreover, the box-like potential contains dimples with a depth of up to the size of the offset potential and the potential floor has a certain roughness. Taking the full width at half maximum of the electric-field distribution as a lower bound for the roughness, one finds that the median kinetic energy is only a factor of six larger than the roughness of the 'magic' potential floor. For colder molecules the situation is even worse: the kinetic energy of the coldest ensemble produced in this thesis [final $(f_{\mathrm{RF}} - f_{\mathrm{offset}}) = 3.1\,\mathrm{MHz}$] would not exceed the roughness of the offset potential any more.

Nevertheless, experimental investigations were carried out with molecules cooled to a final $(f_{\mathrm{RF}} - f_{\mathrm{offset}}) = 11\,\mathrm{MHz}$, with the final two cooling steps performed at $\mathcal{E}_{\mathrm{offset}} = 165\,\mathrm{V/cm}$ according to the developed cooling sequence (Fig. 4.4). We performed all preparatory measurements, simulated, and measured the spectrum. The simulated spectrum is plotted in Fig. 5.4 with the simulations for the remaining cooling sequences. It is emphasized that the simulated spectrum contains the measured energy distribution at the 'magic' offset electric field. Apparently, the anticipated Doppler width is not significantly reduced compared to the ensemble with a factor of two more kinetic energy [final $(f_{\mathrm{RF}} - f_{\mathrm{offset}}) = 22\,\mathrm{MHz}$], for the reasons outlined above. Therefore, the measured spectral shapes for these two ensembles show no significant deviation, which is why the one for $(f_{\mathrm{RF}} - f_{\mathrm{offset}}) = 11\,\mathrm{MHz}$ is not shown here. In essence, further cooling at a reduced trap voltage with subsequent ramping to high offset fields reduces the number of molecules due to losses during cooling but does not shift the molecular velocity distribution to lower values. Note that different voltage ramps from low to high offset electric field were tested with the colder molecule ensemble [final $(f_{\mathrm{RF}} - f_{\mathrm{offset}}) =$

11 MHz]. In particular, slow ramps (250 ms ramp time) as used for the remaining sequences, and fast ramps (1 ms) were compared. Neither of the two resulted in slower molecules at the high offset electric field.

The issues discussed here limit the experimental tunability of the two relevant parameters, molecular temperature and offset electric field strength. If the target offset electric field is high, the coldest molecule ensembles cannot be used for spectroscopy with the present electric trap and experimental sequence. Nevertheless, the experiment offers possibilities for obtaining narrower spectra with trapped formaldehyde molecules as will be elaborated in the next section. Note that these restrictions are purely technical. With an improved design of the trap electrodes, the relative roughness of the offset electric fields could be reduced [Zep13], enabling cooling to ultracold temperatures at higher offset electric fields.

5.5 Prospects for narrower spectra

Summary of present results. With the presented experiments we transferred well-known concepts for precision spectroscopy in traps, namely the choice of a narrow 'clock' transition and measurement in a 'magic' trapping field, from atoms and simple diatomic molecules to electrically trapped and cooled polyatomic molecules. Doppler-limited line widths down to 3.8 kHz were observed yielding a relative precision of 10^{-8} for the investigated transition and a new record for electrically trapped polyatomic molecules. The observed spectra were modeled and are well-understood theoretically. The experiment on precision spectroscopy demonstrates the versatility of our electric trap and the advantage of the specific trap design over previous electric traps: Stark broadening could be reduced to a minimum because of the tunable, box-like trapping potential. Moreover, this first use of Sisyphus-cooled molecules for precision spectroscopy illuminates the value of optoelectrical Sisyphus cooling and our rotational-state control techniques for further applications in general.

Future prospects. Technical improvements of the electric trap could allow the observation of even narrower spectra, as described in the previous section. Apart from that, the physical properties of our system can be exploited to perform more precise spectroscopy. Two directions are highlighted. First, possibilities for the observation of a Doppler-free spectroscopy signal were examined theoretically, taking into account coherence between the two states coupled with the investigated transition. Preliminary results from numerical simulations using the measured molecular energy distributions at the 'magic' offset electric field suggest that effects related to saturation of the 'clock' transition could allow observation of a narrow Doppler-free feature with a different set of experimental parameters. However, a detailed discussion of these simulations is beyond the scope of this text. Second, investigation of another rotational transition could allow a further reduction of the Doppler width while keeping the advantage of minimal Stark broadening due to a 'magic' electric field, as exemplified below.

Other 'clock' transitions. The condition for vanishing first-order differential Stark shift is fulfilled for many transitions in formaldehyde and similar molecules, namely for transitions $|0; J, K, J/2\rangle \leftrightarrow |0; J{+}1, K, J/2{+}1\rangle$ with J even (Sec. 5.2). In these cases,

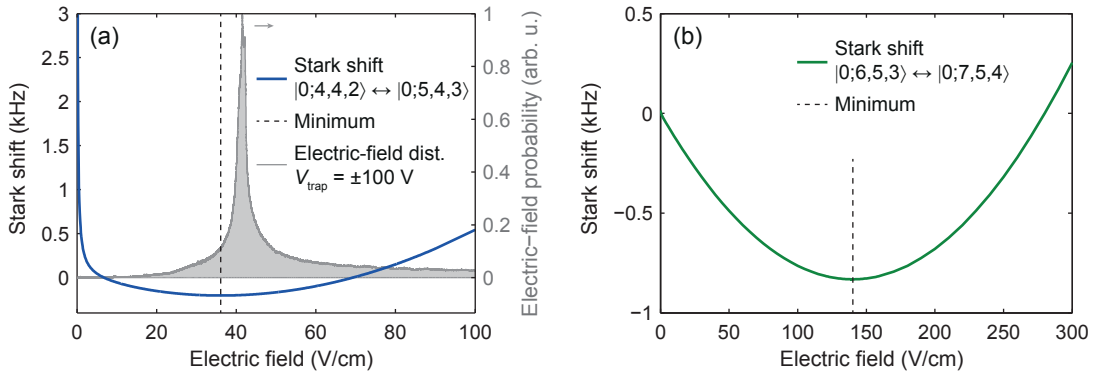

Figure 5.7: Differential Stark shift of two more 'clock' transitions of formaldehyde. (a) Differential Stark shift of $|0;4,4,2\rangle \leftrightarrow |0;5,4,3\rangle$, with respect to the zero-field center frequency 364103.222 MHz coupling the two relevant inversion-doublet states. The minimum of the Stark shift is at low electric field strengths, at which ultracold molecules can be produced in the trap. As a comparison, the simulated electric-field distribution is plotted for $V_{\mathrm{trap}} = \pm 100\,\mathrm{V}$, the trap voltage configuration used in the last cooling steps of the optoelectrical Sisyphus cooling sequence (Fig. 4.4). **(b)** Differential Stark shift of $|0;6,5,3\rangle \leftrightarrow |0;7,5,4\rangle$, with respect to the center transition frequency 509562.126 MHz.

the differential Stark shift features a minimum or maximum at some 'magic' electric field strength. The 'magic' field has to be calculated for every transition and can vary over orders of magnitude. Therefore, there exist transitions having minimal differential Stark shift at an electric field strength of only a few V/cm and ultracold ($T < 1\,\mathrm{mK}$) formaldehyde can be produced and investigated in such electric fields with the present trap.

The differential Stark shift of one such transition, $|0;4,4,2\rangle \leftrightarrow |0;5,4,3\rangle$, is shown in Fig. 5.7(a). Here, the 'magic' electric field strength is 36 V/cm, close to the offset electric field strength used for the two final cooling steps in the complete optoelectrical Sisyphus cooling sequence producing molecules at a temperature of about 400 µK. Hence, a spectroscopic line with smaller Doppler width could be observed in this case. It would require to implement optoelectrical Sisyphus cooling around the rotational states $|0;\{4,5\},4,M\rangle$. This is feasible, despite the fact that the initial thermal population of those states, $\sim 5\,\%$, is reduced to about one fifth of the population in the states used presently for cooling with our source parameters (Fig. 2.9). In fact, a series of proof-of-principle experiments was already performed during the time of this thesis work and produced a signal of cooled molecules in this set of states. Due to K being even, the $|K| = 4$ rotational states combine with a nuclear-spin singlet state (Sec. 2.2) and a hyperfine splitting is not present in this case. In contrast, the $|K| = 5$ manifold of rotational states features another 'clock' transition with hyperfine splitting and a comparably low 'magic' field of 140 V/cm. Moreover, the most suited set of states for cooling in the $|K| = 5$ manifold, $|0;\{5,6\},5,M\rangle$, has an even higher thermal population of $\sim 9\,\%$ than the states in $|K| = 4$ (Fig. 2.9). The differential Stark shift of the corresponding transition with vanishing first-order differential Stark shift, $|0;6,5,3\rangle \leftrightarrow |0;7,5,4\rangle$, is shown in Fig. 5.7(b).

The presented results and the prospects for experiments with even higher precision show the feasibility of high-resolution spectroscopy of trapped polar molecules. With future developments it should be possible to resolve the hyperfine structure of formaldehyde with sub-kHz line splittings (in a moderately strong electric field, Sec. 2.2). With colder molecules we should be able to observe Rabi oscillations in a two-level system coupled by a transition with vanishing first-order differential Stark shift, a key step towards coherent control over the internal molecular states. The combination of box-like trapping fields with extremely long storage times of cooled polar molecules also offers new possibilities for the investigation of weak forbidden transitions. As the employed techniques rely on generic properties of polar molecules, the method presented here is transferable to other species: transitions with vanishing first-order differential Stark shift coupling trapped molecular states can be found in any symmetric-top molecule or similar species.

6 Outlook

In this thesis, we reported on the production of an electrically trapped gas of formaldehyde at submillikelvin temperatures and a method to perform high-resolution spectroscopy on electrically trapped and cooled molecules. Some directions towards improving optoelectrical Sisyphus cooling with the present apparatus were already outlined in Sec. 4.4. Here, we present an overview of further advances and experiments which are now possible.

The detection efficiency of the present detection setup, built around the quadrupole mass spectrometer, is low, on the order of 10^{-4} (Table 4.4), resulting only in a small number of detection events, although large samples of cooled molecules are created. As a consequence, many repetitive measurements are required to obtain signals with a small statistical uncertainty. A more efficient detection of cold beams of formaldehyde, as generated in our setup, could be feasible via laser-induced fluorescence (LIF). In this approach, each molecule is electronically excited with an ultraviolet laser and the fluorescence photon which is subsequently emitted with a certain probability is collected with some optics and counted with a single photon detector. LIF was already used to detect formaldehyde molecules in a cold beam before by Hudson *et al.* [Hud06c, Hud06a]. Preparatory experiments on LIF of formaldehyde at room temperature, performed in our group by Erich Dobler, suggest that formaldehyde molecules with a temperature of 400 µK and in the state $|0;3,3,3\rangle$ could be counted with an efficiency of about one percent, a predicted improvement by a factor of 30 [Dob16]. Next to the much higher efficiency, detection via LIF resolves the rotational state of the molecules because the excitation frequency is state dependent. Thus, the use of LIF in our apparatus would enable faster or more precise and systematic measurements. It is currently being implemented in the laboratory and will be investigated with cooled molecules in the doctoral thesis of Martin Ibrügger.

The presently used effusive molecule source with liquid-nitrogen precooling practically restricts the range of molecule species one can consider for optoelectrical Sisyphus cooling in our setup to those with comparably large rotational constants. This constraint ensures a sufficient thermal population of the rotational states used in the cooling scheme (Secs. 2.1 and 2.4). The variety of usable species can be extended by using a cryogenic buffer-gas source and a subsequent decelerator to create a beam of slow trappable molecules. In particular, this makes Sisyphus cooling of polyatomic molecules much heavier than formaldehyde feasible. As already outlined in Sec. 1.3, a buffer-gas source and a centrifuge decelerator were combined to a very bright source of slow, trappable molecules in our group [Wu17]. This so-called cryofuge not only enabled the observation of dipolar collisions of CH_3F or ND_3 molecules in the electric quadrupole guide, but also the generation of large fluxes of slow CF_3CCH molecules. The successful experiments on optoelectrical Sisyphus cooling of formaldehyde presented in this thesis motivated the installation of a second copy of our electric trap at the output of the cryofuge where optoelectrical Sisyphus cooling of other species will

soon be investigated. Here, the molecule CF_3CCH with a mass of 94 u is particularly suited for Sisyphus cooling because of its large dipole moment of 2.3 Debye [Lid18] and fast vibrational decay rate of about 87 Hz [Zep09]. Cooling of CF_3CCH requires the cryofuge as a source because the species has a rather broad rotational-state distribution even at cryogenic temperatures of a few Kelvin owing to the small rotational constants. The broader state distribution, however, offers the possibility to investigate the performance of Sisyphus cooling with different level schemes, e.g., with a larger number of M sublevels or with more rotational J-state manifolds. In general, experiments involving a large number of rotational states and transitions can be performed more easily because rotational transition frequencies are closer together and many of them can be accessed with a single broad microwave source. For example, this allows to investigate state preparation and rotational cooling via optical pumping in a large set of states. If applied successfully, state-preparation schemes encompassing a large number of states could further broaden the range of molecule species coolable by optoelectrical Sisyphus cooling to even more complex molecules.

An important motivation for cold and ultracold molecule research is the interest in precise spectroscopy of chemically and structurally diverse species. In the previous chapter, this field was introduced and a method for high-resolution spectroscopy of trapped molecules was demonstrated. However, long interrogation times for precise measurements can also be obtained by launching molecules in a fountain [Che16], with the potential advantage of being able to probe the molecules in a field-free environment. The large numbers of ultracold molecules produced by our method at tunable velocities would constitute an ideal alternative source for such a device. In fact, the bunches of slow, guided molecules which are extracted from our trap for detection at the moment could easily by used for further experiments.

One of the long-term goals of our experiments is reaching quantum degeneracy with directly cooled polar molecules. This requires cooling to much lower temperatures. As we have outlined in Sec. 4.4, Sisyphus cooling to temperatures $T \ll 70\,\mu\text{K}$ is probably impossible in the current, comparably large, box-like electric trap because of slow diffusion of molecules between different regions of the trap. However, Sisyphus cooling could still be applied in a harmonic microwave or optical dipole trap. The temperature reached with optoelectrical Sisyphus cooling now should already be low enough to allow an efficient transfer to such a microwave trap [DeM04]. Possible transfer schemes include switching on the microwave trap exactly when molecules launched in a fountain pass the trap or using a Sisyphus-type spontaneous decay event [Nar09] to continuously accumulate molecules in a state which is trapped by the microwave trap. The latter process allowed loading of NH [Rie11] and CaH [Lu14] molecules into a magnetic trap. A transfer to a microwave or optical dipole trap is not only needed for further cooling but also to trap molecules in their rotational ground state which is always high-field-seeking and therefore not trapped in our electrostatic trap. Holding the molecules in the ground state is beneficial because inelastic state-changing two-body collisions which could lead to trap loss are then impossible, provided the kinetic energy of the molecules is low enough. As a consequence, the ensemble can be compressed to increase its density, a further advantage of a harmonic trap. Note that we have concentrated on a microwave trap in the preceding discussion because of its (typically) larger volume compared to an optical dipole trap. This facilitates an efficient transfer of molecules into it from our large-volume electric trap.

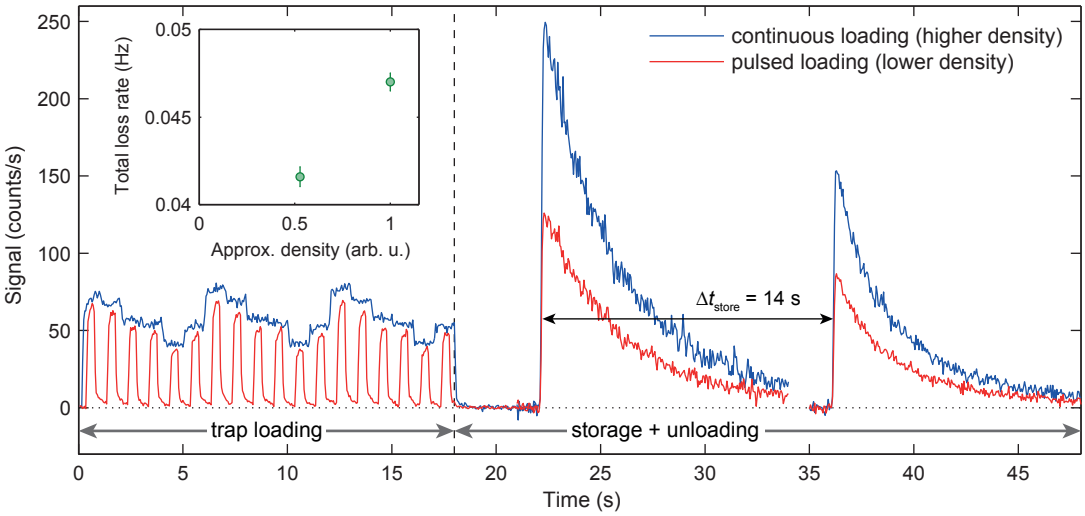

Figure 6.1: First experimental evidence for density-dependent loss. Molecules cooled to a final $f_{\mathrm{RF}} - f_{\mathrm{offset}} = 762\,\mathrm{MHz}$ and populating the rotational states $|0;\{3,4\},3,M\rangle$ used for Sisyphus cooling are probed to search for density-dependent trap losses. Two ensembles with equal initial temperature but differing initial molecule number are generated as follows. Performing the standard trap loading and shortened cooling sequence (Fig. 4.4) results in a molecule ensemble with higher density. A lower-density sample with approximately equal temperature is obtained by loading the trap in a pulsed fashion with a duty cycle of about 40 % but applying Sisyphus cooling identically to before. This is shown in the left part of the figure (the step-like modulation of both loading signals is due to the RF applied for cooling). Then, for each of the two ensembles a total loss rate r_l is estimated by comparing the integrated signal measured directly after cooling and state detection, S_0, with the signal obtained with $\Delta t_{\mathrm{store}} = 14\,\mathrm{s}$ of additional storage time, S_{store}: $r_l = -1/\Delta t_{\mathrm{store}} \log\left(S_{\mathrm{store}}/S_0\right)$. The right part of the plot displays the four trap unloading signals obtained by varying the density and the storage time. The inset shows the loss rates r_l calculated from the lower and higher density data (bars represent the 1σ statistical error). Here, the relative initial densities are obtained from the ratio of integrated signals without additional storage (S_0). This last inference requires that the two ensembles have approximately the same energy and rotational-state distributions and hence all effects related to molecule detection with the QMS affect both ensembles equally. The fact that the normalized time-resolved unloading signals S_0 of the higher and lower density ensembles overlap very well (not shown) supports the expectation of equal unloading and detection conditions for both ensembles. The observed density-dependent loss rate is a first signature of collisions. However, higher densities or a more efficient detection scheme are required for more systematic studies.

When the density is large enough that molecules collide frequently, the temperature could also be further reduced with evaporative or sympathetic [Lar06, Tok11, Lut14] cooling (see also Sec. 1.3). Both approaches require that elastic collisions dominate inelastic ones and could be investigated with molecules held in a microwave trap in their rotational ground state. Nonetheless, the collisional properties of formaldehyde which are of interest not only for further cooling but also for the field of cold and ultracold chemistry [Bel09, Stu14] can also be examined in the present apparatus. The ability to control the final kinetic energy, the rotational state, and the offset electric field as well as minute-long trapping times in our trap are ideal starting points for collision studies and could provide valuable information before an extended experimental setup is constructed. In fact, we already observed first experimental evidence for density-dependent losses in the trap, a first indication of collisions. The measurement is shown and explained in Fig. 6.1. From the data, basically two conclusions can be drawn. First, there is hope to investigate collisions between cooled formaldehyde molecules in our trap and the good control over experimental parameters in principle allows systematic experiments. However, the effects observed so far and the count rates are small and averaging over many experimental runs is required to obtain significant results. Thus, second, it would be very tedious to explore collisions with the rather inefficient detector used so far. But with a successful implementation of LIF detection in the laboratory, systematic studies of cold and ultracold collisions of formaldehyde present a very interesting research opportunity. For example, one could study the effect of the electric-field strength on collisions, deduce thermalization rates and search for scattering resonances [Boh09].

The rich internal level structure and the permanent electric dipole moment of polar molecules allows to couple molecules to other physical systems in different frequency domains, as already outlined in the introduction (Sec. 1.1). Two particularly interesting systems are superconducting microwave stripline resonators and Rydberg atoms. The former platform in combination with molecules was suggested for quantum information processing [And06, Rab06, Rab07]. Since direct cooling of molecules has now reached the submillikelvin temperature regime, molecules are cold enough to be potentially trappable in shallow traps close to such resonators. Rydberg atoms, on the other hand, are interesting because of their large dipole moment of several thousand Debye. This leads to large coupling rates and can be exploited for, e.g., a non-destructive and efficient detection scheme for polar molecules [Zep17]. For the realization of such hybrid systems, formaldehyde as an asymmetric-rotor molecule has an additional benefit over other types of molecules: the inversion-doublet states are coupled by dipole-allowed transitions and their splitting varies over orders of magnitude depending on the rotational state. Hence, a coupling frequency can be chosen with great flexibility. Moreover, the choice of rotational-state manifolds with odd or even $|K|$ determines whether the rotational states interact with magnetic fields via the nuclear spin.

Appendix A

The electric trap and surface charges: additional measurements

A crucial step towards producing an ultracold ensemble of molecules in our electric trap was the removal of severe surface charges which distort the electric fields and had accumulated in the previous version of the trap. As one consequence of these unwanted additional charges, the measured electric-field distribution deviated substantially from the expectation for the previous trap, even for high offset fields (Fig. 3.2). Prior to the experiments performed for this thesis, the (large) surface charges could be removed by installing a new pair of microstructured capacitor plates (Sec. 3.1.2). In the course of the thesis, it turned out that the problem with surface charges persists, but on a substantially reduced level (Sec. 4.2.3). This improvement is attributed to operation of the trap with lower maximum voltages. Here, we show additional measurements which were performed around the time of the exchange of the trap and show the removal of severe disturbances of the trap electric fields.

One experiment giving hints to surface charges is measuring the lifetime of molecules in the trap with the microstructured capacitor plates switched off, i.e. with $V_\mu = V_{\text{offset}} = 0\,\text{V}$. Ideally, a very fast decay of the molecule signal is expected for increasing duration of the switch-off, with the decay time depending on the kinetic energy of the molecules. Such a measurement is displayed in Fig. A.1 for the previous trap and shows that the signal decays with a time constant at least one order of magnitude too long. In contrast, the curve obtained with the newly installed current trap and plotted in the same figure satisfies the expectation of a fast signal decay.

Presumably, the unwanted charges accumulate in the dielectric coating of the microstructured capacitor plates, as already noted in Sec. 3.1. Moreover, an increased ambient temperature should increase the mobility of these charges and might remove them from the surface of the trap. This was tested experimentally with the previous trap before its replacement. We heated up the entire vacuum chamber to 200 °C for a few days and repeated the measurement after the bake-out. Indeed, the result is very close to the one obtained with the new trap immediately after installation (Fig. A.1). This suggests that the large surface charges which we had on the previous trap could be removed with this procedure. Note, however, that the currently persisting issue with small surface charges, visible as distorted electric-field distributions for low trap voltages of $V_{\text{trap}} = \pm 100\,\text{V}$ and $V_{\text{trap}} = \pm 50\,\text{V}$ [Fig. 4.9(b)], could not be solved by heating up the setup a second time.

Further evidence for disturbed electric fields can be obtained by measuring the signal of trapped molecules and varying the offset electric field. If no offset field is applied, trap losses due to Majorana flips to untrapped, high-field-seeking rotational states are

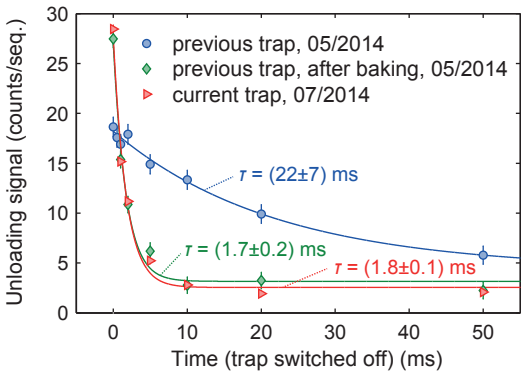

Figure A.1: Decay of the molecule signal with $V_\mu = V_{\text{offset}} = 0\,\text{V}$ for the previous and current electric trap. The measurement was performed with uncooled CH_3F molecules [Kro14]. Molecules were loaded into the trap for 4 s, stored for 2 s, and unloaded and detected for 6 s with $V_{\text{trap}} = \pm 300\,\text{V}$ applied to the trap during the entire sequence ($V_{\text{ring}} = \Delta V_{\text{guide}} = 3|V_\mu|$), except for a varying short time at the end of the storage period during which $V_\mu = V_{\text{offset}} = 0\,\text{V}$. For these uncooled molecules one would expect that the molecules cover the distance of 3 mm between the microstructured capacitor plates in $\lessapprox 1\,\text{ms}$ and get lost on approximately this time scale. The slow decay of the signal for the previous trap prior to baking is attributed to severe surface charges. Apart from the slower decay constant, the signal level without switch-off is considerably reduced in this case, showing a poor performance of the trap. Both heating up the vacuum chamber hosting the trap and installation of a new pair of microstructured capacitor plates give a larger signal initially and a signal decay roughly satisfying the expectation. Note that the offset (or rather slow additional decay) for the two lower curves is due to a small number of molecules residing in the input and exit quadrupole guides during the time of trap switch-off.

much more probable [Zep13]. Therefore, the smallest signal of trapped molecules and the shortest lifetime of molecules in the trap is expected if $V_{\text{offset}} = 0\,\text{V}$. However, this was not the case for the previous trap, as shown in Figs. A.2(a) and (b). The poorest trap performance was observed with a small offset field applied. Installation of the new trap not only restored the expected behavior but also increased the signal of trapped molecules, as demonstrated with Figs. A.2(a) and (c). Note that all measurements shown in this appendix were performed with uncooled molecules, without application of any radiation fields or state detection, and with the molecule CH_3F.

Fig. A.3 shows a photograph of the currently installed electric trap.

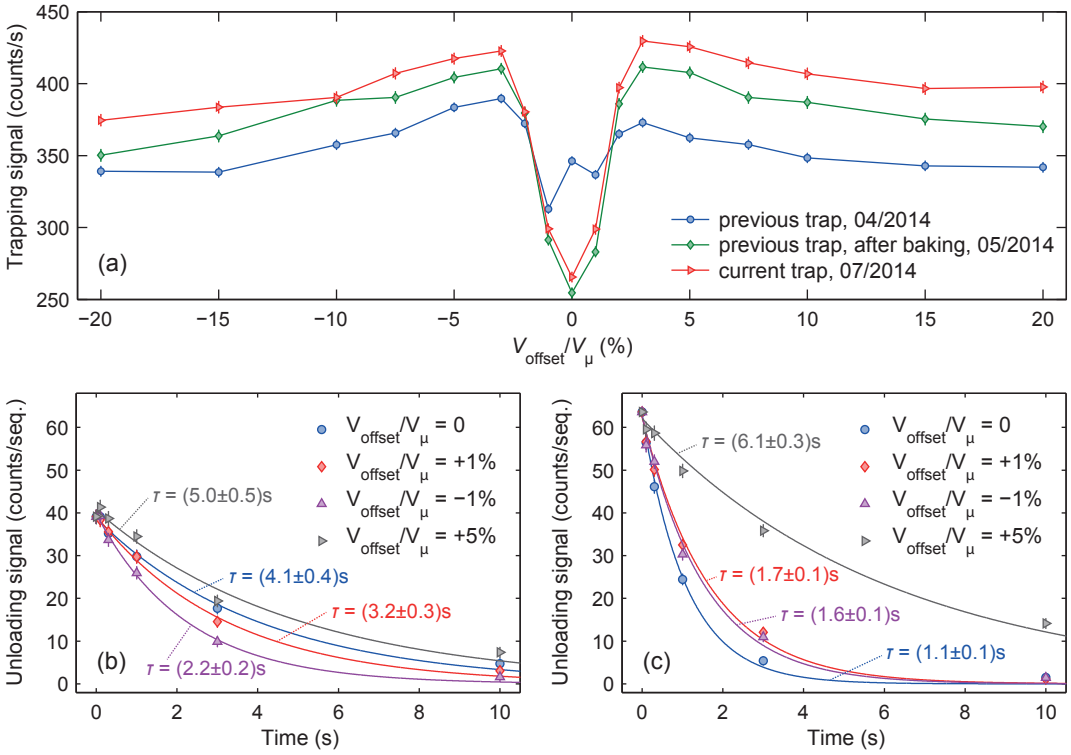

Figure A.2: Signal of trapped molecules and lifetime of uncooled molecules in the trap, before and after replacement of the microstructured capacitor plates. (a) Signal of trapped molecules vs. $V_{\mathrm{offset}}/V_\mu$. A modified, continuous measurement sequence was used. The voltages $V_\mu = \pm 600\,\mathrm{V}$ and $V_{\mathrm{ring}} = \Delta V_{\mathrm{guide}} = 3|V_\mu|$ were applied to the trap and the quadrupole guides and the signal was measured continuously. The data shown is the difference of the signal obtained with all trapping fields applied and the signal recorded with half of the trap left off. Consequently, the data contains only contributions from molecules which actually entered the trap and stayed there for a while. The smallest signal is expected for $V_{\mathrm{offset}}/V_\mu = 0$. **(b), (c)** Lifetime of uncooled molecules in the trap for the previous and current trap. The trap was loaded with $V_{\mathrm{trap}} = \pm 300\,\mathrm{V}$ for 6 s, molecules were stored for a fixed time of 0.4 s with $V_{\mathrm{trap}} = \pm 300\,\mathrm{V}$ and 0.6 s with $V_{\mathrm{trap}} = \pm 600\,\mathrm{V}$, then stored for varying time and with varying V_{offset} ($V_\mu = \pm 600\,\mathrm{V}$). Finally, the trap was unloaded for 6 s with $V_{\mathrm{trap}} = \pm 300\,\mathrm{V}$. With the new trap, a higher initial signal is measured and the fastest decay is observed for $V_{\mathrm{offset}}/V_\mu = 0$ as expected. All data was obtained with CH_3F.

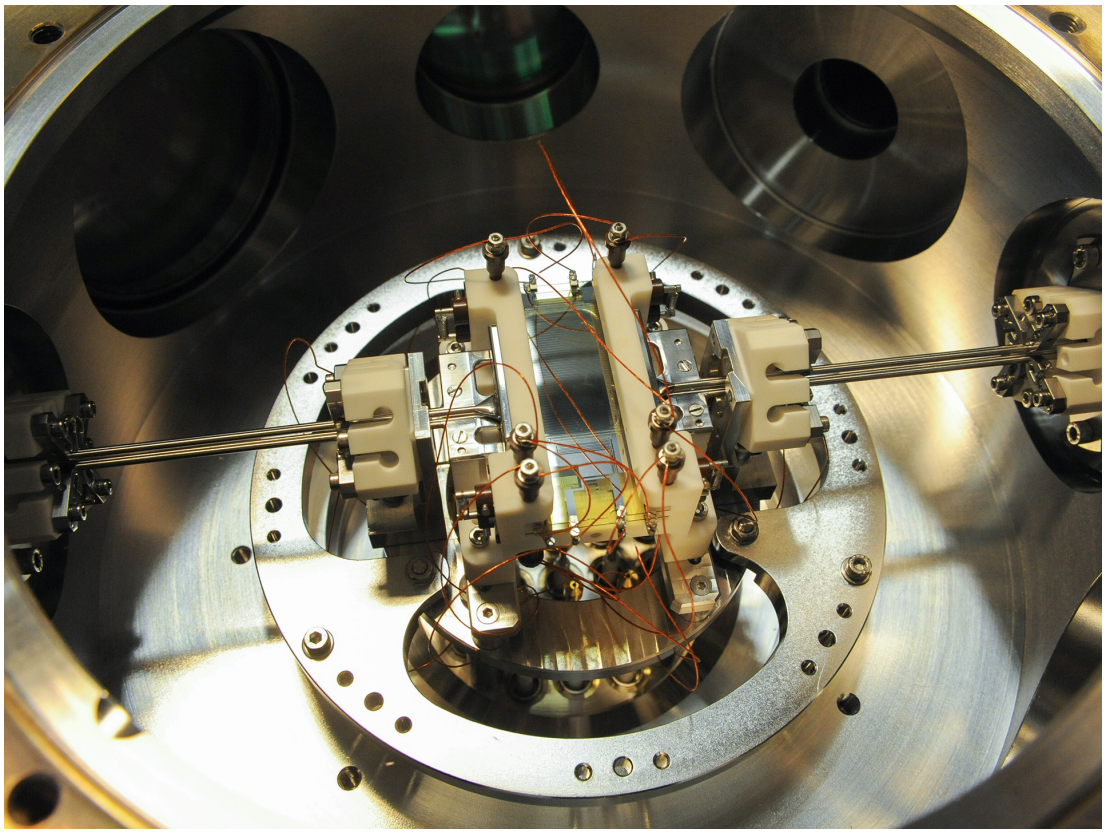

Figure A.3: Photograph of the electric trap. The picture shows the current version of the trap in the vacuum chamber before the chamber was closed. One can see the input and output electric quadrupole guides, the two glass pates holding the electrode microstructure, and the perimeter electrode (cf. Fig. 3.1). The high-voltage electrical feedthroughs are situated below the trap. The electrodes are connected to the feedthroughs with Kapton-insulated wires. Photographs of other parts of the experimental setup are included in the Diploma thesis of Manuel Mielenz [Mie10].

Appendix B

Measurement of the electric-field distribution in the trap

To measure the electric-field distribution in the trap [Sec. 3.1.3, Figs. 3.2, 4.7, 4.9(b), and 5.5(a)], Stark spectroscopy on the single MW transition $|0;3,3,3\rangle \leftrightarrow |0;4,3,4\rangle$ is performed. We use a slightly refined version of the scheme developed earlier [Glö15b] to measure the spectrum and extract the field distribution.

In brief, we prepare a sample of molecules with sufficient population in the state $|0;4,3,4\rangle$ (cooling is applied and stopped at $f_{\mathrm{RF}} - f_{\mathrm{offset}} = 189\,\mathrm{MHz}$ to obtain large signals). Then, we drive suitable IR and MW transitions to optically pump molecules in the states $|0;3,3,M\rangle$ and $|0;4,3,M{\neq}4\rangle$ to untrapped states and thus deplete all molecules in those states from the trap. The frequencies are chosen such that the transitions are driven resonantly in the homogeneous offset electric field and enough power is applied to saturate the transitions (see Ref. [Glö16] for more details). Adding another MW which couples the state manifolds $|0;3,3,M\rangle$ and $|0;4,3,M\rangle$ and varying its frequency, results in a depletion spectrum of the desired transition $|0;3,3,3\rangle \leftrightarrow |0;4,3,4\rangle$, as molecules still left in the state $|0;4,3,4\rangle$ can now only be depleted from the trap through this channel. The investigated Stark-shifted transition is always driven resonantly at an electric-field strength corresponding to the applied probe frequency. Thus, the amount of additional depletion (depending on MW power and frequency) caused by the scanned MW samples the probability for a specific electric-field strength to occur in the trap.

The number of molecules N remaining in the state $|0;4,3,4\rangle$ after depletion is related to the probability $\rho(\mathcal{E})$ of finding an electric-field strength $\mathcal{E}$ in the trap via a simple model [Glö15b]. The rate Γ at which molecules are depleted is proportional to $\rho(\mathcal{E})$ and the effective power P of the scanned MW. Additionally, we assume $N \propto \exp(-\Gamma \cdot t)$, where t is the depletion time. We then find $\rho(\mathcal{E}) \propto \log(N)/P$.

For the measurement we choose the duty cycle, meaning the effective power, of the scanned probe MW in an iterative approach such that for every applied probe frequency approximately half of the molecules are depleted from the state $|0;4,3,4\rangle$. Using the described model we plot the electric-field distribution versus electric-field strength. To validate the applicability of the model we measured the field distribution for the highest trap voltage also with half and twice the original MW duty cycle. The three resulting curves for the electric-field distribution overlap. Note that the measurement samples the electric field only up to a value of about $1200\,\mathrm{V/cm}$ for $V_{\mathrm{trap}} = \pm 1500\,\mathrm{V}$ due to the limited kinetic energy of the molecular ensemble used for spectroscopy. Additionally, the method actually measures the distribution of electric fields weighted with a factor of about $\sqrt{\mathcal{E}_0 - \mathcal{E}}$ with $\mathcal{E}_0$ being the maximum electric field strength a molecule with

given total energy can reach in the trap. Thus, this factor accounts for the probability for molecules to reach a given potential energy. For both reasons, the high-field tail of the distribution is not reproduced correctly. However, these systematics do not affect the peak of the distribution, which we are mostly interested in, very much.

Appendix C

Details on molecule detection with the quadrupole mass spectrometer

In this appendix, a few details on the detection of cold molecules with our quadrupole mass spectrometer (QMS) are explained. Specifically, the used settings are summarized in Sec. C.1. Experimental evidence for the claim that very cold and slow molecules are deflected from the ionization volume of the QMS due to a potential barrier is presented in Sec. C.2. Further, the effects of parametric heating of the trapped molecules which was employed to overcome the issue of the potential barrier is discussed in Sec. C.3. Finally, data for the determination of the sensitivity coefficient of the QMS is shown in Sec. C.4.

C.1 QMS settings

The settings used for molecule detection with the commercial QMS are specified in Table C.1. To obtain a good signal to noise ratio for the detection of beams of slow formaldehyde molecules, a few parameters were optimized experimentally. In particular, the exact mass setting for ion filtering and the "resolution" have to be adjusted to the molecule species and the settings noted in the table gave the largest signal to noise ratio and were used for all measurements of this thesis performed with formaldehyde.

C.2 Deflection of slow molecules from the ionization region of the QMS

The process of unloading cooled molecules from the trap for detection with the QMS was discussed in Sec. 4.2.4. There, it was stated that very cold and thus slow molecular beams are deflected from the ionization volume of the QMS by an unwanted potential barrier. Here, we present experimental evidence supporting this claim.

The detection setup built around the QMS is sketched in Fig. C.1. Molecules exit the electric trap and are guided to the ionization volume through an electrostatic quadrupole guide. Potentially problematic is the voltage difference between the cage around the ionization volume and the grounded end cap of the quadrupole guide. The voltage difference depends on the so-called ion reference voltage $V_{\mathrm{ion,ref}}$ which has to be applied to the cage for efficient electron-impact ionization of the molecules and extraction of the resulting molecular ions. The voltage difference and the associated electric field $\mathcal{E}_{\mathrm{barrier}}$ can cause a potential barrier and inhibit slow molecules in low-field-seeking rotational states from reaching the ionization volume. This could explain the abrupt drop

Parameter	Setting
Device configuration	
Analyser detector type	SEM
Ion source type	crossbeam
Mass range	340 amu
Ion source parameters	
Emission current	0.6 mA
Protection current	4 mA
Ion reference voltage $V_{\mathrm{ion,ref}}$	105 V
Kathode voltage	-85 V
Focus voltage	-18.5 V
Field Axis voltage	-16 V
Extraction voltage	-135 V
Inner Deflection voltage	-240 V
Protocol: Multiple Ion Detection	
Mass	28.90 a.u.
Detector type	Ion-Counter
SEM voltage	2400 V
CP Level	25
Resolution	90

Table C.1: Settings for the quadrupole mass spectrometer (QMS) used during all experiments (Model: Pfeiffer Vacuum QMG700 + QMA410 + QMH 410-3 + Quadera software).

in trap-unloading efficiency which was observed in Fig. 4.8 for the coldest molecules, i.e. for molecules cooled to a final $(f_{\mathrm{RF}} - f_{\mathrm{offset}}) \leq 189\,\mathrm{MHz}$. Of course, the height of the potential barrier depends on the electric-field strength which, in turn, depends on the exact shape of the metal surfaces in the detection region. Thus, $\mathcal{E}_{\mathrm{barrier}}$ is probably position dependent and certainly difficult to measure or calculate without opening the vacuum chamber. To test the hypothesis nonetheless, we systematically investigated molecule unloading with a smaller $V_{\mathrm{ion,ref}}$ which should result in a smaller potential barrier if such a barrier exists.

Towards this end, the measurement usually used to optimize the trap voltage applied during unloading and detection was repeated with two $V_{\mathrm{ion,ref}}$ and otherwise equal experimental parameters. Specifically, the integrated molecule signal was determined for different trap voltages during unloading and for molecule samples with differing kinetic energies. The data for the usual $V_{\mathrm{ion,ref}} = 105\,\mathrm{V}$ and a reduced voltage $V_{\mathrm{ion,ref}} = 65\,\mathrm{V}$ is displayed in Fig. C.2. Evidently, the smaller $V_{\mathrm{ion,ref}}$ dramatically reduces the overall detection efficiency by about a factor of ten. This is expected because the QMS is not operated with optimized parameters any more. Apart from that, more subtle effects are visible in a direct comparison of the curves obtained for different $V_{\mathrm{ion,ref}}$, as shown in Fig. C.3.

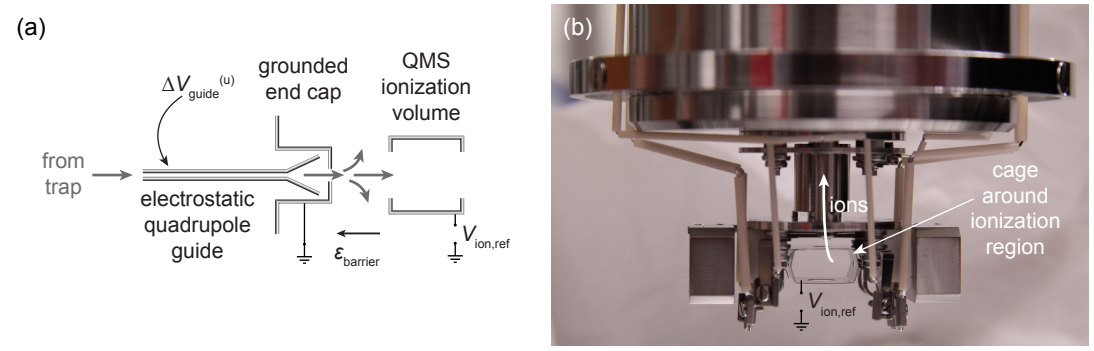

Figure C.1: Sketch of the molecule detection setup. (a) Detection geometry. Molecules leave the trap through the electrostatic quadrupole guide which is bent outwards to focus the molecular beam into the ionization region of the QMS [Mie10]. Around the quadrupole guide, there is a grounded metal cap to shield the QMS from the high electric fields present in the guide. In the setup used in this thesis work, it was not possible to apply a static voltage to the cap. For efficient electron-impact ionization and ion collection in the QMS, a voltage $V_{\mathrm{ion,ref}}$ has to be applied to the cage around the ionization volume of the QMS. **(b)** Photograph of the QMS detection region showing the ionization region and the path the molecular ions take. Molecules fly into the plane of the picture, the electron beam for ionization comes from the side of the cage. The photograph was taken in 2009 by Martin Zeppenfeld.

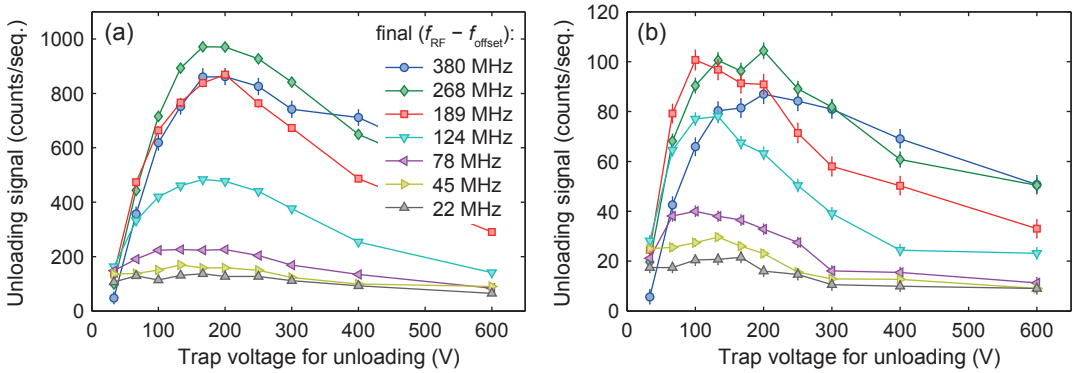

Figure C.2: Trap unloading voltage for two ion reference voltages at the QMS. The integrated molecule signal vs. trap voltage $\pm V_{\mu}^{(u)}$ (with $V_{\mathrm{offset}} = \frac{1}{5}V_{\mu}^{(u)}$ and $V_{\mathrm{ring}}^{(u)} = \Delta V_{\mathrm{guide}}^{(u)} = \frac{3}{2}|V_{\mu}^{(u)}|$) applied during unloading was recorded for various cooling sequences and with the usual ion reference voltage $V_{\mathrm{ion,ref}} = 105\,\mathrm{V}$ **(a)** and a reduced $V_{\mathrm{ion,ref}} = 65\,\mathrm{V}$ **(b)**. The measurement is very similar to the one presented in Fig. 4.8 and discussed in Sec. 4.2.4. However, the molecules were prepared in the state $|0;3,3,3\rangle$ prior to unloading and state detection for the states $|0;3,3,M\rangle$ was applied. Thus, the majority of the detected molecules are in a well-defined internal state. Solid lines are guides to the eye and keys specify when cooling was stopped. The lower $V_{\mathrm{ion,ref}}$ results in a dramatically reduced detection efficiency. The data for the two cases is compared to each other in Fig. C.3.

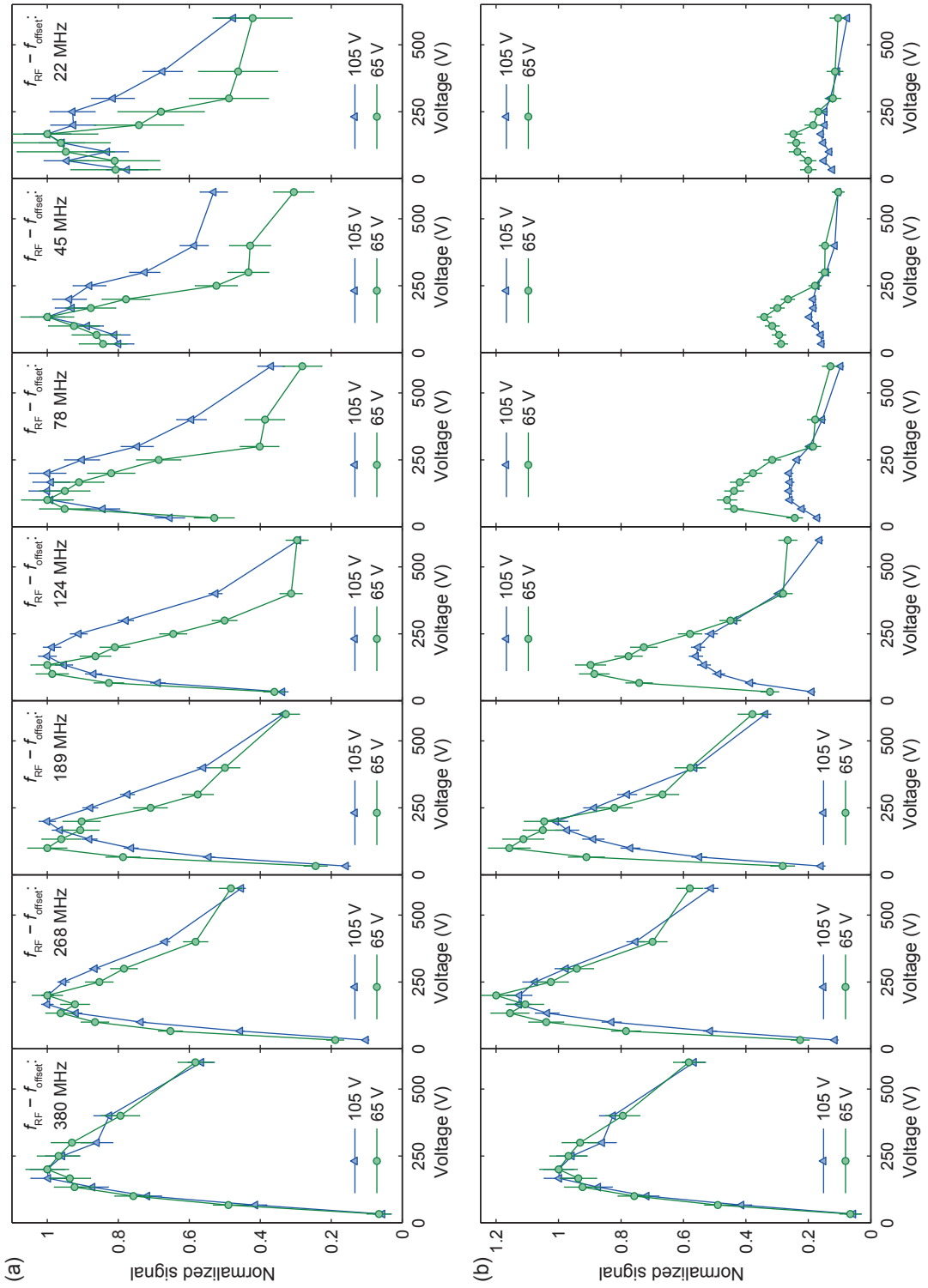

Figure C.3: Comparison of signals obtained with different ion reference voltages at the QMS. The data (plotted vs. trap unloading voltage) for the normal and reduced $V_{\mathrm{ion,ref}}$ at the QMS shown here is identical to Fig. C.2 but normalized in two different ways to facilitate comparison. **(a)** All curves normalized to their individual maximum. **(b)** The curves for each $V_{\mathrm{ion,ref}}$ are normalized to the maximum of the leftmost curve for a final $(f_{\mathrm{RF}} - f_{\mathrm{offset}}) = 380\,\mathrm{MHz}$ corresponding to the respective $V_{\mathrm{ion,ref}}$. The keys specify $V_{\mathrm{ion,ref}}$ in all panels. In each row, equal molecule ensembles are investigated, with the final $f_{\mathrm{RF}} - f_{\mathrm{offset}}$ for cooling named in part (a).

Conclusions about the unwanted potential barrier can be drawn by inspecting data measured with molecule ensembles of different energy. It is expected that the optimal trap unloading voltage, i.e. the maximum signal, for a specific molecule ensemble scales with its kinetic energy. Thus, for smaller final $f_{\mathrm{RF}} - f_{\mathrm{offset}}$ we expect the maximum as well as both flanks of the curves to be shifted to lower voltages. This was indeed observed in Fig. 4.8 for final $(f_{\mathrm{RF}} - f_{\mathrm{offset}}) > 189\,\mathrm{MHz}$. For the range of molecular kinetic energies investigated here there is hardly any shift of the maximum and the flanks observable for $V_{\mathrm{ion,ref}} = 105\,\mathrm{V}$ [Fig. C.2(a)], but from $f_{\mathrm{RF}} - f_{\mathrm{offset}} = 380\,\mathrm{MHz}$ to $f_{\mathrm{RF}} - f_{\mathrm{offset}} = 124\,\mathrm{MHz}$ a shift is visible for $V_{\mathrm{ion,ref}} = 65\,\mathrm{V}$ [Fig. C.2(b)]. For even colder molecules and $V_{\mathrm{ion,ref}} = 65\,\mathrm{V}$, only the right flank shifts with smaller kinetic energy while the maximum and the left flank of the curve do not move further to the left and the relative optimal unloading signal drops abruptly. Thus, for smaller $V_{\mathrm{ion,ref}}$ the same behavior is observed as for the usual $V_{\mathrm{ion,ref}}$ (cf. Sec. 4.2.4). However, the drop in molecule unloading and detection efficiency occurs for smaller molecular kinetic energies. This is seen best in Fig. C.3(b). As the possible potential barrier should scale with $V_{\mathrm{ion,ref}}$, this observation backs the above claim. Moreover, Fig. C.3(a) shows that the optimal trap unloading voltage for different molecule energies depends on $V_{\mathrm{ion,ref}}$. This behavior would not be expected if the voltages around the QMS ionization volume would not produce a potential barrier. Consequently, the data discussed in this section backs the assumption that the drop in unloading and detection efficiency for cold and slow molecules is caused by the electric fields around the QMS ionization volume. Hence, it should be possible to extract very cold and slow molecules from the trap, once the new detection setup employing laser-induced fluorescence is operational (Ch. 6). This would eliminate the need for parametric heating which was applied to detect the coldest molecule samples produced in this thesis work.

C.3 Parametric heating of trapped molecules

To efficiently unload the coldest molecules from the trap and detect them with the QMS parametric heating had to be applied (Sec. 4.2.4). Here, we detail how the trap electric fields were switched for heating and discuss the energy distribution of the molecule ensemble after heating.

For parametric heating we exploit the fact that the electric fields can be chosen independently in the two halves of the trap [Eng11]. Rapidly ramping to an increased offset electric field in one half of the trap ($V_\mu = \pm 100\,\mathrm{V}$, $V_{\mathrm{offset}} = 0.25 \cdot V_\mu$) with the other half remaining at the usual offset ($V_\mu = \pm 100\,\mathrm{V}$, $V_{\mathrm{offset}} = 0.05 \cdot V_\mu$) allows molecules residing in the region with higher field to roll down an electric field gradient and be accelerated. After a hold time of 50 ms, the configuration of offset electric fields in the two halves of the trap is reversed. In total, we switch the offset electric fields 20 times during 1 s, with the ramps performed in about 1 ms. In particular, $V_\mu = \pm 100\,\mathrm{V}$ for the first ten ramps and $V_\mu = \pm 200\,\mathrm{V}$ for the last ten ramps, with the remaining voltages scaled accordingly. The same heating protocol is applied after all cooling sequences with a final $(f_{\mathrm{RF}} - f\mathrm{offset}) < 189\,\mathrm{MHz}$.

After parametric heating, all molecule samples to which heating is applied have approximately the same energy distribution. This was investigated using RF-knife-edge filters (Sec. 4.1). A measurement for two cooling sequences resulting in median kinetic

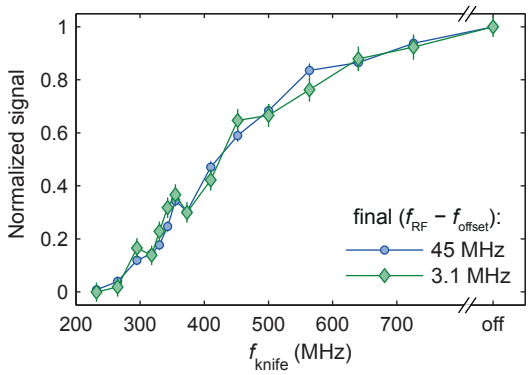

Figure C.4: Energy distribution of parametrically heated molecules in the trap. The energy distribution after heating was measured for the least energetic molecule ensemble for which parametric heating was applied [final $(f_{\mathrm{RF}} - f\mathrm{offset}) = 3.1\,\mathrm{MHz}$] and an ensemble with a kinetic energy about a factor of eight higher (see also Table 4.3). The results show that the energy distributions after heating almost overlap, independent of molecular energy before heating, as claimed in Sec. 4.2.4. As usual, the molecules were prepared in the state $|0;3,3,3\rangle$ prior to application of the RF knife for energy measurement. The data was taken at a trap voltage of $V_{\mathrm{trap}} = \pm 1500\,\mathrm{V}$ where $f_{\mathrm{offset}} = 184\,\mathrm{MHz}$.

energies differing by a factor of about eight prior to heating is shown in Fig. C.4. As the measured curves overlap, all ensembles to which heating is applied can be unloaded from the trap with the same set of unloading voltages ($V_\mu^{(u)} = \pm 200\,\mathrm{V}$, $V_{\mathrm{offset}}^{(u)} = \frac{1}{5} V_\mu^{(u)}$). Moreover, the calibration of the molecule number performed for the coldest ensemble can be directly transferred to all other molecule ensembles detected after parametric heating: except for the measured integrated QMS signal S all quantities influencing the molecule number N in Eq. (4.8) are identical. The QMS signal S for all molecule samples in question was shown in Fig. 4.12.

Note that the velocity v of molecules in the QMS needed for the calibration of the molecule number, for the cooled molecules, was calculated from the data in Fig. C.4. Towards this end, the median kinetic energy of the parametrically heated molecules was determined as $E_{\mathrm{kin}} = 3h\,(f_{\mathrm{knife,median}} - f_{\mathrm{offset}})$ with $f_{\mathrm{knife,median}} = (430 \pm 20)$ MHz, as described in Sec. 4.3.1. Assuming that the entire kinetic energy and offset potential energy of the molecules in the trap ($E_{\mathrm{pot}} = 3h f_{\mathrm{offset}}^{(u)}$ with $f_{\mathrm{offset}}^{(u)} = 78\,\mathrm{MHz}$ during unloading) is converted to forward velocity during unloading, one finds the velocity in the QMS

$$v = \sqrt{\frac{6h}{m_{\mathrm{H_2CO}}}\left(f_{\mathrm{knife,median}} - f_{\mathrm{offset}} + f_{\mathrm{offset}}^{(u)}\right)} = (5.1 \pm 0.9)\ \frac{\mathrm{m}}{\mathrm{s}}, \tag{C.1}$$

the value stated in Table 4.4.

C.4 Determination of the sensitivity coefficient of the QMS

The general approach used to measure the number of cooled molecules exiting the trap was outlined in Sec. 4.3.3. It requires determination of the sensitivity coefficient C of

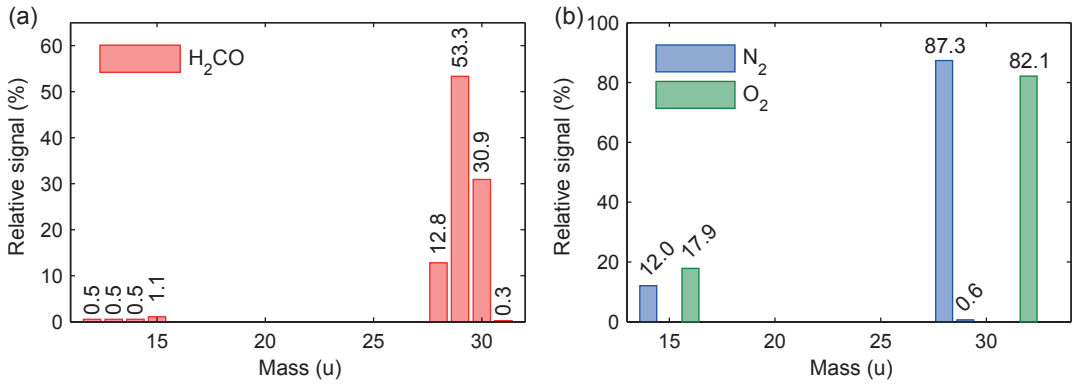

Figure C.5: Fragmentation probabilities for electron-impact ionization of H_2CO (a) as well as N_2 and O_2 (b) [Lin15].

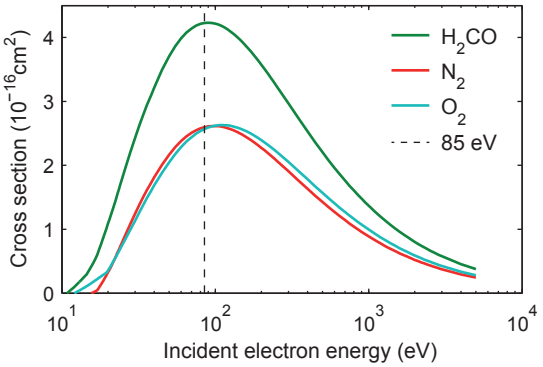

Figure C.6: Ionization cross sections for electron-impact ionization of H_2CO, N_2, and O_2 [Kim04]. The ionizing electrons have an energy of 85 eV for our QMS parameters (Table C.1).

the QMS. This quantity defines the QMS count rate $s = C \cdot n$ measured for a given number density n of molecules in the ionization volume. In the main text, we already sketched our procedure of extrapolating C for formaldehyde, H_2CO, by measuring it with the two test gases N_2 and O_2. Here, we briefly note down the performed steps and show the obtained data without justifying and explaining every step in detail.

Measuring C of H_2CO directly would require applying a constant pressure of the gas at room temperature and monitoring the count rate with the QMS and the pressure with the Bayard-Alpert gauge. Both the QMS and the Bayard-Alpert gauge employ electron-impact ionization to measure the partial or total pressure in a given ionization volume, respectively. Consequently, the direct measurement could be distorted due to an over-estimated total pressure caused by fragmentation of H_2CO [Fig. C.5(a)]. Therefore, we chose to determine C of H_2CO indirectly by applying a constant pressure of a test gas which produces less fragments to the vacuum chamber, measure the count rate as well as the pressure for the test gas, and use known fragmentation probabilities (Fig. C.5) and ionization cross sections (Fig. C.6) to deduce the expected H_2CO count rate for a given pressure. As a consistency check, the procedure was performed for N_2 and O_2.

First, mass spectra were measured for different total pressures of test gas in the

QMS vacuum chamber. These are shown in Figs. C.7(a) and (d). Since there is an unknown background pressure of residual unknown gas in the vacuum chamber, differences between each of the measured mass spectra and recorded pressure values are used in the further evaluation.

From the test-gas difference spectra $s_{tg}(m,p)$ for a pressure difference p, an expected H_2CO signal $s_{H_2CO,calc}(m,p)$ is deduced as follows. First, a sum of three shifted components $s_{tg,i}(m,p)$ of the test gas spectrum around the strongest peak is fitted to a measured mass spectrum of formaldehyde (the three strongest peaks of it):

$$s_{H_2CO,fit}(m) = a_1 s_{tg,1}(m,p) + a_2 s_{tg,2}(m,p) + a_3 s_{tg,3}(m,p). \tag{C.2}$$

Here, the $s_{tg,i}(m,p)$ are obtained by shifting the test-gas difference spectra $s_{tg}(m,p)$ [in the mass range marked in Figs. C.7(a) and (d)] to the mass values of the three strong formaldehyde fragmentation peaks, i.e. $s_{tg,i}(m,p) = s_{tg}(m+\Delta m_i, p)$. The coefficients a_i in Eq. (C.2) are scaling factors determined with a fitting routine. Note that the formaldehyde spectrum was obtained with a guided beam of uncooled formaldehyde molecules. Thus, no pressure p can be associated with it. The $s_{H_2CO,fit}(m)$ constructed in this way and the measured spectrum of guided formaldehyde are shown in Figs. C.7(b) and (e). They show a good overlap.

Next, the H_2CO count rate expected for the pressure p is calculated as

$$s_{H_2CO,calc}(m,p) = \frac{1}{F_{tg}} \frac{\sigma_{H_2CO}}{\sigma_{tg}} \left[b_1 s_{tg,1}(m,p) + b_2 s_{tg,2}(m,p) + b_3 s_{tg,3}(m,p) \right], \tag{C.3}$$

with test gas fragmentation probability F_{tg} (Fig. C.5) and the ionization cross sections σ (Fig. C.6). The b_i scale the fitted spectra to the signal level corresponding to p via the relation

$$b_i = \frac{1}{F_{H_2CO}} \frac{a_i(p)}{\sum_i a_i(p)} \tag{C.4}$$

which also takes into account the total fragmentation probability for the three strongest formaldehyde mass peaks, $F_{H_2CO} = 0.971$.

In our normal experiments, formaldehyde molecules are counted by setting the mass filter of the QMS to a fixed mass of 28.9 u (Table C.1). Therefore, finally, we use the expected, pressure-dependent count rate for this mass setting, $s_{H_2CO,calc}(m{=}28.9\,\mathrm{u}, p)$, and plot it vs. number density n [using $n = p/(k_B T)$] to fit the desired sensitivity coefficient C of the QMS. The data and the fit results are shown in Figs. C.7(c) and (f). As already noted in Sec. 4.3.3, the coefficient determined with nitrogen differs from the one obtained with oxygen by about 15 %. The sources of error causing this discrepancy were discussed before in that section of the main text. The coefficients obtained here were used to calibrate the number of molecules unloaded from the trap in Sec. 4.3.4.

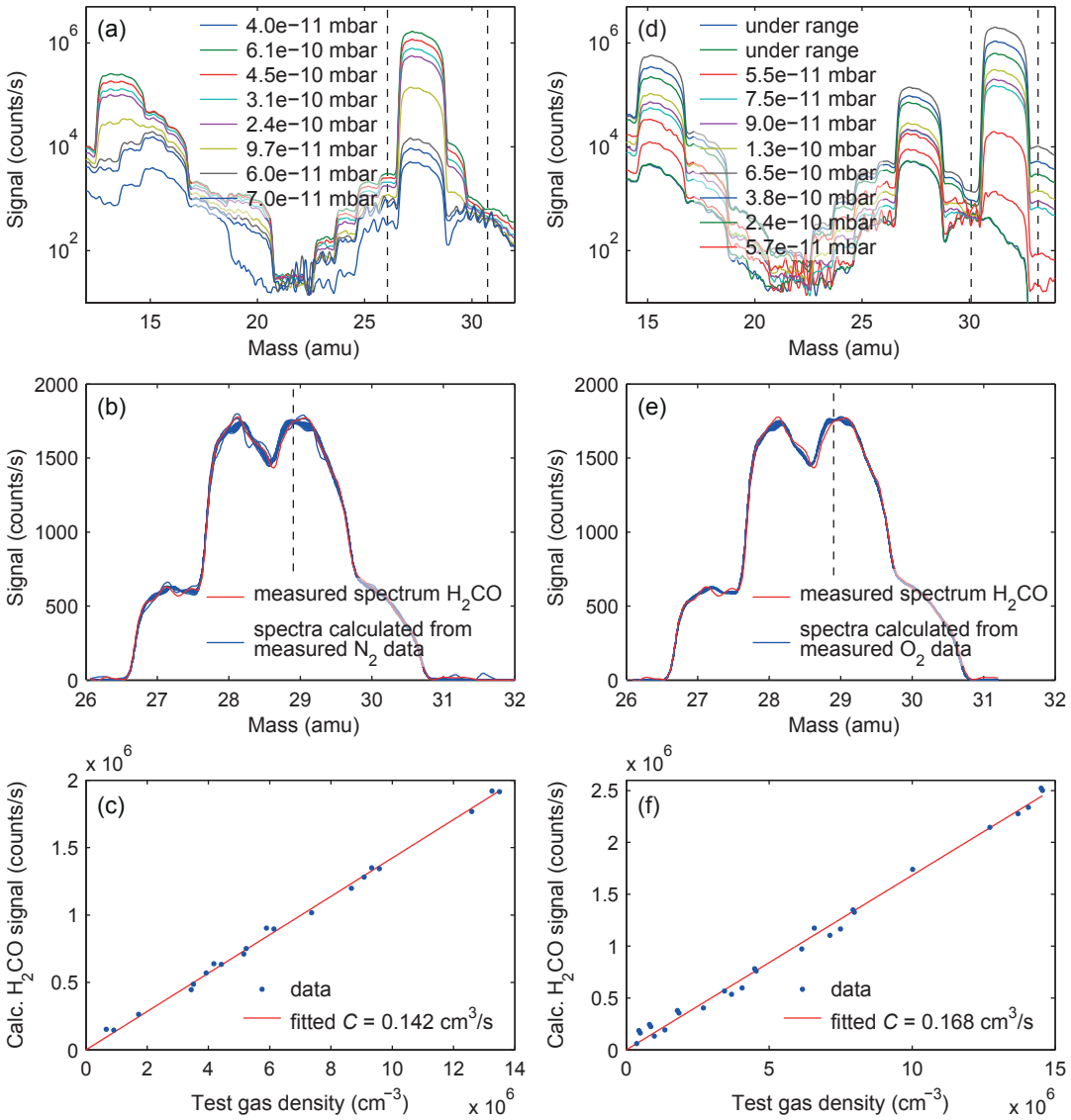

Figure C.7: Sensitivity calibration of the QMS. Panels **(a)**–**(c)** show the data measured with N_2, whereas panels **(d)**–**(f)** display the corresponding measurements with O_2. **(a)**, **(d)** Mass spectra for varying test-gas pressure. The mass range enclosed by the vertical dashed lines was used in the further evaluation. **(b)**, **(e)** H_2CO mass spectra constructed from the test-gas spectra and fitted to the H_2CO mass spectrum obtained with guided molecules (see main text for further details). **(c)**, **(f)** Calculated, density-dependent H_2CO count rate at mass 28.9 u with fitted sensitivity coefficient C of the QMS. These coefficients were used to calibrate the number of (cooled) molecules unloaded from the trap.

Appendix D

Data evaluation and statistics

All error bars associated with experimental data shown in this thesis represent the 1σ statistical error deduced from the molecule count measured with the QMS. Due to the low detection efficiency of the QMS, the number of molecules detected after a single run of an experimental sequence is comparably low. To reduce the statistical uncertainty measurements are typically repeated several or many times and the obtained signals are averaged (Sec. 3.2). Tables D.1 and D.2 specify the number of repetitions and the date of the measurement for all data plots included in this thesis.

Measurement	Label	Repetitions	Date
Fig. 3.2	current trap	11	03/08/2015
	previous trap	279	20/12/2013
		~ 114	09/01/2014
Fig. 3.3	$f_{\mathrm{RF}} - f_{\mathrm{offset}} = 22\,\mathrm{MHz}$	8	15/09/2015
	$f_{\mathrm{RF}} - f_{\mathrm{offset}} = 3.1\,\mathrm{MHz}$	~ 36	30/08/2015
Fig. 3.5(b)		6	19/06/2015
Fig. 3.5(c)		19	17/09/2015
Fig. 3.6		23	29/04/2015
Fig. 3.7(b)		4	21/05/2015
Fig. 3.7(c)		10	21/05/2015
Fig. 3.9(a)		~ 26, ~ 10	23, 24/09/2014
Fig. 4.1(b)		15	24/08/2015
Fig. 4.2		21, 18	10,25/07/2015
Fig. 4.3		22	09/09/2015

Table D.1: Number of repetitions of the experimental sequence (and date of the measurement) for all data plots shown in this thesis. For some data series the number of repetitions deliberately varies for different data points. Then, a range is specified. Occasionally, important single data points, e.g., a reference signal level to which the remaining data is normalized, were measured a multiple of the given number of repetitions. This is not specified in the table but is often visible in the plot because these points thus have smaller error bars. Note that a plotted data point is often a difference signal extracted from two or more experimental sequences, a consequence of our state-detection method (Sec. 3.3.1).

Measurement	Label	Repetitions	Date
Fig. 4.5		~ 200, ~ 3500	21, 29/08/2014
Fig. 4.6(a), (b)		~ 133	06/08/2015
Fig. 4.6(c)		57	14/06/2012
Fig. 4.7(a)		11	03/08/2015
Fig. 4.7(b)		7	03/08/2015
Fig. 4.7(c)		13	04/08/2015
Fig. 4.8		2 – 10	22/06/2015
		3	10/07/2015
Fig. 4.9(a)	$V_{\mathrm{trap}} = \pm 100\,\mathrm{V}$	47	03/07/2015
Fig. 4.9(a)	$V_{\mathrm{trap}} = \pm 50\,\mathrm{V}$	~ 11	08/07/2015
Fig. 4.9(b)	$V_{\mathrm{trap}} = \pm 100\,\mathrm{V}$	13	04/08/2015
Fig. 4.9(b)	$V_{\mathrm{trap}} = \pm 50\,\mathrm{V}$	17	05/08/2015
Fig. 4.10		47	03/07/2015
Fig. 4.12		18	19/08/2015
Fig. 4.13(a), (b)		~ 180	16/09/2015
Fig. 4.13(c)		~ 70	21/09/2015
Fig. 5.3(a)	$f_{\mathrm{RF}} - f_{\mathrm{offset}} = 762\,\mathrm{MHz}$	8	18/08/2016
Fig. 5.3(a)	$f_{\mathrm{RF}} - f_{\mathrm{offset}} = 189\,\mathrm{MHz}$	21	11/08/2016
Fig. 5.3(a)	$f_{\mathrm{RF}} - f_{\mathrm{offset}} = 22\,\mathrm{MHz}$	33	26/07/2016
Fig. 5.5(a)	$\mathcal{E}_{\mathrm{offset}} = 1.05\,\mathrm{kV/cm}$	~ 14	21/09/2016
Fig. 5.5(a)	$\mathcal{E}_{\mathrm{offset}} = 0.81\,\mathrm{kV/cm}$	12	24/09/2016
Fig. 5.5(a)	$\mathcal{E}_{\mathrm{offset}} = 1.32\,\mathrm{kV/cm}$	10	25/09/2016
Fig. 5.5(c)	$\mathcal{E}_{\mathrm{offset}} = 1.05\,\mathrm{kV/cm}$	41	26/08/2016
Fig. 5.5(c)	$\mathcal{E}_{\mathrm{offset}} = 0.81\,\mathrm{kV/cm}$	~ 35	16/07/2016
Fig. 5.5(c)	$\mathcal{E}_{\mathrm{offset}} = 1.32\,\mathrm{kV/cm}$	~ 39	13/07/2016
Fig. 5.6(a)		71	23/08/2016
Fig. 5.6(b)		41	26/08/2016
Fig. 5.6(c)		254 – 570	08–09/2016
Fig. 6.1		96 – 384	02/05/2015
Fig. A.1	previous trap	90	15/05/2014
Fig. A.1	after baking	370	21/05/2014
Fig. A.1	current trap	390	01/07/2014
Fig. A.2(a)	previous trap	34	01/04/2014
Fig. A.2(a)	after baking	23	22/05/2014
Fig. A.2(a)	current trap	27	04/07/2014
Fig. A.2(b)		27	07/04/2014
Fig. A.2(c)		29	04/07/2014
Fig. C.2(a)		2 – 30	04/2016
Fig. C.2(b)		16 – 68	04/2016
Fig. C.4		10	01/09/2015

Table D.2: Continuation of the preceding table.

Bibliography

[Agú13] M. Agúndez and V. Wakelam. Chemistry of Dark Clouds: Databases, Networks, and Models. *Chem. Rev.* **113**, 8710 (2013) [cited on p. 4].

[Ake17] N. Akerman, M. Karpov, Y. Segev, N. Bibelnik, J. Narevicius, and E. Narevicius. Trapping of Molecular Oxygen together with Lithium Atoms. *Phys. Rev. Lett.* **119**, 073204 (2017) [cited on pp. 4, 8, 9].

[And06] A. André, D. DeMille, J. M. Doyle, M. D. Lukin, S. E. Maxwell, P. Rabl, R. J. Schoelkopf, and P. Zoller. A coherent all-electrical interface between polar molecules and mesoscopic superconducting resonators. *Nat. Phys.* **2**, 636 (2006) [cited on pp. 5, 112].

[And17] L. Anderegg *et al.* Radio Frequency Magneto-Optical Trapping of CaF with High Density. *Phys. Rev. Lett.* **119**, 103201 (2017) [cited on p. 11].

[Bag13] J. Bagdonaite, P. Jansen, C. Henkel, H. L. Bethlem, K. M. Menten, and W. Ubachs. A Stringent Limit on a Drifting Proton-to-Electron Mass Ratio from Alcohol in the Early Universe. *Science* **339**, 46 (2013) [cited on p. 91].

[Bal01] N. Balakrishnan and A. Dalgarno. Chemistry at ultracold temperatures. *Chem. Phys. Lett.* **341**, 652 (2001) [cited on p. 3].

[Bal16] N. Balakrishnan. Perspective: Ultracold molecules and the dawn of cold controlled chemistry. *J. Chem. Phys.* **145**, 150901 (2016) [cited on p. 3].

[Bar12] J. F. Barry, E. S. Shuman, E. B. Norrgard, and D. DeMille. Laser Radiation Pressure Slowing of a Molecular Beam. *Phys. Rev. Lett.* **108**, 103002 (2012) [cited on p. 9].

[Bar14a] J. Baron *et al.* Order of Magnitude Smaller Limit on the Electric Dipole Moment of the Electron. *Science* **343**, 269 (2014) [cited on pp. 2, 91, 92].

[Bar14b] J. F. Barry, D. J. McCarron, E. B. Norrgard, M. H. Steinecker, and D. DeMille. Magneto-optical trapping of a diatomic molecule. *Nature* **512**, 286 (2014) [cited on p. 9].

[Bar17] J. Baron *et al.* Methods, analysis, and the treatment of systematic errors for the electron electric dipole moment search in thorium monoxide. *New J. Phys.* **19**, 073029 (2017) [cited on pp. 2, 91].

[Bel09] M. T. Bell and T. P. Softley. Ultracold molecules and ultracold chemistry. *Mol. Phys.* **107**, 99 (2009) [cited on pp. 1, 3, 112].

[Ber07] E. A. Bergin and M. Tafalla. Cold Dark Clouds: The Initial Conditions for Star Formation. *Annu. Rev. Astron. Astrophys.* **45**, 339 (2007) [cited on pp. 4, 5].

[Ber14] B. Bertsche, J. Jankunas, and A. Osterwalder. Low-temperature Collisions between Neutral Molecules in Merged Molecular Beams. *Chim. Int. J. Chem.* **68**, 256 (2014) [cited on p. 4].

[Ber98] K. Bergmann, H. Theuer, and B. W. Shore. Coherent population transfer among quantum states of atoms and molecules. *Rev. Mod. Phys.* **70**, 1003 (1998) [cited on p. 6].

[Bet00] H. L. Bethlem, G. Berden, F. M. H. Crompvoets, R. T. Jongma, A. J. A. van Roij, and G. Meijer. Electrostatic trapping of ammonia molecules. *Nature* **406**, 491 (2000) [cited on pp. 7, 8].

[Bet08] H. L. Bethlem, M. Kajita, B. Sartakov, G. Meijer, and W. Ubachs. Prospects for precision measurements on ammonia molecules in a fountain. *Eur. Phys. J. Spec. Top.* **163**, 55 (2008) [cited on p. 92].

[Bet99] H. L. Bethlem, G. Berden, and G. Meijer. Decelerating Neutral Dipolar Molecules. *Phys. Rev. Appl.* **83**, 1558 (1999) [cited on p. 8].

[Bie16] J. Biesheuvel, J. P. Karr, L. Hilico, K. S. E. Eikema, W. Ubachs, and J. C. J. Koelemeij. Probing QED and fundamental constants through laser spectroscopy of vibrational transitions in HD^+. *Nat. Commun.* **7**, 10385 (2016) [cited on p. 91].

[Boh09] J. L. Bohn, M. Cavagnero, and C. Ticknor. Quasi-universal dipolar scattering in cold and ultracold gases. *New J. Phys.* **11**, 055039 (2009) [cited on pp. 1, 112].

[Boh17] J. L. Bohn, A. M. Rey, and J. Ye. Cold molecules: Progress in quantum engineering of chemistry and quantum matter. *Science* **357**, 1002 (2017) [cited on pp. 3–5].

[Bra49] J. K. Bragg and A. H. Sharbaugh. Microwave Spectrum of Formaldehyde. *Phys. Rev.* **75**, 1774 (1949) [cited on p. 18].

[Bro78] L. R. Brown and R. H. Hunt. The ground state of H_2CO. *J. Mol. Spectrosc.* **73**, 277 (1978) [cited on p. 18].

[Bro79] L. R. Brown, R. H. Hunt, and A. S. Pine. Wavenumbers, line strengths, and assignments in the Doppler-limited spectrum of formaldehyde from 2700 to 3000 cm^{-1}. *J. Mol. Spectrosc.* **75**, 406 (1979) [cited on p. 18].

[Brü03] S. Brünken, H. S. P. Müller, F. Lewen, and G. Winnewisser. High accuracy measurements on the ground state rotational spectrum of formaldehyde (H_2CO) up to 2 THz. *Phys. Chem. Chem. Phys.* **5**, 1515 (2003) [cited on pp. 3, 17, 18, 21, 23, 27, 36–38, 92, 94, 95, 103].

[Bun12] P. R. Bunker and P. Jensen. *Molecular Symmetry and Spectroscopy*. E-book. NRC Research Press, Ottawa, Ontario, Canada (2012) [cited on p. 18].

[Buu09] L. van Buuren, C. Sommer, M. Motsch, S. Pohle, M. Schenk, J. Bayerl, P. Pinkse, and G. Rempe. Electrostatic Extraction of Cold Molecules from a Cryogenic Reservoir. *Phys. Rev. Lett.* **102**, 033001 (2009) [cited on p. 8].

[Cah14] S. B. Cahn, J. Ammon, E. Kirilov, Y. V. Gurevich, D. Murphree, R. Paolino, D. A. Rahmlow, M. G. Kozlov, and D. DeMille. Zeeman-Tuned Rotational Level-Crossing Spectroscopy in a Diatomic Free Radical. *Phys. Rev. Lett.* **112**, 163002 (2014) [cited on pp. 91, 92].

[Cai17] W. B. Cairncross, D. N. Gresh, M. Grau, K. C. Cossel, T. S. Roussy, Y. Ni, Y. Zhou, J. Ye, and E. A. Cornell. Precision Measurement of the Electron's Electric Dipole Moment Using Trapped Molecular Ions. *Phys. Rev. Lett.* **119**, 153001 (2017) [cited on p. 91].

[Car09] L. D. Carr, D. DeMille, R. V. Krems, and J. Ye. Cold and ultracold molecules: Science, technology and applications. *New J. Phys.* **11** (2009) [cited on pp. 1, 3].

[Cha73] J. Chardon and D. Guichon. Structure hyperfine du spectre basse fréquence de H_2CO. *J. Phys. France* **34**, 791 (1973) [cited on pp. 18, 25, 103].

[Che14] S. Chervenkov, X. Wu, J. Bayerl, A. Rohlfes, T. Gantner, M. Zeppenfeld, and G. Rempe. Continuous Centrifuge Decelerator for Polar Molecules. *Phys. Rev. Lett.* **112**, 013001 (2014) [cited on p. 8].

[Che16] C. Cheng, A. P. P. van der Poel, P. Jansen, M. Quintero-Pérez, T. E. Wall, W. Ubachs, and H. L. Bethlem. Molecular Fountain. *Phys. Rev. Lett.* **117**, 253201 (2016) [cited on pp. 8, 92, 110].

[Chu98] S. Chu. Nobel Lecture: The manipulation of neutral particles. *Rev. Mod. Phys.* **70**, 685 (1998) [cited on p. 1].

[Clo83] D. J. Clouthier and D. A. Ramsay. The Spectroscopy of Formaldehyde and Thioformaldehyde. *Annu. Rev. Phys. Chem.* **34**, 31 (1983) [cited on p. 18].

[Coh98] C. N. Cohen-Tannoudji. Nobel Lecture: Manipulating atoms with photons. *Rev. Mod. Phys.* **70**, 707 (1998) [cited on p. 1].

[Cor02] E. A. Cornell and C. E. Wieman. Nobel lecture: Bose-Einstein condensation in a dilute gas, the first 70 years and some recent experiments. *Rev. Mod. Phys.* **74**, 875 (2002) [cited on p. 1].

[Cor80] R. Cornet and G. Winnewisser. A precise study of the rotational spectrum of formaldehyde $H_2^{12}C^{16}O$, $H_2^{13}C^{16}O$, $H_2^{12}C^{18}O$, $H_2^{13}C^{18}O$. *J. Mol. Spectrosc.* **80**, 438 (1980) [cited on pp. 18, 22, 38, 56, 102, 103].

[Cro09] A. D. Cronin, J. Schmiedmayer, and D. E. Pritchard. Optics and interferometry with atoms and molecules. *Rev. Mod. Phys.* **81**, 1051 (2009) [cited on p. 1].

[Cro44] P. C. Cross, R. M. Hainer, and G. W. King. The Asymmetric Rotor II. Calculation of Dipole Intensities and Line Classification. *J. Chem. Phys.* **12**, 210 (1944) [cited on p. 27].

[Dan08] J. G. Danzl, E. Haller, M. Gustavsson, M. J. Mark, R. Hart, N. Bouloufa, O. Dulieu, H. Ritsch, and H.-C. Nägerl. Quantum Gas of Deeply Bound Ground State Molecules. *Science* **321**, 1062 (2008) [cited on p. 6].

[Dau07] C. Daussy, M. Guinet, A. Amy-Klein, K. Djerroud, Y. Hermier, S. Briaudeau, C. J. Bordé, and C. Chardonnet. Direct Determination of the Boltzmann Constant by an Optical Method. *Phys. Rev. Lett.* **98**, 250801 (2007) [cited on p. 91].

[Dau99] C. Daussy, T. Marrel, A. Amy-Klein, C. Nguyen, C. Bordé, and C. Chardonnet. Limit on the Parity Nonconserving Energy Difference between the Enantiomers of a Chiral Molecule by Laser Spectroscopy. *Phys. Rev. Lett.* **83**, 1554 (1999) [cited on pp. 2, 91].

[Dei08] J. Deiglmayr, A. Grochola, M. Repp, K. Mörtlbauer, C. Glück, J. Lange, O. Dulieu, R. Wester, and M. Weidemüller. Formation of Ultracold Polar Molecules in the Rovibrational Ground State. *Phys. Rev. Lett.* **101**, 133004 (2008) [cited on p. 7].

[DeM02] D. DeMille. Quantum Computation with Trapped Polar Molecules. *Phys. Rev. Lett.* **88**, 067901 (2002) [cited on p. 5].

[DeM04] D. DeMille, D. R. Glenn, and J. Petricka. Microwave traps for cold polar molecules. *Eur. Phys. J. D* **31**, 375 (2004) [cited on p. 110].

[DeM08] D. DeMille, S. B. Cahn, D. Murphree, D. A. Rahmlow, and M. G. Kozlov. Using Molecules to Measure Nuclear Spin-Dependent Parity Violation. *Phys. Rev. Lett.* **100**, 023003 (2008) [cited on p. 91].

[DeM17] D. DeMille, J. M. Doyle, and A. O. Sushkov. Probing the frontiers of particle physics with tabletop-scale experiments. *Science* **357**, 990 (2017) [cited on pp. 2, 91].

[Di 04] M. D. Di Rosa. Laser-cooling molecules. *Eur. Phys. J. D* **31**, 395 (2004) [cited on pp. 9, 10, 16].

[Die15] P. Dietiker, E. Miloglyadov, M. Quack, A. Schneider, and G. Seyfang. Infrared laser induced population transfer and parity selection in $^{14}NH_3$: A proof of principle experiment towards detecting parity violation in chiral molecules. *J. Chem. Phys.* **143**, 244305 (2015) [cited on pp. 2, 91].

[Die34] G. H. Dieke and G. B. Kistiakowsky. The Structure of the Ultraviolet Absorption Spectrum of Formaldehyde. I. *Phys. Rev.* **45**, 4 (1934) [cited on p. 18].

[Dob16] E. Dobler. *Untersuchungen zur Laser-induzierten Fluoreszenz als Detektionsmethode für ultrakalte Formaldehyd Moleküle.* Master's Thesis. Technische Universität München (2016) [cited on pp. 18, 109].

[Doy16] J. M. Doyle, B. Friedrich, and E. Narevicius. Physics and Chemistry with Cold Molecules. *ChemPhysChem* **17**, 3581 (2016) [cited on p. 3].

[Dul11] O. Dulieu, R. Krems, M. Weidemüller, and S. Willitsch. Physics and Chemistry of Cold Molecules. *Phys. Chem. Chem. Phys.* **13**, 18703 (2011) [cited on p. 3].

[Eli12] S. Eliet, A. Cuisset, M. Guinet, F. Hindle, G. Mouret, R. Bocquet, and J. Demaison. Rotational spectrum of formaldehyde reinvestigated using a photomixing THz synthesizer. *J. Mol. Spectrosc.* **279**, 12 (2012) [cited on p. 3].

[Eng11] B. G. U. Englert, M. Mielenz, C. Sommer, J. Bayerl, M. Motsch, P. Pinkse, G. Rempe, and M. Zeppenfeld. Storage and Adiabatic Cooling of Polar Molecules in a Microstructured Trap. *Phys. Rev. Lett.* **107**, 263003 (2011) [cited on pp. 2, 7, 41, 42, 47, 52, 80, 123].

[Eng13] B. G. U. Englert. *Sisyphus-Kühlung von polyatomaren Molekülen*. Dissertation. Technische Universität München (2013) [cited on pp. 10, 11, 13, 16, 17, 38, 41–44, 49–52, 55, 57, 65, 74, 76, 79, 87].

[Fab14] M. I. Fabrikant, T. Li, N. J. Fitch, N. Farrow, J. D. Weinstein, and H. J. Lewandowski. Method for traveling-wave deceleration of buffer-gas beams of CH. *Phys. Rev. A* **90**, 033418 (2014) [cited on p. 8].

[Fab77] B. Fabricant, D. Krieger, and J. S. Muenter. Molecular beam electric resonance study of formaldehyde, thioformaldehyde, and ketene. *J. Chem. Phys.* **67**, 1576 (1977) [cited on pp. 17–19, 25, 37, 59, 94, 95].

[Ful04] R. Fulton, A. I. Bishop, and P. F. Barker. Optical Stark Decelerator for Molecules. *Phys. Rev. Lett.* **93**, 243004 (2004) [cited on p. 8].

[Glö15a] R. Glöckner, A. Prehn, B. G. U. Englert, G. Rempe, and M. Zeppenfeld. Rotational Cooling of Trapped Polyatomic Molecules. *Phys. Rev. Lett.* **115**, 233001 (2015) [cited on pp. 33, 41, 51, 53, 56, 61].

[Glö15b] R. Glöckner, A. Prehn, G. Rempe, and M. Zeppenfeld. Rotational state detection of electrically trapped polyatomic molecules. *New J. Phys.* **17**, 055022 (2015) [cited on pp. 46, 50, 53, 55, 62, 79, 117].

[Glö16] R. Glöckner. *Rotational-state cooling and detection of trapped CH_3F molecules*. Dissertation. Technische Universität München (2016) [cited on pp. 11, 33, 42, 43, 45–47, 53, 55–57, 61, 117].

[Gri09] W. C. Griffith, M. D. Swallows, T. H. Loftus, M. V. Romalis, B. R. Heckel, and E. N. Fortson. Improved Limit on the Permanent Electric Dipole Moment of ^{199}Hg. *Phys. Rev. Lett.* **102**, 101601 (2009) [cited on p. 91].

[Gro17] C. Gross and I. Bloch. Quantum simulations with ultracold atoms in optical lattices. *Science* **357**, 995 (2017) [cited on p. 1].

[Guo16] M. Guo *et al.* Creation of an Ultracold Gas of Ground-State Dipolar ^{23}Na^{87}Rb Molecules. *Phys. Rev. Lett.* **116**, 205303 (2016) [cited on p. 6].

[Hen12] A. B. Henson, S. Gersten, Y. Shagam, J. Narevicius, and E. Narevicius. Observation of Resonances in Penning Ionization Reactions at Sub-Kelvin Temperatures in Merged Beams. *Science* **338**, 234 (2012) [cited on p. 4].

[Her45] G. Herzberg. *Molecular Spectra and Molecular Structure. II. Infrared and Raman Spectra of Polyatomic Molecules*. Van Nostrand Reinhold, New York (1945) [cited on pp. 18, 19].

[Her66] G. Herzberg. *Molecular Spectra and Molecular Structure. III. Electronic Spectra and Electronic Structure of Polyatomic Molecules*. Van Nostrand Reinhold, New York (1966) [cited on p. 15].

[Hog11] S. D. Hogan, M. Motsch, and F. Merkt. Deceleration of supersonic beams using inhomogeneous electric and magnetic fields. *Phys. Chem. Chem. Phys.* **13**, 18705 (2011) [cited on p. 7].

[Hos10] K. Hosaka, H. Shimada, H. Chiba, H. Katsuki, Y. Teranishi, Y. Ohtsuki, and K. Ohmori. Ultrafast Fourier Transform with a Femtosecond-Laser-Driven Molecule. *Phys. Rev. Lett.* **104**, 180501 (2010) [cited on p. 5].

[Hud06a] E. R. Hudson. *Experiments on Cold Molecules Produced via Stark Deceleration*. PhD Thesis. University of Colorado (2006) [cited on p. 109].

[Hud06b] E. R. Hudson, H. J. Lewandowski, B. C. Sawyer, and J. Ye. Cold Molecule Spectroscopy for Constraining the Evolution of the Fine Structure Constant. *Phys. Rev. Lett.* **96**, 143004 (2006) [cited on pp. 91, 92].

[Hud06c] E. R. Hudson, C. Ticknor, B. C. Sawyer, C. A. Taatjes, H. J. Lewandowski, J. R. Bochinski, J. L. Bohn, and J. Ye. Production of cold formaldehyde molecules for study and control of chemical reaction dynamics with hydroxyl radicals. *Phys. Rev. A* **73**, 063404 (2006) [cited on pp. 3, 4, 8, 109].

[Hud11] J. J. Hudson, D. M. Kara, I. J. Smallman, B. E. Sauer, M. R. Tarbutt, and E. A. Hinds. Improved measurement of the shape of the electron. *Nature* **473**, 493 (2011) [cited on p. 2].

[Hut12] N. R. Hutzler, H.-I. Lu, and J. M. Doyle. The Buffer Gas Beam: An Intense, Cold, and Slow Source for Atoms and Molecules. *Chem. Rev.* **112**, 4803 (2012) [cited on p. 8].

[Ibr13] M. Ibrügger. *Progress in opto-electrical cooling: Implementation of Formaldehyde and of an improved microwave source*. Diploma Thesis. Technische Universität München (2013) [cited on pp. 13, 18, 27, 37, 49].

[Isa16] T. A. Isaev and R. Berger. Polyatomic Candidates for Cooling of Molecules with Lasers from Simple Theoretical Concepts. *Phys. Rev. Lett.* **116**, 063006 (2016) [cited on pp. 9, 16].

[Jan14a] J. Jankunas, B. Bertsche, K. Jachymski, M. Hapka, and A. Osterwalder. Dynamics of gas phase Ne^* + NH_3 and Ne^* + ND_3 Penning ionisation at low temperatures. *J. Chem. Phys.* **140**, 244302 (2014) [cited on p. 4].

[Jan14b] J. Jankunas, B. Bertsche, and A. Osterwalder. Study of the $Ne(^3P_2)$ + CH_3F electron-transfer reaction below 1 K. *J. Phys. Chem. A* **118**, 3875 (2014) [cited on p. 4].

[Jan15] J. Jankunas, K. Jachymski, M. Hapka, and A. Osterwalder. Observation of orbiting resonances in $He(^3S_1)$ + NH_3 Penning ionization. *J. Chem. Phys.* **142**, 164305 (2015) [cited on p. 4].

[Jin12] D. S. Jin and J. Ye. Introduction to Ultracold Molecules: New Frontiers in Quantum and Chemical Physics. *Chem. Rev.* **112**, 4801 (2012) [cited on p. 3].

[Jun04] T. Junglen, T. Rieger, S. A. Rangwala, P. W. H. Pinkse, and G. Rempe. Slow ammonia molecules in an electrostatic quadrupole guide. *Eur. Phys. J. D* **31**, 365 (2004) [cited on p. 50].

[Ket02] W. Ketterle. Nobel lecture: When atoms behave as waves: Bose-Einstein condensation and the atom laser. *Rev. Mod. Phys.* **74**, 1131 (2002) [cited on p. 1].

[Kim04] Y.-K. Kim *et al. Electron-Impact Ionization Cross Section for Ionization and Excitation Database*. http://physics.nist.gov/ionxsec, (retrieved Sep. 29, 2015). National Institute of Standards and Technology, Gaithersburg MD (2004) [cited on pp. 86, 125].

[Kle16] A. Klein *et al.* Directly probing anisotropy in atom–molecule collisions through quantum scattering resonances. *Nat. Phys.* **13**, 35 (2016) [cited on p. 4].

[Koz16] I. Kozyryev, L. Baum, K. Matsuda, and J. M. Doyle. Proposal for Laser Cooling of Complex Polyatomic Molecules. *ChemPhysChem* **17**, 3641 (2016) [cited on pp. 9, 16].

[Koz17a] I. Kozyryev, L. Baum, K. Matsuda, B. L. Augenbraun, L. Anderegg, A. P. Sedlack, and J. M. Doyle. Sisyphus Laser Cooling of a Polyatomic Molecule. *Phys. Rev. Lett.* **118**, 173201 (2017) [cited on p. 9].

[Koz17b] I. Kozyryev and N. R. Hutzler. Precision Measurement of Time-Reversal Symmetry Violation with Laser-Cooled Polyatomic Molecules. *Phys. Rev. Lett.* **119**, 133002 (2017) [cited on pp. 9, 92].

[Kra09] F. Krausz and M. Ivanov. Attosecond physics. *Rev. Mod. Phys.* **81**, 163 (2009) [cited on p. 1].

[Kra16] S. A. Krasnokutski, M. Kuhn, M. Renzler, C. Jäger, T. Henning, and P. Scheier. Ultra-Low-Temperature Reactions of Carbon Atoms With Hydrogen Molecules. *Astrophys. J.* **818**, L31 (2016) [cited on p. 5].

[Kre05] R. V. Krems. Molecules near absolute zero and external field control of atomic and molecular dynamics. *Int. Rev. Phys. Chem.* **24**, 99 (2005) [cited on p. 3].

[Kre09] R. V. Krems, B. Friedrich, and W. C. Stwalley, eds. *Cold Molecules: Theory, Experiment, Applications*. CRC Press, Boca Raton (2009) [cited on pp. 1, 3].

[Kro14] M. Krottenmüller. *Fabrication of Microstructures for Trapping of Polar Molecules*. Master's Thesis. Technische Universität München (2014) [cited on pp. 43, 44, 90, 114].

[Kro75] H. W. Kroto. *Molecular Rotation Spectra*. John Wiley & Sons, New York (1975) [cited on pp. 18–22, 24, 25].

[Kuz08] E. Kuznetsova, R. Côté, K. Kirby, and S. F. Yelin. Analysis of experimental feasibility of polar-molecule-based phase gates. *Phys. Rev. A* **78**, 012313 (2008) [cited on p. 5].

[Lan08] F. Lang, K. Winkler, C. Strauss, R. Grimm, and J. H. Denschlag. Ultracold Triplet Molecules in the Rovibrational Ground State. *Phys. Rev. Lett.* **101**, 133005 (2008) [cited on p. 6].

[Lar06] M. Lara, J. L. Bohn, D. Potter, P. Soldán, and J. M. Hutson. Ultracold Rb-OH Collisions and Prospects for Sympathetic Cooling. *Phys. Rev. Lett.* **97**, 183201 (2006) [cited on pp. 9, 112].

[Law51] R. B. Lawrance and M. W. P. Strandberg. Centrifugal Distortion in Asymmetric Top Molecules. I. Ordinary Formaldehyde, $H_2C^{12}O$. *Phys. Rev.* **83**, 363 (1951) [cited on p. 18].

[Lem13] M. Lemeshko, R. V. Krems, J. M. Doyle, and S. Kais. Manipulation of molecules with electromagnetic fields. *Mol. Phys.* **111**, 1648 (2013) [cited on pp. 1, 3].

[Lid18] D. R. Lide. Dipole moments. *CRC Handb. Chem. Phys.* Ed. by J. R. Rumble. 98th Edition. CRC Press/Taylor & Francis, Boca Raton (2018) [cited on p. 110].

[Lin15] P. J. Linstrom and W. G. Mallard, eds. *NIST Chemistry WebBook, NIST Standard Reference Database Number 69*. http://webbook.nist.gov, (retrieved Sep. 29, 2015). National Institute of Standards and Technology, Gaithersburg MD (2015) [cited on pp. 86, 125].

[Liu17] Y. Liu, M. Vashishta, P. Djuricanin, S. Zhou, W. Zhong, T. Mittertreiner, D. Carty, and T. Momose. Magnetic Trapping of Cold Methyl Radicals. *Phys. Rev. Lett.* **118**, 093201 (2017) [cited on p. 8].

[Lu14] H.-I. Lu, I. Kozyryev, B. Hemmerling, J. Piskorski, and J. M. Doyle. Magnetic Trapping of Molecules via Optical Loading and Magnetic Slowing. *Phys. Rev. Lett.* **112**, 113006 (2014) [cited on p. 110].

[Lud15] A. D. Ludlow, M. M. Boyd, J. Ye, E. Peik, and P. O. Schmidt. Optical atomic clocks. *Rev. Mod. Phys.* **87**, 637 (2015) [cited on p. 91].

[Lut14] J. J. Lutz and J. M. Hutson. Reactions between cold methyl halide molecules and alkali-metal atoms. *J. Chem. Phys.* **140**, 014303 (2014) [cited on pp. 9, 112].

[Man12] I. Manai, R. Horchani, H. Lignier, P. Pillet, D. Comparat, A. Fioretti, and M. Allegrini. Rovibrational Cooling of Molecules by Optical Pumping. *Phys. Rev. Lett.* **109**, 183001 (2012) [cited on p. 6].

[McG15] B. H. McGuyer, M. McDonald, G. Z. Iwata, M. G. Tarallo, A. T. Grier, F. Apfelbeck, and T. Zelevinsky. High-precision spectroscopy of ultracold molecules in an optical lattice. *New J. Phys.* **17**, 055004 (2015) [cited on p. 91].

[Mee01] S. Y. T. van de Meerakker, R. T. Jongma, H. L. Bethlem, and G. Meijer. Accumulating NH radicals in a magnetic trap. *Phys. Rev. A* **64**, 041401 (2001) [cited on p. 10].

[Mee09] S. A. Meek, H. Conrad, and G. Meijer. A Stark decelerator on a chip. *New J. Phys.* **11**, 055024 (2009) [cited on p. 8].

[Mee12] S. Y. T. van de Meerakker, H. L. Bethlem, N. Vanhaecke, and G. Meijer. Manipulation and Control of Molecular Beams. *Chem. Rev.* **112**, 4828 (2012) [cited on p. 7].

[Mej15] S. Mejri *et al.* Measuring the Boltzmann constant by mid-infrared laser spectroscopy of ammonia. *Metrologia* **52**, S314 (2015) [cited on p. 91].

[Men15] C. Meng, A. P. P. van der Poel, C. Cheng, and H. L. Bethlem. Femtosecond laser detection of Stark-decelerated and trapped methylfluoride molecules. *Phys. Rev. A* **92**, 023404 (2015) [cited on p. 8].

[Mer12] S. Merz, N. Vanhaecke, W. Jäger, M. Schnell, and G. Meijer. Decelerating molecules with microwave fields. *Phys. Rev. A* **85**, 063411 (2012) [cited on p. 8].

[Met99] H. Metcalf and P. van der Straten. *Laser cooling and trapping*. Springer New York, New York (1999) [cited on pp. 9, 11, 16].

[Mie10] M. Mielenz. *Speichern von polaren Molekülen in einer mikrostrukturierten elektrischen Falle*. Diploma Thesis. Julius-Maximilians-Universität Würzburg (2010) [cited on pp. 17, 43, 44, 49, 52, 86, 116, 121].

[Mir11] M. H. de Miranda, A. Chotia, B. Neyenhuis, D. Wang, G. Quéméner, S. Ospelkaus, J. L. Bohn, J. Ye, and D. S. Jin. Controlling the quantum stereodynamics of ultracold bimolecular reactions. *Nat. Phys.* **7**, 502 (2011) [cited on p. 4].

[Mol14] P. K. Molony, P. D. Gregory, Z. Ji, B. Lu, M. P. Köppinger, C. R. Le Sueur, C. L. Blackley, J. M. Hutson, and S. L. Cornish. Creation of Ultracold $^{87}Rb^{133}Cs$ Molecules in the Rovibrational Ground State. *Phys. Rev. Lett.* **113**, 255301 (2014) [cited on p. 6].

[Moo83] C. B. Moore and J. C. Weisshaar. Formaldehyde Photochemistry. *Annu. Rev. Phys. Chem.* **34**, 525 (1983) [cited on p. 10].

[Mos15] S. A. Moses, J. P. Covey, M. T. Miecnikowski, B. Yan, B. Gadway, J. Ye, and D. S. Jin. Creation of a low-entropy quantum gas of polar molecules in an optical lattice. *Science* **350**, 659 (2015) [cited on p. 6].

[Mos16] S. A. Moses, J. P. Covey, M. T. Miecnikowski, D. S. Jin, and J. Ye. New frontiers for quantum gases of polar molecules. *Nat. Phys.* **13**, 13 (2016) [cited on p. 3].

[Mot07] M. Motsch, M. Schenk, L. D. van Buuren, M. Zeppenfeld, P. W. H. Pinkse, and G. Rempe. Internal-state thermometry by depletion spectroscopy in a cold guided beam of formaldehyde. *Phys. Rev. A* **76**, 061402(R) (2007) [cited on p. 7].

[Mot08] M. Motsch, M. Schenk, M. Zeppenfeld, M. Schmitt, W. Leo Meerts, P. W. Pinkse, and G. Rempe. Spectroscopy of the $\tilde{A}^1A_2 \leftarrow \tilde{X}^1A_1$ transition of formaldehyde in the 30140–30790 cm^{-1} range: The $2_0^1 4_0^3$ and $2_0^2 4_0^1$ rovibrational bands. *J. Mol. Spectrosc.* **252**, 25 (2008) [cited on p. 18].

[Mot09a] M. Motsch, C. Sommer, M. Zeppenfeld, L. D. van Buuren, P. W. H. Pinkse, and G. Rempe. Collisional effects in the formation of cold guided beams of polar molecules. *New J. Phys.* **11**, 055030 (2009) [cited on pp. 8, 50].

[Mot09b] M. Motsch. *Cold Guided Beams of Polar Molecules*. Dissertation. Technische Universität München (2009) [cited on pp. 7, 22, 33, 50].

[Mou75] D. C. Moule and A. D. Walsh. Ultraviolet spectra and excited states of formaldehyde. *Chem. Rev.* **75**, 67 (1975) [cited on p. 18].

[Mül17] H. S. Müller and F. Lewen. Submillimeter spectroscopy of $H_2C^{17}O$ and a revisit of the rotational spectra of $H_2C^{18}O$ and $H_2C^{16}O$. *J. Mol. Spectrosc.* **331**, 28 (2017) [cited on pp. 5, 18, 25].

[Nar09] E. Narevicius, S. T. Bannerman, and M. G. Raizen. Single-photon molecular cooling. *New J. Phys.* **11**, 055046 (2009) [cited on pp. 10, 110].

[Ni08] K.-K. Ni *et al.* A high phase-space-density gas of polar molecules. *Science* **322**, 231 (2008) [cited on p. 6].

[Ni09] K.-K. Ni, S. Ospelkaus, D. J. Nesbitt, J. Ye, and D. S. Jin. A dipolar gas of ultracold molecules. *Phys. Chem. Chem. Phys.* **11**, 9626 (2009) [cited on pp. 6, 7].

[Ni10] K. K. Ni, S. Ospelkaus, D. Wang, G. Quéméner, B. Neyenhuis, M. H. De Miranda, J. L. Bohn, J. Ye, and D. S. Jin. Dipolar collisions of polar molecules in the quantum regime. *Nature* **464**, 1324 (2010) [cited on p. 4].

[Nie10] M. A. Nielsen and I. L. Chuang. *Quantum Computation and Quantum Information*. Cambridge University Press, Cambridge (2010) [cited on p. 5].

[Nie34] H. H. Nielsen. The Infrared Absorption Spectrum of Formaldehyde. Part I. *Phys. Rev.* **46**, 117 (1934) [cited on p. 18].

[Nij14] A. de Nijs, W. Ubachs, and H. Bethlem. Ramsey-type microwave spectroscopy on CO ($a^3\Pi$). *J. Mol. Spectrosc.* **300**, 79 (2014) [cited on p. 92].

[Nor16] E. B. Norrgard, D. J. McCarron, M. H. Steinecker, M. R. Tarbutt, and D. DeMille. Submillikelvin Dipolar Molecules in a Radio-Frequency Magneto-Optical Trap. *Phys. Rev. Lett.* **116**, 063004 (2016) [cited on p. 10].

[Osp10] S. Ospelkaus *et al.* Quantum-State Controlled Chemical Reactions of Ultracold Potassium-Rubidium Molecules. *Science* **327**, 853 (2010) [cited on p. 4].

[Par11] L. P. Parazzoli, N. J. Fitch, Żuchowski, J. M. Hutson, and H. J. Lewandowski. Large Effects of Electric Fields on Atom-Molecule Collisions at Millikelvin Temperatures. *Phys. Rev. Lett.* **106**, 193201 (2011) [cited on p. 4].

[Par15] J. W. Park, S. A. Will, and M. W. Zwierlein. Ultracold Dipolar Gas of Fermionic $^{23}Na^{40}K$ Molecules in Their Absolute Ground State. *Phys. Rev. Lett.* **114**, 205302 (2015) [cited on p. 6].

[Par17] J. W. Park, Z. Z. Yan, H. Loh, S. A. Will, and M. W. Zwierlein. Second-scale nuclear spin coherence time of ultracold $^{23}Na^{40}K$ molecules. *Science* **357**, 372 (2017) [cited on pp. 5, 92].

[Per06] A. Perrin, A. Valentin, and L. Daumont. New analysis of the $2v_4$, v_4+v_6, $2v_6$, v_3+v_4, v_3+v_6, v_1, v_5, v_2+v_4, $2v_3$, v_2+v_6 and v_2+v_3 bands of formaldehyde $H_2^{12}C^{16}O$: Line positions and intensities in the 3.5 µm spectral region. *J. Mol. Struct.* **780–781**, 28 (2006) [cited on p. 37].

[Per09] A. Perrin, D. Jacquemart, F. Kwabia Tchana, and N. Lacome. Absolute line intensities measurements and calculations for the 5.7 and 3.6 µm bands of formaldehyde. *J. Quant. Spectrosc. Radiat. Transf.* **110**, 700 (2009) [cited on pp. 3, 37].

[Phi98] W. D. Phillips. Nobel Lecture: Laser cooling and trapping of neutral atoms. *Rev. Mod. Phys.* **70**, 721 (1998) [cited on p. 1].

[Pin78] A. Pine. Doppler-limited spectra of the C–H stretching fundamentals of formaldehyde. *J. Mol. Spectrosc.* **70**, 167 (1978) [cited on p. 18].

[Pre12] A. Prehn. *Cooling of an electrically trapped gas of Fluoromethane*. Diploma Thesis. Technische Universität München (2012) [cited on pp. 10, 13, 65, 74, 87].

[Pre16] A. Prehn, M. Ibrügger, R. Glöckner, G. Rempe, and M. Zeppenfeld. Optoelectrical Cooling of Polar Molecules to Submillikelvin Temperatures. *Phys. Rev. Lett.* **116**, 063005 (2016) [cited on pp. 10, 12, 44, 45, 65].

[Pre17] A. Prehn, R. Glöckner, G. Rempe, and M. Zeppenfeld. Fast, precise, and widely tunable frequency control of an optical parametric oscillator referenced to a frequency comb. *Rev. Sci. Instrum.* **88**, 033101 (2017) [cited on pp. 51, 61].

[Pri83] D. E. Pritchard. Cooling neutral atoms in a magnetic trap for precision spectroscopy. *Phys. Rev. Lett.* **51**, 1336 (1983) [cited on pp. 14–16].

[Qua11] M. Quack. Frontiers in spectroscopy. *Faraday Discuss.* **150**, 533 (2011) [cited on p. 91].

[Qué08] G. Quéméner and N. Balakrishnan. Cold and ultracold chemical reactions of F+HCl and F+DCl. *J. Chem. Phys.* **128**, 224304 (2008) [cited on p. 3].

[Qui13] M. Quintero-Pérez, P. Jansen, T. E. Wall, J. E. van den Berg, S. Hoekstra, and H. L. Bethlem. Static Trapping of Polar Molecules in a Traveling Wave Decelerator. *Phys. Rev. Lett.* **110**, 133003 (2013) [cited on p. 8].

[Qui14] M. Quintero-Pérez, T. E. Wall, S. Hoekstra, and H. L. Bethlem. Preparation of an ultra-cold sample of ammonia molecules for precision measurements. *J. Mol. Spectrosc.* **300**, 112 (2014) [cited on p. 8].

[Rab06] P. Rabl, D. DeMille, J. Doyle, M. Lukin, R. Schoelkopf, and P. Zoller. Hybrid Quantum Processors: Molecular Ensembles as Quantum Memory for Solid State Circuits. *Phys. Rev. Lett.* **97**, 033003 (2006) [cited on pp. 5, 112].

[Rab07] P. Rabl and P. Zoller. Molecular dipolar crystals as high-fidelity quantum memory for hybrid quantum computing. *Phys. Rev. A* **76**, 042308 (2007) [cited on pp. 5, 112].

[Ran03] S. A. Rangwala, T. Junglen, T. Rieger, P. W. H. Pinkse, and G. Rempe. Continuous source of translationally cold dipolar molecules. *Phys. Rev. A* **67**, 043406 (2003) [cited on pp. 7, 50].

[Ree17] D. Reens, H. Wu, T. Langen, and J. Ye. Controlling spin flips of molecules in an electromagnetic trap. *Phys. Rev. A* **96**, 063420 (2017) [cited on p. 9].

[Rei15] A. Reiserer and G. Rempe. Cavity-based quantum networks with single atoms and optical photons. *Rev. Mod. Phys.* **87**, 1379 (2015) [cited on p. 1].

[Rie05] T. Rieger, T. Junglen, S. A. Rangwala, P. W. H. Pinkse, and G. Rempe. Continuous Loading of an Electrostatic Trap for Polar Molecules. *Phys. Rev. Lett.* **95**, 173002 (2005) [cited on p. 7].

[Rie11] J. Riedel, S. Hoekstra, W. Jäger, J. J. Gilijamse, S. Y. Van De Meerakker, and G. Meijer. Accumulation of Stark-decelerated NH molecules in a magnetic trap. *Eur. Phys. J. D* **65**, 161 (2011) [cited on pp. 10, 110].

[Ros08] T. Rosenband *et al.* Frequency Ratio of Al^+ and Hg^+ Single-Ion Optical Clocks; Metrology at the 17th Decimal Place. *Science* **319**, 1808 (2008) [cited on p. 91].

[Rot13] L. Rothman *et al.* The HITRAN2012 molecular spectroscopic database. *J. Quant. Spectrosc. Radiat. Transf.* **130**, 4 (2013) [cited on pp. 4, 17–19, 22, 24, 35, 37–39, 58].

[Sag05] J. M. Sage, S. Sainis, T. Bergeman, and D. DeMille. Optical Production of Ultracold Polar Molecules. *Phys. Rev. Lett.* **94**, 203001 (2005) [cited on p. 7].

[See18] F. Seesselberg, N. Buchheim, Z.-K. Lu, T. Schneider, X.-Y. Luo, E. Tiemann, I. Bloch, and C. Gohle. Modeling the adiabatic creation of ultracold polar $^{23}Na^{40}K$ molecules. *Phys. Rev. A* **97**, 013405 (2018) [cited on p. 6].

[Sha12a] Y. Shagam and E. Narevicius. Density and phase-space compression of molecular gases in magneto-electrostatic traps. *Phys. Rev. A* **85**, 053406 (2012) [cited on p. 10].

[Sha12b] M. Shapiro and P. Brumer. *Quantum Control of Molecular Processes*. 2nd Edition. Wiley-VCH Verlag GmbH & Co. KGaA, Weinheim, Germany (2012) [cited on p. 1].

[She08] A. Shelkovnikov, R. J. Butcher, C. Chardonnet, and A. Amy-Klein. Stability of the Proton-to-Electron Mass Ratio. *Phys. Rev. Lett.* **100**, 150801 (2008) [cited on p. 91].

[Shu10] E. S. Shuman, J. F. Barry, and D. DeMille. Laser cooling of a diatomic molecule. *Nature* **467**, 820 (2010) [cited on p. 9].

[Smi11] I. W. Smith. Laboratory Astrochemistry: Gas-Phase Processes. *Annu. Rev. Astron. Astrophys.* **49**, 29 (2011) [cited on p. 5].

[Sny69] L. E. Snyder, D. Buhl, B. Zuckerman, and P. Palmer. Microwave Detection of Interstellar Formaldehyde. *Phys. Rev. Lett.* **22**, 679 (1969) [cited on p. 5].

[Som11] C. Sommer. *Construction and Operation of a Cryogenic Source for Cold Polar Molecules*. Dissertation. Technische Universität München (2011) [cited on p. 18].

[Ste14] T. Steimle and W. Ubachs. Introduction to the special issue spectroscopic tests of fundamental physics. *J. Mol. Spectrosc.* **300**, 1 (2014) [cited on p. 91].

[Ste16] M. H. Steinecker, D. J. McCarron, Y. Zhu, and D. DeMille. Improved Radio-Frequency Magneto-Optical Trap of SrF Molecules. *ChemPhysChem* **17**, 3664 (2016) [cited on p. 10].

[Stu13] B. K. Stuhl, M. Yeo, M. T. Hummon, and J. Ye. Electric-field-induced inelastic collisions between magnetically trapped hydroxyl radicals. *Mol. Phys.* **111**, 1798 (2013) [cited on pp. 4, 9].

[Stu14] B. K. Stuhl, M. T. Hummon, and J. Ye. Cold State-Selected Molecular Collisions and Reactions. *Annu. Rev. Phys. Chem.* **65**, 501 (2014) [cited on p. 112].

[Tak14] T. Takekoshi, L. Reichsöllner, A. Schindewolf, J. M. Hutson, C. R. Le Sueur, O. Dulieu, F. Ferlaino, R. Grimm, and H.-C. Nägerl. Ultracold Dense Samples of Dipolar RbCs Molecules in the Rovibrational and Hyperfine Ground State. *Phys. Rev. Lett.* **113**, 205301 (2014) [cited on p. 6].

[Tar13] M. R. Tarbutt, B. E. Sauer, J. J. Hudson, and E. A. Hinds. Design for a fountain of YbF molecules to measure the electron's electric dipole moment. *New J. Phys.* **15**, 053034 (2013) [cited on p. 92].

[Tes02] C. Tesch and R. de Vivie-Riedle. Quantum Computation with Vibrationally Excited Molecules. *Phys. Rev. Lett.* **89**, 157901 (2002) [cited on p. 5].

[Tha64] P. Thaddeus, L. C. Krisher, and J. H. N. Loubser. Hyperfine Structure in the Microwave Spectrum of HDO, HDS, CH_2O, and CHDO: Beam-Maser Spectroscopy on Asymmetric-Top Molecules. *J. Chem. Phys.* **40**, 257 (1964) [cited on p. 25].

[Tok11] S. K. Tokunaga, W. Skomorowski, P. S. Żuchowski, R. Moszynski, J. M. Hutson, E. A. Hinds, and M. R. Tarbutt. Prospects for sympathetic cooling of molecules in electrostatic, ac and microwave traps. *Eur. Phys. J. D* **65**, 141 (2011) [cited on pp. 9, 112].

[Tok17] S. K. Tokunaga, R. J. Hendricks, M. R. Tarbutt, and B. Darquié. High-resolution mid-infrared spectroscopy of buffer-gas-cooled methyltrioxorhenium molecules. *New J. Phys.* **19**, 053006 (2017) [cited on pp. 2, 8, 91].

[Tow75] C. H. Townes and A. L. Schawlow. *Microwave Spectroscopy*. Dover, New York (1975) [cited on pp. 15, 16, 18, 20–24, 26, 28, 31, 96].

[Tru13] S. Truppe, R. J. Hendricks, S. K. Tokunaga, H. J. Lewandowski, M. G. Kozlov, C. Henkel, E. A. Hinds, and M. R. Tarbutt. A search for varying fundamental constants using hertz-level frequency measurements of cold CH molecules. *Nat. Commun.* **4**, 2600 (2013) [cited on pp. 91, 92].

[Tru17a] S. Truppe, H. J. Williams, M. Hambach, L. Caldwell, N. J. Fitch, E. A. Hinds, B. E. Sauer, and M. R. Tarbutt. Molecules cooled below the Doppler limit. *Nat. Phys.* **13**, 1173 (2017) [cited on pp. 10, 11].

[Tru17b] S. Truppe, H. J. Williams, N. J. Fitch, M. Hambach, T. E. Wall, E. A. Hinds, B. E. Sauer, and M. R. Tarbutt. An intense, cold, velocity-controlled molecular beam by frequency-chirped laser slowing. *New J. Phys.* **19**, 022001 (2017) [cited on pp. 8, 9].

[Tsc15] T. V. Tscherbul and R. V. Krems. Tuning Bimolecular Chemical Reactions by Electric Fields. *Phys. Rev. Lett.* **115**, 023201 (2015) [cited on p. 3].

[Tuc71] K. D. Tucker, G. R. Tomasevich, and P. Thaddeus. Laboratory Measurement of the 6-centimeter Formaldehyde Transitions. *Astrophys. J.* **169**, 429 (1971) [cited on p. 25].

[Ulm12] J. Ulmanis, J. Deiglmayr, M. Repp, R. Wester, and M. Weidemüller. Ultracold Molecules Formed by Photoassociation: Heteronuclear Dimers, Inelastic Collisions, and Interactions with Ultrashort Laser Pulses. *Chem. Rev.* **112**, 4890 (2012) [cited on pp. 6, 7].

[Vel04] J. Veldhoven, J. Küpper, H. L. Bethlem, B. Sartakov, A. J. A. Roij, and G. Meijer. Decelerated molecular beams for high-resolution spectroscopy. *Eur. Phys. J. D* **31**, 337 (2004) [cited on p. 92].

[Vit08] M. Viteau, A. Chotia, M. Allegrini, N. Bouloufa, O. Dulieu, D. Comparat, and P. Pillet. Optical pumping and vibrational cooling of molecules. *Science* **321**, 232 (2008) [cited on p. 6].

[Wal13] M. L. Wall, K. Maeda, and L. D. Carr. Simulating quantum magnets with symmetric top molecules. *Ann. Phys.* **525**, 845 (2013) [cited on p. 2].

[Wal15] M. L. Wall, K. Maeda, and L. D. Carr. Realizing unconventional quantum magnetism with symmetric top molecules. *New J. Phys.* **17**, 025001 (2015) [cited on p. 2].

[Wal16] T. E. Wall. Preparation of cold molecules for high-precision measurements. *J. Phys. B* **49**, 243001 (2016) [cited on pp. 2, 92].

[Wan29] S. C. Wang. On the Asymmetrical Top in Quantum Mechanics. *Phys. Rev.* **34**, 243 (1929) [cited on p. 23].

[Wec05a] P. F. Weck and N. Balakrishnan. Reactivity enhancement of ultracold $O(^3P)+H_2$ collisions by van der Waals interactions. *J. Chem. Phys.* **123**, 144308 (2005) [cited on p. 3].

[Wec05b] P. F. Weck and N. Balakrishnan. Quantum dynamics of the Li + HF $\rightarrow$ H + LiF reaction at ultralow temperatures. *J. Chem. Phys.* **122**, 154309 (2005) [cited on p. 3].

[Wei11] Q. Wei, S. Kais, B. Friedrich, and D. Herschbach. Entanglement of polar symmetric top molecules as candidate qubits. *J. Chem. Phys.* **135**, 154102 (2011) [cited on p. 5].

[Wei98] J. D. Weinstein, R. DeCarvalho, T. Guillet, B. Friedrich, and J. M. Doyle. Magnetic trapping of calcium monohydride molecules at millikelvin temperatures. *Nature* **395**, 148 (1998) [cited on p. 8].

[Wes17] C. M. Western. PGOPHER: A program for simulating rotational, vibrational and electronic spectra. *J. Quant. Spectrosc. Radiat. Transf.* **186**, 221 (2017) [cited on pp. 27, 36, 37].

[Wil17] H. J. Williams, S. Truppe, M. Hambach, L. Caldwell, N. J. Fitch, E. A. Hinds, B. E. Sauer, and M. R. Tarbutt. Characteristics of a magneto-optical trap of molecules. *New J. Phys.* **19**, 113035 (2017) [cited on pp. 10, 11].

[Wil18] H. J. Williams, L. Caldwell, N. J. Fitch, S. Truppe, J. Rodewald, E. A. Hinds, B. E. Sauer, and M. R. Tarbutt. Magnetic Trapping and Coherent Control of Laser-Cooled Molecules. *Phys. Rev. Lett.* **120**, 163201 (2018) [cited on p. 11].

[Wu17] X. Wu, T. Gantner, M. Koller, M. Zeppenfeld, S. Chervenkov, and G. Rempe. A cryofuge for cold-collision experiments with slow polar molecules. *Science* **358**, 645 (2017) [cited on pp. 4, 8, 9, 109].

[Yan13] B. Yan, S. A. Moses, B. Gadway, J. P. Covey, K. R. A. Hazzard, A. M. Rey, D. S. Jin, and J. Ye. Observation of dipolar spin-exchange interactions with lattice-confined polar molecules. *Nature* **501**, 521 (2013) [cited on p. 2].

[Ye08] J. Ye, H. J. Kimble, and H. Katori. Quantum State Engineering and Precision Metrology Using State-Insensitive Light Traps. *Science* **320**, 1734 (2008) [cited on p. 92].

[Yel06] S. F. Yelin, K. Kirby, and R. Côté. Schemes for robust quantum computation with polar molecules. *Phys. Rev. A* **74**, 050301 (2006) [cited on p. 5].

[Yeo15] M. Yeo, M. T. Hummon, A. L. Collopy, B. Yan, B. Hemmerling, E. Chae, J. M. Doyle, and J. Ye. Rotational State Microwave Mixing for Laser Cooling of Complex Diatomic Molecules. *Phys. Rev. Lett.* **114**, 223003 (2015) [cited on p. 9].

[Zep07] M. Zeppenfeld, M. Motsch, P. Pinkse, and G. Rempe. Doppler-free spectroscopy of weak transitions: An analytical model applied to formaldehyde. *Appl. Phys. B* **89**, 475 (2007) [cited on p. 18].

[Zep09] M. Zeppenfeld, M. Motsch, P. Pinkse, and G. Rempe. Optoelectrical cooling of polar molecules. *Phys. Rev. A* **80**, 041401(R) (2009) [cited on pp. 10, 13–17, 38, 40, 42, 89, 110].

[Zep12] M. Zeppenfeld, B. G. U. Englert, R. Glöckner, A. Prehn, M. Mielenz, C. Sommer, L. D. van Buuren, M. Motsch, and G. Rempe. Sisyphus cooling of electrically trapped polyatomic molecules. *Nature* **491**, 570 (2012) [cited on pp. 10, 13, 15–17, 38, 39, 41, 43, 47, 56, 65, 73, 75, 79].

[Zep13] M. Zeppenfeld. *Electric Trapping and Cooling of Polyatomic Molecules*. Dissertation. Technische Universität München (2013) [cited on pp. 10, 11, 13, 15, 41–44, 47, 52, 56, 65, 90, 105, 114].

[Zep17] M. Zeppenfeld. Nondestructive detection of polar molecules via Rydberg atoms. *EPL* **118**, 13002 (2017) [cited on p. 112].

List of Publications

High-resolution spectroscopy on cold electrically trapped formaldehyde
A. Prehn, M. Ibrügger, G. Rempe, M. Zeppenfeld
arXiv:1807.06618 [physics.atom-ph] (2018)

Fast, precise, and widely tunable frequency control of an optical parametric oscillator referenced to a frequency comb
A. Prehn, R. Glöckner, G. Rempe, M. Zeppenfeld
Rev. Sci. Instr. **88**, 033101 (2017)

An experimental toolbox for the generation of cold and ultracold polar molecules
M. Zeppenfeld, T. Gantner, R. Glöckner, M. Ibrügger, M. Koller, A. Prehn, X. Wu, S. Chervenkov, G. Rempe
J. Phys.: Conf. Ser. **793**, 012035 (2017)

Optoelectrical cooling of polar molecules to submillikelvin temperatures
A. Prehn, M. Ibrügger, R. Glöckner, G. Rempe, M. Zeppenfeld
Phys. Rev. Lett. **116**, 063005 (2016)

Rotational cooling of trapped polyatomic molecules
R. Glöckner, A. Prehn, B.G.U. Englert, G. Rempe, M. Zeppenfeld
Phys. Rev. Lett. **115**, 233001 (2015)

Rotational state detection of electrically trapped polyatomic molecules
R. Glöckner, A. Prehn, G. Rempe, M. Zeppenfeld
New J. Phys. **17**, 055022 (2015)

Sisyphus cooling of electrically trapped polyatomic molecules
M. Zeppenfeld, B.G.U. Englert, R. Glöckner, A. Prehn, M. Mielenz, C. Sommer, L.D. van Buuren, M. Motsch, G. Rempe
Nature **491**, 570 (2012)

Acknowledgments

Throughout my time in the Quantum Dynamics Division of the Max Planck Institute of Quantum Optics, I had the pleasure of and benefited from working with many inspiring people in this group and this institute. Here, I want to show my gratitude to all scientists and friends whose countless contributions and continuous support have made this thesis possible and work in the institute enjoyable.

First of all, I am deeply grateful to my doctoral advisor, Gerhard Rempe, for giving me the opportunity to work on this exciting project in his group. He offered guidance and scientific input as well as a lot of freedom to pursue own ideas and to organize one's work independently. Moreover, his curiosity and enthusiasm for physics created a stimulating research environment, while his special and strict way of thinking ensured that any scientific reasoning was rock-solid. I also want to thank him for supporting my colleagues' and my idea to organize an international conference and invite about one hundred fellow doctoral researchers to Garching for a week of stimulating scientific and personal exchange.

Secondly, I am very thankful to Martin Zeppenfeld who has envisioned and built the experiment I then took over and led the cold molecule subgroup basically throughout the whole duration of my thesis work, although he was busy finishing his own thesis in the first months of this period. His constant stream of brilliant, unconventional ideas, thoughtful explanations of observed effects, and spontaneous and enthusiastic mini-lectures in front of the white board contributed significantly to the results presented here. Other things I learned from him range from how to write or not write a paper to molecular theory. Further, I thank him for carefully proof-reading this thesis.

Operating and developing the complex experimental setup would not have been possible without the support of many colleagues in the *Ultrastark* lab. I thank Barbara Englert and Rosa Glöckner for introducing me to the apparatus, Sisyphus cooling of molecules, the art of baking vacuum, and the psyche of the group—and for the fun time in the lab. Martin Ibrügger, who rejoined the group shortly after the measurements on cooling of formaldehyde began and took over the lab recently, deserves many thanks for his great commitment to our experiments, excellent collaboration and laid-back attitude. I want to thank both Rosa and Martin, with whom I shared an office and the lab for the longest time, for the open and cooperative atmosphere and many fruitful discussions, the serious and not so serious ones. Moreover, I would like to thank Markus Krottenmüller for his proactive attempt to develop a high-voltage-proof lithography process for our electric-trap microstructure and his great help with the installation of our new trap during his master's thesis. The students Jannik Luhn and Ömer Bayraktar contributed parts of the experimental control and data evaluation software.

I also want to thank the remaining current and former members of the cold molecule team for their helpfulness, support with any technical or physics question, and nice atmosphere in the group, in particular, Sotir Chervenkov, Xing Wu, Thomas Gantner, Manuel Koller, Erich Dobler, Ferdinand Jarisch as well as Maximilian Löw and Isabel Rabey who joined recently. I thank Martin Ibrügger, Maximilian and Isabel for proof-reading parts of this thesis.

The team of retired and current technicians formed by Josef Bayerl, Franz Denk, Helmuth Stehbeck, Tobias Urban, Florian Furchtsam, Johannes Siegl and Thomas Wiesmeier not only offered professional support whenever a new part of the experiment was designed and set up but also quick help in case of a technical emergency. I thank Iris Schwaiger for her organizational support.

Furthermore, would I like to thank Simon Baur for supervising my first student project in the group's electronics lab and his BEC experiment as well as Matthias Körber and Thomas Gantner for kicking off the organization of the YAO conference with me. In addition, I thank Stephan Dürr, Stephan Ritter, Christoph Hamsen, Manuel Uphoff and Andreas Neuzner for advice and chat. I thank the whole Quantum Dynamics Group for the excellent cooperation, insightful discussions, group retreats, beer garden visits, barbecues, hiking trips, regular bouldering sessions and more: the team spirit was great!

Finally, I am very grateful to my friends, my family and Helene for their constant encouragement, great support and wonderful distraction—at home or while traveling.

Thank you!